

An Experimental Investigation into the Validity of Leeson's Equation for Low Phase Noise Oscillator Design

by

John van der Merwe

*Thesis presented in partial fulfilment of the requirements for the
degree Master of Science in Engineering at
the University of Stellenbosch*



Supervisor: Prof. J.B. de Swardt
Co-supervisor: Prof. P.W. van der Walt
Department of Electrical & Electronic Engineering

December 2010

Declaration

By submitting this thesis electronically, I declare that the entirety of the work contained therein is my own, original work, and that I have not previously in its entirety or in part submitted it for obtaining any qualification.

Date: December 2010

Copyright © 2010 Stellenbosch University
All rights reserved.

Abstract

In 1966, D.B. Leeson presented his model on phase noise in a letter entitled *A Simple Model of Feedback Oscillator Noise Spectrum*. This model usually requires an additional *effective noise figure* in order to conform with measured results. (This *effective noise figure* has to be determined by means of curve-fitting Leeson's model with the measured results.) The model is, however, relatively simple to use, compared with other more accurate phase noise models that have since been developed and which can only be solved numerically with the aid of computers. It also gives great insight regarding component choices during the design process.

Therefore several experiments were conducted in order to determine conditions under which Leeson's model may be considered valid and accurate. These experiments, as well as the conclusions drawn from their results, are discussed in this document.

Opsomming

In 1966 stel D.B. Leeson sy faseruis model bekend in 'n brief getiteld *A Simple Model of Feedback Oscillator Noise Spectrum*. Hierdie model vereis gewoonlik die gebruik van 'n bykomende effektiewe ruissyfer, sodat die model ooreenstem met die gemete resultate. (Hierdie effektiewe ruissyfer kan slegs bepaal word deur middel van krommepassings tussen Leeson se model en die gemete resultate.) Die model is egter relatief eenvoudig om te gebruik in teenstelling met ander, meer akkurate, faseruis modelle wat sedertdien ontwikkel is en slegs met behulp van rekenaars opgelos kan word. Dit bied ook onoortreflike insig ten opsigte van komponent keuses tydens die ontwerpsproses.

Om hierdie rede is verskeie eksperimente uitgevoer met die doel om toestande te identifiseer waaronder Leeson se model as geldig en akkuraat geag kan word. Hierdie eksperimente, asook die gevolgtrekkings wat van hul resultate gemaak is, word in hierdie dokument behandel.

Acknowledgements

I would like to take this opportunity to thank everyone who contributed to this thesis.

A special word of thanks is extended to my supervisors, Prof. J.B. De Swardt and Prof. P.W. van der Walt, for their guidance, motivation and inspiration during the course of this project.

I would also like to express my gratitude to Stellenbosch University and Reutech Radar Systems for the use of their equipment and facilities. Thank you also to Mr. Clive Whaits and the Cape Peninsula University of Technology, for facilitating the use of their signal-source analyser.

Thank you to Dr. C. van Niekerk and Dr. R. Wolhuter for facilitating funds from the Department of Trade and Industry, without which this study would not have been possible.

I am grateful to my parents, Carel and Laura van der Merwe, for their sacrifices and support throughout my years of study. A special thank you is also extended to Madelé van der Walt for her encouragement and support.

Contents

Declaration	i
Abstract	ii
Opsomming	iii
Acknowledgements	iv
Contents	v
List of Figures	x
List of Tables	xvii
List of Abbreviations	xviii
1 Introduction	1
1.1 Problem Statement	2
1.2 Organisation of Thesis	2
2 An Introduction to Electronic Oscillators	4
2.1 Introduction	4
2.2 Oscillator Specifications	6
2.2.1 Output Power	6
2.2.2 Frequency Drift	6
2.2.3 Harmonic Distortion	7

3	An Introduction to Phase Noise	8
3.1	Introduction	8
3.2	Phase Noise Modelled	9
3.3	Phase Noise Distribution	11
3.4	Leeson's Equation (an LTI model)	16
3.4.1	A Heuristic Approach	16
3.4.2	A Mathematical Approach	20
3.4.3	Conclusion	24
3.5	Conclusion	25
4	Experiment 1:	27
4.1	Purpose of the experiment	27
4.2	The design and characterisation of the different circuit modules	29
4.2.1	Cascode amplifier	29
4.2.2	Wilkinson power divider	29
4.2.3	Phase shift network	30
4.2.4	Attenuator	30
4.2.5	Resonator	30
4.3	System measurements and evaluation	33
4.3.1	Phase noise measurements	36
4.4	Conclusion	39
5	Experiment 2:	41
5.1	Purpose of the experiment	41
5.2	The design and characterisation of the various circuit models	41
5.2.1	Resistive Feedback Amplifier	42
5.2.2	Amplifier without Feedback	42
5.2.3	Resonator	43
5.2.4	Phase Shifter	43
5.2.5	Power Divider and Attenuators	43
5.3	Method of the Experiment	43
5.4	Conclusion	46

6 Experiment 3:	47
6.1 Purpose of the Experiment	47
6.2 Method of the Experiment	47
6.3 Measurements and Discussion	49
6.3.1 Comparing Measured Phase Noise with Leeson's Model	51
6.3.2 Discussion of Phase Noise Measurements	53
6.4 Conclusion	56
7 Experiment 4:	58
7.1 Purpose of the Experiment	58
7.2 Method of the Experiment	58
7.3 Measurements and Discussions	59
7.3.1 Comparing Phase Noise Measurements with Leeson's Model	61
7.3.2 Discussion of Phase Noise Measurements and Approximations	62
7.4 Conclusion	65
8 Experiment 5:	68
8.1 Purpose of the Experiment	68
8.2 Method of the Experiment and Measured Results	68
8.2.1 Open Loop Simulations and Measurements	69
8.2.2 Phase Noise Measurements	77
8.3 Conclusion	78
9 Experiment 6:	80
9.1 Purpose of the Experiment	80
9.2 Method of the Experiment	81
9.2.1 Open Loop Measurements	82
9.2.2 Phase Noise Measurements	84
9.3 Conclusion	93

10 Final Conclusions and Future Work	95
10.1 Conclusions	95
10.2 Future Work	96
Bibliography	98
A The Modules Used in Experiment 1	A-1
A.1 Cascode Amplifier	A-1
A.1.1 Design and Simulation	A-2
A.1.2 Measurements and Conclusions	A-4
A.2 Wilkinson Power Divider	A-8
A.2.1 Design and Simulation	A-9
A.2.2 Measurements and Conclusions	A-13
A.3 270° Phase Shift Network	A-15
A.3.1 Design and Simulation	A-15
A.3.2 Measurements and Conclusions	A-18
A.4 Π -Attenuators	A-20
A.5 Π -Resonator	A-25
A.5.1 Measurements and Conclusions	A-30
B Mini-Circuits Attenuators	B-1
C Hardware Used in Experiment 2 and Experiment 3	C-1
C.1 Resistive Feedback Amplifier	C-1
C.2 Amplifier without Feedback	C-6
C.3 10 MHz Resonator	C-8
C.4 10 MHz Wilkinson Divider	C-10
C.5 Phase Shift Network	C-12
C.6 Variable Attenuator	C-14

D Hardware Used in Experiments 4 to 6	D-1
D.1 SC-Cut Crystal Resonator	D-1
D.1.1 Design and Measurement	D-1
D.2 Modified Resistive Feedback Amplifier	D-4
D.2.1 Measurements	D-4
D.3 AT-Cut Crystal Resonator	D-8
D.3.1 Design and Measurements	D-8

List of Figures

2.1	Basic oscillator block diagram	4
2.2	The Colpitts, the Hartley and the Clapp oscillator configurations.	6
3.1	The relationship between $S_{\Phi}(f)$ and $\mathcal{L}(f)$	9
3.2	Spectrum broadens as a result of phase noise	10
3.3	Conversion of voltage noise to phase noise	12
3.4	The effect of resonator BW on the oscillator's phase noise distribution .	13
3.5	$S_{\Phi}(f)$ and $S_y(f)$	15
3.6	Variation on basic oscillator block diagram	17
3.7	Amplitude and phase conditions for oscillations	18
3.8	Decomposition of resonator input signal and resulting response	22
3.9	Oscillator block diagram in the phase domain	23
4.1	Experimental circuit layout	28
4.2	A generic oscillator circuit.	32
4.3	Simulated collector current against time	34
4.4	Simulated oscillator signal out	35
4.5	Measured harmonic distortion of oscillator circuits	35
4.6	Measured output signal strengths	35
4.7	Block diagram of measurement setup with external reference oscillator .	36
4.8	Phase noise performance for different attenuation settings	37
4.9	Digitally filtered phase noise measurements	38
5.1	The experimental circuit layout	42

5.2	Measured fundamental frequency of the linearly driven oscillator	44
5.3	Measured fundamental frequency of the nonlinearly driven oscillator . .	45
5.4	Phase noise performances of linearly and nonlinearly driven oscillator networks	45
6.1	The experimental setup	48
6.2	Phase noise vs. compression	49
6.3	Signal magnitude vs. compression	50
6.4	Oscillator loop broken in order to calculate system noise figure.	53
6.5	Discrepancy between measured and predicted phase noise at 0.1 dB amplifier saturation.	54
6.6	Discrepancy between measured and predicted phase noise at 0.2 dB amplifier saturation.	54
6.7	Discrepancy between measured and predicted phase noise at 0.3 dB amplifier saturation.	55
6.8	Discrepancy between measured and predicted phase noise at 0.4 dB amplifier saturation.	55
7.1	Crystal loop oscillator setup used in experiment 4	58
7.2	Experimental setup	59
7.3	Phase noise vs. compression	60
7.4	Phase noise vs compression for compression levels of less than 0.6 dB .	60
7.5	Measured and predicted phase noise at 0.1 dB amplifier compression. .	62
7.6	Measured and predicted phase noise at 0.2 dB amplifier compression. .	63
7.7	Measured and predicted phase noise at 0.5 dB amplifier compression. .	63
7.8	Measured and predicted phase noise at 0.9dB amplifier compression. . .	64
7.9	Measured and predicted phase noise at 1.2 dB amplifier compression. .	64
7.10	Measured phase noise @ 0.1 dB amplifier saturation vs. FSUP8 mini- mum phase noise specifications.	67
8.1	The oscillator network	69
8.2	The oscillator network with the loop broken	70

8.3	Simulated passband and group delay at 0.1 dB open loop gain	70
8.4	Simulated passband and group delay at 0.2 dB open loop gain	71
8.5	Simulated phase deviation and group delay at 0.1 dB open loop gain . .	71
8.6	Measured passband and group delay at 0.1 dB open loop gain	73
8.7	Measured phase deviation and group delay at 0.1 dB open loop gain . .	73
8.8	Calculated maximum and minimum amplitude measurement errors at 0.1 dB amplifier saturation	74
8.9	Measured passband and group delay at 0.2 dB open loop gain	75
8.10	Measured phase deviation and group delay at 0.2 dB open loop gain . .	76
8.11	Calculated maximum and minimum amplitude measurement errors at 0.2 dB open loop gain	76
8.12	Oscillator measurements with FSUP8	77
8.13	Phase noise @ 0.1 dB amplifier saturation.	78
8.14	Phase noise @ 0.2 dB amplifier saturation.	79
9.1	Oscillator network using an AT-cut crystal resonator	80
9.2	The oscillator network	81
9.3	The Oscillator network with the loop broken	82
9.4	Oscillation conditions @ 0.1 dB open loop gain	83
9.5	Group delay @ 0.1 dB open loop gain	83
9.6	Oscillation conditions @ 0.2 dB open loop gain	85
9.7	Group delay @ 0.2 dB open loop gain	85
9.8	Oscillation conditions @ 0.3 dB open loop gain	86
9.9	Group delay @ 0.3 dB open loop gain	86
9.10	Oscillation conditions @ 0.4 dB open loop gain	87
9.11	Group delay @ 0.4 dB open loop gain	87
9.12	Oscillation conditions @ 0.5 dB open loop gain	88
9.13	Group delay @ 0.5 dB open loop gain	88
9.14	Measured and predicted phase noise @ 0.1 dB amplifier saturation . . .	90
9.15	Measured and predicted phase noise @ 0.2 dB amplifier saturation . . .	91

9.16	Measured and predicted phase noise @ 0.3 dB amplifier saturation . . .	91
9.17	Measured and predicted phase noise @ 0.4 dB amplifier saturation . . .	92
9.18	Measured and predicted phase noise @ 0.5 dB amplifier saturation . . .	92
9.19	The deviation between the measured phase noise and that predicted by Leeson's model at offset frequencies of 1 MHz and 800 Hz.	93
A.1	Cascode amplifiers	A-1
A.2	Simplified BJT cascode amplifier	A-2
A.3	Schematic diagram of cascode amplifier	A-3
A.4	Cascode amplifier: simulated gain	A-3
A.5	Cascode amplifier: simulated phase deviation	A-4
A.6	Cascode amplifier: simulated input and output port matching	A-5
A.7	Cascode amplifier: measured input port matching	A-6
A.8	Cascode amplifier: output port matching	A-6
A.9	Cascode amplifier: measured gain and bandwidth	A-7
A.10	Cascode amplifier: measured input output phase deviation	A-7
A.11	Cascode amplifier: input power vs. output power	A-8
A.12	Wilkinson power dividers used in experiment 1	A-8
A.13	Wilkinson power divider	A-9
A.14	Quarter wave equivalent LC network	A-10
A.15	LC wilkinson power divider	A-10
A.16	The simulated normalised power delivered at the output ports of the divider shown against frequency.	A-11
A.17	The simulated phase deviation from input to output against frequency.	A-11
A.18	The simulated isolation factor between the output ports against frequency.	A-12
A.19	The simulated reflection coefficient at all three ports	A-12
A.20	The measured normalised power delivered at the output ports of the divider shown against frequency.	A-13
A.21	The measured phase deviation from input to output against frequency.	A-14
A.22	The measured isolation factor between the output ports against frequency.	A-14

A.23	The measured reflection coefficient at all three ports	A-15
A.24	270° Phase shifters	A-15
A.25	$\frac{3}{4}$ Wavelength transmission line LC equivalent circuit	A-16
A.26	Simulated reflection coefficient $\frac{3}{4}$ wavelength transmission line equivalent	A-16
A.27	Simulated pass band of $\frac{3}{4}$ wavelength equivalent.	A-17
A.28	Simulated phase deviation of $\frac{3}{4}$ wavelength equivalent against frequency.	A-17
A.29	Measured reflection coefficient $\frac{3}{4}$ wavelength transmission line equivalent	A-18
A.30	Measured pass band of $\frac{3}{4}$ wavelength equivalent.	A-19
A.31	Measured phase deviation of $\frac{3}{4}$ wavelength equivalent against frequency.	A-19
A.32	Attenuators used	A-20
A.33	Schematic diagram of a π -attenuator	A-20
A.34	3 dB Attenuator port matching	A-21
A.35	3 dB Attenuator losses	A-21
A.36	3 dB Attenuator phase deviation	A-22
A.37	11 dB Attenuator port matching	A-22
A.38	11 dB Attenuator loss	A-23
A.39	11 dB Attenuator phase deviation	A-23
A.40	15 dB Attenuator port matching	A-24
A.41	15 dB Attenuator loss	A-24
A.42	15 dB Attenuator phase deviation	A-25
A.43	LC Π -resonator schematic	A-26
A.44	Simplified Π -resonator schematic	A-26
A.45	Simulated fixed resonator: port matching	A-28
A.46	Simulated fixed resonator: pass band	A-29
A.47	Simulated fixed resonator: phase shift between input and output ports	A-29
A.48	Schematic diagram of voltage adjustable resonator	A-30
A.49	Adjustable resonator	A-30
A.50	Comparison of port matching of fixed and adjustable resonators	A-31

A.51	Simulated comparison of resonance frequencies of fixed and adjustable resonators	A-31
A.52	Measured fixed resonator port matching	A-32
A.53	Measured resonance frequency of fixed resonator	A-33
A.54	Resonance frequency of adjustable resonator for various varactor biasing voltages	A-34
A.55	Measured comparison of resonance frequencies of fixed and adjustable resonators.	A-35
C.1	Resistive feedback amplifier	C-1
C.2	Schematic of resistive feedback amplifier	C-2
C.3	Resistive feedback amplifier:input port matching	C-3
C.4	Resistive feedback amplifier: output port matching	C-3
C.5	Resistive feedback amplifier: gain vs frequency	C-4
C.6	Resistive feedback amplifier:isolation between the input and output ports	C-4
C.7	Resistive feedback amplifier: gain vs input power	C-5
C.8	Resistive feedback amplifier: output power vs input power	C-5
C.9	Amplifier without feedback used in experiment 2	C-6
C.10	Amplifier without feedback: input port matching	C-6
C.11	Amplifier without Feedback: Amplifier Gain	C-7
C.12	Amplifier without Feedback: Phase Deviation	C-7
C.13	10 MHz LC resonator	C-8
C.14	10 MHz LC resonator with resistive matching	C-8
C.15	10 MHz resonator: port matching	C-9
C.16	10 MHz resonator: magnitude and phase response	C-9
C.17	10 MHz Wilkinson power divider	C-10
C.18	10 MHz LC Wilkinson power divider: port matching	C-10
C.19	10 MHz LC wilkinson power divider:	C-11
C.20	10 MHz LC Wilkinson power divider: output port isolation	C-11
C.21	10 MHz LC Wilkinson power divider: phase deviation	C-12

C.22	Phase shifter	C-12
C.23	68°Phase Shifter: port matching	C-13
C.24	68°Phase shifter: magnitude and phase response	C-14
C.25	Variable attenuator	C-14
C.26	Variable attenuator: schematic diagram	C-15
C.27	Variable attenuator: attenuative losses	C-16
C.28	Variable attenuator: input port matching	C-16
C.29	Variable attenuator: output port matching	C-17
C.30	Variable attenuator: phase deviation	C-17
D.1	Crystal resonator	D-1
D.2	Crystal resonator schematic	D-2
D.3	Crystal resonator: pass band	D-2
D.4	Crystal resonator: phase deviation	D-3
D.5	Crystal resonator: port matching	D-3
D.6	Crystal resonator: fitted group delay with regard to pass band	D-4
D.7	Modified resistive feedback amplifier schematic	D-5
D.8	Modified resistive amplifier: port matching	D-6
D.9	Modified resistive amplifier: port isolation	D-6
D.10	Modified resistive amplifier: amplifier gain	D-7
D.11	Modified resistive amplifier: phase deviation	D-7
D.12	Modified resistive amplifier: input power vs output power	D-8
D.13	AT-cut crystal resonator	D-8
D.14	AT-cut crystal resonator: reflection coefficients	D-9
D.15	AT-cut crystal resonator: pass band and phase deviation	D-10
D.16	AT-cut crystal resonator:pass band and group delay	D-10

List of Tables

3.1	Power spectral densities of noise types	14
4.1	Calculated input signal power and losses at measured centre frequency.	38
4.2	Calculated noise figures and open loop gains for different levels of attenuation	39
6.1	Noise figures and resulting ultimate phase noise.	52
7.1	Ultimate phase noise and cascaded noise figure for various levels of amplifier saturation.	61
8.1	Simulated quality factors and Leeson frequencies	72
8.2	Open loop data at the oscillation frequency	75
8.3	Maximum calculated error in amplitude measurement	75
9.1	Leeson frequency and related variables @ various open loop gains	89
9.2	Ultimate phase noise and related variables @ various open loop gains .	89
A.1	Component values of the nonadjustable resonator	A-27
C.1	Component values of the resistive feedback amplifier.	C-2
C.2	Component values of the 10 MHz matched resonator	C-8
C.3	Variable attenuator: attenuation settings	C-15

List of Abbreviations

AC	alternating current
AM	amplitude modulated
BW	Bandwidth
CW	continuous wave
dBc	decibel relative to carrier
dBm	decibel relative to one milliwatt
DC	direct current
DUT	Device Under Test
FM	frequency modulated
Hz	hertz
ISF	impulse sensitivity function
i.t.o.	in terms of
LC	Inductor and Capacitor
LTI	Linear time-invariant
LTV	Linear time-variant
LO	Local Oscillator
MWO	Microwave Office
MTD	Moving Target Detector
MTI	Moving Target Indication

NLTV	Nonlinear time-variant
PM	phase modulated
QAM	Quadrature Amplitude Modulation
RCS	Radar Cross Section
RMS	root mean square
SSB	single sideband
VGA	Variable Gain Amplifier
VNA	Vector Network Analyser

Chapter 1

Introduction

Electronic oscillators are used as time references in a wide variety of applications ranging from radar to communication systems. The need for greater oscillator stability is becoming ever more pertinent: Quadrature amplitude modulation (QAM) communication systems such as WiMAX require very stable local oscillators (LOs), since the data is modulated onto the carrier by varying both amplitude and phase. Undesired variances in amplitude or phase as a result of noise would therefore place a fundamental limit on the achievable bit rates. This implies that the greater the stability of the LO, the greater the bit rate that can theoretically be achieved in a given channel. This statement holds true as long as the thermal noise limit is not reached.

When considering radar applications, on the other hand, a noisy LO can impair the detection threshold of the system. This is especially true in the case of continuous wave (CW) radars, but also for pulse radar systems such as MTI or MTD radars. This is due to the fact that clutter suppression is limited by phase noise. Clutter suppression entails echoes of sequential measurements being subtracted from each other. Should there be any variation in the carrier wave's phase during the time between the sending of the signal and the reception of the echo, the result would be that stationary targets would no longer be eliminated. This would imply an increase in the radar's detection threshold. In CW radar applications, the phase noise of a large reflected signal can also increase the system's noise threshold, making it impossible to detect small targets at long range. Phase noise can also lead to an error in the Doppler frequency. The problem intensifies for radially slow-moving targets.

Phase noise, which manifests as jitter in the time domain, can also lead to synchronisation problems and bit errors in digital systems.

These are but a few examples. In this document the phase noise performance of oscillator circuits and the effects of the linearity of the circuits themselves on this performance will be investigated.

1.1 Problem Statement

When designing an oscillator for low phase noise, as with the design of most electronic circuits, it is often easiest to start off with a linear model in order to develop greater insight into the problem. Such a phase noise model was presented by D.B. Leeson in 1966, using a heuristic approach. His model is linear time-invariant in nature and is still one of the phase noise models most widely used by oscillator designers today. This is irrespective of the fact that other phase noise models, which are nonlinear time-variant or linear time-variant and which are much more accurate, have been developed. This can be attributed to the fact that with the methods of the newer phase noise models, the effect of individual components within the system (transistors, resistors, inductors, etc.) upon the system's phase noise is lost within layers of obscurity. These phase noise models (LTV and NLTV models) are also usually only solvable by means of numerical computer simulations, which negates approaches to design by hand.

As has just been mentioned, Leeson's model is not as accurate as the LTV and NLTV models and usually requires the addition of an effective noise figure in order to conform with measured or simulated phase noise. However, given the insight that Leeson's model provides into a component choice with regard to its effect on the oscillator's phase noise performance, it stands to reason that the circumstances under which this model is indeed valid should be defined. Another point to evaluate, is how quickly, and under which conditions, the model becomes invalid.

In the following chapters the author will attempt to determine just that: The conditions under which Leeson's model may be considered as valid and accurate will be investigated and verified by means of a set of experiments.

1.2 Organisation of Thesis

In Chapter 2, basic principles concerning the functioning of oscillators as well as a few oscillator properties are discussed.

Chapter 3 deals with phase noise. It illustrates how phase noise could be described as a random FM or PM signal modulated onto a carrier. The phase noise distribution is

also described, along with a detailed discussion on the derivation of Leeson's model for phase noise.

In Chapter 4 an experiment concerning the effect of circuit non-linearity on the oscillator's phase noise performance is outlined and evaluated. In particular, the effect that the linearity of the circuit has on its effective noise figure is assessed. It is also demonstrated that the magnitude of the output signal level increases with circuit non-linearity. It is found that Leeson's model describes an oscillator's phase noise distribution with increasing accuracy as the circuit approaches linear operation. A hypothesis is made that, should a linearly driven oscillator have an output signal similar in magnitude to that of a nonlinearly driven oscillator, the linearly driven oscillator will show superior phase noise performance. In Chapter 5 this hypothesis is evaluated and confirmed.

Chapters 6 and 7 evaluate the phase noise of, respectively, an LC oscillator network and a crystal oscillator network, as the level of amplifier saturation is adjusted in steps of approximately 0.1dB. In both cases the measured phase noise is approximated using Leeson's phase noise model. The loaded quality factors of the resonators are used to determine the Leeson frequency in both experiments. In Chapter 6, the resonator's bandwidth is used to determine the Q , whereas in Chapter 7, it is determined using the group delay of the resonator.

The experiments of Chapters 8 and 9 are similar to those discussed in Chapters 6 and 7, but differ from these in that the network's open loop group delay instead of the resonator's bandwidth, is used in order to determine the Leeson frequency.

Chapter 10 completes this thesis by reflecting upon the conclusions drawn from these experiments and suggests a low phase noise oscillator design procedure.

Chapter 2

An Introduction to Electronic Oscillators

2.1 Introduction

An oscillator is a circuit that converts direct current (DC) power into a periodic alternating current (AC) waveform with a fixed frequency[1]. The basic frequency domain block diagram of a linear oscillator is shown in figure 2.1. The figure shows the conceptual operation of a sinusoidal oscillator in terms of a linear amplifier with linear feedback between its output and input ports. The amplifier has a gain of A and an output voltage $V_{out}(s)$. From the block diagram we see that the output

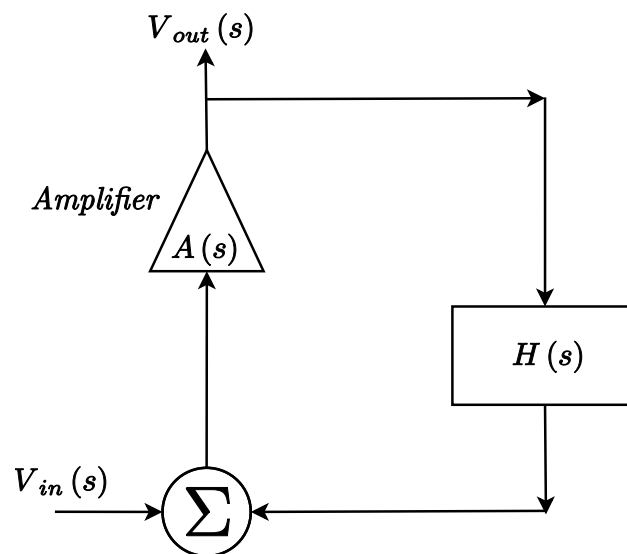


Figure 2.1: Basic oscillator block diagram

voltage can be written as:

$$V_{out}(s) = AV_{in}(s) + H(s)AV_{out}(s) \quad (2.1)$$

where $V_{in}(s)$ and $V_{out}(s)$ are the Laplace transforms of the time domain input and output signals respectively. Equation 2.1 can be rewritten in the form:

$$V_{out}(s) = \frac{A}{1 - AH(s)}V_{in}(s) \quad (2.2)$$

From equation 2.2 it can be deduced that, should the denominator of this equation become zero at a certain frequency, f_0 (when $AH(j2\pi f_0) = 1$), a non-zero output voltage could be obtained, given a zero input voltage. (At this oscillation frequency $s = j2\pi f_0$) This is known as the Nyquist or Barkhausen criterion [1, 2]. This model is, however, linear and does not allow for the output signal's amplitude to be determined. The amplitude of the output signal is usually governed by nonlinearities in the active device. This is due to the fact that real-world active devices are only capable of handling finite amounts of power before they are driven into saturation. Once saturation sets in, the effective gain of the amplifier decreases until the oscillator stabilises. It is, however, also possible to govern the output signal's amplitude by linear means. An example of this would be the filament of a light bulb, often used in Wien bridge oscillator configurations. Therefore the criteria for oscillation can be stated another way: Should an active two port device be provided with a feedback path, an oscillation will occur if the signal being fed back is larger than, and in phase with, the input signal. These oscillations will continue to grow until saturation sets in or the effective loop gain is reduced to unity by other means[3]. Therefore the criterion for oscillation is that a feedback path must exist, providing an open loop gain of at least unity and precisely zero (or $n \times 360^\circ$, where n is an integer) phase shift [3].

It is useful to note some of the more traditional oscillator circuit configurations, such as those shown in figure 2.2, even though this document will not be evaluating their designs [1, 4, 5, 6]. Also note that all oscillator circuits can be made to fit the block diagram of figure 2.1.

Oscillators may also be analysed by means of a negative resistance model, to which any oscillator can be made to fit. This document will, however, be making use of the previously discussed loop oscillator model, due to the insight it provides into the working of the oscillator.

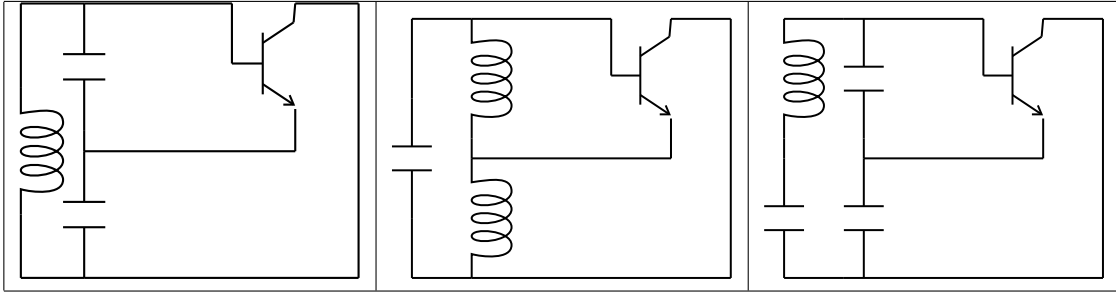


Figure 2.2: The Colpitts, the Hartley and the Clapp oscillator configurations.

2.2 Oscillator Specifications

Oscillators are specified and characterised in terms of various properties. For the purposes of this document, the most important of these properties is the oscillator's phase noise. This will be discussed in detail in the following chapter. Other important properties are listed below. The list is incomplete and limited to the properties most relevant to the purposes of this document.

2.2.1 Output Power

The signal power at the fundamental frequency of the oscillator, as measured with a spectrum analyser at the oscillator's output, is referred to as the oscillator's output power [4]. It is usually measured in dBm. The output power is relevant to the purpose of this document since, as will be discussed in the following chapter, the phase noise spectral density is measured relative to the output signal power in dBc/Hz.

2.2.2 Frequency Drift

Frequency drift or oscillator drift, as it is sometimes referred to, is the undesired phenomenon by which the oscillation frequency is continuously changing. This will occur over long periods of time and is then referred to as *aging* [4]. Oscillators may also drift as a result of environmental changes, such as temperature changes in the active device or resonator. It is important to note that temperature fluctuations may also affect the load resistance of the oscillator, which could result in load pulling. Another environmental change would be fluctuations in the biasing of the active device, which will result in changes of in the oscillation frequency.

It is of interest that, should the previously mentioned environmental changes only occur with regard to the active device and not affect the resonator (for example

an oscillator with an ovenised resonator), the amount of drift would be inversely proportional to the quality factor of the oscillator's resonator.

Aging is measured over a specified time as the difference between the maximum and the minimum frequency deviation. Mathematically it can be stated as: $(f_{max} - f_{min})$ [Hz] during x amount of time.

2.2.3 Harmonic Distortion

When the amplitude of the input signal to the active device surpasses the active device's saturation level, the signal at the output of the active device is clipped. As the input signal amplitude is increased, the active device is driven deeper into saturation. This results in a decrease in effective gain at the fundamental frequency f_0 and the appearance of harmonics at frequency multiples of f_0 [2].

Second harmonic distortion is the ratio of the power magnitude of the second harmonic to that of the power magnitude of the fundamental frequency component and is measured in dBc [4]. High harmonic distortion indicates that the active device has been driven deep into saturation. Note that the opposite is not necessarily true. Should the oscillator's output signal be obtained off the resonator through electromagnetic coupling, the resonator will act as a filter and suppress any harmonics that may be present within the oscillator loop.

Chapter 3

An Introduction to Phase Noise

3.1 Introduction

Phase noise is a measure of a signal's short term stability. This short term signal stability is ordinarily measured over a period of time ranging from fractions of seconds to 1 second and sometimes up to a minute. It is often given as an integrated number in RMS degrees or radians [7]. Oscillator phase noise is best described in terms of power spectral density, $S_{\Phi}(f)$, which is given in $\frac{\text{rad}^2}{\text{Hz}}$. It is usually plotted on a logarithmic scale, in which case it is then given in $\frac{\text{dBc}}{\text{Hz}}$. These notations are equivalent in the sense that $S_{dB} = 10 \log_{10}(S)$. A mathematical derivation will follow soon.

In technical documentation phase noise is normally given as the quantity $\mathcal{L}(f)$. $\mathcal{L}(f)$ is interchangeable with $S_{\Phi}(f)$, since $\mathcal{L}(f) = \frac{1}{2}S_{\Phi}(f)$, which is always in $\frac{\text{dBc}}{\text{Hz}}$ [8],[2]. It refers to the ratio of single sideband (SSB) noise power in a 1 Hz bandwidth to the total carrier signal power and is plotted against the frequency offset from the carrier [7]. Note that $S_{\Phi}(f)$ is a single sided spectral density due to the fact that the Fourier frequency, f , ranges from 0 to ∞ . It does, however, include fluctuations from both the lower as well as the upper sideband [8]. The relationship between $S_{\Phi}(f)$ and $\mathcal{L}(f)$, is illustrated in figure 3.1.

The term *jitter* should also be mentioned. It is related to phase noise in the time domain and refers to variations in the time domain signal's zero crossings [7].

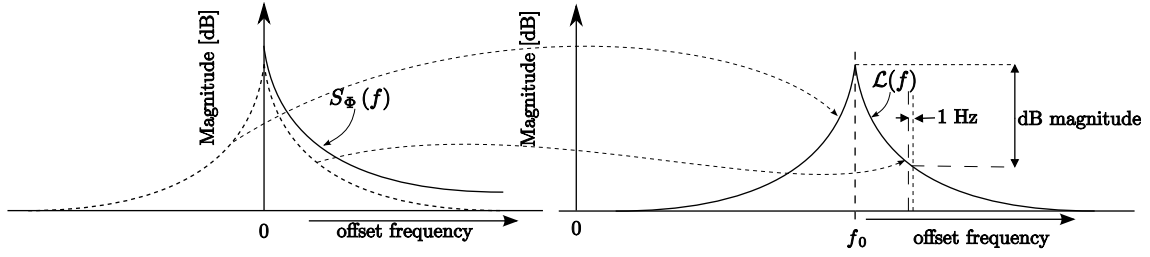


Figure 3.1: The relationship between $S_{\Phi}(f)$ and $\mathcal{L}(f)$

3.2 Phase Noise Modelled

Consider a time dependent oscillator output voltage signal to be of the form:

$$v(t) = V(t) \cos(\theta(t)) \quad (3.1)$$

$$v(t) = V_0 [1 + \alpha(t)] \cos(\omega_0 t + \phi(t)) \quad (3.2)$$

The instantaneous frequency of the signal, $v(t)$, given in equation 3.1, can be determined by the time derivative, $\frac{d\theta(t)}{dt}$. It is constantly changing with time and has an average value of ω_0 . This implies that equation 3.1 can be expanded to the form given in equation 3.2. In this equation ω_0 is the fundamental or carrier frequency in radians per second, $\alpha(t)$ is the fractional amplitude noise and $\phi(t)$ is the phase noise. The unit of measure for $\phi(t)$ is radians, while $\alpha(t)$ is dimensionless. Both of these are random variables [2]. If $v(t)$ had been a noiseless signal, its spectrum would ideally have been the Dirac function $\frac{V_0}{2} \delta(\omega - \omega_0)$. In the presence of noise, however, the spectrum broadens. This is due to the fact that the signal is being randomly modulated in both amplitude and phase [7]. The broadened spectrum, illustrated in figure 3.2, could be viewed as a series of closely spaced discrete side bands.

Amplitude (AM) noise is normally much less than phase noise. AM noise usually also has less of an effect on a system's performance [7]. Therefore the AM noise can be considered constant and the previously mentioned broadened spectrum will be explained only as a result of phase noise, $\phi(t)$ [7].

Consider a frequency modulated (FM) signal with the following instantaneous frequency deviation:

$$f(t) = \Delta f \cos(\omega_m t) \quad (3.3)$$

Since phase is the time integral of frequency, equation 3.4 holds true and gives the

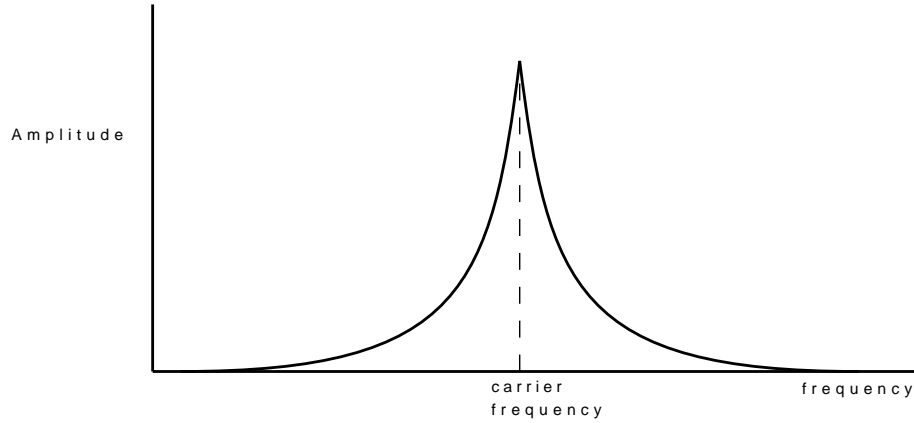


Figure 3.2: Spectrum broadens as a result of phase noise

instantaneous phase deviation. This equation clearly illustrates that an FM signal with a maximum frequency deviation of Δf and a carrier frequency of f_0 , will result in a phase modulated (PM) signal at f_0 with a peak phase deviation of Φ_p , where $\Phi_p = \frac{\Delta f}{f_0}$ radians [7].

$$\phi(t) = \int 2\pi f(t) dt = \frac{\Delta f}{f_0} \sin(\omega_m t) = \Phi_p \sin(\omega_m t) \quad (3.4)$$

In the absence of AM noise, and with V_0 set to 1, equation 3.2 can be reduced to equation 3.5.

$$v(t) = \cos(\omega_0 t + \phi(t)) \quad (3.5)$$

Equation 3.6 is obtained when equation 3.4 is substituted into equation 3.5.

$$\begin{aligned} v(t) &= \cos(\omega_0 t + \Phi_p \sin(\omega_m t)) \\ &= \cos(\omega_0 t) \cos(\Phi_p \sin(\omega_m t)) - \sin(\omega_0 t) \sin(\Phi_p \sin(\omega_m t)) \end{aligned} \quad (3.6)$$

In the case of narrow band FM (an FM signal with a small modulation index), Φ_p is very small. Should Φ_p be much smaller than 1, the following approximations may be made:

$$\cos(\Phi_p \sin(\omega_m t)) \approx 1 \quad (3.7)$$

and

$$\sin(\Phi_p \sin(\omega_m t)) \approx \Phi_p \sin(\omega_m t) \quad (3.8)$$

Therefore, for a narrow band FM signal, equation 3.6 can be reduced to equation 3.9. This equation clearly illustrates that the carrier signal has two side bands with

peak amplitudes of $\frac{\Phi_p}{2}$ at a frequency offset of f_m Hz or ω_m radians [7].

$$\begin{aligned} v(t) &= \cos(\omega_0 t) - \Phi_p \sin(\omega_0 t) \sin(\omega_m t) \\ &= \cos(\omega_0 t) + \frac{\Phi_p}{2} \cos((\omega_0 + \omega_m)t) - \frac{\Phi_p}{2} \cos((\omega_0 - \omega_m)t) \end{aligned} \quad (3.9)$$

As was noted previously, phase noise has a continuous spectral distribution. Should this noise distribution be divided into 1 Hz intervals, the energy in each of these 1 Hz bands can be viewed as the result of an FM signal with a variation proportional to the amplitude of the power spectrum at the offset frequency being considered. Phase noise can therefore be modelled as a large number of random FM signals around a single carrier, with their offset frequencies spaced 1 Hz apart.

3.3 Phase Noise Distribution

From the previous section, one might assume that phase noise would have a homogeneous distribution around the carrier. This is, of course, not the case. An oscillator's phase noise distribution is in fact largely determined by its resonator's response, as well as the noise inherent to its power source and active device, that will inevitably enter the system. Various models exist to determine the phase noise distribution [9, 10, 11, 12]; these will be discussed in the following sections.

The noise voltage or noise current power spectral density of the oscillator's power source and active device, can be considered to be as depicted in figure 3.3.a. It has a predominantly white noise distribution, but a $\frac{1}{f}$ -noise distribution (flicker noise) will also be present at low frequencies. Due to the nonlinear operation of the oscillator network, noise components situated at integer multiples(n) of the oscillation frequency(f_0), are transformed to low frequency noise sidebands in the phase domain. These phase noise sidebands are in turn transformed to the power spectral density of the oscillator's output signal. $S_\Phi(f)$ is obtained by means of the superposition of all of the phase noise inputs that have been transformed from device noise at $n \times f_0$ [10, 11].

Each of these phase noise inputs is weighted by a coefficient, k_n . White noise sources give rise to a $\frac{1}{f^2}$ dependency in the phase domain within the bandwidth of the resonator, whereas $\frac{1}{f}$ -dependent noise sources are transformed to $\frac{1}{f^3}$ -dependent phase noise sources. Note that the previously mentioned frequency dependence is i.t.o. the offset frequency with regard to the carrier frequency. (The mechanism for the transformation is described in the following section.) Low frequency noise

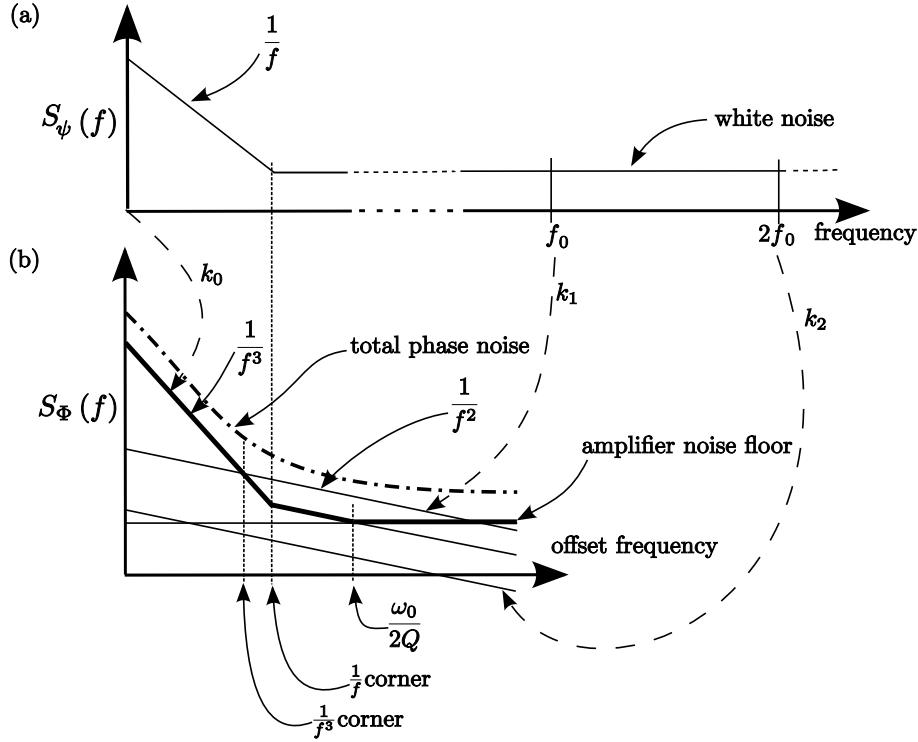


Figure 3.3: Conversion of voltage noise to phase noise

sources are weighted by the coefficient k_0 , while noise sources at positive integer multiples of the oscillation frequency are weighted by coefficients k_n [11, 10]. This weighted transformation is illustrated in figure 3.3.

In linear time-invariant models, the weight of k_0 dominates the phase noise distribution and the remaining coefficients are ignored. Such a system is described by Leeson’s model. (See section 3.4) Given the dominance of k_0 , it is obvious from figure 3.3.b, that in linear time-invariant models, the $\frac{1}{f^3}$ - and $\frac{1}{f}$ -corner frequencies will coincide. This would not be the case were the phase noise to be modeled using a linear time-variant model. In such cases, the effects of the other coefficients, k_n , become more discernable and the previously mentioned frequency-corners may occur at different frequencies[10, 11]. Note also that an oscillator’s ultimate phase noise can never be lower than the noise floor of the active device.

The effect of the resonator’s phase response on the phase noise distribution should also be taken into account. In particular, the position of the resonator’s half power bandwidth frequency (or half bandwidth frequency), $\frac{f_0}{2Q}$ [Hz], with regard to the $\frac{1}{f}$ -corner frequency, f_c , of the device noise, S_ψ . This is illustrated in figure 3.4, which can be derived from the linear time-invariant model (LTI) discussed in the next section. Figure 3.4 depicts the phase noise distribution of an oscillator should $\frac{f_0}{2Q}$ be smaller than f_c (case 1), as well as for the case where $\frac{f_0}{2Q}$ is greater than f_c (case

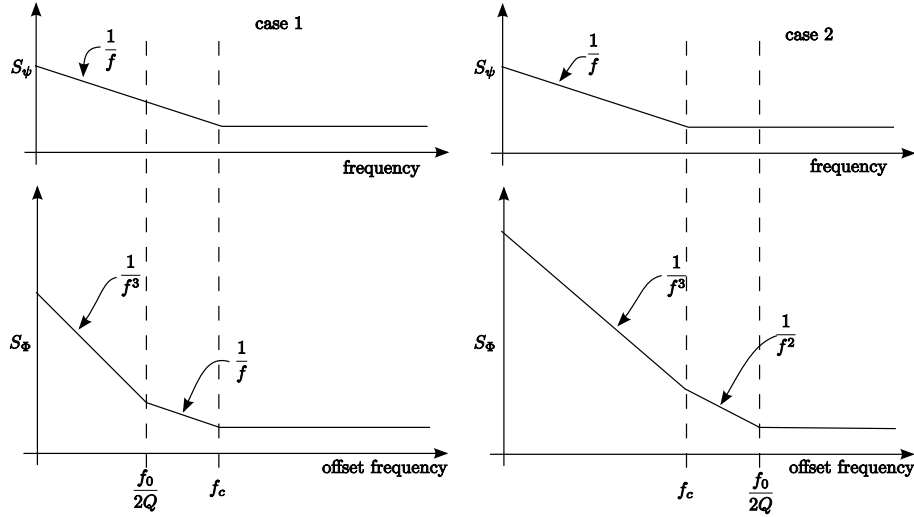


Figure 3.4: The effect of resonator BW on the oscillator’s phase noise distribution

2). This phenomenon will be explained in the following sections. In this section it merely serves to illustrate the effect of the resonator’s bandwidth (and consequently its Q) on the phase noise distribution. Notice the presence of a $\frac{1}{f}$ dependency in case 1, and a $\frac{1}{f^2}$ dependency in case 2 of figure 3.4.

At this point it may be noted that, in order to design an oscillator with low phase noise, an active device with a low noise figure and a low flicker noise corner frequency is needed. A resonator with a high quality factor will also have greater phase noise suppression near the carrier frequency.

Only the effect of white noise and flicker noise entering the oscillator network have been discussed thus far. It must be pointed out that, should noise with other distributions, e.g. $\frac{1}{f^3}$, enter the system, it would be subjected to the same transformation that white and flicker noise are subjected to. Therefore oscillator phase noise can be described by means of the following power law:

$$S_{\Phi}(f) = \sum_{i=0}^{-4} b_i f^i \tag{3.10}$$

It should be mentioned that equation 3.10 can be expanded by adding additional negative terms [2]. The phase noise terms are shown in table 3.1. Phase noise can also be described in terms of phase time fluctuation and fractional frequency fluctuation given, respectively, in equations 3.11 and 3.12. Phase time fluctuations, $x(t)$, are the phase fluctuations, $\phi(t)$, converted into time and measured in seconds. (This is sometimes called phase jitter.) Fractional frequency fluctuations are the instantaneous frequency variations normalised with respect to the carrier frequency,

f_0 , and are dimensionless[8, 2].

$$x(t) = \frac{\phi(t)}{2\pi f_0} \quad (3.11)$$

$$y(t) = \frac{\dot{\phi}(t)}{2\pi f_0} \quad (3.12)$$

Their power spectral densities are given by equations 3.13 and 3.14 respectively[8, 2].

$$S_x(f) = \frac{1}{f_0^2} S_\Phi(f) \quad (3.13)$$

$$S_y(f) = \frac{f^2}{f_0^2} S_\Phi(f) \quad (3.14)$$

Equation 3.14 is derived from equation 3.12 using the Fourier transform property that differentiation in the time domain maps to multiplication by $j2\pi f$ in the frequency domain. This implies that the spectrum has to be multiplied by $4\pi^2 f^2$ [2]. Subsequently the power law given in equation 3.15 can be obtained. The individual power spectral density terms of the frequency fluctuation power law are also shown in table 3.1, along with a list of conversions between $S_\Phi(f)$ and $S_y(f)$ [2]. The relationship between phase noise and fractional frequency fluctuation is graphically illustrated in figure 3.5.

$$S_\Phi(f) = \sum_{i=2}^{-2} h_i f^i \quad (3.15)$$

Table 3.1: Power spectral densities of noise types

Noise Type	$S_\Phi(f)$	$S_y(f)$	$S_\Phi(f) \leftrightarrow S(f)$
White phase	b_0	$h_2 f^2$	$h_2 = \frac{b_0}{f_0^2}$
Flicker phase	$b_{-1} f^{-1}$	$h_1 f$	$h_1 = \frac{b_{-1}}{f_0^2}$
White frequency	$b_{-2} f^{-2}$	h_0	$h_0 = \frac{b_{-2}}{f_0^2}$
Flicker frequency	$b_{-3} f^{-3}$	$h_{-1} f^{-1}$	$h_{-1} = \frac{b_{-3}}{f_0^2}$
Random walk frequency	$b_{-4} f^{-4}$	$h_{-2} f^{-2}$	$h_{-2} = \frac{b_{-4}}{f_0^2}$

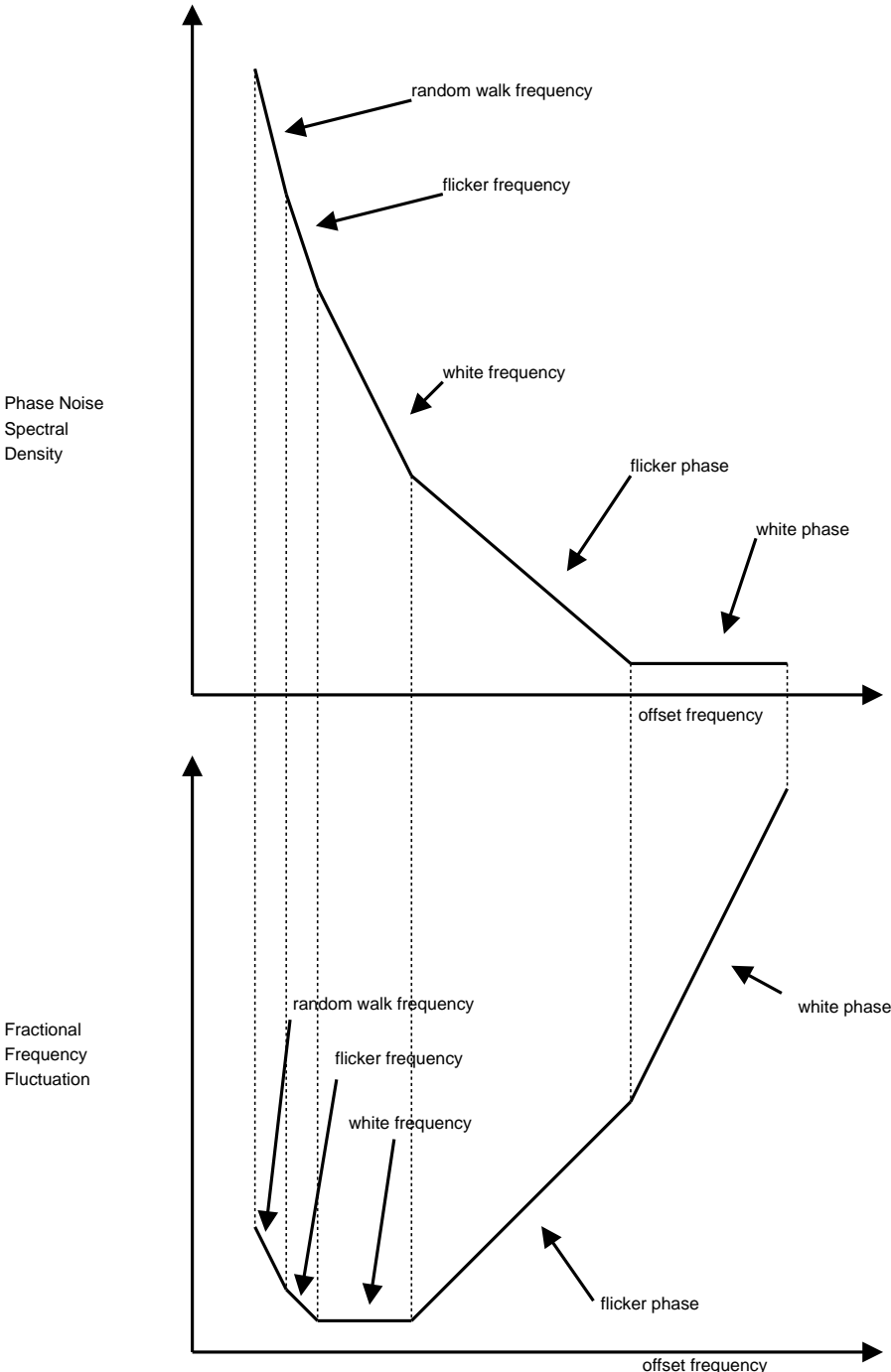


Figure 3.5: $S_{\Phi}(f)$ and $S_y(f)$

3.4 Leeson's Equation (an LTI model)

3.4.1 A Heuristic Approach

Consider the variation on the basic oscillator network in figure 3.6. (The block diagram shown is the same as the one in figure 2.1, but with a static phase shift added.) $H(f)$ is assumed to be an ideal resonator with no frequency deviations and a high quality factor. The half power bandwidth of the resonator is given by $\frac{\pi f_0}{Q}$ [4]. The half power bandwidth can also be expressed as $\frac{1}{\tau}$, where τ is the resonator's group delay or relaxation time[2]. For example the impedance of a series RLC resonator is:

$$Z_{series}(j\omega) = R + j\omega L + \frac{1}{j\omega C} \quad (3.16)$$

The group delay of such a resonator may be calculated as follows: The circuit is resonant when $Z_{series} = R$. This will occur at a frequency

$$\omega_0 = \frac{1}{\sqrt{LC}} \quad (3.17)$$

The circuit's quality factor can be calculated at this point to be

$$Q = \frac{L\omega_0}{R} \quad (3.18)$$

By substituting equations 3.17 and 3.18 into equation 3.16, equation 3.19 can be obtained, which has a first order bandpass response.

$$Z_{series} = \sqrt{\frac{L}{C}} \left[\frac{1}{Q} + j \left(\frac{\omega}{\omega_0} - \frac{\omega_0}{\omega} \right) \right] \quad (3.19)$$

The group delay of this bandpass response is given by

$$\begin{aligned} \tau &= -\frac{d \arg Y_{series}(j\omega)}{d\omega} \\ &= \frac{d}{d\omega} \arctan \left(Q \left(\frac{\omega}{\omega_0} - \frac{\omega_0}{\omega} \right) \right) \\ &= \frac{Q \left(\frac{1}{\omega_0} + \frac{\omega_0}{\omega^2} \right)}{Q \left(\frac{\omega}{\omega_0} - \frac{\omega_0}{\omega} \right)^2 + 1} \end{aligned}$$

where $Y_{series} = \frac{1}{Z_{series}}$.¹

¹ Y_{series} is used instead of Z_{series} , due to the fact that Y_{series} has a pair of complex poles on

For the case where $\omega = \omega_0$, the group delay reduces to

$$\tau_0 = \frac{2Q}{\omega_0} \quad (3.20)$$

From equation 3.20, it can be seen that the quality factor can be expressed in terms of the group delay. Mathematically it may be stated

$$\begin{aligned} Q &= \frac{\omega_0 \tau_0}{2} \\ &= \pi f_0 \tau_0 \end{aligned} \quad (3.21)$$

The previous derivation shows that the group delay is directly related to the quality factor for a simple RLC resonator. Group delay may, however, be considered to be a more fundamental characteristic of the resonator, since it can be applied to all resonators and is easy to measure. For example group delay may be applied to delay line resonators where the quality factor has no meaning.

Figures 3.6 and 3.7 show how the frequency of an oscillator network can be pulled by adding a static phase, ψ , into the loop. As was mentioned previously, the Barkhausen conditions for oscillation are closed loop gain of unity while simultaneously achieving a 0° phase deviation. Figure 3.7 illustrates how these conditions can be satisfied across multiple frequencies for the same resonator. By adding additional phase to the loop, the frequency at which the phase condition is satisfied, is shifted. As long as the gain condition is also being satisfied at this shifted frequency, the network will oscillate at the shifted frequency [4, 2].

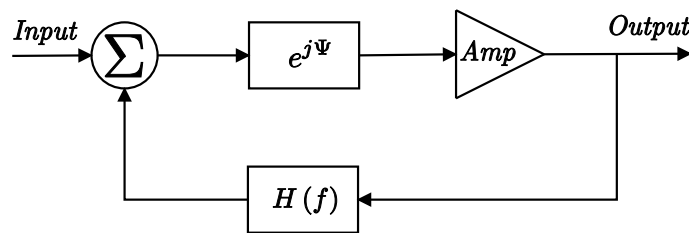


Figure 3.6: Variation on basic oscillator block diagram

In mathematical terms: the oscillator will oscillate at a frequency of $f_0 + \Delta f$ when equation 3.22 holds true. f_0 denotes the resonant frequency of the network in the absence of the static phase. Δf denotes the amount by which the oscillation frequency of the network is shifted should a static phase be added.

the imaginary axis and would result in a decreasing phase and a positive group delay. Z_{series} has a pair of complex zeros on the imaginary axis and will therefore have a resulting negative group delay.

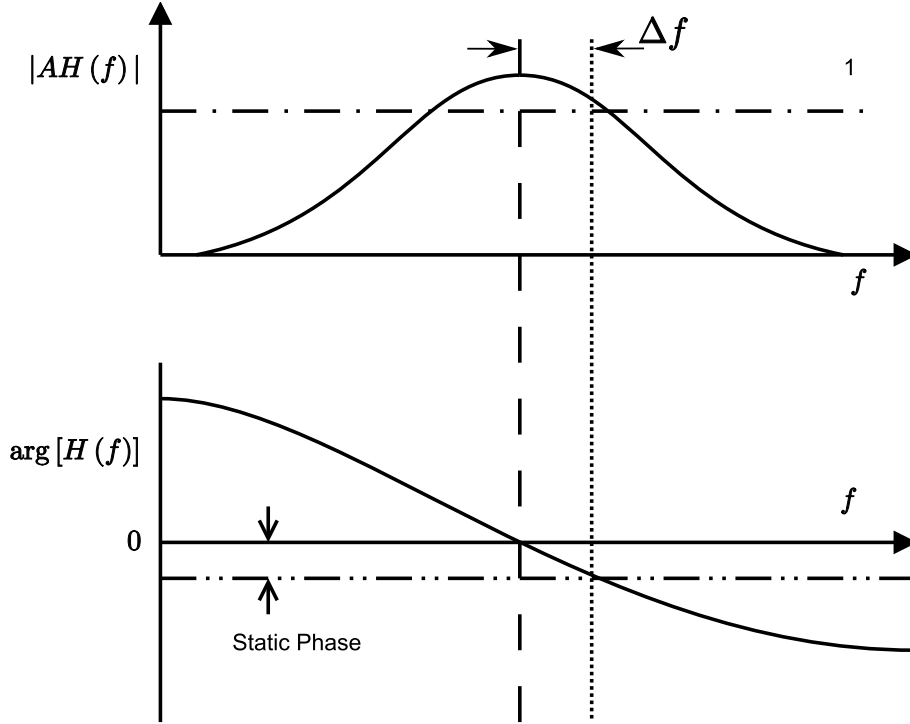


Figure 3.7: Amplitude and phase conditions for oscillations

$$\arg [H (f)] + \psi = 0 \quad (3.22)$$

this can be rewritten in the form

$$\psi = -\arg [H (f)] \quad (3.23)$$

The effect of ψ on the oscillation frequency can be obtained by inverting equation 3.23 and using linearisation to arrive at equation 3.24 [2]

$$\Delta f = \frac{-\psi}{\frac{d}{df} \arg [H (f)]} \quad (3.24)$$

Should the static phase, ψ , be replaced with a randomly varying phase $\psi (t)$ that accounts for all the phase noise sources in the loop, the oscillator in figure 3.6 would have the following voltage output signal:

$$v (t) = V_0 \cos [\omega_0 t + \Phi (t)] \quad (3.25)$$

where $\omega_0 = 2\pi f_0$ and $\Phi (t)$ is the effect of $\psi (t)$ [2]. In the following paragraphs, the mechanism by which the power spectral density of ψ is converted to that of Φ will

be analysed.

For the slow moving components of $\psi(t)$, slower than the half power bandwidth of the resonator, ψ may be treated as a quasi-static perturbation [2, 4]. This implies that:

$$\Delta f = \frac{f_0}{2Q} \psi(t) \quad (3.26)$$

therefore

$$S_{\Delta f}(f) = \left(\frac{f_0}{2Q}\right)^2 S_{\psi}(f) \quad (3.27)$$

The instantaneous output phase would be given as

$$\Phi(t) = 2\pi \int (\Delta f) dt \quad (3.28)$$

Since time domain integration maps to multiplication by $\frac{1}{j\omega}$ in the Fourier transform domain and consequently to multiplication by $\frac{1}{(2\pi f)^2}$ in the spectrum domain, the oscillator's spectrum density is given by equation 3.29 [2, 4].

$$S_{\Phi}(f) = \frac{1}{f^2} \left(\frac{f_0}{2Q}\right)^2 S_{\psi}(f) \quad (3.29)$$

For fast varying changes in $\psi(t)$, faster than the half power bandwidth of the resonator, the resonator acts as a band stop filter for ψ . This means that any fast component of $\psi(t)$ that enters the amplifier in figure 3.6, is passed straight through to the output without being affected by the resonator. This is mathematically stated as

$$\Phi(t) = \psi(t) \quad (3.30)$$

This implies that

$$S_{\Phi}(f) = S_{\psi}(f) \quad (3.31)$$

Assume that no correlation exists between the slow and fast moving components of $\psi(t)$. This implies that the effects of equations 3.29 and 3.31 can now be summed. This leads to the Leeson equation for phase noise:

$$S_{\Phi}(f) = \left[1 + \frac{1}{f^2} \left(\frac{f_0}{2Q}\right)^2\right] S_{\psi}(f) \quad (3.32)$$

which can be rewritten in the form

$$S_{\Phi}(f) = \left[1 + \frac{f_L^2}{f^2} \right] S_{\psi}(f)$$

where

$$f_L = \frac{f_0}{2Q} \quad (3.33)$$

Equation 3.33 is sometimes referred to as the Leeson frequency [2].

Inspection of the Leeson formula (equation 3.32), indicates that oscillator behaviour is similar to that of a first order filter with a pole at the origin in the Laplace transform domain and a cutoff frequency at f_L (zero on real axis on left-hand side).

It should be noted that the Leeson equation explains only those phase to frequency transformations that are inherently inside the loop illustrated in figure 3.6. The noise of the resonator must still be taken into account.

3.4.2 A Mathematical Approach

Leeson's formula can be mathematically deduced in the following manner [2]. Let $b(t)$ be the phase transfer function of the resonator with $B(s)$ its Laplace transform. Let the resonator be driven with a sinusoidal signal with a frequency of ω . This may be any frequency, including the natural frequency of the resonator. Under quasi-static conditions, the phase transfer function, $b(t)$, is the resonator's phase response to a phase impulse function, $\delta(t)$, in the input signal [2]. Mathematically this can be written as

$$v_i(t) = \cos[\omega_0 t + \delta(t)] \quad (3.34)$$

$$v_o(t) = \cos[\omega_0 t + b(t)] \quad (3.35)$$

The response to the unit step function, $U(t)$, can be used to derive $b(t)$, since it is a characteristic of linear systems that the impulse response, $b(t)$, is the derivative of the step response, $b_U(t)$. In mathematical form

$$b(t) = \frac{d}{dt} b_U(t) \quad (3.36)$$

The response for small signal conditions is evaluated by making use of a phase step, $\kappa U(t)$, with $\kappa \rightarrow 0$. The unit step function can be defined as $U(t) = 0$ for $t < 0$

and $U(t) = 1$ for $t > 0$, or:

$$U(t) = \int_{-\infty}^{\infty} \delta(t) dt \quad (3.37)$$

The approximation for κ may be considered accurate, since the phase noise in an oscillator is indeed a small signal. In the following method the input signal, $v_i(t)$, is split into two terms at $t = 0$.

$$v_i(t) = v_i'(t) + v_i''(t) \quad (3.38)$$

where, for $t > 0$,

$$v_i'(t) = v_i(t) U(-t) \quad (\text{signal off}) \quad (3.39)$$

$$v_i''(t) = v_i(t) U(t) \quad (\text{signal on}). \quad (3.40)$$

Consequently, the resonator's output phase response can be written as:

$$v_o(t) = v_o'(t) + v_o''(t)$$

where $v_o'(t)$ is the response to $v_i'(t)$ (the signal switched off) and $v_o''(t)$ is the response to $v_i''(t)$ (the signal switched on) for $t > 0$. The splitting in two of the input signal allows for the insertion of $\kappa U(t)$ into the phase of $v_i''(t)$ [2].

Now consider the phase response of a resonator with an input signal tuned to its exact resonance frequency. The input signal can be written in the form shown in equation 3.41.

$$\begin{aligned} v_i(t) &= \cos[\omega_0 t + \kappa U(t)] \\ &= \cos(\omega_0 t) U(-t) + \cos(\omega_0 t + \kappa) U(t) \end{aligned} \quad (3.41)$$

The last two terms of equation 3.41, are depicted in figures 3.8.a and 3.8.b [2]. The resonator response for the sinusoidal input signal switched off (figure 3.8.a), is the exponentially decaying signal given in equation 3.42, which holds true for $t > 0$. Where again $\tau = \frac{2Q}{\omega_0}$.

$$v_o'(t) = \cos(\omega_0 t) e^{-\frac{t}{\tau}} \quad (3.42)$$

For the sinusoidal input signal switched on, the resonator has an exponentially increasing response. This is given by equation 3.43, which is valid for $t > 0$.

$$v_o''(t) = \cos(\omega_0 t + \kappa) \left[1 - e^{-\frac{t}{\tau}} \right] \quad (3.43)$$

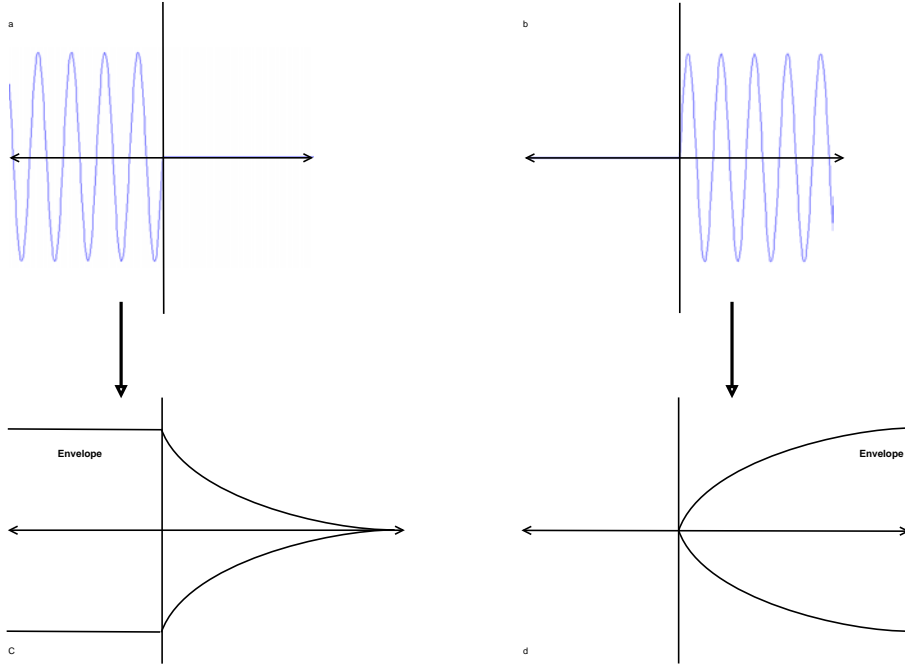


Figure 3.8: Decomposition of resonator input signal and resulting response

Equations 3.42 and 3.43 are, respectively, illustrated in figure 3.8.c and figure 3.8.d.

For a sinusoidal input signal at the exact resonance frequency of the resonator, such as the one given in equation 3.41, the resonator's signal response will be given by equation 3.44.

$$v_o = v_o' + v_o'' \quad (3.44)$$

Substituting equations 3.42 and 3.43 into equation 3.44, yields:

$$v_o = \cos(\omega_0 t) e^{-\frac{t}{\tau}} + \cos(\omega_0 t + \kappa) \left[1 - e^{-\frac{t}{\tau}}\right]$$

which could be written in phasor form as:

$$V_o(t) = e^{j0} e^{-\frac{t}{\tau}} + e^{j\kappa} \left[1 - e^{-\frac{t}{\tau}}\right] \quad (3.45)$$

From the phasor definition $e^{j\kappa} = \cos(\kappa) + j \sin(\kappa)$, equation 3.45 can be expanded to

$$V_o(t) = e^{-\frac{t}{\tau}} + [\cos(\kappa) + j \sin(\kappa)] \left[1 - e^{-\frac{t}{\tau}}\right] \quad (3.46)$$

since $\kappa \rightarrow 0$

$$V_o(t) \approx e^{-\frac{t}{\tau}} + [1 + j\kappa] \left[1 - e^{-\frac{t}{\tau}}\right] = 1 + j\kappa \left[1 - e^{-\frac{t}{\tau}}\right] \quad (3.47)$$

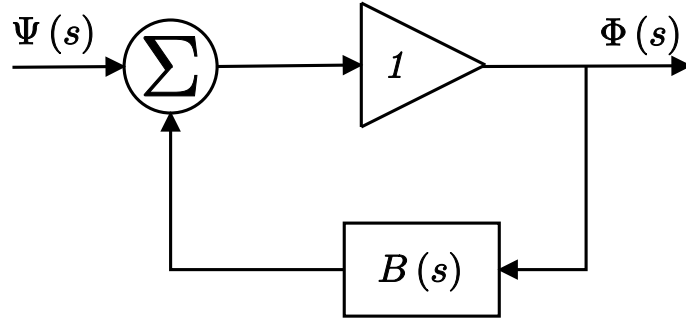


Figure 3.9: Oscillator block diagram in the phase domain

The phase variation of the signal at the output of the resonator will be given by $\arctan\left(\frac{\Im V_o(t)}{\Re V_o(t)}\right) = \kappa - \kappa e^{-\frac{t}{\tau}}$. Therefore the phase step response, $b_U(t)$, is given by equation

$$b_U(t) = 1 - e^{-\frac{t}{\tau}} \quad (3.48)$$

which is the phase variation of the resonator's output signal, normalised to κ . Utilising equation 3.36, equation 3.49 is obtained [2].

$$b(t) = \frac{1}{\tau} e^{-\frac{t}{\tau}} \quad (3.49)$$

As previously stated, $B(s)$ is the Laplace transform of $b(t)$. It can be obtained from equation 3.49, using mathematical tables [13].

$$B(s) = \frac{1}{s\tau + 1} \quad (3.50)$$

Now consider an oscillator network in the phase domain. A block diagram of such a network is illustrated in figure 3.9. The phase noise of the amplifier, as well as resonator fluctuations, are modelled by $\Psi(s)$, which could also represent the phase of any external signal to which the oscillator is locked. Notice that the amplifier in the block diagram, has unity gain. This correlates with the assumption that an ideal amplifier will let any phase deviation at its input pass unhindered to its output. From the block diagram it can be seen that the oscillator phase transfer function would be given by equation 3.51

$$\mathcal{H}(s) = \frac{\Phi(s)}{\Psi(s)} \quad (3.51)$$

By applying simple block diagram algebra, equation 3.51, can be expanded to:

$$\mathcal{H}(s) = \frac{1}{1 - B(s)} \quad (3.52)$$

In the case where the oscillation frequency of such a network is tuned to the exact natural frequency of the resonator, equation 3.50 may be substituted into equation 3.52. Consequently equation 3.52 is reduced to:

$$\mathcal{H}(s) = \frac{s\tau + 1}{s\tau} \quad (3.53)$$

By substituting $j\omega$ for s , the square of equation 3.53 can be written as:

$$|\mathcal{H}(j\omega)|^2 = \frac{\tau^2\omega^2 + 1}{\tau^2\omega^2} \quad (3.54)$$

Now consider the spectral densities of $\Phi(t)$, namely $S_\Phi(f)$, and $\psi(t)$, namely $S_\psi(f)$. From equation 3.51, it follows that

$$S_\Phi(\omega) = |\mathcal{H}(j\omega)|^2 S_\psi(\omega) \quad (3.55)$$

By substituting equation 3.54 into equation 3.55, the following is obtained

$$S_\Phi(\omega) = \left[1 + \frac{1}{\tau^2\omega^2} \right] S_\psi(\omega) \quad (3.56)$$

Given that $\omega = 2\pi f$ and that $\tau = \frac{2Q}{\omega_0} = \frac{Q}{\pi f_0}$, equation 3.57, Leeson's equation, can be derived from equation 3.56.

$$S_\Phi(f) = \left[1 + \frac{1}{f^2} \left(\frac{f_0}{2Q} \right)^2 \right] S_\psi(f) \quad (3.57)$$

3.4.3 Conclusion

The above model was published by D.B. Leeson in 1966. It is linear time-invariant in nature and therefore does not account for the nonlinear and time-variant nature of oscillators, unlike linear time-variant (LTV) and non-linear time-variant (NLTV) models. It is, however, relatively simple to calculate the phase noise distribution of an oscillator network using this model. (LTV and NLTV models have to be solved numerically with the use of computers.) Also, given the relationship between the

components of the circuit and its quality factor, the effect of an individual component on the oscillator's phase noise can be determined.

Leeson's model is usually inaccurate and requires the addition of an *effective noise figure*. This effective noise figure is not to be confused with the noise figure of an amplifier. It can be derived by curve-fitting the results of Leeson's model upon a phase noise measurement.

3.5 Conclusion

In this chapter the concept of phase noise was introduced. The method by which it is created was explained and three models for determining an oscillator's phase noise distribution were mentioned. It was shown that Leeson's model gives the best insight as to the effect of physical components within the oscillator upon its phase noise, but lacks the accuracy of the LTV and NLTV models. It is also much simpler to implement.

Roadmap to Experiments

The following experiments evaluate the phase noise predicted by Leeson's model and compare it with the measured phase noise of various oscillators. The purpose, or focus, of each experiment is discussed in the following paragraphs.

In Chapter 4, an experiment concerning the effect of circuit non-linearity on the oscillator's phase noise performance is outlined and evaluated. In particular, the effect that the linearity of the circuit has on its effective noise figure, is assessed. It is also demonstrated that the magnitude of the output signal level increases with circuit non-linearity. It is found that Leeson's model describes an oscillator's phase noise distribution with increasing accuracy as the circuit approaches linear operation. A hypothesis is made that should a linearly driven oscillator have an output signal similar in magnitude to that of a nonlinearly driven oscillator, the linearly driven oscillator will show superior phase noise performance. In Chapter 5 this hypothesis is evaluated and confirmed.

Chapters 6 and 7 evaluate the phase noise of, respectively, an LC oscillator network and a crystal oscillator network, as the level of amplifier saturation is adjusted in steps of approximately 0.1dB. In both cases the measured phase noise is approximated using Leeson's phase noise model. The loaded quality factor of the resonators are used to determine the Leeson frequency in both experiments. In chapter 6, the resonator's bandwidth is used to determine the Q , whereas in chapter 7, it is determined using the group delay of the resonator.

The experiments of chapters 8 and 9 are similar to those discussed in chapters 6 and 7, but differ from them in that the network's open loop group delay instead of the resonator's bandwidth is used in order to determine the Leeson frequency.

These experiments will now be discussed.

Chapter 4

Experiment 1:

4.1 Purpose of the experiment

In the previous chapters it was noted that the nonlinear operation of oscillator networks allows for the low frequency noise, present near DC, to be translated to phase noise around the carrier. It was also shown that a similar process takes place for noise present around integer multiples of the carrier frequency. In this experiment the author proposes to evaluate how the measured phase noise distribution of an oscillator network differs from that suggested by Leeson's model when the linearity of the network is altered. The experimental circuit layout is shown in figure 4.1. The amplifier in the block diagram was designed to have a high gain. If the loop gain of the circuit should be left unrestricted, the amplifier will quickly be driven into saturation and the circuit will operate in a non-linear manner. Electric current that flows in short pulses at the transistor's collector is indicative of this mode of operation. The circuit's loop gain can, however, be limited by increasing the losses in the attenuator shown in the block diagram. Should the attenuation be increased to the point where the loop gain is near unity, the circuit will operate in a linear mode. In this mode the electric current flowing through the collector should be sinusoidal, perfectly following the output voltage. The aim of the following experiment is to evaluate the system's performance in terms of signal power, noise figure and phase noise, as a function of system linearity. Previous experiments have been performed in terms of drive level [4]. These experiments suggest that an oscillator's phase noise performance is improved by increasing the amount of feedback in the network. However, they do not take into account the variations in the magnitude of the oscillator's output signal. In the following experiment the signal power is measured at the input of the amplifier and is then related to the measured phase noise.

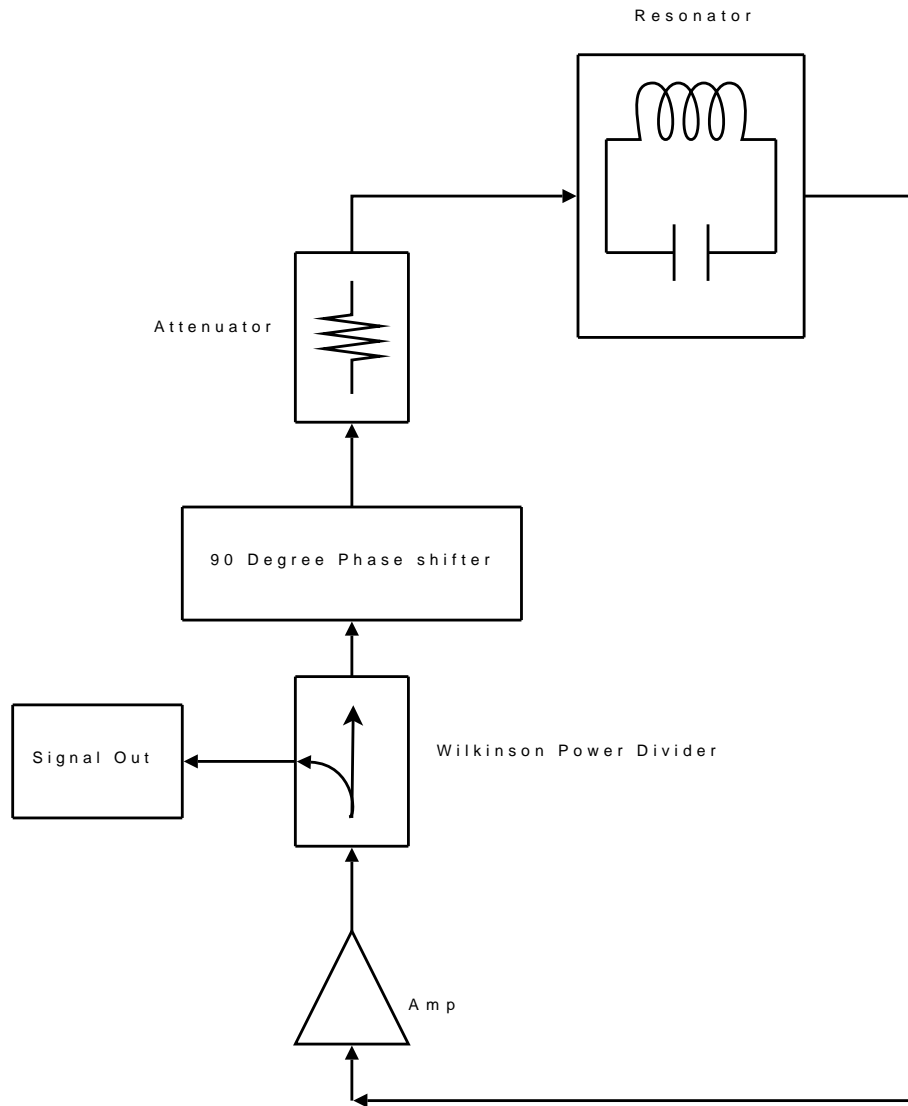


Figure 4.1: Experimental circuit layout

Two near identical 5 MHz oscillator circuits were designed, the difference between the two circuits being that one of the resonators was designed to be voltage controlled. This is so that the oscillators can be locked to oscillate at exactly the same frequency. One oscillator serves as a reference oscillator in order to measure the combined phase noise of the two oscillators. The phase noise measurement procedure will be explained later in this chapter.

4.2 The design and characterisation of the different circuit modules

A modular design was decided upon. This will enable characterisation and measurement of each of the individual components or modules. It also allows for variation of one circuit aspect without affecting any of the others, since all of the modules were designed for a system with a characteristic impedance of 50Ω . In other words, any change in the phase noise performance of the oscillator circuit is as a result of the previously mentioned circuit change. This is true because the loading of the other components remains unaltered.

In the following sections the various considerations for the design of each of the different modules will be discussed. Most of these components are quite simple, they must, however, be characterised accurately, especially in terms of gains or losses and phase deviation, since this data will be used later on in system calculations. Subsequently, both the simulated and measured results of these modules are shown and compared in Appendix A.

4.2.1 Cascode amplifier

The amplifier's purpose in this experiment is to deliver the necessary signal gain to the system. It should be capable of driving the circuit into non-linearity with ease if left unlimited. This would imply a gain of at least 20 dB. For this purpose it was decided upon a cascode amplifier design. The design and verification of this amplifier is discussed in Appendix A.1.

4.2.2 Wilkinson power divider

In order to perform the necessary measurements, a method is needed of diverting part of the signal power to the measurement device without allowing the measurement device to interfere with the experimental setup. In other words: the measurement device must not be allowed to provide additional loading, or to deliver extra noise to the circuit. Therefore the measurement port should be isolated from the rest of the experimental setup. For this purpose it was decided to use a Wilkinson power divider, since Wilkinson dividers inherently provide good isolation between the output ports. They are further beneficial in that they allow for all ports to be matched, unlike lossless T-junction dividers, and they do not have the losses

associated with resistive power dividers[1]. An LC version of the Wilkinson divider was designed and built, the design and verification of which is shown in Appendix A.2.

4.2.3 Phase shift network

The power dividers add an additional 90° phase shift to the oscillator circuits, due to their quarter wavelength characteristics. This can be seen in both the simulated and measured results discussed in Appendix A.2 of the previously described module. The results are illustrated in figures A.17 and A.21. In order to compensate for this phase shift another 270° or -90° of phase deviation is required.

In Appendix A.2 it was mentioned that a quarter wave transmission line equivalent circuit could be designed using an LC network. It is also possible to employ a similar design in order to obtain a $\frac{3}{4}$ wavelength transmission line equivalent. The design, simulation and measurements of this module are discussed in Appendix A.3.

4.2.4 Attenuator

The purpose of the attenuator in the test setup is to limit the loop gain of the system. This will allow for the evaluation of the oscillator circuit's phase noise performance at various levels of system linearity: The more closely the loop gain approaches unity, the more linear the operation of the oscillator will be, since the active device is not being driven as deeply into saturation as would otherwise be the case. The attenuators should provide gain losses in the oscillator circuit while still remaining impedance matched to the rest of the circuit. Otherwise stated: the attenuators must have a characteristic impedance of 50Ω so as not to provide additional loading to the oscillator system or cause signals to be reflected within this system.

For the purposes of the experiment a combination of Mini-circuits attenuators, shown in Appendix B, as well as a few resistive π -attenuators, the schematic diagram of which is shown in figure A.33, were used. Please note that the attenuator in this figure is for a matched system. The design and verification of a few such attenuators are discussed in Appendix A.4.

4.2.5 Resonator

The resonator is an integral part of any oscillator circuit, since it largely determines the operating frequency of the circuit, as well as the frequency drift and the phase

noise. Great care must therefore be taken when designing a resonator for a low phase noise oscillator. Arguably the most important consideration to be made when designing a resonator is in terms of its quality factor (Q). It will be shown that there is an optimum point for minimum oscillator phase noise that relates to Q .

In [9], D.B. Leeson denoted the uncertainty of the oscillator input phase noise due to noise and parameter variations as $\Delta\theta(t)$ and its two-sided power spectral density (PSD) as $S_{\Delta\theta}(\omega_m)$. He denoted the total output PSD as:

$$S_{\Phi}(\omega_m) = S_{\Delta\theta}(\omega_m) \left[1 + \left(\frac{\omega_0}{2Q\omega_m} \right)^2 \right] \quad (4.1)$$

where ω_0 is the resonance frequency and ω_m is the frequency offset relative to the resonance frequency. For $\omega_m < \left(\frac{\omega_0}{2Q}\right)$, in other words for offset frequencies smaller than the half-power bandwidth of the resonator, equation 4.1 can be reduced to:

$$S_{\Phi}(\omega_m) = \left(\frac{\omega_0}{2Q\omega_m} \right)^2 S_{\Delta\theta}(\omega_m) \quad (4.2)$$

If one now assumes that the noise component of $S_{\Delta\theta}$ is white, then its double sideband noise power spectral density would be given by:

$$S_{\Delta\theta}(\omega_m) = \frac{1}{2} \cdot \frac{FkT}{P_S} \quad (4.3)$$

where F is the effective noise figure of the resonator, k is Boltzmann's constant, T is the noise temperature in kelvin and P_S is the signal level at the input of the oscillator's active element. Substituting equation 4.3 into equation 4.2, one can now write:

$$S_{\Phi}(\omega_m) = \frac{\omega_0^2 FkT}{8P_S Q^2 \omega_m^2} \quad (4.4)$$

From equation 4.4, it can be seen that;

$$S_{\Phi}(\omega_m) \propto \frac{1}{P_S Q^2} \quad (4.5)$$

This implies that the output PSD of the phase noise will be at its minimum if $P_S Q^2$ is at its maximum. Now consider an oscillator circuit or a driven and loaded resonator like the one shown in figure 4.2. The power delivered to the resonator by the the generator is:

$$P_{gen} = \frac{|I_{gen}|^2}{4G_{gen}} \quad (4.6)$$

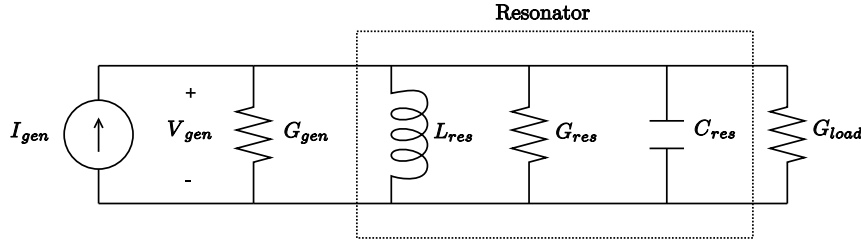


Figure 4.2: A generic oscillator circuit.

furthermore, the unloaded and loaded Q of the resonator can be written as equation 4.7 and equation 4.8 respectively:

$$Q_U = \omega_0 \times L_{res} \times G_{res} \quad (4.7)$$

$$Q_L = \omega_0 \times L_{res} \times G_{eqv} \quad (4.8)$$

where G_{res} is the conductance of the resonator alone, L_{res} is the inductance of the resonator and G_{eqv} is the equivalent conductance of the entire circuit expressed in equation 4.9.

$$G_{eqv} = G_{res} + G_{load} + G_{gen} \quad (4.9)$$

If one now sets $P_S = P_{gen}$ and subsequently substitutes equations 4.8 and 4.6 into equation 4.5, then the proportionality of the output PSD of the phase noise becomes:

$$S_{\Phi}(\omega_m) \propto \frac{4 \times G_{gen}}{|I_{gen}|^2 \times L_{res}^2 \times G_{eqv}^2 \times \omega_0^2} \quad (4.10)$$

which can be reduced to:

$$S_{\Phi}(\omega_m) \propto \frac{G_{gen}}{G_{eqv}^2} \quad (4.11)$$

Now consider the special case where $G_{gen} = G_{load}$; equation 4.11 can then be rewritten as:

$$S_{\Phi}(\omega_m) \propto \frac{G_{gen}}{(G_{res} + 2G_{gen})^2} \quad (4.12)$$

This means that for the case of $G_{gen} = G_{load}$, the output PSD of the phase noise will

be at its minimum when:

$$\begin{aligned} \frac{\partial}{\partial G_{gen}} \left(\frac{G_{gen}}{(G_{res} + 2G_{gen})^2} \right) &= 0 \\ \frac{G_{res} - 4G_{gen}^2}{(G_{res} + 4G_{gen})^4} &= 0 \\ 2G_{gen} &= G_{res} \end{aligned}$$

Therefore the optimum minimum phase noise level will be reached when the load impedance is equal to that of the source impedance and double that of the resonator impedance. Otherwise stated: The optimum phase noise level will be reached when a quarter of the available power is dissipated in the source, a quarter in the load and half of the available power is dissipated in the resonator. In other words, the loaded Q must be equal to half of the unloaded Q in order achieve a level of optimum phase noise[14]. The design, simulation and verification of the resonator used is shown in Appendix A.5

4.3 System measurements and evaluation

At the beginning of this chapter it was stated that the purpose of the experiment was to evaluate the performance of the oscillator circuit depicted in the block diagram of figure 4.1, in particular with regard to phase noise. In the previous section of this chapter specifications have been set up for the different modules to be used in the following experiment. In Appendix A it has also been confirmed that these modules conformed to their various specifications.

Spice simulations indicate that the circuit will perform as expected. The collector is driven in short current pulses when the system operates in a very non-linear way, in other words when no attenuation is added. As more attenuation is added, however, the collector current becomes more and more sinusoidal in nature as the system becomes more linear; this is illustrated in figure 4.3. In addition to this, it can be seen that the peak amplitude of the collector current is much greater for the non-linear case than it is for the more linear case.

Also consider the output signal of the systems for both the highly non-linear as well as the more linear case shown in figure 4.4. It is shown that the signal amplitude is much greater in magnitude in the case of the highly non-linear system than in the case of the more linear system. In the case of the more linear system, the signal's sinusoidal swing is, however, much more symmetrical than that of its non-linear counterpart. This is due to the fact that harmonic distortion is greater in non-linear

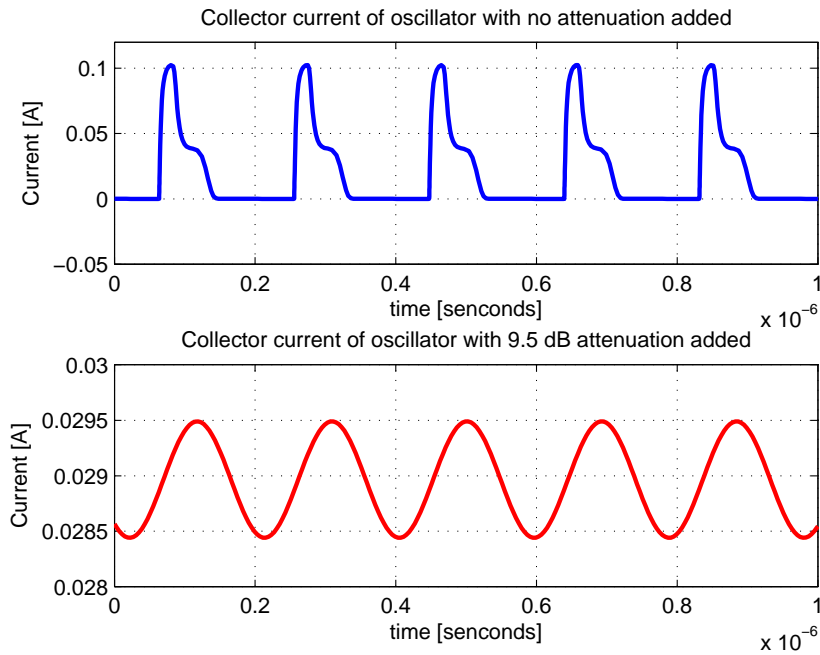


Figure 4.3: Simulated collector current against time

oscillators than in linear oscillators.

This phenomenon is verified by measurements shown in figure 4.5. This figure illustrates that the harmonic distortion for the linear case, where 15.1 dB of attenuation was added to the oscillator circuit, is approximately -28 dBc. Now consider a more non-linear case, where only 3 dB of attenuation was added; it is shown that the harmonic distortion is increased to roughly -10.5 dBc. In both cases the system was set up with amplifier A as the amplifier, phase shifter 1 as phase shift network and LC Wilkinson divider A as the power divider used in the block diagram of figure 4.1, only the amount of attenuation was altered. (See Appendix A, for the characterisation of the previously mentioned modules.) It must be mentioned that the difference in the noise floor level for the two graphs shown in figure 4.5 is the result of different resolution bandwidth being used during the measurements and has nothing to do with the linearity of the circuits.

Figure 4.6, indicates that the magnitude of the output signal is indeed proportional to the non-linearity of the oscillator circuit. In this figure it can be seen that the signal magnitude for the linear case, where 15.1 dB attenuation was added, is 6.27 dBm, whereas in the more non-linear case, where only 6 dB of attenuation was added, the signal magnitude is found to be 7.32 dB. The difference in fundamental frequency between the two levels of attenuation can be explained with the help of the Barkhausen criterion for oscillation. Since there are small differences in the

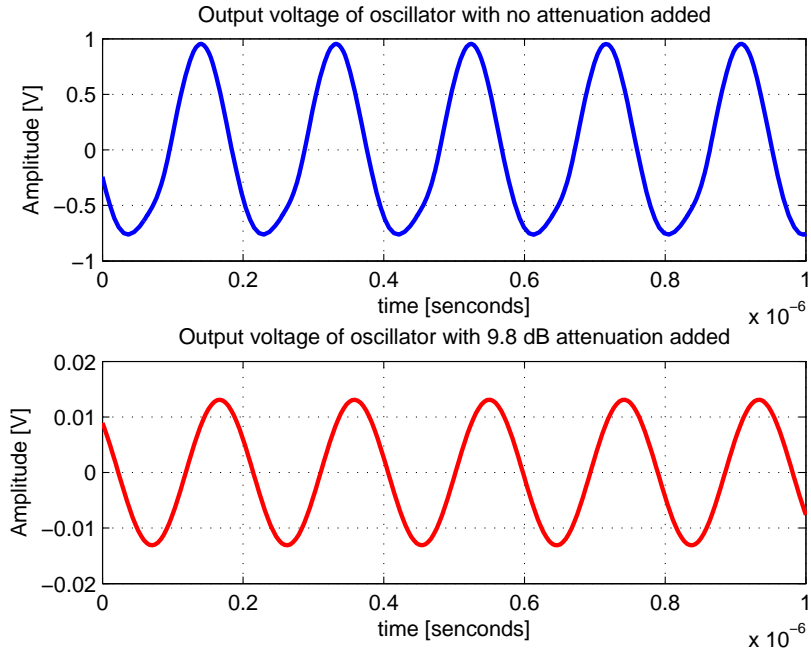


Figure 4.4: Simulated oscillator signal out

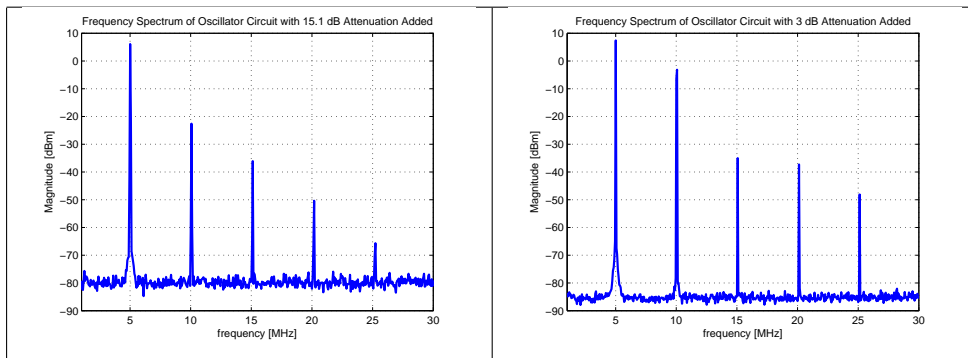


Figure 4.5: Measured harmonic distortion of oscillator circuits

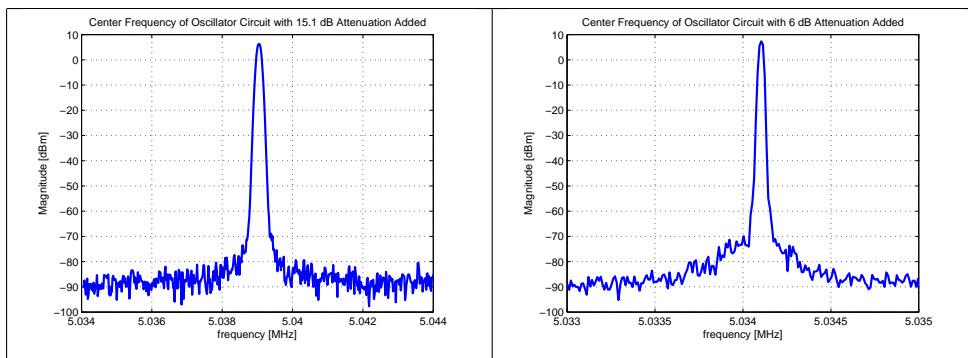


Figure 4.6: Measured output signal strengths

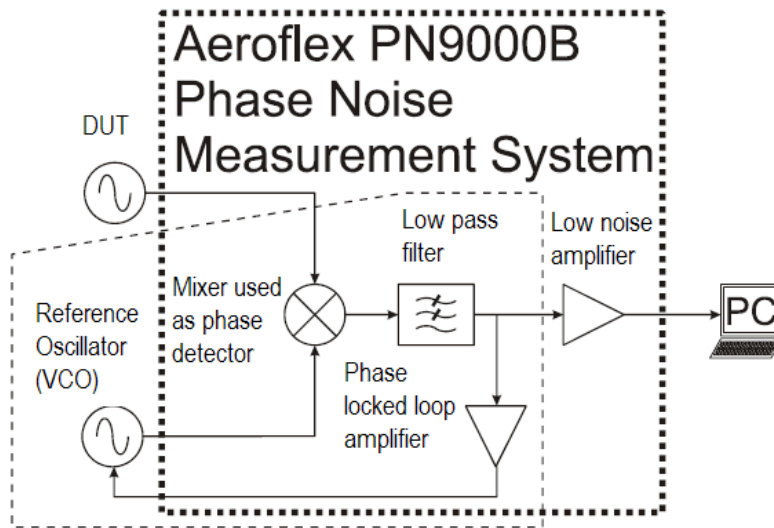


Figure 4.7: Block diagram of measurement setup with external reference oscillator

phase deviation of the attenuators, less than one degree, the phase conditions of this criterion are satisfied at slightly different frequencies.

4.3.1 Phase noise measurements

A PN9000B phase noise measurer, from Aeroflex, was used in order to perform the following measurements. It makes use of a phase demodulation method for analysing phase noise [15]. The PN9000B has the advantage that the measuring equipment is very sensitive. It also has a very wide measuring bandwidth and the ability to detect spurious responses. Furthermore, it allows for hundreds of measurements to be repeated and averaged automatically.

Due to the fact that the expected phase noise performance of the DUT was better than that of the PN9000B's internal reference oscillator, an external reference oscillator comprising of amplifier B, LC Wilkinson divider B, phase shifter 2 and a 13 dB attenuator configured as in figure 4.1, was used. A block diagram illustrating the measurement setup used, is shown in figure 4.7.

As DUT, amplifier A, LC Wilkinson divider A and phase shifter 1 were used, configured as in figure 4.1. The level of attenuation was varied in order to evaluate the phase noise as a function of system linearity. The measured results are shown in figure 4.8. In order to facilitate distinction between the phase noise levels for the different attenuation settings, the measurements were digitally filtered. These filte-

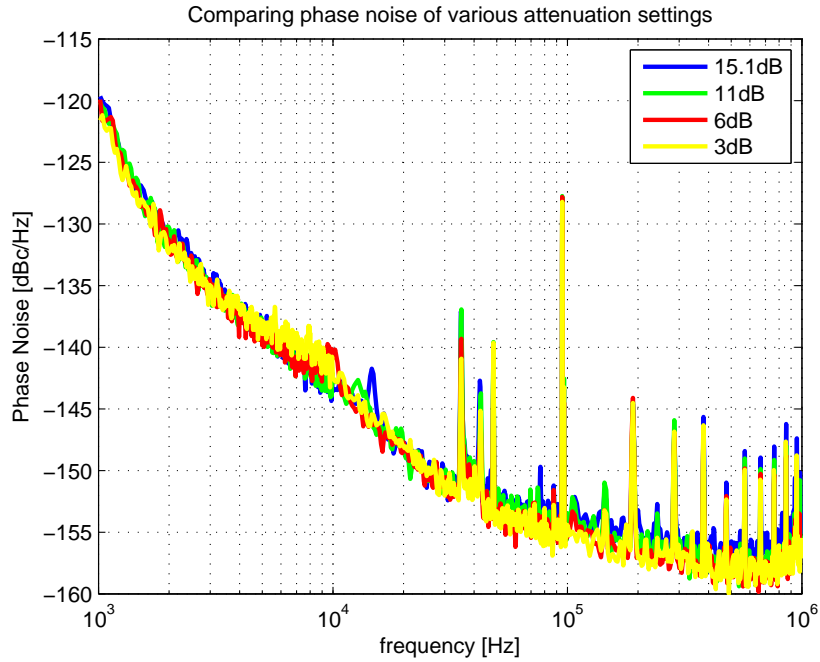


Figure 4.8: Phase noise performance for different attenuation settings

red results are shown in figure 4.9. The graphs appear to indicate that the ultimate phase noise improves as the system becomes more non-linear. If, however, one looks at the magnitude of the signal entering the amplifier, this conclusion is called into question.

The magnitude of the input signal can be derived by performing a loop calculation. Consider again the block diagram of figure 4.1. Since the outputs of the LC Wilkinson Divider A are symmetrical, it can be concluded that the magnitude of the measured signal out, is the same as that of the signal entering Phase Shifter 1. Therefore if one were to subtract the losses of phase shifter 1, the attenuator used and the fixed resonator from the measured output signal, one would arrive at the magnitude of the signal available to amplifier A. This data is tabulated in table 4.1. The *centre frequency* listed in the table denotes the oscillator's centre frequency measured while *Power Out* refers to the signal power at the fundamental frequency measured at the output of the oscillator. The losses occurring as a result of the phase shifter, the resonator and the attenuator used are listed below *Phase Shifter*, *Resonator* and *Attenuation* respectively. *Power Avail* is the calculated signal power available to the amplifier. Note that the resonator losses given, are the losses in the resonator occurring at a frequency equal to that of the oscillator's centre frequency.

Now consider what happens when one applies the data in figure 4.9 and table 4.1 to equation 4.13. Where \mathcal{L}_{floor} is the ultimate phase noise in dBc/Hz , F_{dB} is the

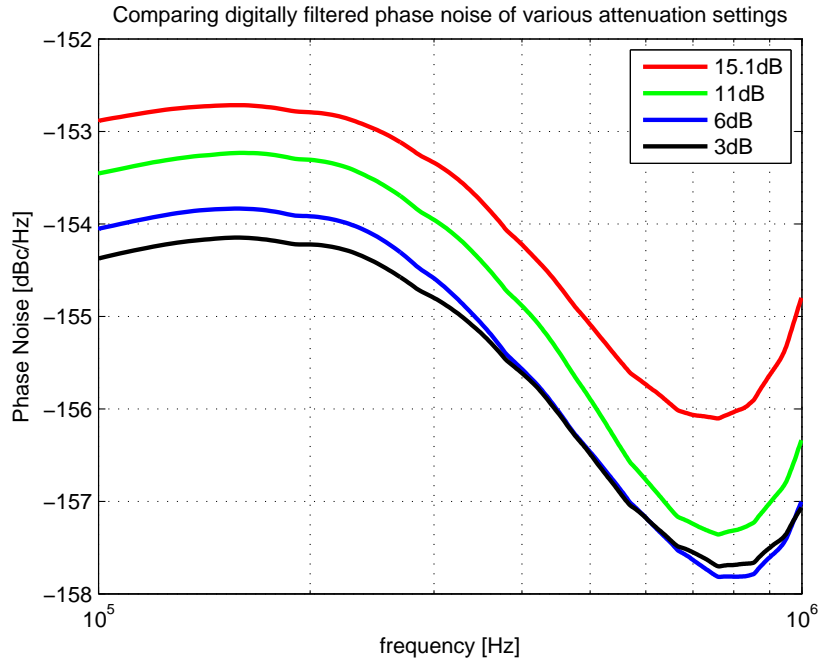


Figure 4.9: Digitally filtered phase noise measurements

noise figure in dB and P_{in} is the signal power entering the amplifier in dBm [15]. Since the phase noise has been measured and the power entering the amplifier has been calculated, the noise figure of the amplifier can be determined.

$$\mathcal{L}_{floor} = 10 \log_{10} \left(\frac{kT}{0.001} \right) - 3.01 + F_{dB} - P_{in} \quad (4.13)$$

The calculated noise figures, as well as the open loop gains for each of the attenuation levels of the circuit, are shown table 4.2. The open loop gain serves as an indication of system linearity. The closer to unity it is, the more linearly the system is operating. The open loop gain is calculated by subtracting all the losses in the system at the operating frequency from the amplifier gain at this frequency.

Table 4.2, therefore, clearly illustrates that the system's effective noise figure increases as it becomes more non-linear. It should be noted that the effective noise

Table 4.1: Calculated input signal power and losses at measured centre frequency.

Center frequency	Power Out	Phase Shifter	Resonator	Attenuation	Power Avail.
5.035 MHz	6.20 dBm	0.3 dB	6.054 dB	15.1 dB	-15.254 dBm
5.031 MHz	8.17 dBm	0.3 dB	6.509 dB	11 dB	-9.639 dBm
5.026 MHz	8.60 dBm	0.3 dB	7.266 dB	6 dB	-4.966 dBm
5.023 MHz	8.75 dBm	0.3 dB	7.603 dB	3 dB	-2.153 dBm

figure mentioned here is the actual noise figure of the oscillator. The increase in the amplifier's noise figure can be attributed to noise at integer multiples of the oscillation frequency being mixed down to frequencies situated around the carrier. An increase in the power magnitude of the oscillator's harmonics would, therefore, lead to an increase in the amount of noise being transformed to frequencies around the fundamental oscillation frequency.

4.4 Conclusion

At first glance, it appears that the ultimate phase noise level improves as the circuit becomes more non-linear. On closer inspection, however, it can be seen that this improvement is more likely the result of the increased output signal power level, associated with the non-linearity, than as a result of the non-linearity itself. Furthermore, it was shown that the amplifier's effective noise figure increases as it is driven deeper into saturation. It could be hypothesised that the increase in the oscillator's effective noise figure is the result of white noise situated around integer multiples of the oscillation frequency being mixed down to frequencies near DC and then transformed to phase noise around the carrier. This phenomenon was mentioned in Chapter 3.3. It could be assumed that the greater the magnitude of the oscillator's harmonics, the greater the effect of the white noise surrounding them will be on the oscillator circuit's total phase noise.

Therefore the following hypothesis can be made: A non-linearly driven oscillator will have a greater output signal level, as well as greater harmonic distortion, than one linearly driven. The increase in the effective noise figure associated with non-linearity is greater than the increase in output signal level. Therefore it stands to reason that an oscillator with good phase noise performance should be driven linearly and be capable of handling large input signal levels without the active device being driven into saturation. This hypothesis will be evaluated by means of the following experiments discussed in the next chapters.

The previous conclusion also suggests that Leeson's model approximates linearly dri-

Table 4.2: Calculated noise figures and open loop gains for different levels of attenuation

Attenuation	Open Loop Gain	Noise Figure
15.1 dB	1.3 dB	5.474 dB
11 dB	4.89 dB	9.789 dB
6 dB	9.13 dB	14.062 dB
3 dB	11.797 dB	16.975 dB

ven oscillators better than their non-linearly driven counterparts, since the effective noise figure is much lower in the more linear cases.

Chapter 5

Experiment 2:

5.1 Purpose of the experiment

In the previous chapter it was concluded that the active device in an oscillator circuit should be capable of handling large input signal levels without going into saturation. It was also indicated that, for the same output signal level, a linearly driven oscillator will have better phase noise performance than a non-linearly driven oscillator. In this chapter these conclusions will be evaluated by comparing the measured phase noise performance of a linearly driven oscillator with that of a non-linearly driven oscillator. In order to make a useful comparison, the oscillator circuits will be adjusted to produce the same output signal magnitude in both cases.

The experimental setup is similar to that used in the previous chapter and is shown in figure 5.1. Unlike the oscillators in the previous chapter, the oscillators in this experiment, were designed to operate at 10 MHz. This choice of operating frequency allows for greater ease of measurement as far as noise figure and phase noise measurements are concerned.

5.2 The design and characterisation of the various circuit models

A modular approach was again taken with regard to the oscillator networks used in this experiment. Given the fact that the operating frequency of the oscillators had changed from 5 MHz to 10 MHz, and considering the conclusions reached in the previous chapter, some modules from the previous experiment had to be re-designed. The specifications of these modules are briefly discussed in this section.

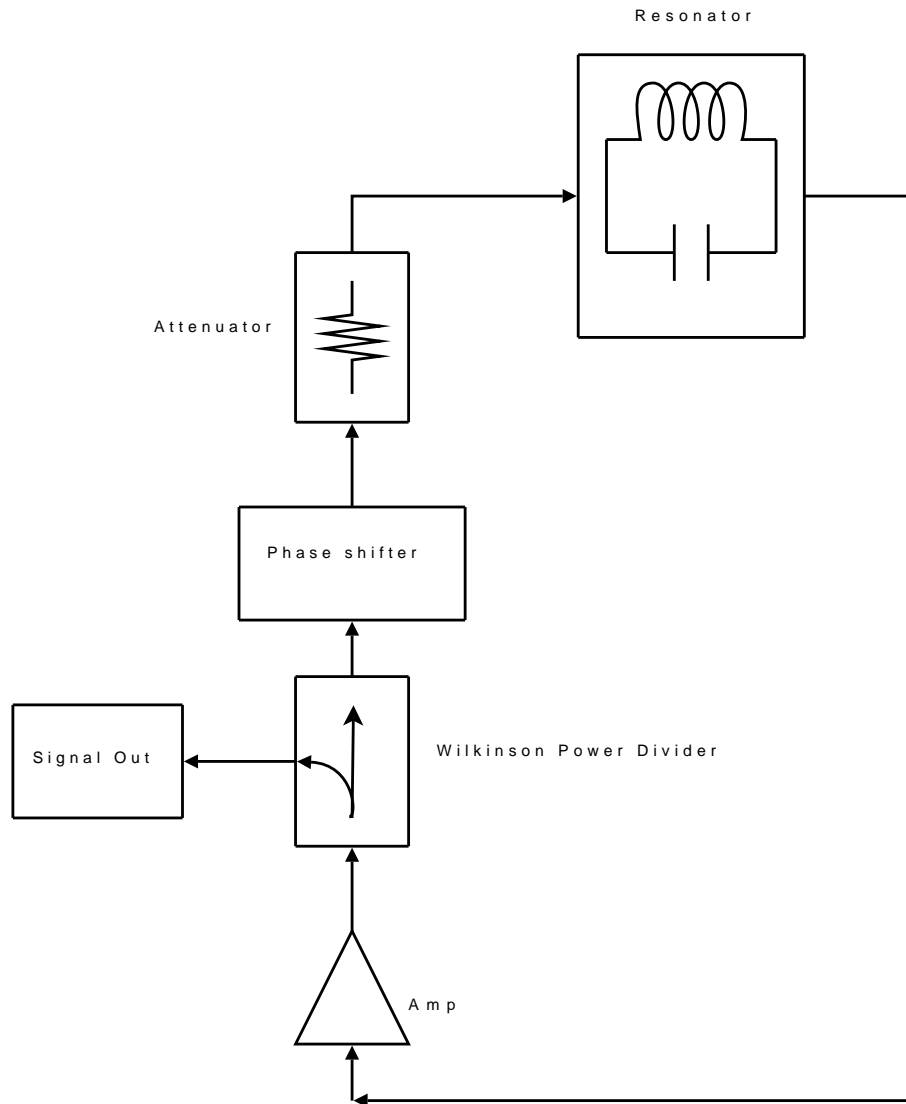


Figure 5.1: The experimental circuit layout

5.2.1 Resistive Feedback Amplifier

As mentioned previously, an active device with the ability to handle large amounts of input power, without being driven into saturation, is needed. For this purpose a resistive feedback amplifier was designed and built. The design and verification of this amplifier are discussed in Appendix C.1, which illustrates that this amplifier adheres to the previously mentioned amplifier criterion.

5.2.2 Amplifier without Feedback

An amplifier identical to the one mentioned in the previous subsection was built, but the feedback resistor and capacitor, R_{fb} and C_{fb} , were omitted. The amplifier

was measured and the results are illustrated in Appendix C.2.

5.2.3 Resonator

A 10 MHz resonator was designed following a procedure similar to that outlined in Chapter 4.2.5 and Appendix A.5. This time, however, a compromise was made regarding the optimal power dissipation within the resonator, required for optimal phase noise performance, in order to obtain a match at both its ports. The design and verifications are shown in Appendix C.3. Note that the quality factor of this resonator is slightly degraded as a result of the resistive port matching applied to it.

5.2.4 Phase Shifter

In the previous experiment a 270° LC phase shifting network was implemented in order to negate the 90° phase shift inherent to Wilkinson power dividers. In this experiment and the next a 68° phase shifter was implemented to negate the phase shift resulting from both the amplifier and the power divider. The layout and measured results of this phase shifter are discussed in Appendix C.5.

5.2.5 Power Divider and Attenuators

The attenuator used in this experiment is the same 1 dB attenuator that was used in the previous experiment. A 10 MHz Wilkinson power divider was designed following the same procedure as discussed in Appendix A.2. The measured results are illustrated in Appendix C.4.

5.3 Method of the Experiment

The experiment is started by first setting up a linearly driven oscillator. This oscillator comprises out of the resistive feedback amplifier, Wilkinson divider, 68° phase shifter, resonator and the 1 dB attenuator mentioned in the previous section. The 1 dB attenuator was chosen in order to limit the open loop gain of the system to approximately 0 dB, thereby ensuring a linearly driven oscillator. The output signal magnitude of this oscillator was subsequently measured and is shown in figure 5.2.

Once the magnitude of the linearly driven oscillator had been determined, the resistive feedback amplifier of subsection 5.2.1 was replaced with a similar amplifier,

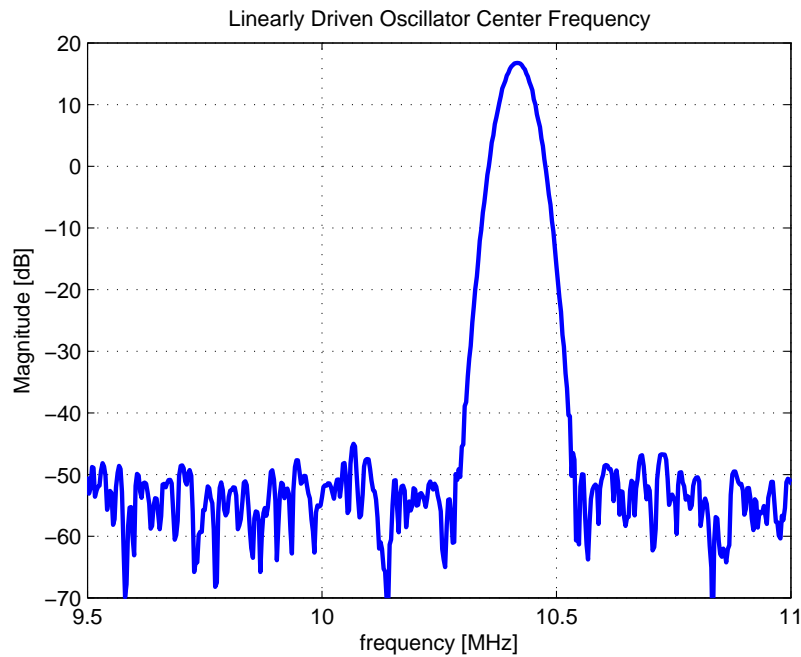


Figure 5.2: Measured fundamental frequency of the linearly driven oscillator

with the feedback resistor and capacitor removed. (This amplifier was mentioned in subsection 5.2.2.) The biasing voltage at the bases of this amplifier’s transistors was adjusted by means of an adjustable voltage regulator, until this oscillator produced an output signal equal in magnitude to that of the previous linearly driven oscillator. This is verified by the measurement shown in figure 5.3.

Once it had been confirmed that the two oscillator networks produced output signals equal in magnitude, the second amplifier could be characterised. These amplifier measurements are discussed in Appendix C.2 and indicate that this amplifier is indeed driven nonlinearly in the oscillator loop of the present experiment: The amplifier’s gain is approximately 5 dB higher than that of the resistive feedback amplifier. This implies that it would necessarily be driven into saturation, since the open loop gain of the network would be 5 dB. This amplifier is also poorly matched, which would inevitably result in large reflections at its input port. These facts indicate that, should the oscillator loop be driven by the amplifier without feedback, the oscillator would be operating in a nonlinear fashion.

The previous paragraphs have illustrated that the resistive feedback amplifier would drive the described oscillator loop linearly, whereas the amplifier without feedback would drive it nonlinearly. Phase noise measurements were performed for both scenarios and the results are illustrated in figure 5.4. The dotted line represents the measured phase noise distribution of the nonlinearly driven network, while the solid

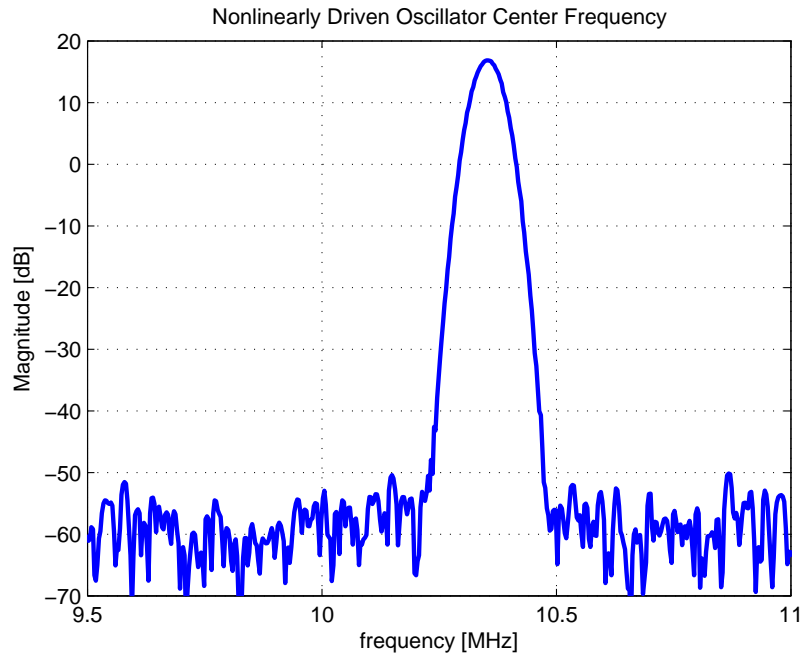


Figure 5.3: Measured fundamental frequency of the nonlinearly driven oscillator

line denotes the phase noise distribution of the linearly driven oscillator.

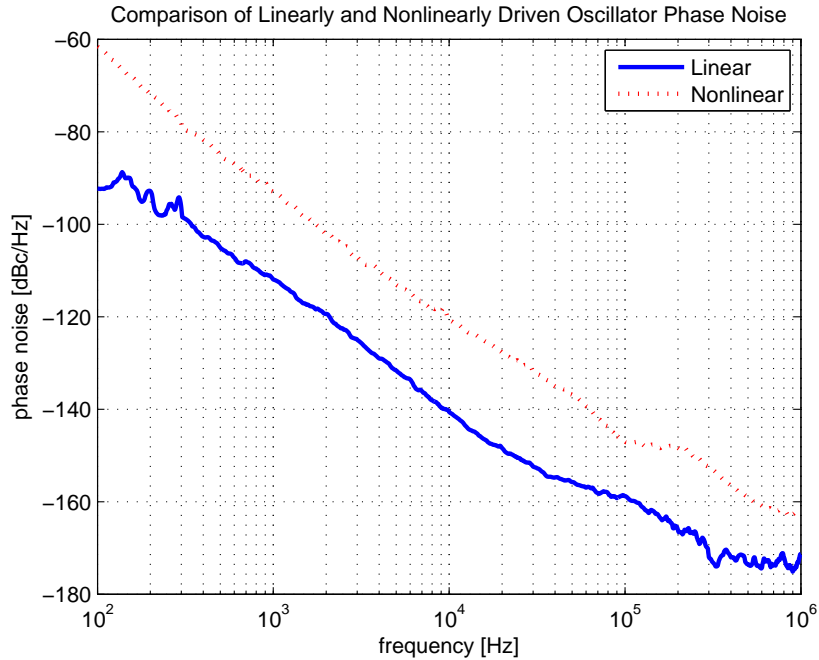


Figure 5.4: Phase noise performances of linearly and nonlinearly driven oscillator networks

Since the amplifiers are the only components that were varied during the execution of

the experiment, it must be concluded that the difference in phase noise performance is a result of the amplifiers driving the two oscillator networks.

5.4 Conclusion

In the previous chapter it was postulated that should a linearly driven oscillator and a nonlinearly driven oscillator produce output signals that are equal in magnitude at the fundamental frequency, the linearly driven oscillator should have superior phase noise performance. From the experiment performed in this chapter it is clear that this is indeed the case. This experiment indicates that the phase noise performance of the linearly driven oscillator network is at least 10 dBc/Hz better than that of the nonlinearly driven oscillator network.

Chapter 6

Experiment 3:

6.1 Purpose of the Experiment

In chapter 4 it was suggested that the more closely an oscillator approaches linear operation, the more closely its phase noise performance would approach the phase noise predicted by Leeson's model. During the course of the following experiment this claim will be evaluated in greater detail.

In this experiment the author assesses just how sensitive the phase noise performance of an oscillator network is with regards to the degree of saturation within which it's active device is operating.

6.2 Method of the Experiment

In the following experiment the oscillator's active device is driven deeper and deeper into compression in steps of approximately 0.1 dB. This is achieved as follows: A variable attenuator was designed, the design of which is discussed in Appendix C.6. This design allows for its attenuation to be adjusted in steps of 0.1 dB, with minimal variations in its phase deviation for the various attenuation settings.

The experimental setup is similar to that described in chapters 4 and 5. The oscillator block diagram is shown in figure 6.1. The resonator, resistive feedback amplifier, power divider and phase shift network used in Chapter 5 is again employed in this experiment. The fixed attenuator has a loss of 1 dB and the variable attenuator is initially set to its maximum loss of approximately 0.8 dB. At this point the loop gain of the network is less than 0 dB and no oscillation takes place. The loss of the

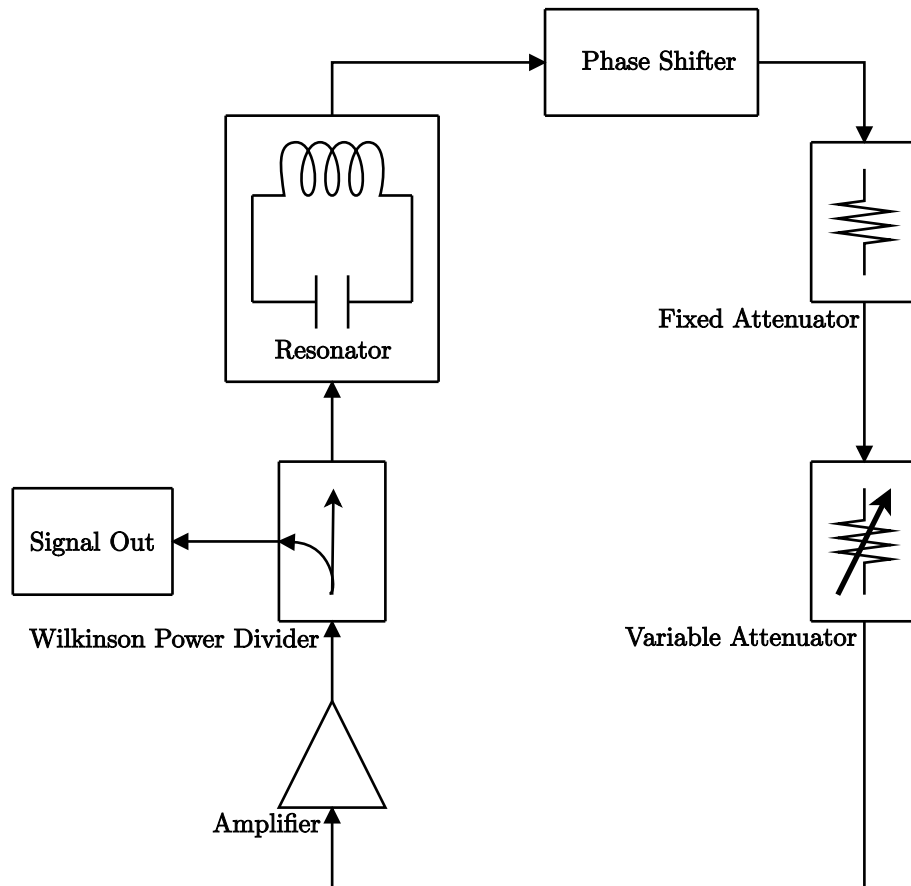


Figure 6.1: The experimental setup

variable attenuator is then reduced in steps of nearly 0.1 dB until oscillation occurs. For the circuit used in this experiment it was found that a total attenuation loss of 1.4 dB is the greatest level of attenuation at which oscillation can still take place.

The gain condition for oscillation states that the open loop gain of an oscillator network must be greater than 0 dB in order for oscillation to take place. Since oscillation did not occur at an attenuation level of 1.5 dB, it may be argued that at this attenuation setting, the open loop gain of the system is less than 0 dB. (Since no oscillation occurs, it may be concluded that no saturation of the active device is occurring either. Therefore the open loop gain is the same as the closed loop gain for an attenuation setting of 1.5 dB or greater.) Following a similar argument, the open loop gain of the network must therefore be greater than 0 dB at an attenuation setting of 1.4 dB. Since these attenuation settings differ by only 0.1 dB, it must be concluded that the open loop gain of the system must be less than or equal to 0.1 dB for a 1.4 dB attenuation setting. At this point, the active device is operating between 0 and 0.1 dB into compression at an attenuation setting of 1.4 dB. This statement can be explained as follows: at the point of stable oscillation, the closed

loop gain of the oscillator network must be unity (0 dB). In an oscillator network such as the one being considered in this experiment, this condition is realised by saturation of the active device. Since the open loop gain of the network is less than or equal to 0.1 dB, it must be concluded that the level of saturation occurring within the active device must also be less than or equal to 0.1 dB. It therefore stands to reason that, should the total amount of attenuation (from the variable and the fixed attenuator) be decreased to 1.3 dB, the active device would be operating between 0.1dB and 0.2 dB into compression. For 1.2 dB of attenuation it will be operating between 0.2 dB and 0.3 dB into compression, etc.

By adjusting the amount of attenuation, the output signal magnitude, as well as the phase noise performance of the oscillator, can be measured as a function of the level of saturation occurring within the active device.

6.3 Measurements and Discussion

The phase noise performance was measured for four levels of amplifier saturation. These measurements were taken with the amplifier operating respectively within 0.1 dB, 0.2 dB, 0.3 dB and 0.4 dB of compression and are illustrated in figure 6.2.

Apart from the measurement taken for the amplifier operating at 0.1 dB of com-

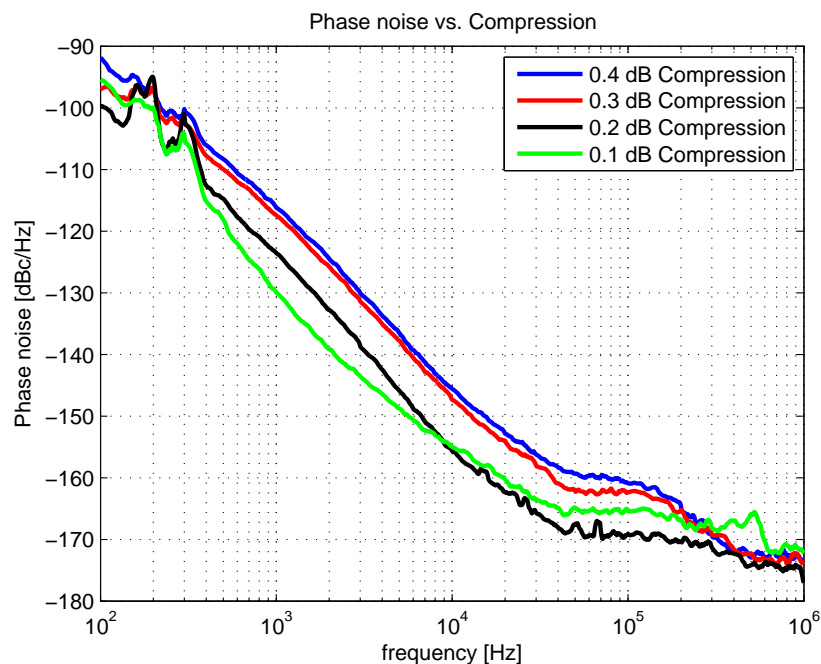


Figure 6.2: Phase noise vs. compression

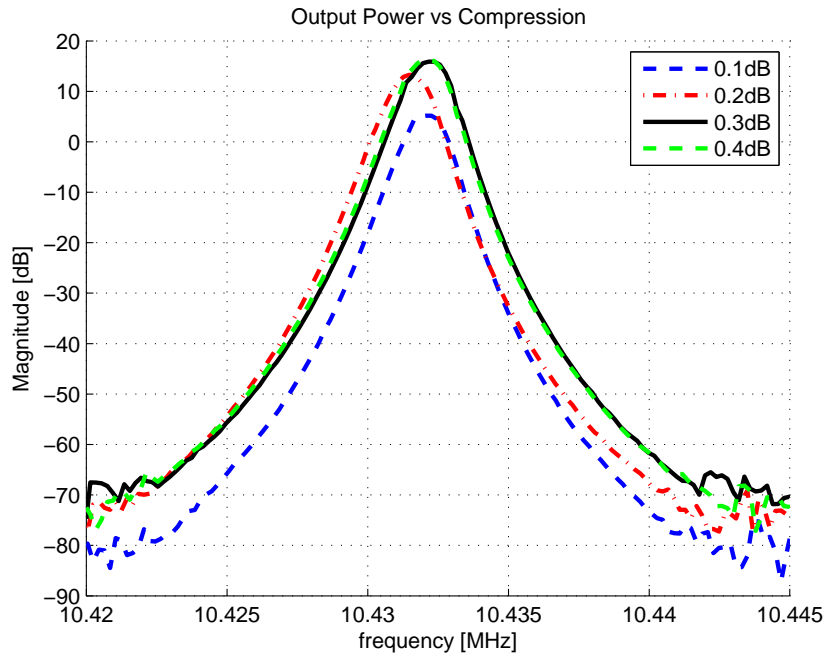


Figure 6.3: Signal magnitude vs. compression

pression, it can be seen that the phase noise performance deteriorates as the level of amplifier saturation increases. The reason for the discrepancy at 0.1 dB of amplifier saturation may be explained as follows: Consider the measured output signal magnitudes of the oscillator for the different levels of amplifier saturation, shown in figure 6.3. These measurements indicate that the magnitude of the output signal is approximately 10 dB smaller when the amplifier operates within 0.1 dB of compression than when it operates at deeper levels of compression. Since the phase noise is represented in dBc/Hz, it stands to reason that the phase noise measured for 0.1 dB of amplifier compression will necessarily be poorer than the phase noise measured while the amplifier is operating within 0.2 dB saturation. This is purely as a result of the difference in carrier magnitude. A more reasonable method of evaluating the phase noise performance with regard to the level of amplifier saturation (or system linearity) is needed. One way to do this would be to compare the phase noise performance at each of the different amplifier saturation settings with the phase noise predicted by Leeson's model.

6.3.1 Comparing Measured Phase Noise with Leeson's Model

Assuming that the noise power density entering the amplifier is white, the phase noise distribution given by Leeson's model may be calculated as follows: First the ultimate phase noise is calculated. This is phase noise far from the carrier and is the lowest achievable phase noise limit that the oscillator can obtain [15]. It is calculated by adding the system noise figure, in dB, to the theoretical minimum phase noise power, in dBm, and then subtracting the signal magnitude, in dBm, from this value. Mathematically this may be stated as:

$$\mathcal{L}(f) = P_{phase} + NF - P \quad (6.1)$$

In equation 6.1, P is the magnitude of the oscillator's output signal and P_{phase} represents the theoretical minimum achievable phase noise power, in dBm, which can be calculated by:

$$P_{phase} = P_{thermal} - 3.01[dB] \quad (6.2)$$

where

$$\begin{aligned} P_{thermal} &= kTB \\ &= -174dBm \end{aligned} \quad (6.3)$$

is the theoretical thermal noise floor. In equation 6.3, k is Boltzmann's constant, $T = 300K$ and $B = 1Hz$. The thermal noise power consists of equal AM and FM/PM components. The phase noise power is therefore 3.01 dB less than the thermal noise power [16].

NF represents the noise figure of the system (the combined noise figure of the cascaded system) in equation 6.1 and may be calculated as follows:

$$F_{sys} = F_1 + \frac{(F_2 - 1)}{G_1} + \frac{(F_3 - 1)}{G_1 G_2} + \dots \quad (6.4)$$

The values in equation 6.4 are all linear. F_{sys} is the total noise factor of the cascaded system. F_1 represents the noise factor of the first element in the cascade, F_2 the second and so forth. Similarly G_1 represents the gain of the first element in the system, G_2 the second and so forth. A lossy element will have a negative gain [17]. The noise figure is simply the noise factor expressed in dB, as is illustrated in equation 6.5 [17].

$$NF = 10 \times \log(F_{sys}) \quad (6.5)$$

In the case of the oscillator network used in this experiment, the loop should be broken at the same point in the chain as that from which the signal is taken, ie. after the power divider, as is shown in figure 6.4, in order to calculate the cascaded noise figure. This implies that the resonator is the first element in the cascaded network and that the Wilkinson divider is the final element in the chain. It should also be noted that the noise figure of a passive element is equal to the loss of the element. Another factor to be taken into consideration is the fact that, while oscillation is occurring, the loop gain of the network is 0 dB. This implies that the gain of the amplifier must be decreased as the amount of attenuation is decreased, in order to compensate for this. The previously mentioned adjustment of the amplifier's gain correlates with the phenomenon of amplifier saturation which will inevitably occur during oscillation and result in a lower amplifier gain. The losses, and therefore the noise figures, of the passive elements in the cascade may be read from the measured results in Appendix C. These values result in the system noise figures shown in table 6.1 at the various levels of saturation.

Table 6.1: Noise figures and resulting ultimate phase noise.

Saturation level	Signal magnitude	Amplifier Gain	NF	Ultimate Phase Noise
0.1 dB	5.18 dBm	12.9 dB	14.4 dB	-167.78 dBc/Hz
0.2 dB	13.27 dBm	12.8 dB	14.3 dB	-175.60 dBc/Hz
0.3 dB	15.89 dBm	12.7 dB	14.2 dB	-178.69 dBc/Hz
0.4 dB	16.20 dBm	12.6 dB	14.1 dB	-179.1 dBc/Hz

The next step in deriving Leeson's phase noise model is to determine the Leeson frequency. This was shown in Chapter 3.4 and is again defined here in equation 6.6.

$$f_L = \frac{f_0}{2Q} \quad (6.6)$$

In this equation Q represents the loaded quality factor of the resonator. Since all of the modules in the oscillator have a characteristic impedance of 50Ω , this value can be determined directly from the resonator passband (S_{21}) measurement shown in Appendix C.3, by using the following equation 6.7.

$$Q = \frac{1}{BW} \quad (6.7)$$

BW represents the half power bandwidth of the resonator. It is determined by subtracting the lower half power frequency from the higher half power frequency and dividing the result by the resonant/centre frequency of the resonator. These

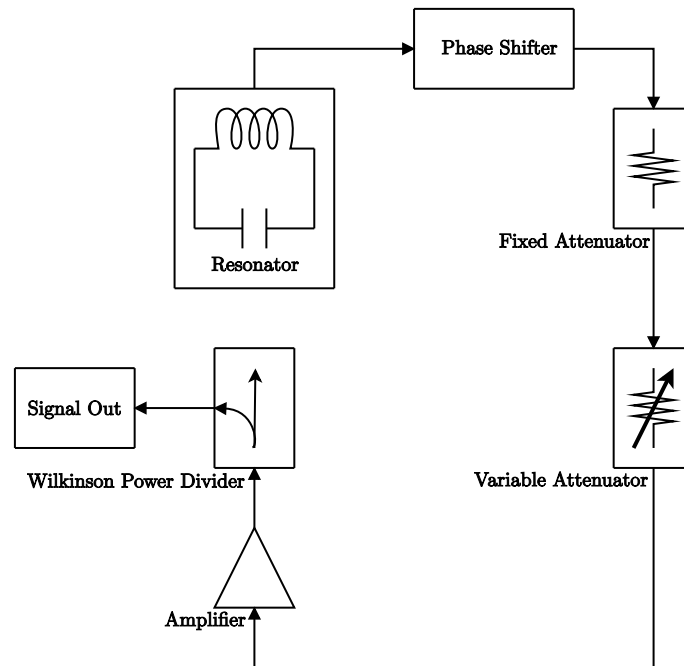


Figure 6.4: Oscillator loop broken in order to calculate system noise figure.

values may be read from figure C.16, and result in $Q = 74.6$. Substituting this value in equation 6.6, yields a Leeson frequency of 70 kHz. In Chapter 3.4, it was shown that for frequencies smaller than the half power bandwidth of the resonator, the phase noise has a $\frac{1}{f^2}$ dependence with regard to the noise power distribution of the loop. This implies that, on a logarithmic scale, the phase noise distribution between the Leeson offset frequency and carrier frequency will increase by 20 dB per decade. Note that this phase noise distribution holds true only for the assumed case of a white noise power distribution entering the resonator. The phase noise distribution as defined by Leeson's model for each of the previously mentioned levels of amplifier compression would, therefore, be as depicted by the dashed lines in figures 6.5 to 6.8.

6.3.2 Discussion of Phase Noise Measurements

The measured phase noise distributions for each of the different levels of compression are illustrated in figures 6.5 to 6.8 by the solid lines. The measurements were taken with an FSUP-8 from Rohde & Schwarz. These figures clearly indicate that Leeson's model is a fair approximation of the measured phase noise for the cases where the amplifier is operating at 0.1 dB (figure 6.5) and 0.2 dB compression (figure 6.6). However, the model rapidly loses accuracy as the level of amplifier compression increases beyond 0.3 dB, as is shown in figures 6.7 and 6.8. It should be noted

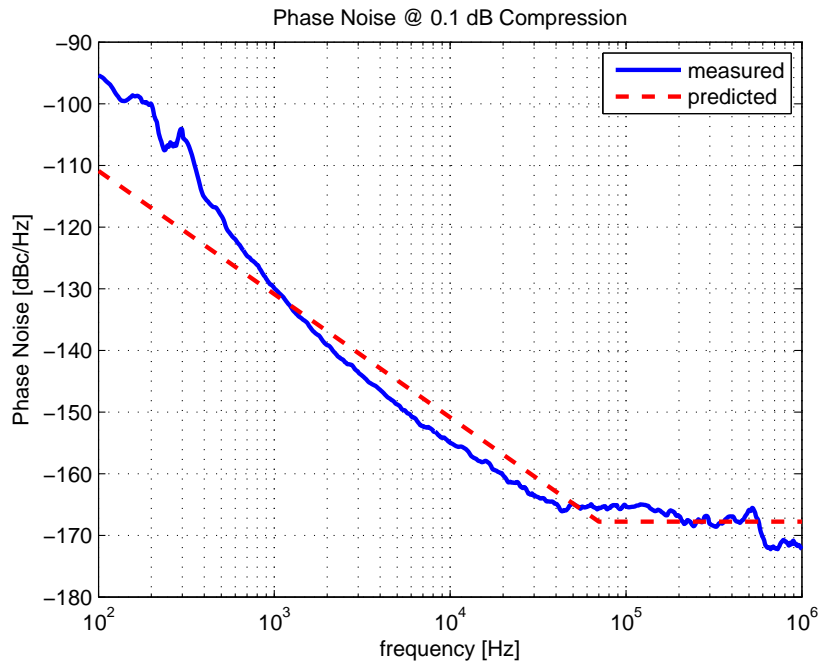


Figure 6.5: Discrepancy between measured and predicted phase noise at 0.1 dB amplifier saturation.

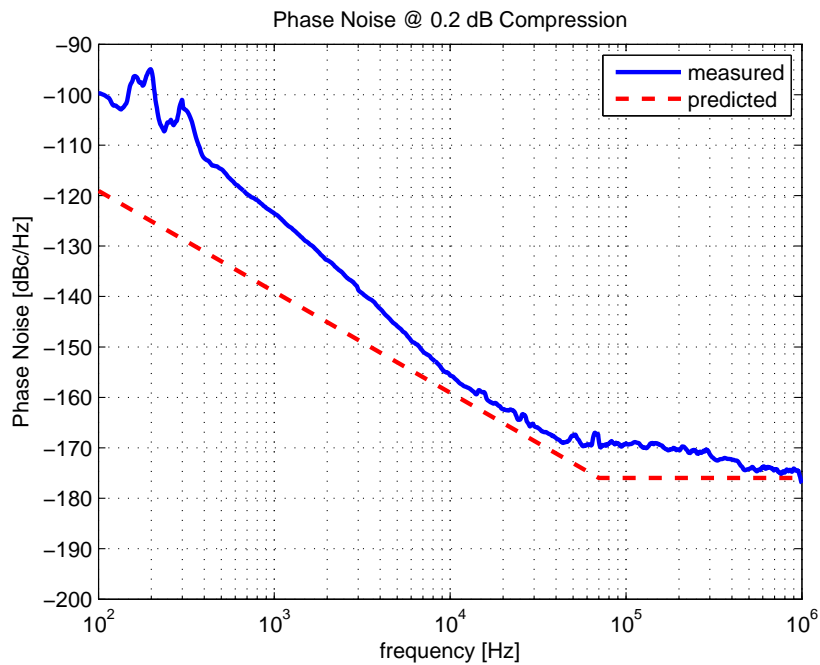


Figure 6.6: Discrepancy between measured and predicted phase noise at 0.2 dB amplifier saturation.

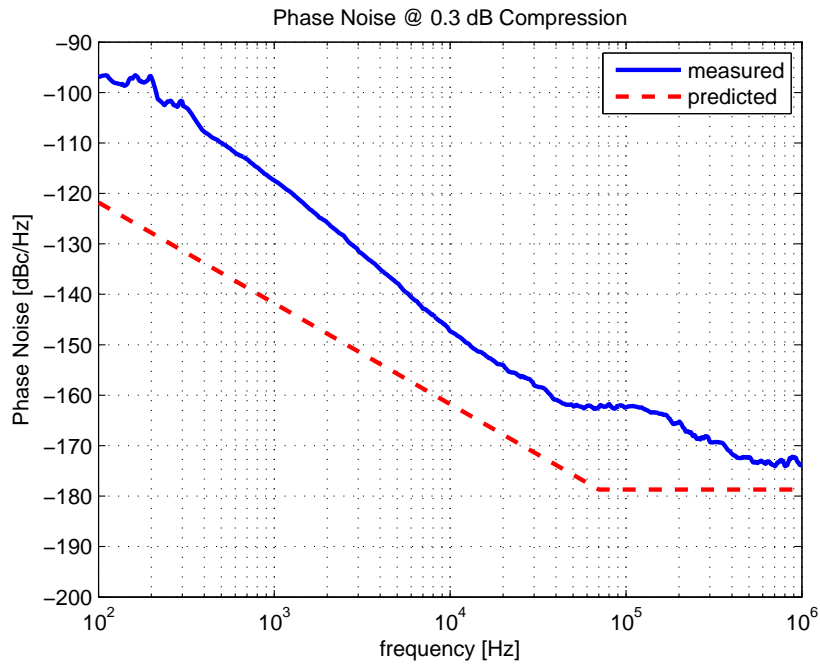


Figure 6.7: Discrepancy between measured and predicted phase noise at 0.3 dB amplifier saturation.

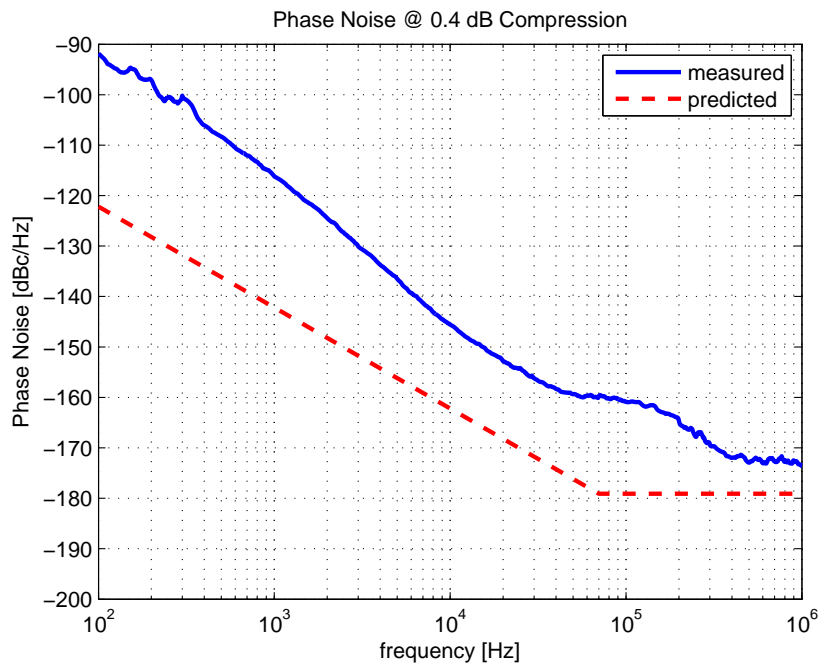


Figure 6.8: Discrepancy between measured and predicted phase noise at 0.4 dB amplifier saturation.

that the author did not take the effect of frequency flicker noise into account while generating the Leeson approximations of the measurements. The effect of this flicker noise is, however, clearly visible in all of the measured results and manifests as a $\frac{1}{f^3}$ component in the phase noise.

It should also be considered that the phase noise measurement in the case where the amplifier is operating at 0.1 dB compression might not be accurate. This claim is made due to the fact that the amplifier's gain would inevitably vary with temperature. Given that the oscillator is operating on the fringe of the loop gain oscillation condition, it may be assumed that the magnitude of the oscillator's output signal will vary. This could account for the measured phase noise showing better performance than that predicted by Leeson's model for oscillator phase noise.

The erratic behaviour of the measured phase noise at offset frequencies of 300 Hz and less is also noticeable. 300 Hz coincides with the bandwidth of the phase noise meter's phase locked loop (PLL) during the measurements. (the FSUP-8) It may therefore be assumed that at offset frequencies smaller than the loop bandwidth of the FSUP-8's PLL, mixer pulling is occurring between the DUT and the FSUP-8's LO. This effect becomes less noticeable as the level of compression into which the oscillator is driven is increased. (This effect could possibly have been avoided had a buffer amplifier been in place between the oscillator's output and the phase noise meter.)

Another anomaly to consider is the *bulge* on the measured phase noise curves between the offset frequencies of 40 kHz and 400 kHz. This phenomenon may be attributed to noise inherent to the oscillator's power source or voltage regulators. (This will be confirmed in a later chapter.) What is of note, is that this *bulge* becomes smaller as the level of amplifier saturation is decreased.

6.4 Conclusion

In chapter 4 it was hypothesised that the more linear the operation of an oscillator's active device, the better its phase noise distribution could be approximated by Leeson's model. During the course of this experiment it was shown that this is indeed true. It was also shown that the phase noise measurements of the linearly driven oscillator are more susceptible to the effects of mixer pulling than their more non-linearly driven counterparts, even if the degree of non-linearity differs by fractions of a decibel. This effect could be negated by placing a buffer amplifier between the oscillator's output and the measuring equipment or by increasing the quality

factor of the resonator. This will be evaluated in the following experiment. Perhaps the most interesting observation in the previous experiment was that the more linear the operation of the amplifier became, the less discernable the effect of the noise inherent to the power source became in the phase noise measurements. This occurrence can again be explained by the same mechanism discussed in chapters 3.3 and 4.4. The low frequency noise originating from the power source and/or voltage regulators situated near DC, is mixed up in frequency to sit around the fundamental frequency as well as around the harmonics of this frequency. The noise situated at these harmonics is then transformed into phase noise situated around the fundamental frequency as was explained in the previously mentioned chapters [11]. This implies that as the level of amplifier saturation is decreased, and consequently also the magnitude of the harmonics being generated, the effect of the source noise becomes less noticeable in the phase noise measurements.

Chapter 7

Experiment 4:

7.1 Purpose of the Experiment

In the previous experiments resonators with relatively low quality factors were used. Low Q resonators allow for more frequency drift to take place during oscillation. During the course of this experiment, the performance of an oscillator with a high quality factor resonator will be evaluated. This is done in order to determine how such an oscillator is affected by the degree of linearity under which it is operating.

7.2 Method of the Experiment

The same technique used in chapter 6.2 is again employed here. The LC resonator of the previous experiment was, however, replaced with the crystal resonator described in Appendix D.1. The experimental setup is illustrated in figure 7.2. The resistive feedback amplifier, phase shifter, Wilkinson power divider and variable attenuator,

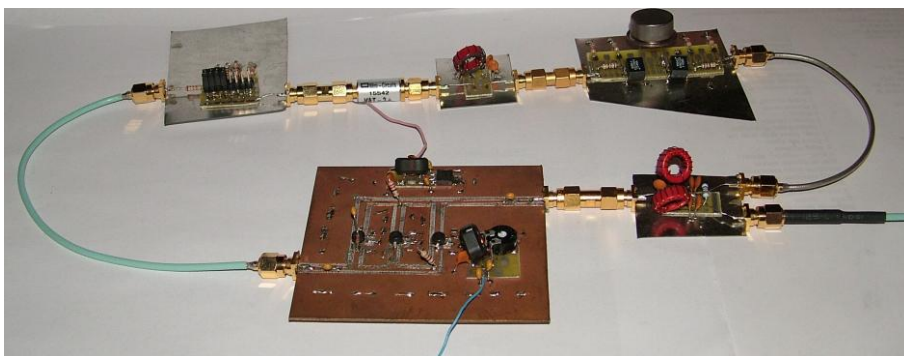


Figure 7.1: Crystal loop oscillator setup used in experiment 4

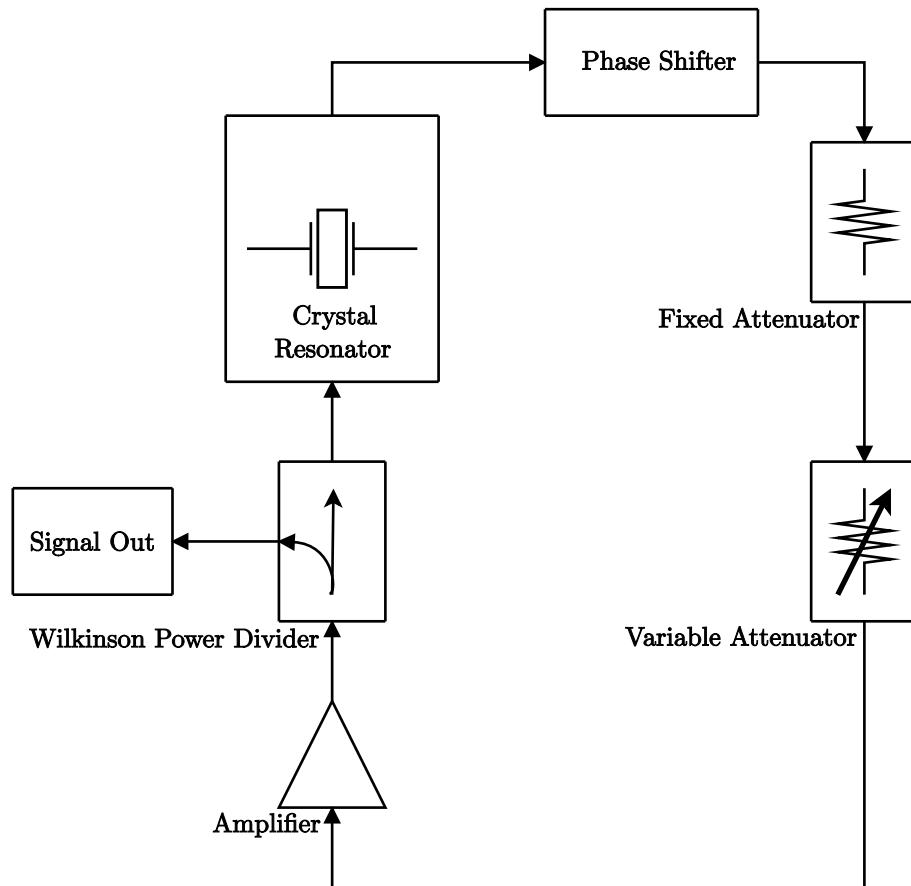


Figure 7.2: Experimental setup

are the same modules used in the previous chapter. As far as the fixed attenuator is concerned, in order to acquire the necessary levels of attenuation, a 4dB and a 3dB attenuator were respectively used in conjunction with the variable attenuator.

As in the previous experiment the amount of attenuation is decreased in steps of approximately 0.1 dB and the phase noise performance was measured for each attenuation setting.

7.3 Measurements and Discussions

Figure 7.3 depicts four phase noise measurements taken at different attenuation settings. In order to keep the graph uncluttered not all of the consecutively taken measurements are shown in this figure. It is noteworthy that there is very little variation in the phase noise performance for the different attenuation levels at offset frequencies close to the carrier. Also of note is that for levels of amplifier compression below 0.6dB there is very little variation in the phase noise performance of the oscillator, as is illustrated in figure 7.4.

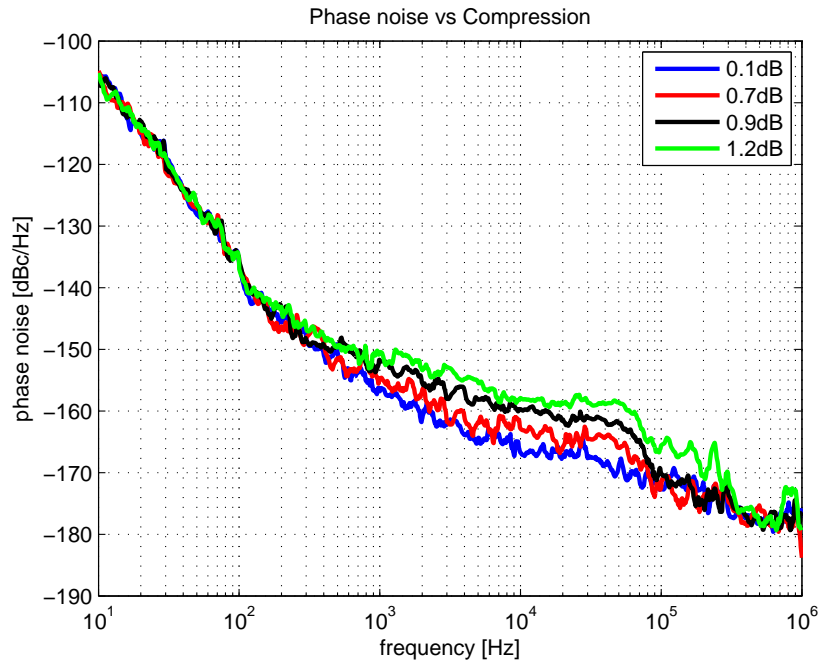


Figure 7.3: Phase noise vs. compression

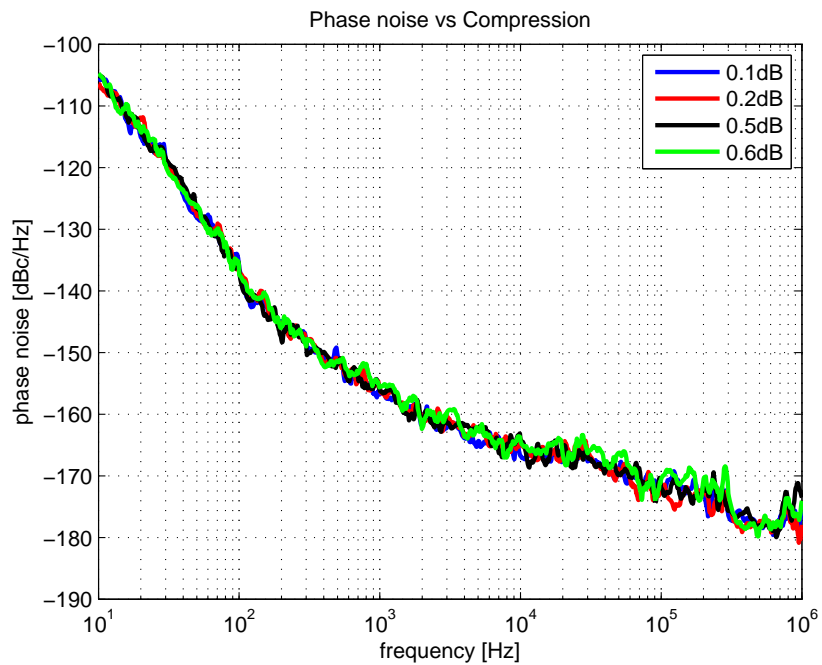


Figure 7.4: Phase noise vs compression for compression levels of less than 0.6 dB

Table 7.1: Ultimate phase noise and cascaded noise figure for various levels of amplifier saturation.

Saturation Level	Signal Magnitude	Amplifier Gain	NF	Ultimate Phase Noise
0.1 dB	15.47 dBm	12.98 dB	14.4828 dB	-177.9872 dBc/Hz
0.2 dB	16.2 dBm	12.88 dB	14.3828 dB	-178.8172 dBc/Hz
0.5 dB	16.26 dBm	12.58 dB	14.0907 dB	-179.1693 dBc/Hz
0.9 dB	17 dBm	12.18 dB	13.6994 dB	-180.3006 dBc/Hz
1.2 dB	17.16 dBm	11.88 dB	13.4064 dB	-180.7536 dBc/Hz

7.3.1 Comparing Phase Noise Measurements with Leeson's Model

In figures 7.5 to 7.9 a few phase noise measurements taken at different levels of amplifier compression are depicted by the solid lines. On the same figures, two phase noise approximations given by Leeson's model are also shown. One approximation assumes that only white noise is entering the resonator and this is depicted by the dashed line. The other assumes that a flicker noise component is also present. For the case where only white noise is assumed to have entered the resonator, the same procedure as was described in the previous chapter is used to draw the approximation. Once again the system noise figure is calculated along with the ultimate phase noise for each of the illustrated levels of amplifier compression. The results, along with the measured magnitude of the oscillator's output signal and corresponding amplifier gain, are shown in table 7.1. Once again the Leeson frequency was calculated using equation 6.6. In this case Q is taken to be 86799.6 (from Appendix D.1). At the fundamental oscillating frequency of 9.9997 MHz, this yields a Leeson frequency of 56.6 Hz

For the case where the presence of a flicker noise component is assumed to have entered the resonator, the same Leeson frequency, as well as the ultimate phase noise, also applies. In order to illustrate a Leeson model which assumes the presence of flicker, or $\frac{1}{f}$ noise, a flicker/ $\frac{1}{f}$ corner frequency must first be determined. This is done as follows. In chapter 3.4, it was shown that for offset frequencies greater than the Leeson frequency the resonator has no effect on the phase noise distribution of the oscillator. For offset frequencies smaller than the Leeson frequency, the phase noise is altered and receives an additional $\frac{1}{f^2}$ dependency. Since flicker noise has a $\frac{1}{f}$ dependency, it therefore stands to reason that for offset frequencies ranging from the flicker corner frequency to the Leeson frequency, the phase noise will increase by 10 dB/decade. For offset frequencies ranging from the Leeson frequency to the carrier frequency, the phase will increase by 30 dB/decade. With this information at

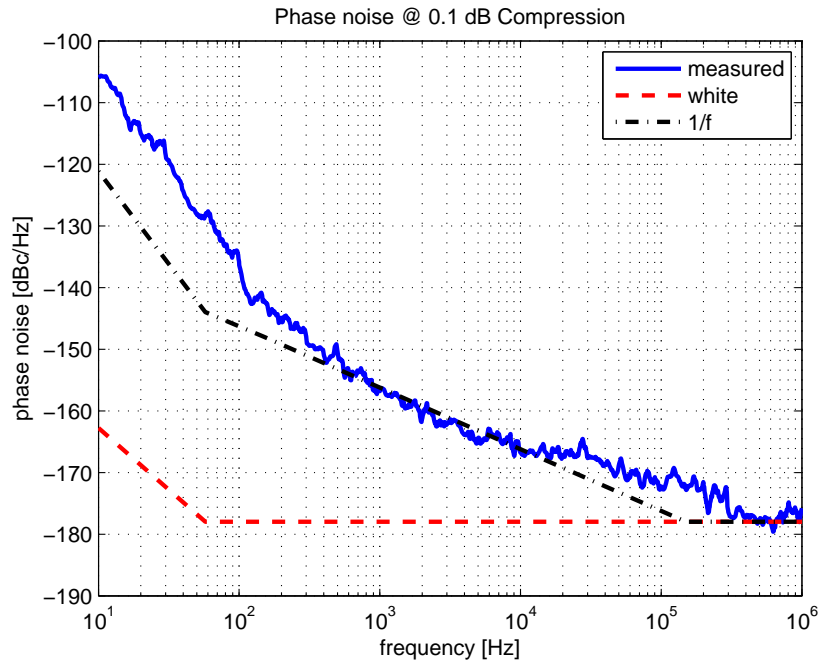


Figure 7.5: Measured and predicted phase noise at 0.1 dB amplifier compression.

hand, a line with 10 dB/decade dependence ($\frac{1}{f}$ dependence) can be fitted onto the measured results. The intersect point of this line and the line of constant ultimate phase noise, results in the $\frac{1}{f}$ corner frequency. It is assumed that the phase noise measurement for the case where the amplifier is operating at less than 0.1 dB of saturation, is the most accurate representation of the noise inherent to the system. This assumption is based upon the results of the previous chapters. The argument is put forward that, when operating in its most linear state, the harmonics generated by the oscillator are minimised. This results in less noise situated at integer multiples of the oscillation frequency being mixed down to near the fundamental frequency. For this reason the $\frac{1}{f}$ corner is determined from the phase noise measurement where the amplifier is operating within 0.1 dB of compression. This results in the line with both dots and dashes depicted in figures 7.5 through 7.9. Note that it is assumed that the $\frac{1}{f}$ corner frequency is the same for all levels of amplifier compression.

7.3.2 Discussion of Phase Noise Measurements and Approximations

In figures 7.5 through 7.9 it is clear from the slope of the measured phase noise that a relatively large flicker noise component is present within the loop. With this in mind, the focus of this discussion shifts to the comparison of the measured phase

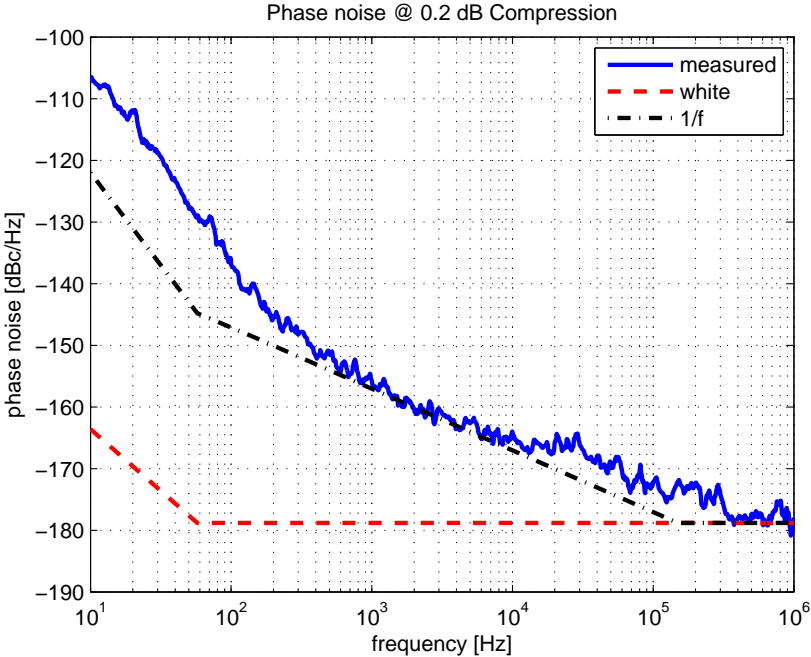


Figure 7.6: Measured and predicted phase noise at 0.2 dB amplifier compression.

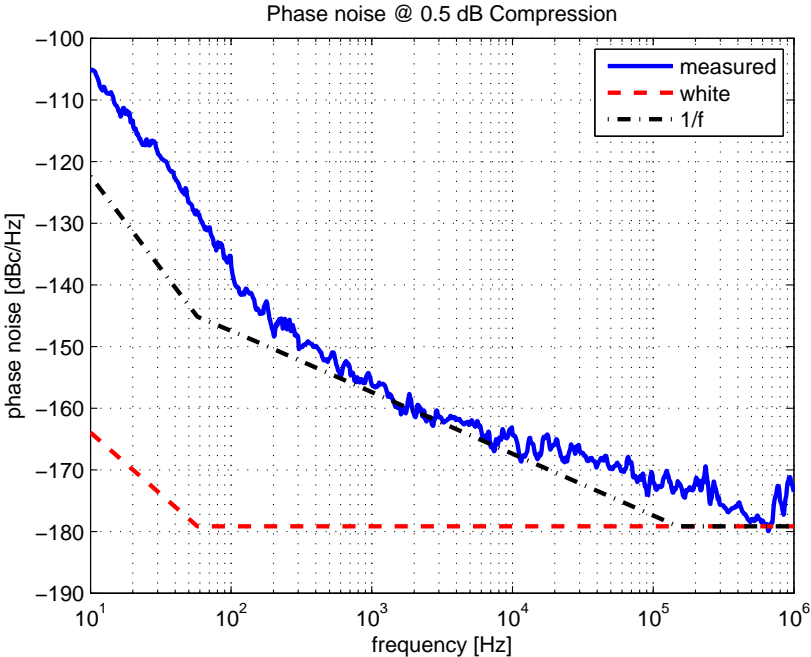


Figure 7.7: Measured and predicted phase noise at 0.5 dB amplifier compression.

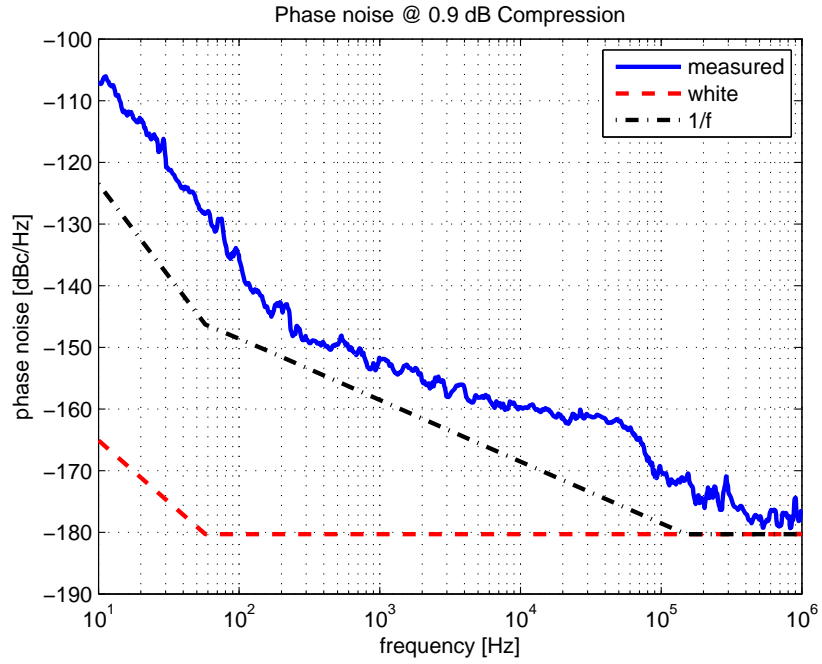


Figure 7.8: Measured and predicted phase noise at 0.9dB amplifier compression.

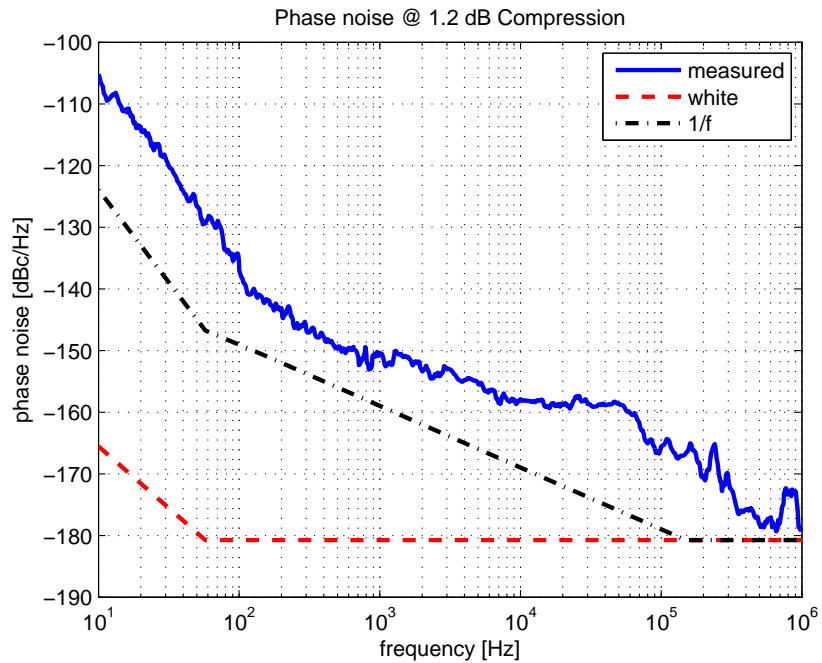


Figure 7.9: Measured and predicted phase noise at 1.2 dB amplifier compression.

noise, depicted by the solid line and the phase noise approximation, which assumes the presence of a flicker noise component. (Depicted by the line with both dots and dashes.) Once again it is shown that as the level of amplifier saturation/compression is increased, so too is the deviation between the measured phase noise and that predicted by Leeson's model.

Also evident is the presence of power source noise between offset frequencies of 10 kHz and 400 kHz. (Noise from voltage supplies and regulators.) In the previous experiment this noise was only visible between 40 kHz and 400 kHz, since it was obscured by the effect of the LC resonator on the phase noise. The effect of this type of noise on the measured phase noise also becomes more distinguishable as the level of amplifier saturation is increased. This was also the case in the previous experiment.

It can also be seen that the Leeson's frequency that was calculated using the crystal resonator's measured data does not compare well with measured phase noise: Compare the measured phase noise with that predicted by Leeson's model in figure 7.5. It can be seen that the measured phase noise assumes a 30 dB/decade dependence at an offset frequency further from the carrier than the predicted Leeson frequency. The same is true for the measurements shown in figures 7.6 to 7.9. This implies that the calculated Leeson frequency must be wrong. This fact could be attributed to the fact that the frequency at which oscillation occurs in the oscillator is not necessarily the same as the resonant frequency of the resonator. As was stated earlier, oscillation will occur at a frequency where both the phase and the gain conditions in the loop are met. It is possible for oscillation to occur at a frequency slightly off the resonant frequency of the resonator. Since the phase condition within the oscillator, at oscillation, may differ from the phase condition at resonance within the resonator, inherently so too must the group delay, and therefore the Leeson frequency.

It is clear from the measurements that phase noise measurements of an oscillator using a resonator with a high quality factor and operating at low levels of amplifier compression, is much less susceptible to mixer pulling between the DUT and phase noise measurer than an oscillator using a low Q resonator under the same conditions.

7.4 Conclusion

Once again it was shown that as the level of amplifier compression decreases, the measured phase noise is better approximated by Leeson's model. It was also shown that the effect of noise inherent to the voltage supplies becomes more prominent

within the phase noise measurements as the amplifier is driven deeper into compression.

The high Q resonator used in this experiment led to a significant improvement in the oscillator's phase noise performance from that of the previous experiment, where a low Q resonator was used. This may be explained using the Leeson equation, equation 3.32. As the loaded Q is increased, the phase noise must decrease. The resonator is only able to affect the phase noise within its half power bandwidth and has no effect on phase noise within the system at offset frequencies outside this band.

A discrepancy between the calculated Leeson frequency and the measurements was pointed out in the previous section. A better estimate of this frequency must be obtained. This will be done in the following chapters.

Another point to be considered, is illustrated in figure 7.10. The solid line indicates the measured phase noise when the amplifier is operating within less than 0.1 dB of saturation. The dashed line depicts the minimum phase noise of the FSUP8 as given by Rohde & Schwarz in its datasheet. This figure shows that the measured phase noise approximates the specified phase noise performance of the machine at some of the offset frequencies. It can therefore be concluded that the phase noise of the oscillator might be lower than that of the machine at these offset frequencies, in which case the measured result would be that of the FSUP8, instead of that of the oscillator.

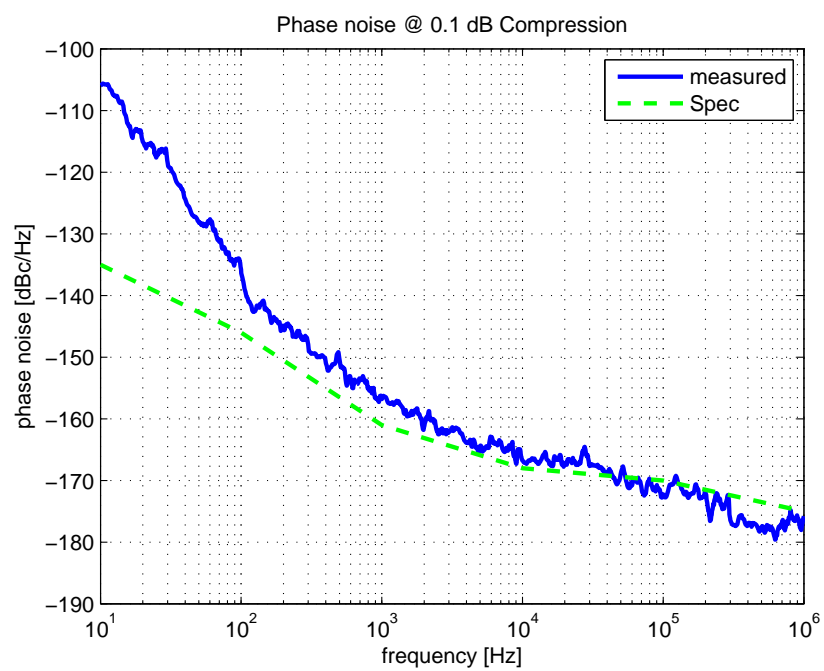


Figure 7.10: Measured phase noise @ 0.1 dB amplifier saturation vs. FSUP8 minimum phase noise specifications.

Chapter 8

Experiment 5:

8.1 Purpose of the Experiment

In the previous two experiments it was shown that noise from the power supplies and/or voltage regulators driving the system had a significant effect on the measured phase noise. In order to negate this occurrence the resistive feedback amplifier used in the previous experiments was modified as is shown in Appendix D.2. The shortcomings of estimating the Leeson frequency by means of the measured bandwidth was also pointed out. This point will be addressed during the following experiment where, instead of the resonator bandwidth, the oscillator's group delay will be used to determine its quality factor.

8.2 Method of the Experiment and Measured Results

The oscillator network is shown in figure 8.1. It uses the same resonator, phase shifter and Wilkinson divider as was used for the experiment in chapter 6.

It was determined that the maximum amount of added attenuation that would still allow oscillation to take place in the network, is 1.2 dB. For this reason the fixed attenuator in figure 8.1 was chosen to be 1 dB and the variable attenuator was set to 0.2 dB. (The same variable attenuator as was used in the previous experiments.)

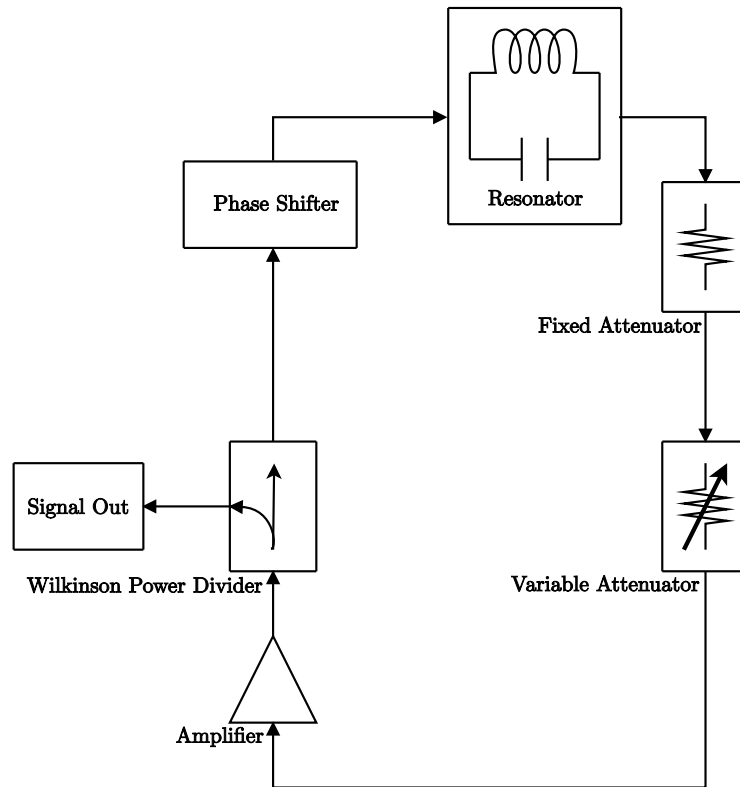


Figure 8.1: The oscillator network

8.2.1 Open Loop Simulations and Measurements

In order to determine the the network's group delay, the oscillator loop must be broken. In this subsection the simulated group delay will be compared with that of the physical system. For both simulation and measurements, consider the output port to be terminated and the loop to be broken between the two attenuators, as is shown in figure 8.2. The frequency at which the circuit will oscillate, should the loop be closed, can be determined using the Barkhausen criterion. Oscillation will occur at a frequency where the total loop gain is greater than 0 dB and the phase deviation is 0° .

First a Spice simulation of the circuit was performed. From these simulations the group delay and passband was extracted for the cases where the amplifier would be operating within 0.1 dB and 0.2 dB of saturation, should the loop be closed. This is shown in figure 8.3 and figure 8.4.

For the simulated oscillator networks, the maximum group delay will occur at the oscillation frequency. This is due to the fact that the phase shift network used, was designed to negate the combined phase shift associated with the amplifier and the power divider. This can be seen figure 8.5, but is not the case for the physical

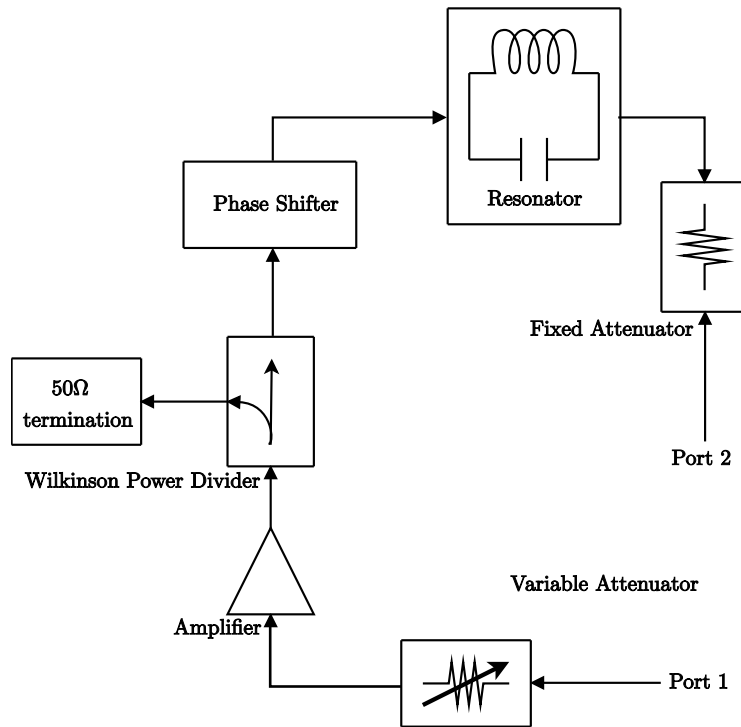


Figure 8.2: The oscillator network with the loop broken

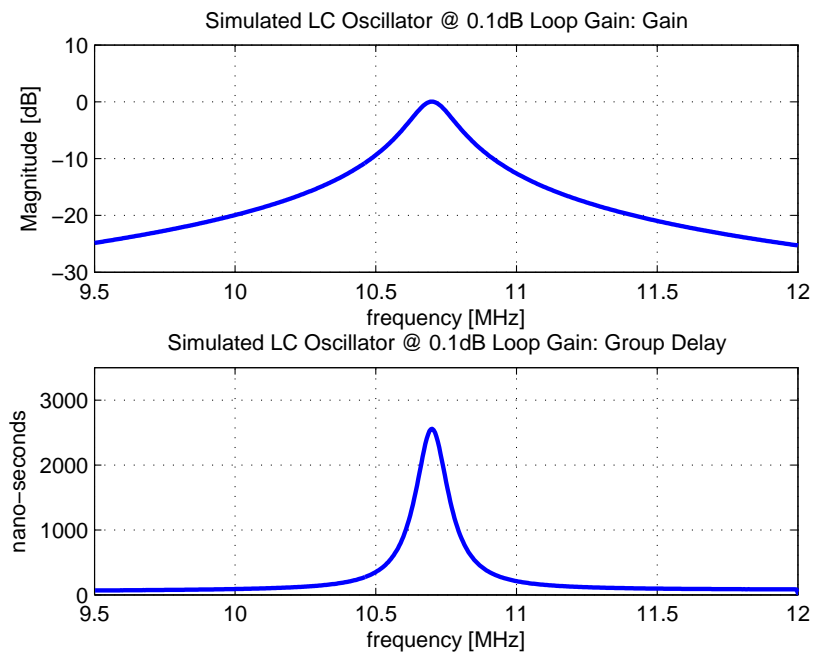


Figure 8.3: Simulated passband and group delay at 0.1 dB open loop gain

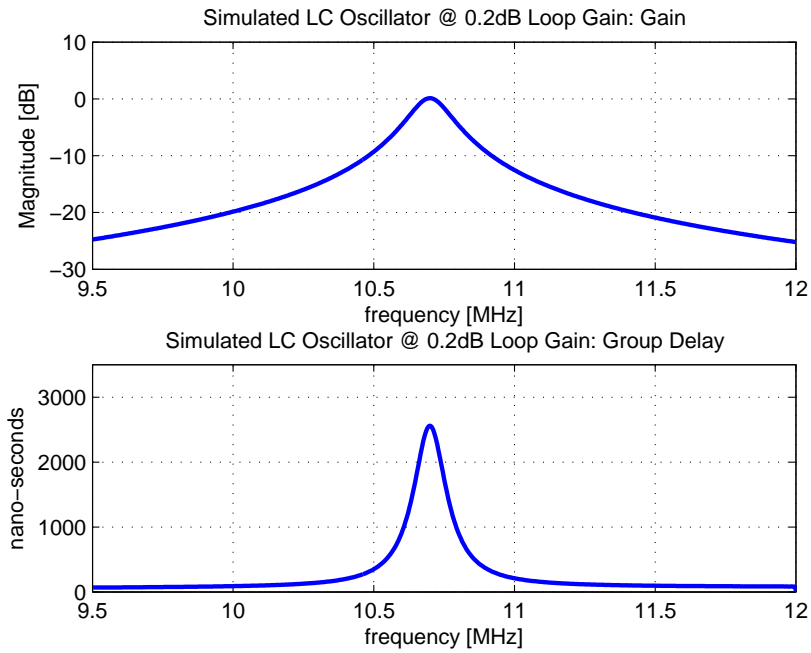


Figure 8.4: Simulated passband and group delay at 0.2 dB open loop gain

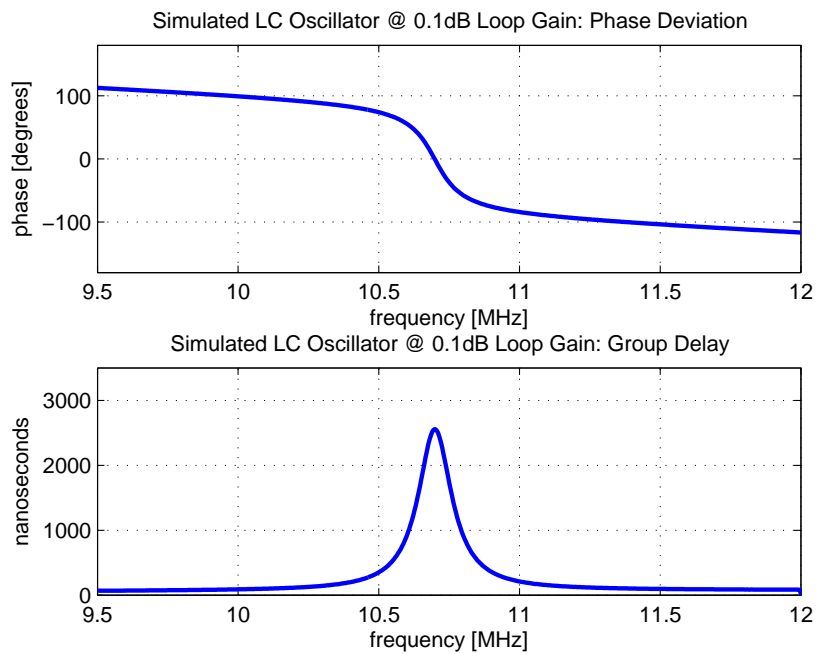


Figure 8.5: Simulated phase deviation and group delay at 0.1 dB open loop gain

network: The phase shift associated with the cables and connectors that connect the different modules have not been taken into account. Their effects will become apparent in the following measurements.

The quality factor of the network at the oscillating frequency can be calculated by using the maximum group delay of the simulated circuit and substituting this value into equation 8.1. This equation was derived in chapter 3.4.

$$Q = \pi f_0 \tau_0 \quad (8.1)$$

By combining equation 8.1 with equation 8.2, which was also derived in chapter 3.4, the Leeson frequency can be determined.

$$f_L = \frac{f_0}{2Q} \quad (8.2)$$

The Q s and Leeson frequencies for the simulated networks that would result in the amplifier operating within 0.1 dB and 0.2 dB of saturation should the loop be closed, were calculated and are indicated in table 8.1.

Table 8.1: Simulated quality factors and Leeson frequencies

Sat. level	τ	Q	f_L
0.1 dB	2557 ns	85.92	62.267 kHz
0.2 dB	2556 ns	85.887	62.292 kHz

The following measurements were taken using a calibrated ZVB VNA from Rhode & Schwarz. Figure 8.6 illustrates the open loop pass band of the circuit, as well as its group delay for the circuit conditions under which the amplifier would be operating within 0.1 dB of saturation should the loop be closed. Ideally the frequency at which the maximum group delay occurs (and therefore the maximum quality factor) will coincide with the oscillating frequency, as was the case with the simulated results. Figure 8.7, however, indicates that this is not the case in this loop network, since the frequency at which the phase condition for oscillation is satisfied differs from the frequency at which the group delay is at its maximum.

The measurements appear to indicate that the loop gain condition for oscillation is not satisfied at the frequency where the phase condition is satisfied. This could be attributed to the measurement uncertainty that inherently occurs during two port measurements. The degree of uncertainty can be calculated in terms of the VSWR or the reflection coefficients, measured at the measurement ports by means of the

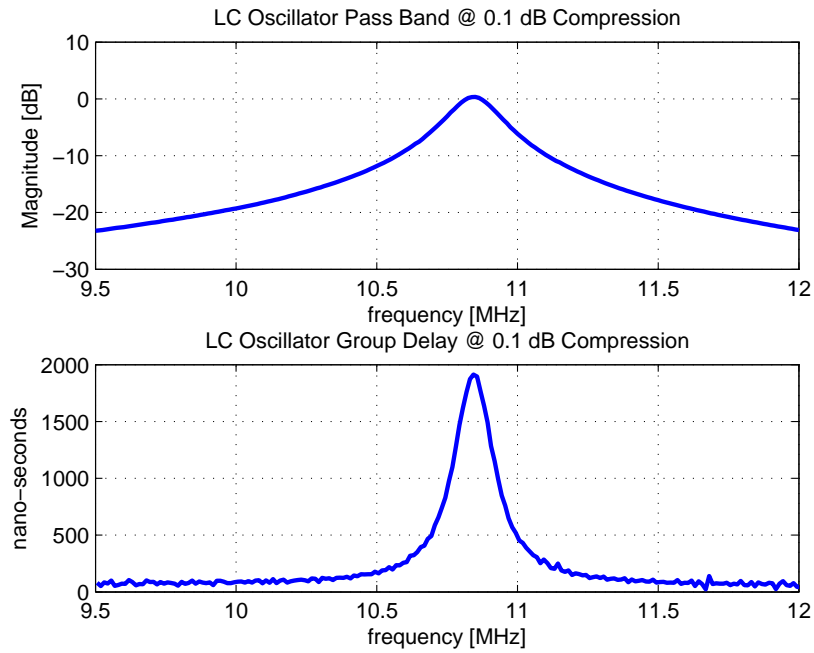


Figure 8.6: Measured passband and group delay at 0.1 dB open loop gain

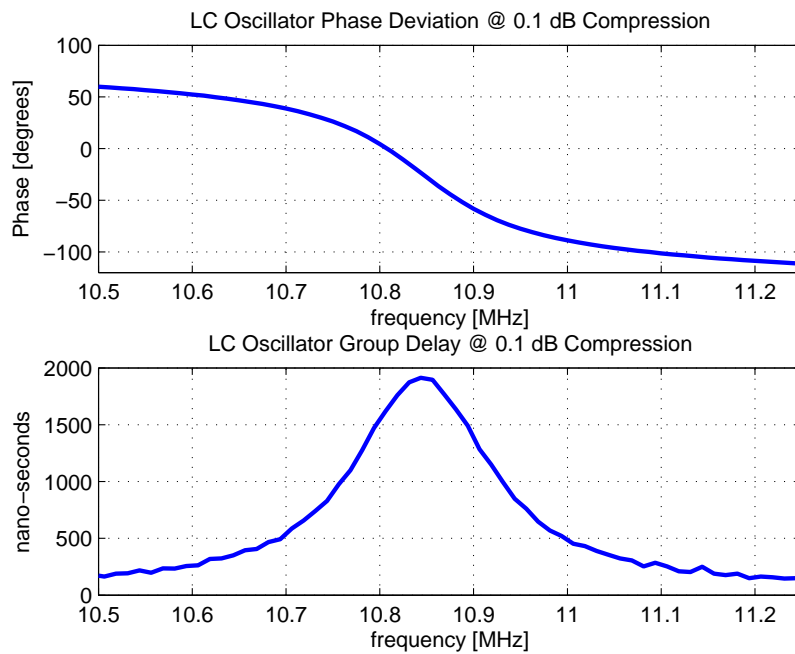


Figure 8.7: Measured phase deviation and group delay at 0.1 dB open loop gain

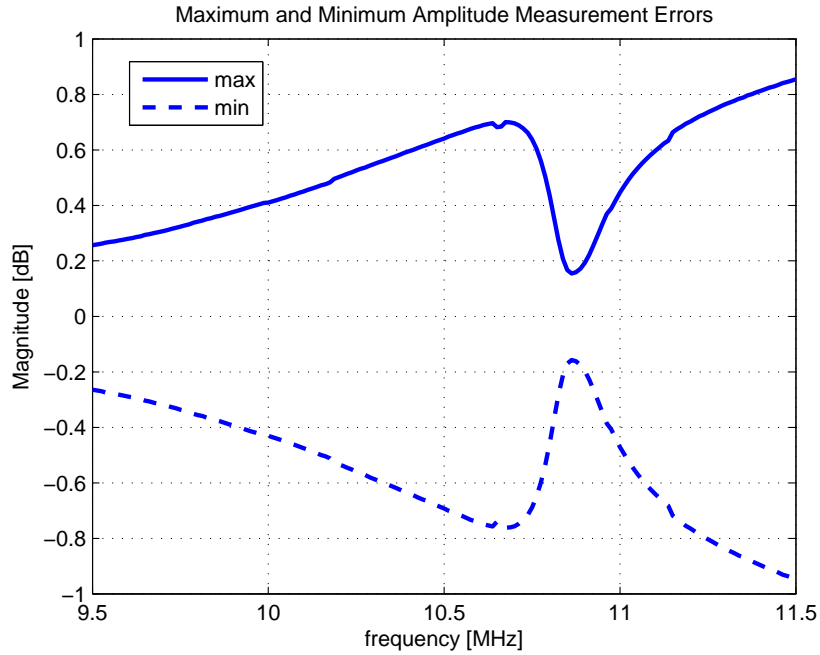


Figure 8.8: Calculated maximum and minimum amplitude measurement errors at 0.1 dB amplifier saturation

following equation[18],[19].

$$A_{error} = 20 \times \log (1 \pm |S_{11}S_{22}|) \quad (8.3)$$

In equation 8.3, A_{error} represents the maximum and minimum error that may occur as a result of mismatches between the DUT and the VNA's ports. By implementing equation 8.3 for the measured reflection coefficients of the network, while the amplifier is operating within 0.1 dB of saturation, the maximum and minimum errors for all frequencies in the band of interest can be calculated. This is illustrated in figure 8.8. These graphs indicate that the S_{21} or pass band measurement might be off by as much as ± 0.355 dB. Should this be taken into account, the gain condition for oscillation is also met.

The group delay measured at 10.815 MHz, the frequency where the phase condition is satisfied, is found to 1619 ns. Substituting these values into equation 8.1 yields a quality factor of 54.98. From this the Leeson frequency is calculated using equation 8.2 and is found to be 98.3 kHz.

The process was repeated for the case where the amplifier is operating within 0.2 dB of saturation. These measurements are illustrated in figures 8.9 through 8.11. The resulting Leeson frequency is shown in table 8.2. Note that the ultimate phase noise

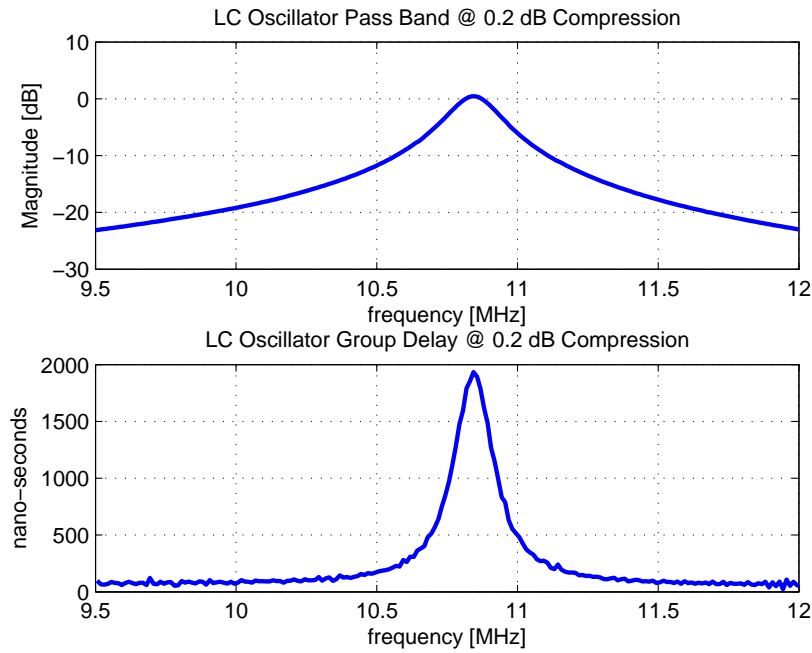


Figure 8.9: Measured passband and group delay at 0.2 dB open loop gain

was determined using the same method as was used in the previous experiments. The maximum calculated amplitude errors are shown in table 8.3.

Table 8.2: Open loop data at the oscillation frequency

Sat level	f_0	τ_0	Q	f_L	Ult. Phase Noise
0.1 dB	10.815 MHz	1619 ns	54.98	98.3 kHz	-173.33 dBc/Hz
0.2 dB	10.810 MHz	1593 ns	54.099	99.9 kHz	-176.69 dBc/Hz

Table 8.3: Maximum calculated error in amplitude measurement

Sat. level	S_{11}	S_{22}	A_{error}
0.1 dB	-14.09 dB	-13.51 dB	0.355 dB
0.2 dB	-13.49 dB	-13.53 dB	0.3788 dB

Significant differences exist between the measured and the corresponding simulated open-loop results. These differences could be minimised if the path lengths of the cables and the connectors were taken into account. The spice simulation also assumed lossless components. A difference in the oscillation frequencies of the simulated and measured results was also indicated. This may be attributed to an alteration of the loop spacings of the resonator's inductor, that could have occurred during the handling of the oscillator. Another contributing factor to the difference in frequency

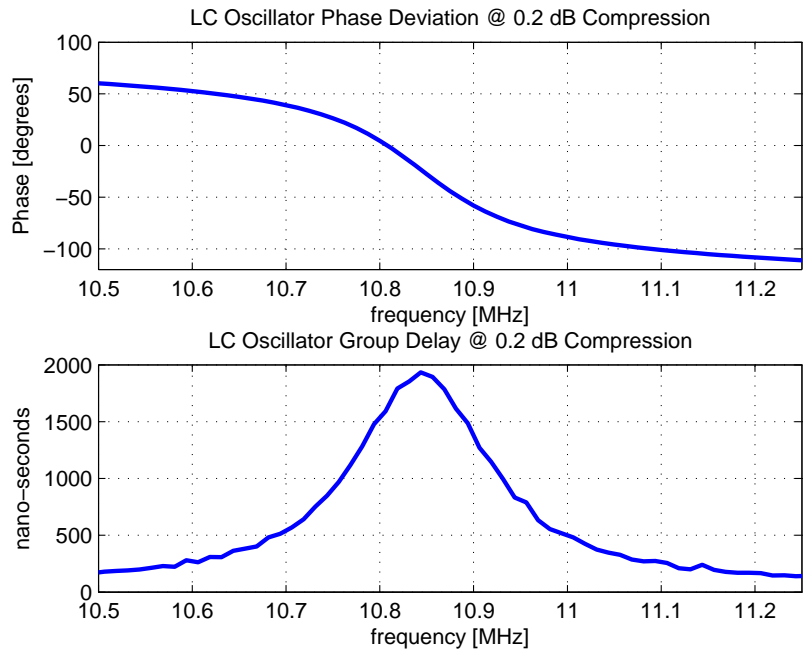


Figure 8.10: Measured phase deviation and group delay at 0.2 dB open loop gain

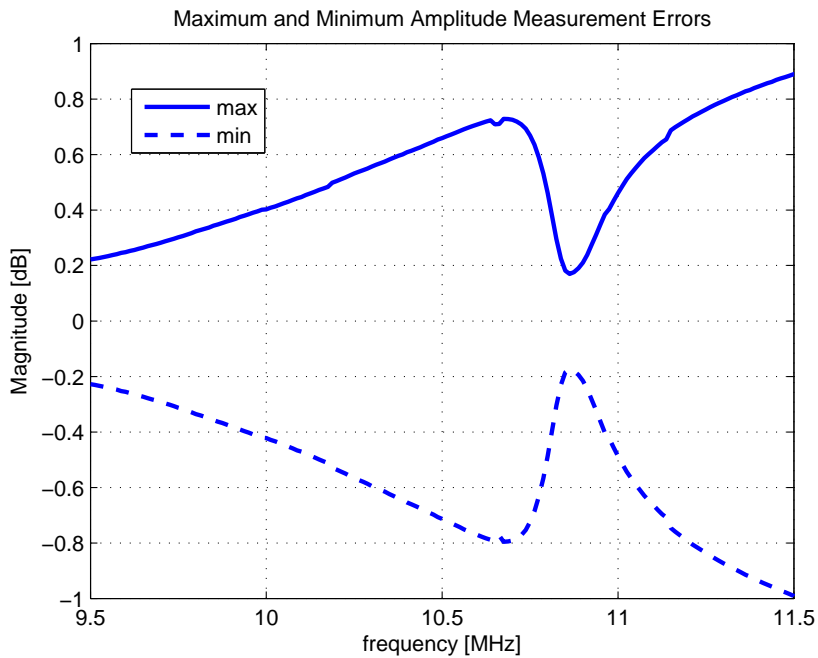


Figure 8.11: Calculated maximum and minimum amplitude measurement errors at 0.2 dB open loop gain



Figure 8.12: Oscillator measurements with FSUP8

would be the previously mentioned added phase shift that resulted from the cables and connectors that connect the different modules.

8.2.2 Phase Noise Measurements

The loop was subsequently closed again and two phase noise measurements were taken using an FSUP8 signal-source analyser, as shown in figure 8.12. These are, respectively, for the scenarios where the amplifier is operating within 0.1 dB and 0.2 dB of saturation. These measurements are depicted by the solid lines in figures 8.13 and 8.14. Once again the bandwidth of the phase noise meter's pll was set to 300 Hz. As was the case in chapter 6, some mixer pulling between the phase noise meter's VCO and the DUT is evident in both of the previously mentioned figures at offset frequencies below this bandwidth.

The dashed line in figures 8.13 and 8.14 represents the Leeson approximation of the phase noise, should the amplifier be driven to within 0.1 dB and 0.2 dB of saturation respectively. Note that these approximations assume a white noise distribution entering the network. These are relatively good approximations of the phase noise. It must, however, be taken into account that the ultimate phase noise was calculated using the assumption that oscillation will occur at the frequency where the resonator's passband is at a maximum. Figures 8.7 and 8.10, however, clearly illustrate that the oscillators' phase conditions are not met at the frequency where the magnitude of the loop pass bands is greatest. Therefore, it may be assumed that the ultimate noise floor is, in fact, larger than anticipated. Adding an additional 3 dB to the ultimate phase noise result in the Leeson approximations depicted with the

dash-dot line in figures 8.13 and 8.14. These lines are near perfect approximations of the measured phase noise at offset frequencies greater than 1 kHz from the carrier.

8.3 Conclusion

Special precautions were taken in order to remove noise from the power sources and regulators. This resulted in less noise entering the system and allows for the elimination of some noise source uncertainties. These are not as apparent when using a low Q resonator, since most of the phase noise effects resulting from source noise are obscured by the resonator's passband.

In this chapter a method of determining the group delay of the oscillator network was introduced by breaking the oscillator loop and terminating its output. It was shown that the group delay measurement serves to obtain a much better approximation of the network's Q and therefore also of its Leeson frequency. Using this method, the author was able to fit a Leeson approximation that closely resembles the measured phase noise data. Allowing for a 3 dB error in the calculation of the ultimate phase noise floor resulted in a near perfect approximation of the measured phase noise.

Perhaps the most significant conclusion that may be drawn from this experiment is the following: For low Q , linearly driven oscillator networks, in the absence of

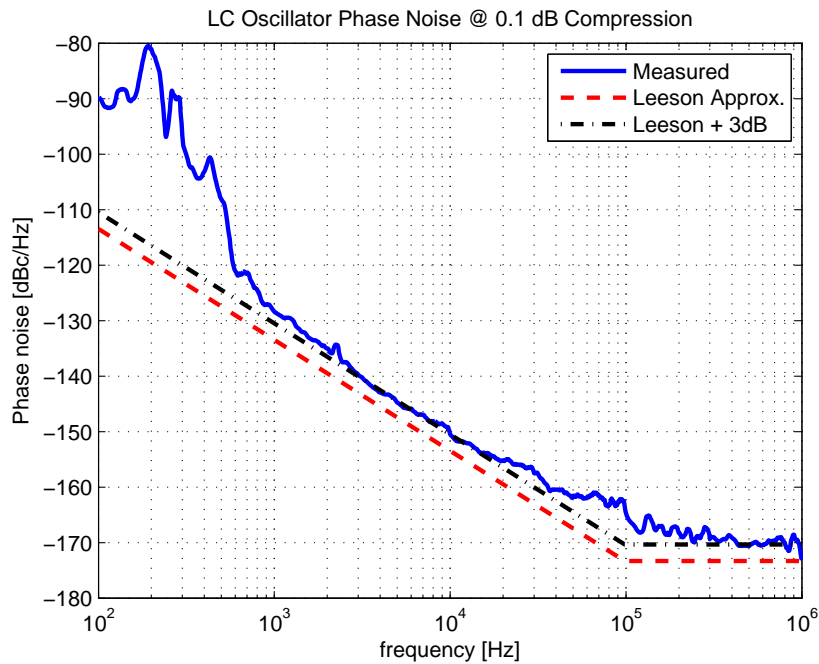


Figure 8.13: Phase noise @ 0.1 dB amplifier saturation.

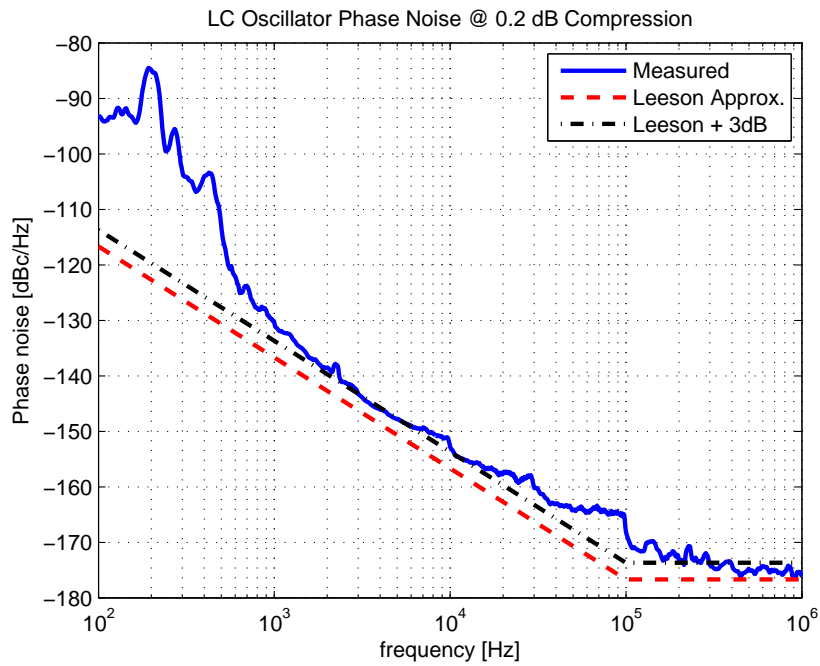


Figure 8.14: Phase noise @ 0.2 dB amplifier saturation.

power source noise, a very accurate approximation of the measured phase noise can be made using Leeson's model. Of further note is that even when assuming that the noise distribution entering the resonator is white, this model maintained its accuracy at offset frequencies greater than 1 kHz.

Chapter 9

Experiment 6:

9.1 Purpose of the Experiment

This experiment acts as a continuation of the experiment performed in chapter 8. Here the low Q resonator of the previous experiment is replaced with the high Q resonator characterised in Appendix D.3. This resonator differs from the one used in chapter 7 in that an AT-cut crystal is used instead of a SC-cut crystal. The reason for this was noted in the conclusion of chapter 7. The reduction of the resonator's Q (by using an AT-cut crystal instead of an SC-cut crystal), leads to a deterioration of the phase noise performance of the oscillators in which it is used. The phase noise performance will therefore be inferior to that of the FSUP8 signal-source analyser, which means that this machine will be capable of accurately measuring the phase noise performance of the following oscillator networks.

The same method used in the previous experiment to determine the Leeson frequency, is applied here again. The purpose of this experiment is to verify that, should this method of determining the Leeson frequency be used, Leeson's model

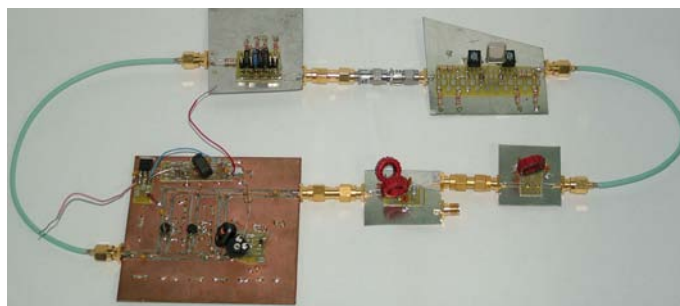


Figure 9.1: Oscillator network using an AT-cut crystal resonator

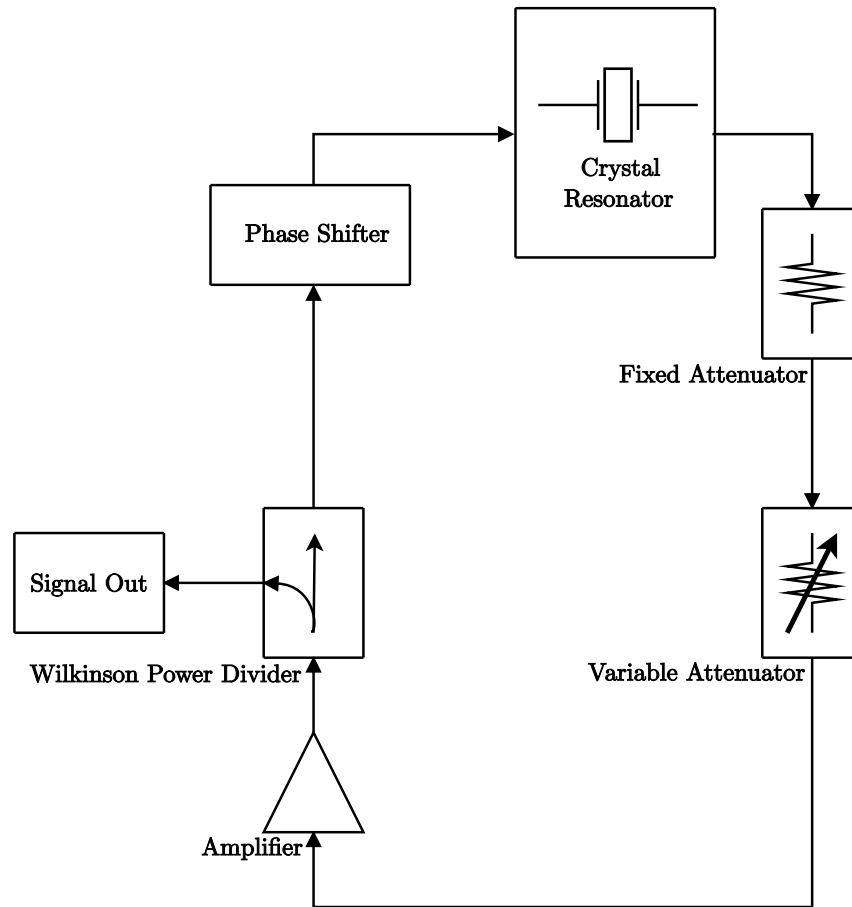


Figure 9.2: The oscillator network

accurately approximates the measured phase noise of this linearly driven oscillator with a high Q resonator.

9.2 Method of the Experiment

The oscillator network used is depicted in figure 9.2. The amplifier, phase shifter and Wilkinson divider are the same modules that were used in the previous experiment. As mentioned previously, the resonator used is the one described in Appendix D.3.

The maximum amount of added attenuation at which oscillation will still occur, was found to be 4.5 dB. This was determined by the same means as described in the previous chapter. This added attenuation comprises a fixed 4 dB attenuator along with the variable attenuator of the previous chapters, set to 0.5 dB.

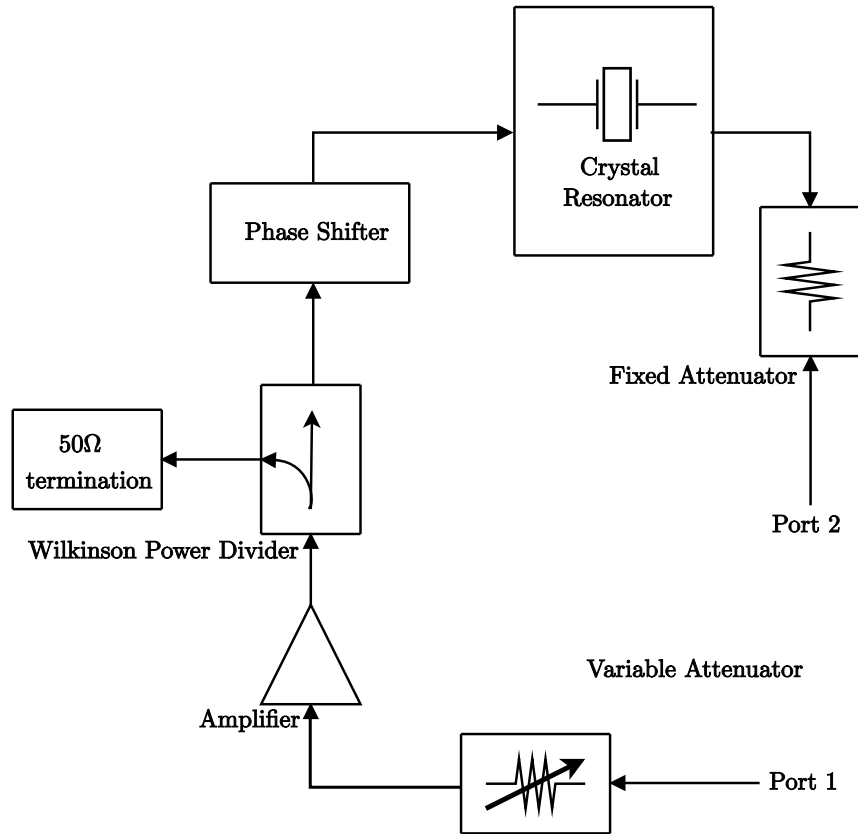


Figure 9.3: The Oscillator network with the loop broken

9.2.1 Open Loop Measurements

As in the previous chapter, the oscillator loop was broken between the two attenuators, as is illustrated in figure 9.3. This was done in order to determine the group delay of the network and thereby also its quality factor.

First consider the case where the network has less than 0.1 dB of open loop gain (when the variable attenuator is set to 0.5 dB attenuation). The measured open loop gain and phase deviation of this circuit is shown in figure 9.4. From these graphs the oscillating frequency of the network, should the loop be closed, is determined to be 10.2409 MHz.

Figure 9.5 depicts the measured group delay of the network. From it, the group delay at the oscillating frequency was read and found to be $19.93 \mu\text{s}$. By substituting the measured group delay (τ_0) and oscillating frequency (f_0) into equation 8.1, given again below, the quality factor is calculated to be

$$\begin{aligned} Q &= \pi f_0 \tau_0 \\ &= 641.2 \end{aligned}$$

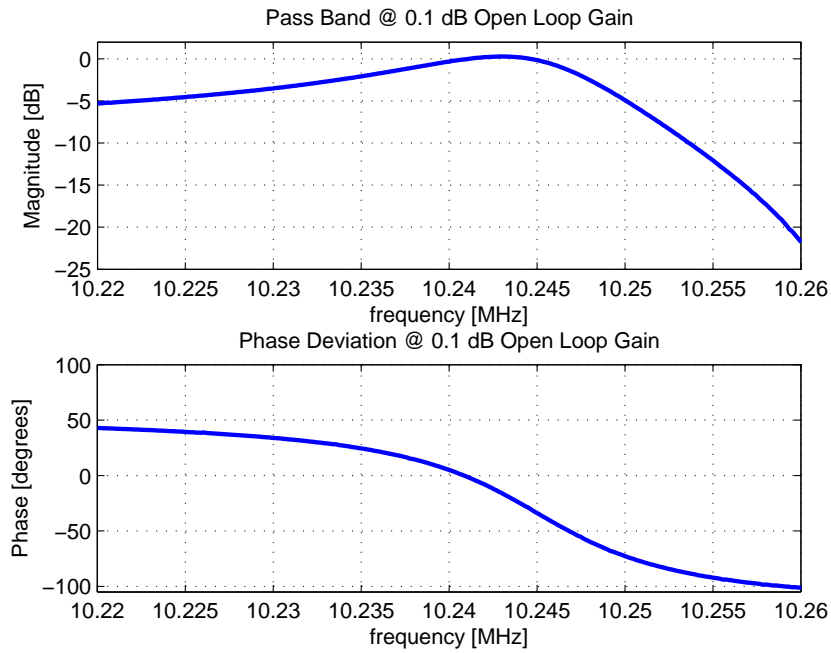


Figure 9.4: Oscillation conditions @ 0.1 dB open loop gain

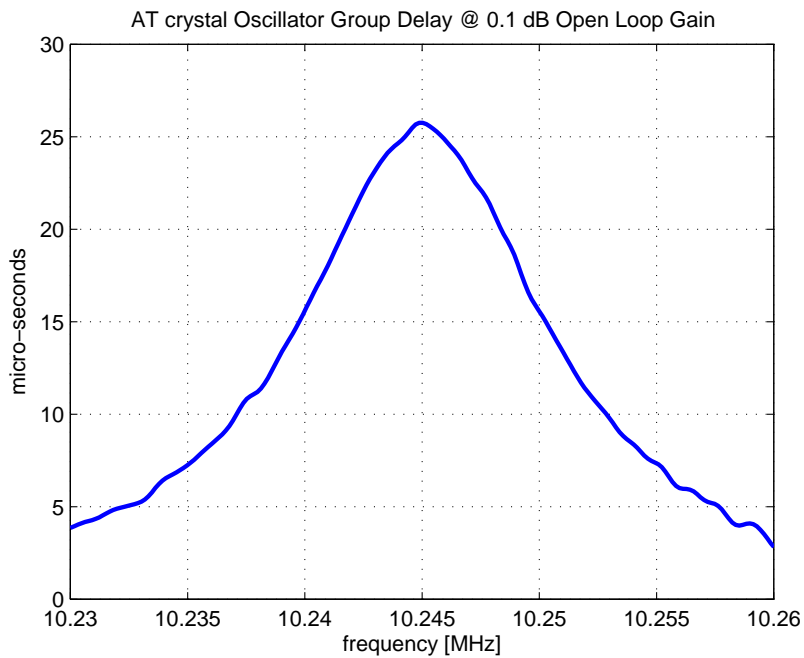


Figure 9.5: Group delay @ 0.1 dB open loop gain

Subsequently the Leeson frequency is determined by substituting Q into equation 8.2 (given below)

$$\begin{aligned} f_L &= \frac{f_0}{2Q} \\ &= 7.986 \text{ kHz} \end{aligned}$$

Next the losses that occur within the resonator, at the oscillating frequency is obtained. This can be read from figure D.15 or figure D.16 in Appendix D.3 and was found to be 4.544 dB. Given that the loss of a passive circuit is equal to its noise figure, the noise figure of the resonator at the oscillating frequency is 4.544 dB. With this information the system noise figure can be determined by using the equations for cascaded noise given in chapter 6.3.1. This noise figure (NF) was calculated to be $NF = 14.2318$ dB.

The loop was then closed in order to measure the magnitude of the oscillator's output signal (P_{signal}). This was measured and found to be 11.85 dBm

The ultimate phase noise ($\mathcal{L}_{ultimate}$) can subsequently be calculated using equation 9.1, which can be obtained from equations 6.1, 6.2 and 6.3.

$$\mathcal{L}_{ultimate} = -177 + NF - P_{signal} \quad (9.1)$$

For the oscillator network, with the amplifier operating within 0.1 dB of saturation, $\mathcal{L}_{ultimate} = -174.62$ dBc

Similarly the group delay, quality factor, Leeson frequency and ultimate phase noise can be determined for the cases where the oscillator's amplifier is operating at 0.2 dB, 0.3 dB, 0.4 dB and 0.5 dB into compression, from the data depicted in figures 9.6 through 9.13. Otherwise stated, the previously mentioned criteria can be determined for the scenarios where the open loop gain of the network is set to 0.2 dB, 0.3 dB, 0.4 dB and 0.5 dB respectively. This is done by switching the variable attenuator from 0.4 dB to 0.1 dB attenuation in steps of 0.1 dB.

The Leeson frequency, at the previously mentioned levels of open loop gain, and the determined criteria needed to calculate it, are listed in table 9.1. Table 9.2 lists the ultimate phase noise at these open loop gain levels, along with the necessary variables to calculate it.

9.2.2 Phase Noise Measurements

From the values in tables 9.1 and 9.2, phase noise approximations can be made using Leeson's model, at the previously specified levels of amplifier saturation.

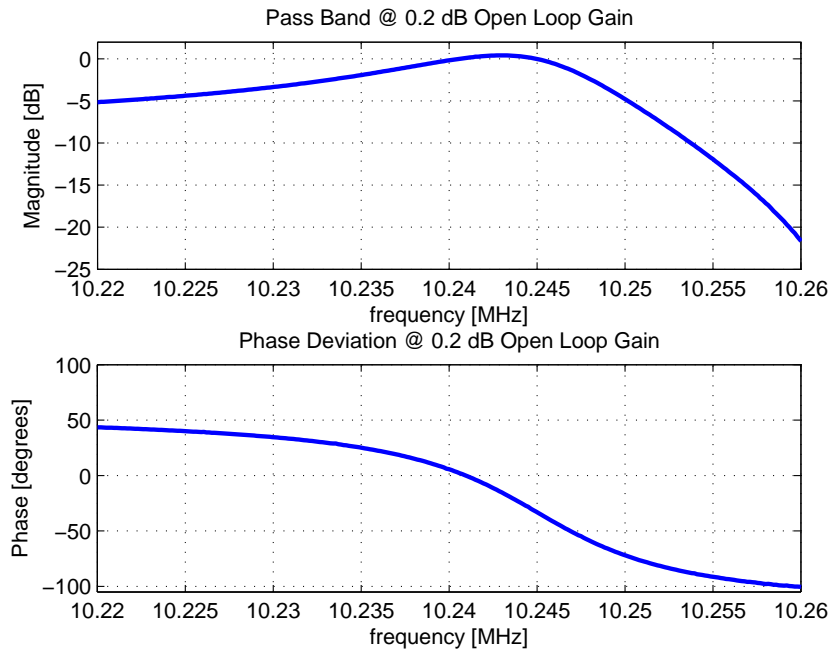


Figure 9.6: Oscillation conditions @ 0.2 dB open loop gain

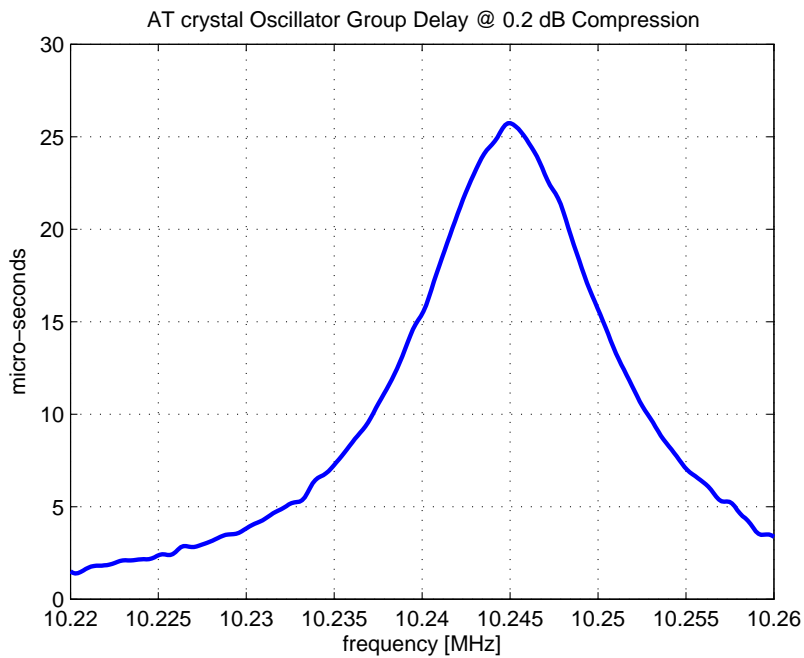


Figure 9.7: Group delay @ 0.2 dB open loop gain

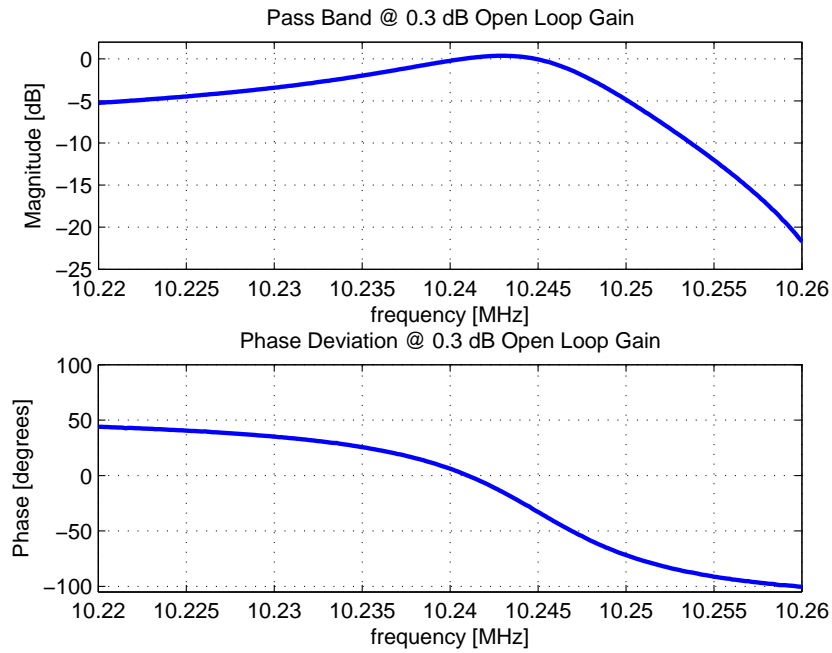


Figure 9.8: Oscillation conditions @ 0.3 dB open loop gain

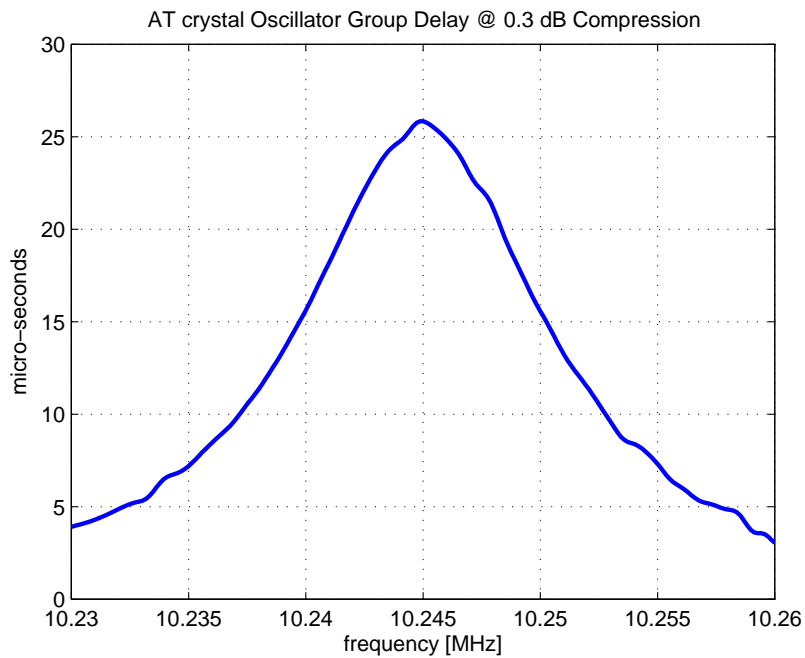


Figure 9.9: Group delay @ 0.3 dB open loop gain

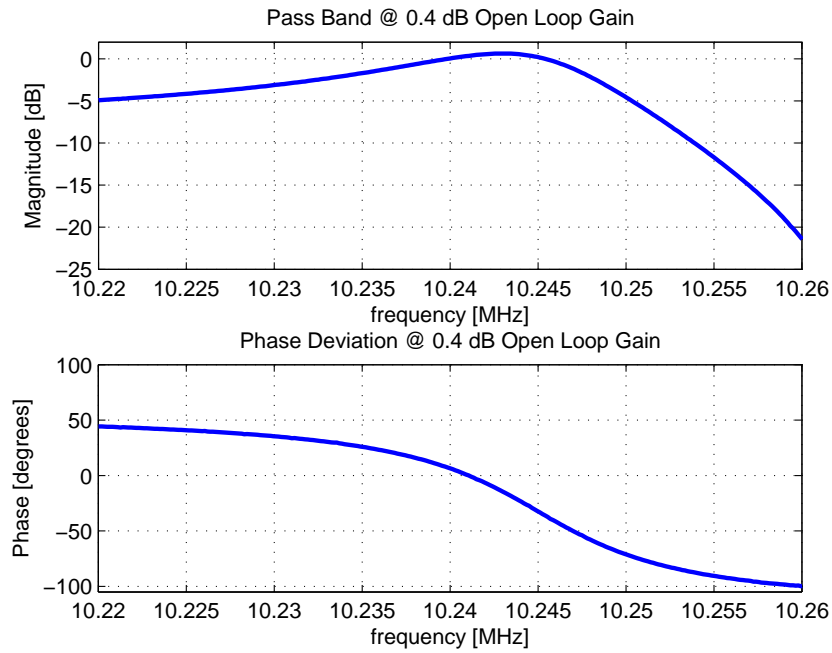


Figure 9.10: Oscillation conditions @ 0.4 dB open loop gain

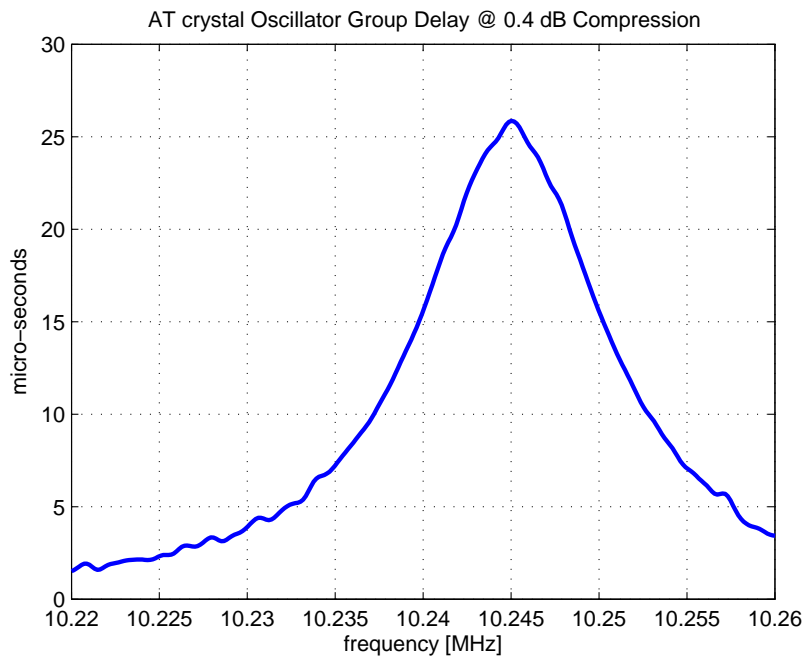


Figure 9.11: Group delay @ 0.4 dB open loop gain

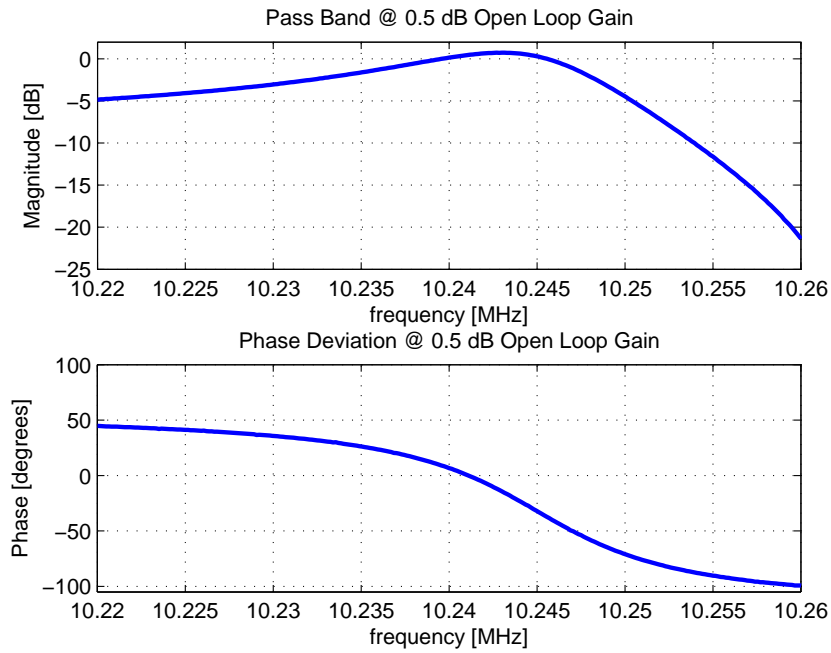


Figure 9.12: Oscillation conditions @ 0.5 dB open loop gain

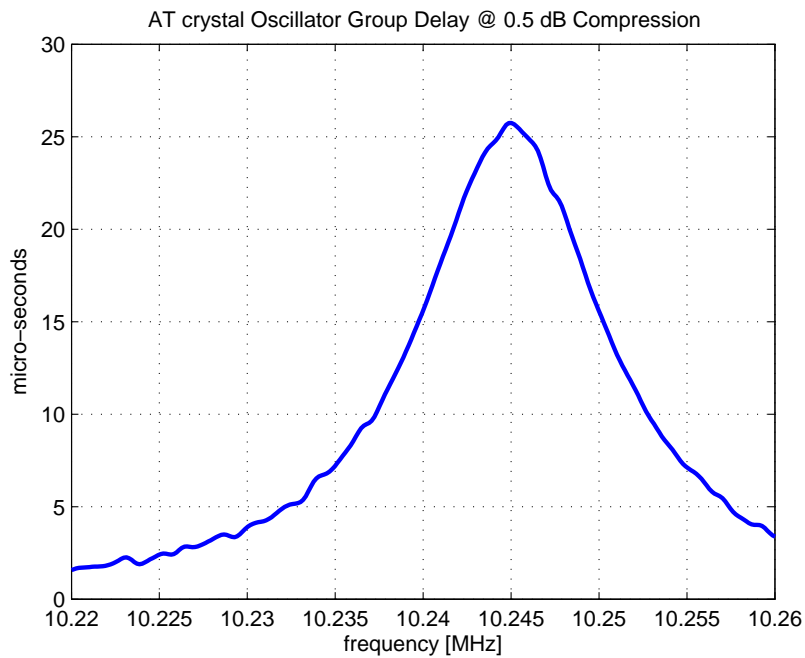


Figure 9.13: Group delay @ 0.5 dB open loop gain

Table 9.1: Leeson frequency and related variables @ various open loop gains

Gain	f_0	τ_0	Q	f_L
0.1dB	10.2409MHz	19.93 μ s	641.2	7.985kHz
0.2dB	10.24105MHz	18.65 μ s	593.76	8.624kHz
0.3dB	10.24105MHz	18.345 μ s	590.22	8.676kHz
0.4dB	10.249MHz	17.8 μ s	572.67	8.941kHz
0.5dB	10.24105MHz	18.33 μ s	589.73	8.683kHz

Table 9.2: Ultimate phase noise and related variables @ various open loop gains

Gain	NF_{res}	NF_{system}	P_{signal}	$\mathcal{L}_{ultimate}$
0.1dB	4.544dB	14.197dB	11.85dBm	-174.62dBc
0.2dB	4.522dB	14.112dB	13.99dBm	-176.88dBc
0.3dB	4.522dB	14.014dB	14.31dBm	-177.30dBc
0.4dB	4.544dB	13.994dB	15.06dBm	-178.12dBc
0.5dB	4.522dB	13.818dB	14.89dBm	-178dBc

Assuming that the noise power entering the resonator has a white spectrum, these approximations, at the indicated levels of amplifier saturation, will be depicted by the dashed lines in the following figures. (Figures 9.14 to 9.18) The solid lines in figures 9.14 through 9.18 represent the measured phase noise at these amplifier saturation levels.

First consider the scenario where the amplifier is operating less than 0.1 dB into compression. Here the amplifier operates in a near linear fashion and only allows for very small frequency harmonics to be present at the oscillator's output and, therefore, in the oscillating loop as well. This means that very little of the noise present near integer multiples of the oscillation frequency, is capable of being mixed down into the frequency band around the desired oscillating frequency. In this case Leeson's model should be a very accurate approximation of the actual phase noise of the oscillator. The measured phase noise, as well as that predicted by Leeson's model for this scenario, are illustrated in figure 9.14. As can be seen, the model correctly approximates the ultimate phase noise. However, it does not make provision for the effect that the transistors' flicker noise has on the measured phase noise. Had the flicker noise corner frequency been known before the measurement was taken, it could have been taken into account. Here, however, the point was not to determine the flicker corner frequency from the measured data, but to predict what the measured phase noise spectrum would look like using only Leeson's model. Figure 9.14 clearly shows that at offset frequencies greater than 1 kHz the model is indeed very accurate, with a slight discrepancy between the measured and predicted

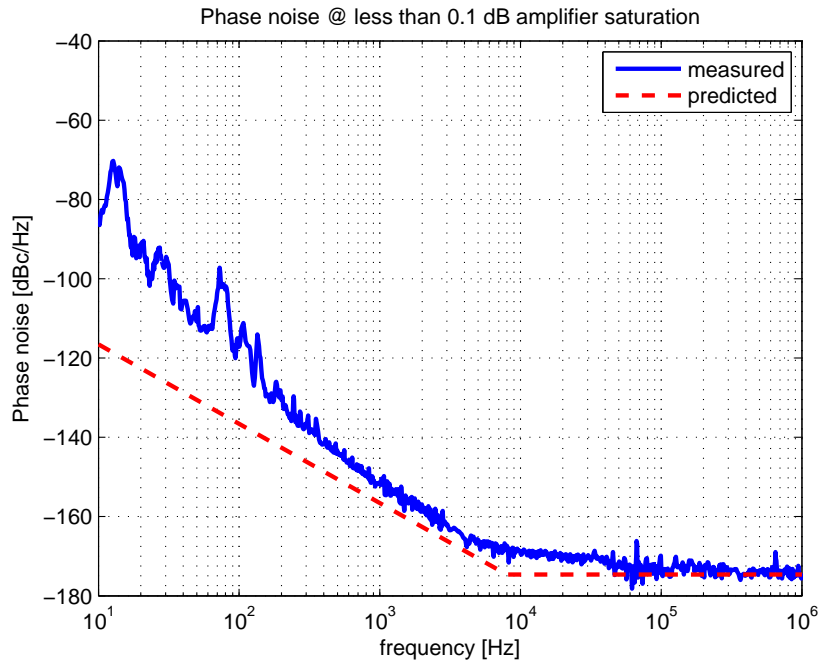


Figure 9.14: Measured and predicted phase noise @ 0.1 dB amplifier saturation

results in the offset frequency region of 3 kHz to 50 kHz. This discrepancy can be attributed to the phase noise of the FSUP8 being greater than that of the oscillator in this region. At offset frequencies smaller than 1 kHz the effect of the previously mentioned flicker noise becomes apparent and the measured phase noise starts to diverge from that which was predicted.

Figures 9.15 through 9.18 demonstrate how the measured and predicted phase noise differ by an increasing degree as the level of saturation, within which the amplifier is operating, is increased. This deviation is especially apparent at offset frequencies closer to the carrier, as is illustrated by figure 9.19.

It can also be seen that measurement errors, resulting from phase noise of the measurement equipment, become more pertinent as the level of saturation is increased. (Although this is more likely as a result of the oscillators' ultimate phase noise being lower than that of the measurement equipment, than as a result of any mixing products that can occur.) Also note that the loop bandwidth of the FSUP8's PLL was set to 100 Hz and that it is possible for mixer pulling to have an effect upon the measured phase noise at offset frequencies smaller than this bandwidth.

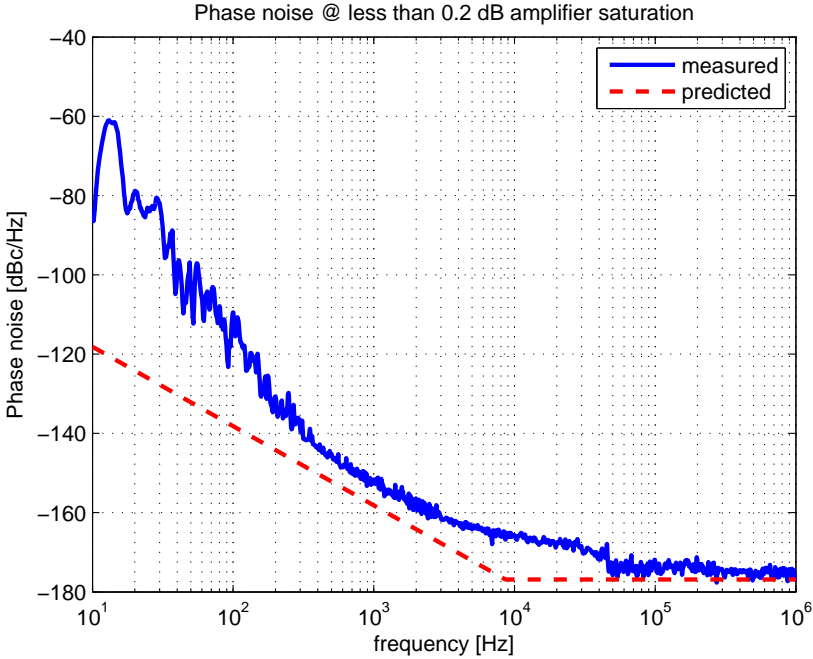


Figure 9.15: Measured and predicted phase noise @ 0.2 dB amplifier saturation

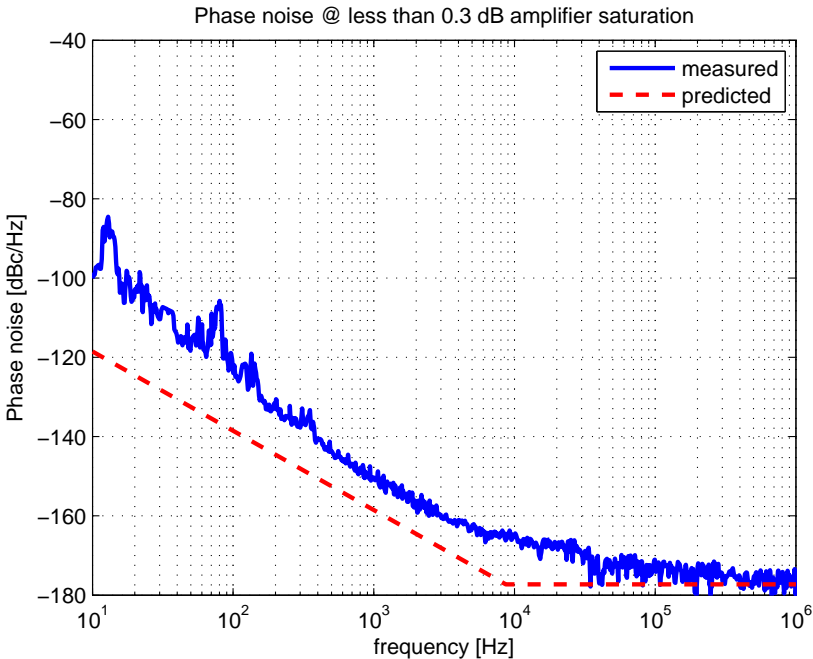


Figure 9.16: Measured and predicted phase noise @ 0.3 dB amplifier saturation

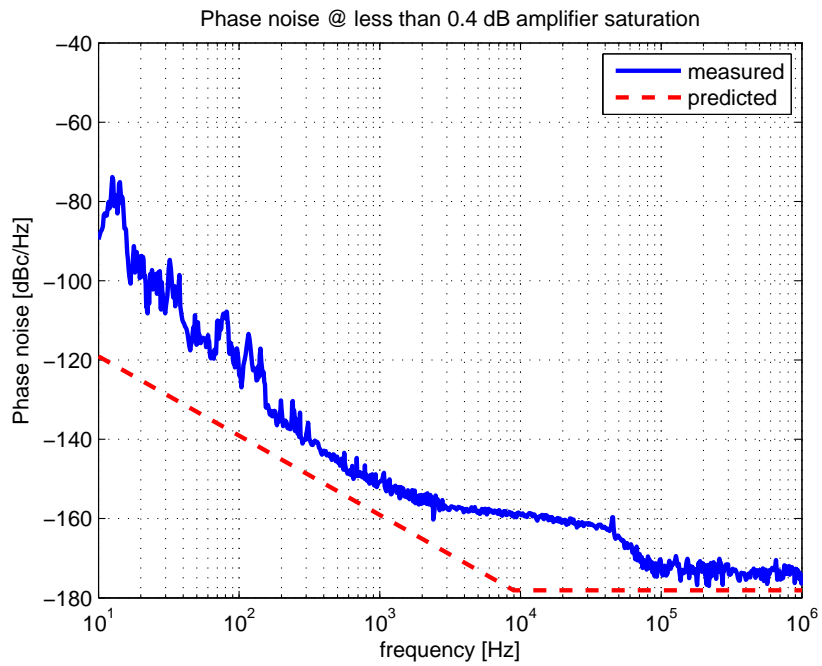


Figure 9.17: Measured and predicted phase noise @ 0.4 dB amplifier saturation

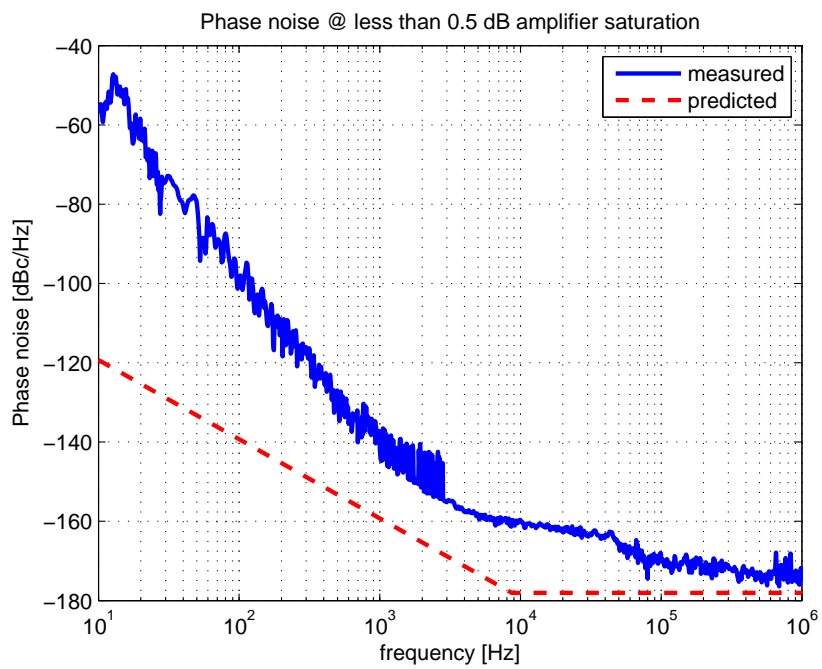


Figure 9.18: Measured and predicted phase noise @ 0.5 dB amplifier saturation

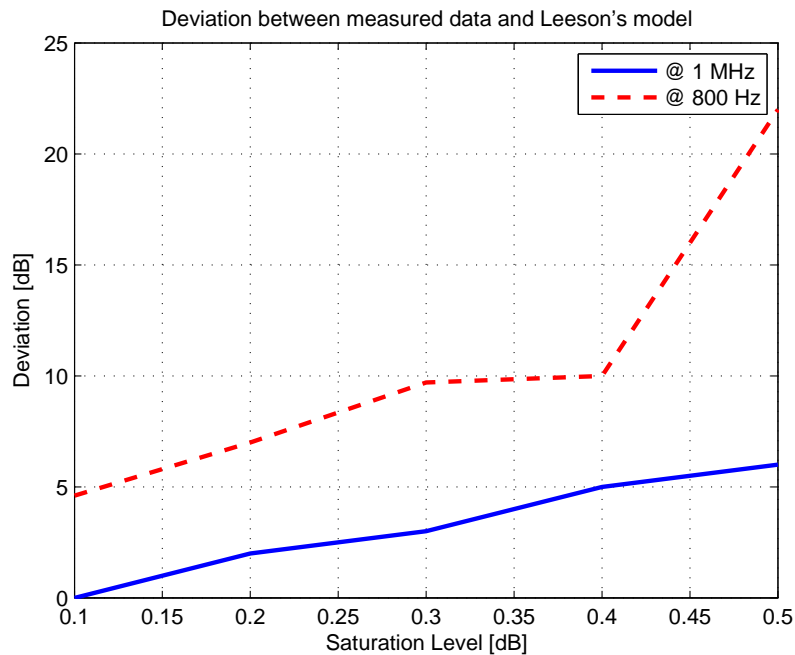


Figure 9.19: The deviation between the measured phase noise and that predicted by Leeson's model at offset frequencies of 1 MHz and 800 Hz.

9.3 Conclusion

When the amplifier is operating within 0.1 dB of compression, Leeson's model provides a very accurate approximation of the measured phase noise. Even when operating within 0.2 dB of compression, this approximation is still good. Figures 9.14 through 9.18, however, demonstrates that this model rapidly loses accuracy as the amplifier is driven deeper into saturation. In other words, the effective noise figure, mentioned in chapter 3.4, becomes larger as the amplifier, or active device, is driven deeper into saturation. This is attributed to an increase in the magnitude of the oscillator's harmonics as saturation sets in, which subsequently allows for noise at frequencies near these harmonics to be mixed into the frequency band around the oscillation frequency of interest.

Should a very accurate circuit model of the oscillator network be available, it would be possible to determine the Leeson frequency through simulation. Such a model would, however, have to factor in the effects of transmission paths upon the phase deviation within the network. This implies that the smaller the oscillator loop (physically), the greater the likelihood of an accurate model being obtained.

The method discussed in this chapter proved that using the open loop group delay of the oscillator network is an accurate means of obtaining an oscillator's Leeson

frequency. It was also shown that, once the magnitude of the oscillator's output signal is known, it is possible to predict its ultimate phase noise. This is, however, only valid when the oscillator's active device is operating in a very linear manner (within 0.2 dB of compression).

Note that no way was found to predict the magnitude of the oscillator's output signal. The author expected the magnitude of the output signal to be 13.72 dBm, using the following argument: The 0.1 dB saturation point of the amplifier occurs at an output signal magnitude of approximately 17 dBm, as shown in Appendix D.2. The loss of the power divider that follows this amplifier in the oscillator network is 3.28 dB. Therefore, if the amplifier is operating within 0.1 dB of saturation, as was determined in the experiment, the magnitude of the output signal should be $17 \text{ dBm} - 3.28 \text{ dBm} = 13.72 \text{ dBm}$, and not 11.85 dBm as was measured.

This does not, however, negate the fact that circumstances have been identified under which Leeson's model may be considered valid and accurate for both high Q (this chapter) and low Q (the previous chapter) oscillator networks.

Chapter 10

Final Conclusions and Future Work

10.1 Conclusions

The focus of this project has been to identify conditions under which Leeson's model could be considered accurate without the use of an *effective noise figure*, thereby validating Leeson's model and providing greater insight into the mechanism that leads to the occurrence of phase noise in oscillators. This was accomplished by means of the execution of the previously discussed experiments, from which the following conclusions can be drawn.

An oscillator of which the active device is operating deep within saturation (nonlinear operation), will have a greater output signal magnitude than a more linearly operating oscillator (an oscillator of which the active device is not driven as deeply into saturation). This may lead to the impression that nonlinearly operating oscillator networks have better phase noise performance than their more linearly operating counterparts, since phase noise is measured relative to the magnitude of the oscillator's output signal. This observation does not, however, take into account the fact that the *effective noise figure* increases as the active device is driven deeper into saturation. This increase in *effective noise figure* is greater than the increase in the magnitude of the oscillator's output signal. It therefore stands to reason that a linearly driven oscillator will have phase noise performance superior to that of a nonlinearly driven oscillator with the same output signal magnitude. This was observed in chapter 4 and proved in chapter 5.

In the experiments following these it was shown that Leeson's model best approxi-

mates an oscillator network of which the active device is operating at less than 0.1 dB of saturation, for oscillators with both high Q and low Q resonators. It was also demonstrated that Leeson's model rapidly loses accuracy as the active device is driven deeper and deeper into compression. A significant deviation between the measured phase noise and that predicted by Leeson's model is already apparent at saturation levels of 0.5 dB.

This deviation, or increase in *effective noise figure*, was attributed to noise situated near integer multiples of the oscillation frequency being mixed down into the frequency band near the oscillating frequency where it is affected by the Leeson effect. The greater the level of saturation within which the active device is operating, the greater the magnitude of the oscillator's harmonics will be and, subsequently, the greater the effect of the noise situated around these harmonics will be on the measured phase noise. By eliminating the harmonics within the oscillator loop, the effect of the noise, situated near these harmonics, upon the phase noise, is also eliminated.

Two ways of limiting these harmonics were demonstrated during the course of these experiments. One was to design an amplifier which was capable of handling a large input signal without being driven into saturation. The second was to limit the loop gain within the oscillator network, by means of additional attenuation. As long as the amplifier is operating on the edge of saturation, the harmonics generated by the oscillator will be small and their effect upon the phase noise minimal.

The experiments also illustrated that the open loop group delay of the oscillator network allows for an accurate method of determining the oscillator's Leeson frequency.

To conclude: Leeson's model is valid when the oscillator network being considered is driven in its most linear manner. It provides a very accurate approximation of the measured phase noise when the level of saturation within which an oscillator's active device is operating is less than 0.2 dB, but rapidly loses accuracy as the level of saturation increases beyond this point.

10.2 Future Work

A clear route for the design of very low phase noise loop oscillators was established in this thesis. By ensuring that the loop amplifier has a very low noise figure and that it operates within its linear region while producing the required output power, the flicker noise and noise at harmonic frequencies of the active device is suppressed.

Driving an oscillator network in such a manner as to ensure that its active device never exceeds a saturation level of 0.1 dB can be problematic. This is due to the fact that the gain of most amplifiers varies as the temperature fluctuates. The design of a loop oscillator, of which the loop gain can be limited to less than 0.1 dB, should therefore be investigated. This could be realised by using a gain comparator in conjunction with an electronically controlled linear attenuator. Care should be taken to ensure that the oscillator is driven by a clean power supply, free of source noise. In order to further improve the phase noise of such an oscillator, a high Q resonator should be used.

Bibliography

- [1] D. M. Pozar, *Microwave Engineering*, 3rd ed. John Wiley & Sons, 2005. 4, 5, 30, A–9
- [2] E. Rubiola, *Phase noise and frequency stability in oscillators*. Cambridge University Press, 2008. 5, 7, 8, 9, 13, 14, 16, 17, 18, 19, 20, 21, 23
- [3] H. L. Krauss, C. W. Bostian, and F. H. Raab, *Solid State Radio Engineering*. John Wiley & Sons, 1980. 5
- [4] U. L. Rohde, “A new and efficient method of designing low noise microwave oscillators,” Ph.D. dissertation, Der Technischen Universität Berlin, 2004. 5, 6, 7, 16, 17, 19, 27
- [5] D. E. Neamen, *Electronic Circuit Analysis and Design*, 2nd ed. McGraw-Hill International, 2001. 5, A–2
- [6] W. Hayward, *Introduction to Radio Frequency Design*. Prentice-Hall, 1982. 5, A–26, C–1
- [7] H. J. Moes, “A low noise pll-based frequency synthesiser for x-band radar,” Master’s thesis, Stellenbosch University, 2008. 8, 9, 10, 11
- [8] E.S.Ferre-Pikal, J.R.Vig, J.C.Camparo, L.S.Cutler, L.Maleki, W.J.Riley, S.R.Stein, C.Thomas, F.L.Walls, and J.D.White, “Draft revision of iee standard 1139-1988 standard definitions of physical quantities for fundamental frequency and time metrology-random instabilities,” *IEEE International Frequency Control Symposium*, 1997. 8, 14
- [9] D. Leeson, “A simple model of feedback oscillator noise spectrum,” *Proceedings of the IEEE*, vol. 54, pp. 329–330, 1966. 11, 31
- [10] A. Hajimiri and T. Lee, “A general theory of phase noise in electrical oscillators,” *IEEE Journal Solid-State Circuits*, vol. 33, pp. 179–194, 1998. 11, 12

- [11] T. H. Lee and A. Hajimiri, "Oscillator phase noise: A tutorial," *IEEE Journal of Solid-State Circuits*, vol. 35, pp. 326–336, 2000. 11, 12, 57
- [12] A. Demir, A. Mehrotra, and J. Roychowdhury, "Phase noise in oscillators: A unifying theory and numerical methods for characterisation," in *Proceedings of Design Automation Conference*, vol. Design Automation Conference, no. 35th, 1998. 11
- [13] M. R. Spiegel and J. Liu, *Mathematical Handbook of Formulas and Tables*, 2nd ed. McGraw-Hill International, 1999. 23
- [14] E. Vermaak, "Development of a low phase noise microwave voltage controlled oscillator," Master's thesis, Stellenbosch University, 2008. 33
- [15] B. Bentley, "An investigation into the phase noise of quartz crystal oscillators," Master's thesis, Stellenbosch University, 2007. 36, 38, 51
- [16] M. M. Driscoll, "Low noise oscillator design and performance." IEEE Frequency Control Symposium, June 2002. 51
- [17] R. E. Ziemer and W. H. Tranter, *Principles of Communications:*. John Wiley and sons Inc., 2001. 51
- [18] "Marconi instruments microwave datamate." 74
- [19] J. Swanzy, "Impact of vswr on the uncertainty analysis of harmonics for a scope calibration instrument," Fluke Application Note. 74
- [20] F. Noriega and P. J. Gonzalez, "Designing lc wilkinson power splitters," *www.rfdesign.com*, 2002. A–9

Appendix A

The Modules Used in Experiment 1

A.1 Cascode Amplifier

A simplified cascode amplifier, where biasing networks are neglected and which has the advantages of having high gain and bandwidth, is shown in figure A.2. These traits of cascode amplifiers are explained as follows.

The transistor Q1 operates in common emitter configuration and therefore will have a gain of $-g_{m1}R_L$, where R_L is the load impedance of the common emitter amplifier and g_{m1} the transconductance of the transistor Q1. Transistor Q2, on the other hand, functions in a common base configuration and therefore will have an input impedance of $\frac{1}{g_{m2}}$, where g_{m2} is the transconductance of transistor Q2. If we assume that transistors Q1 and Q2 are matched, then g_{m1} is equal to g_{m2} and the voltage gain of Q1 will be unity. The voltage gain of a cascode amplifier must therefore be



Figure A.1: Cascode amplifiers

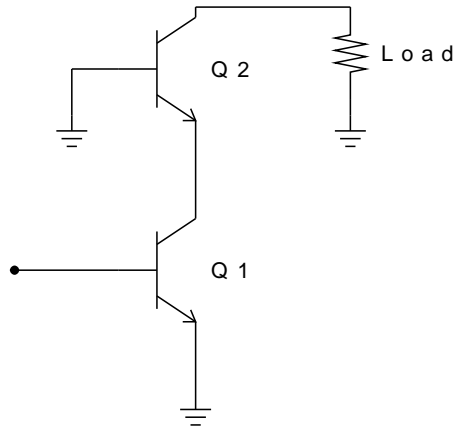


Figure A.2: Simplified BJT cascode amplifier

provided by the common base configured transistor, while the current gain is supplied by the transistor in common emitter configuration. Now consider the Miller effect.

The Miller capacitance is defined as:

$$C_{Miller} = C_{BC} (1 - A_v) \quad (\text{A.1})$$

Where C_{BC} is the base-collector capacitance and A_v is the transistor's voltage gain. This means that the Miller capacitance for a cascode amplifier reduces to twice that of the base-collector capacitance of Q1. There is no Miller multiplication for transistor Q2 since its gain is non-inverting and the collector-emitter capacitance is negligible. This inevitably results in greater bandwidth [5]. The amplifier's slew rate, and therefore the phase shift between its input and output ports, is also reduced as a result of this.

A.1.1 Design and Simulation

A cascode amplifier was designed to have gain of approximately 25 dB and a collector current of nearly 30 mA, the maximum collector current allowed for the BFR90A. The schematic diagram is shown in figure A.3. The matching L-section at the amplifier's input is not shown in the schematic, but comprises a series inductor of approximately $5 \mu H$ and a shunt capacitor of $82 pF$. Simulations indicate that this design should have a gain of almost 29 dB, as is shown in figure A.4. It should be noted at this point that the previously mentioned L-section severely reduces the amplifier's bandwidth, as is also apparent in figure A.4. The benefit of minimised phase deviation, shown in figure A.5 is, however, not lost - as would have been the case for a common emitter amplifier with similar gain and bandwidth. Figure A.6

indicates that both the input and output ports should be well matched to the rest of the system.

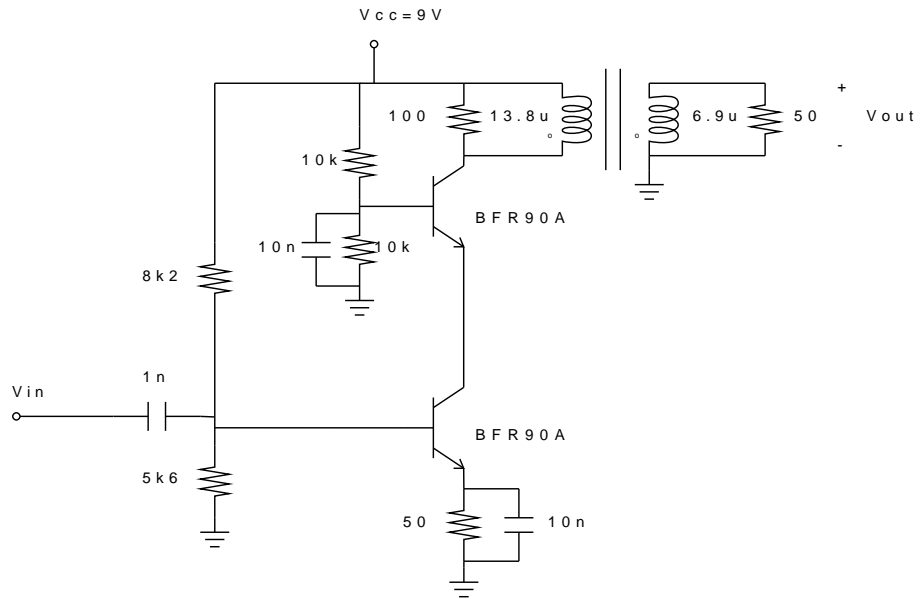


Figure A.3: Schematic diagram of cascode amplifier

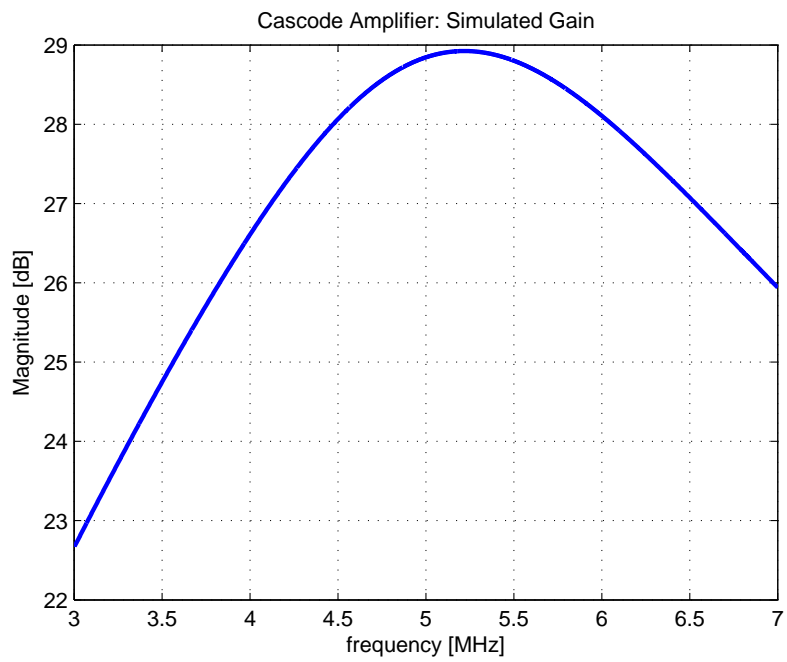


Figure A.4: Cascode amplifier: simulated gain

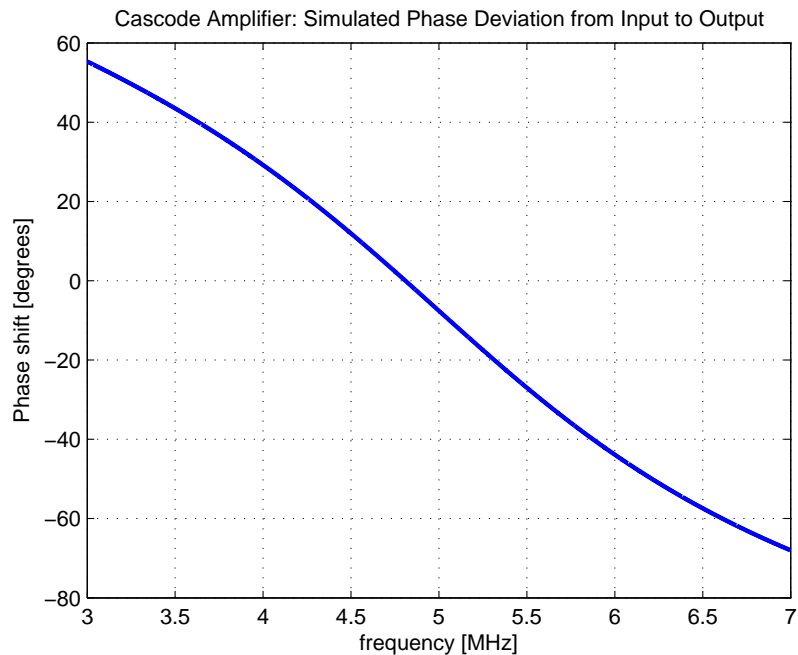


Figure A.5: Cascode amplifier: simulated phase deviation

A.1.2 Measurements and Conclusions

Two amplifiers, one for the system acting as DUT and one for the reference system, were built subsequent to the design. These were measured and the results are discussed below.

The input and output reflection coefficients for both amplifiers are illustrated in figure A.7 and figure A.8 respectively. These measurements, performed on a calibrated vector network analyser (VNA), indicate that the port matching at both the input and output ports is not as good as those simulated. This could be attributed to unaccounted parasitic components of the various elements. It should be noted, however, that for both amplifiers less than one tenth of the signals at both the input and the output ports is reflected. The ports could therefore still be considered matched to 50Ω .

Figure A.9 shows the gain and bandwidth of both amplifiers. It shows that, although the bandwidth of both amplifiers is about the same as that of the simulated amplifier, the amplifier gains are nearly 3 dB less than the simulated gain. Amplifier A has a maximum gain of 26 dB at 5.225 MHz and Amplifier B has a maximum gain of 26.5 dB at 5.225 MHz. The variations could be the result of differences between the physical transistors and their simulated counterparts, as well as tolerances and parasitic components of the different elements. The fact that the input ports are

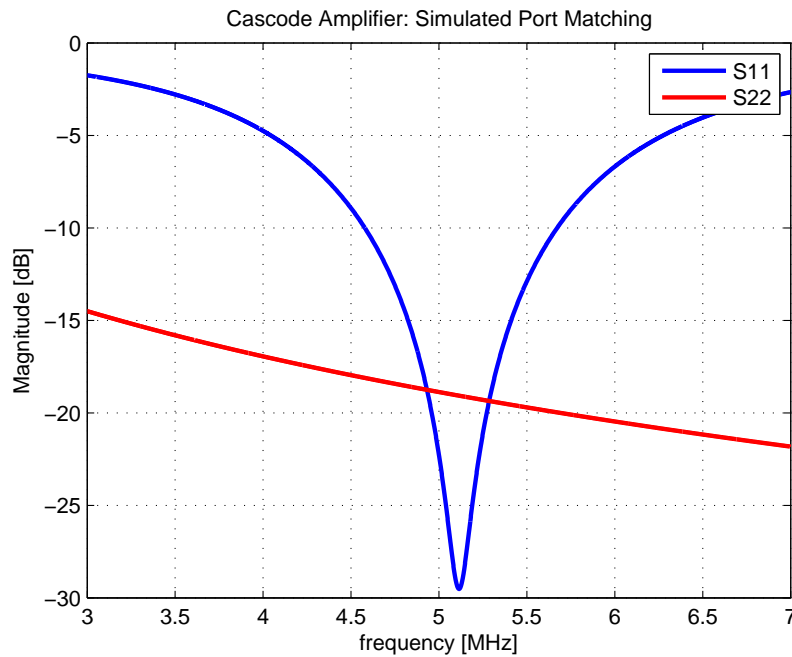


Figure A.6: Cascode amplifier: simulated input and output port matching

not as well matched as those of the simulated amplifier will also mean that less of the input signal power will be amplified.

The phase shifts between the input and output ports of the amplifiers are depicted in figure A.10. It is noteworthy that the phase deviation around 5 MHz is almost linear and nearly the same as the simulated phase deviation.

Figure A.11 shows the output power as a function of the input power for both amplifiers. The dotted lines in the graph indicate the linear increase in output power against input power should the amplifiers not go into saturation. From this graph the 1 dB compression point of both amplifiers can be obtained. For Amplifier A the input 1 dB compression point is -14.85 dBm and for Amplifier B this point is at -16.15 dBm.

It can therefore be concluded that both amplifiers are sufficiently matched to 50Ω , and that they have enough gain for our purposes. The phase shifts between the input and output ports are minimal. The amplifier bandwidths are great enough not to be a deciding factor in the oscillator circuits' resonance frequencies.

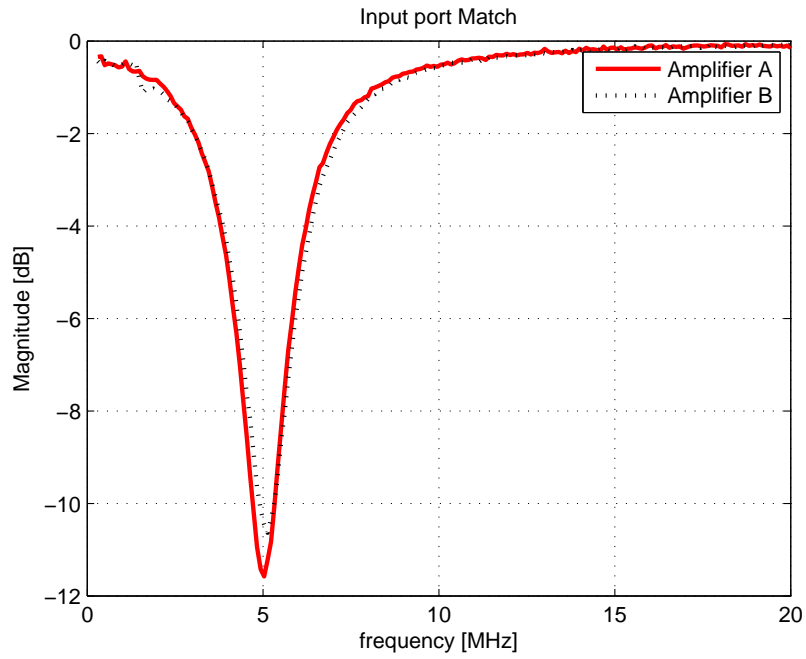


Figure A.7: Cascode amplifier: measured input port matching

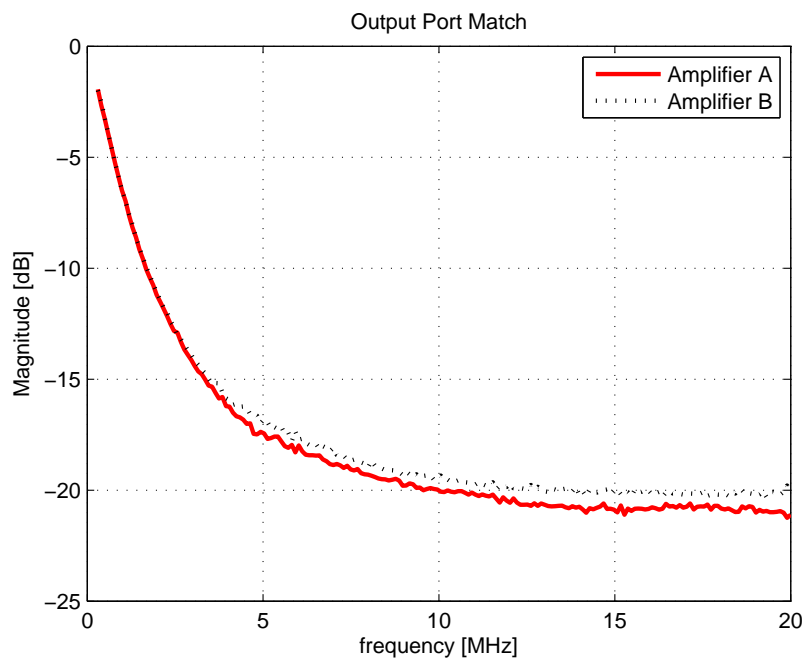


Figure A.8: Cascode amplifier: output port matching

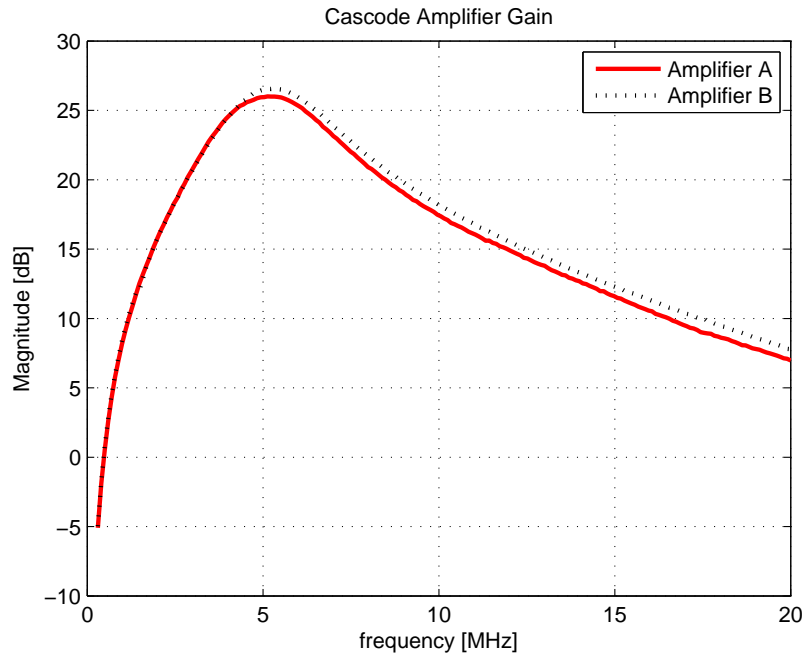


Figure A.9: Cascode amplifier: measured gain and bandwidth

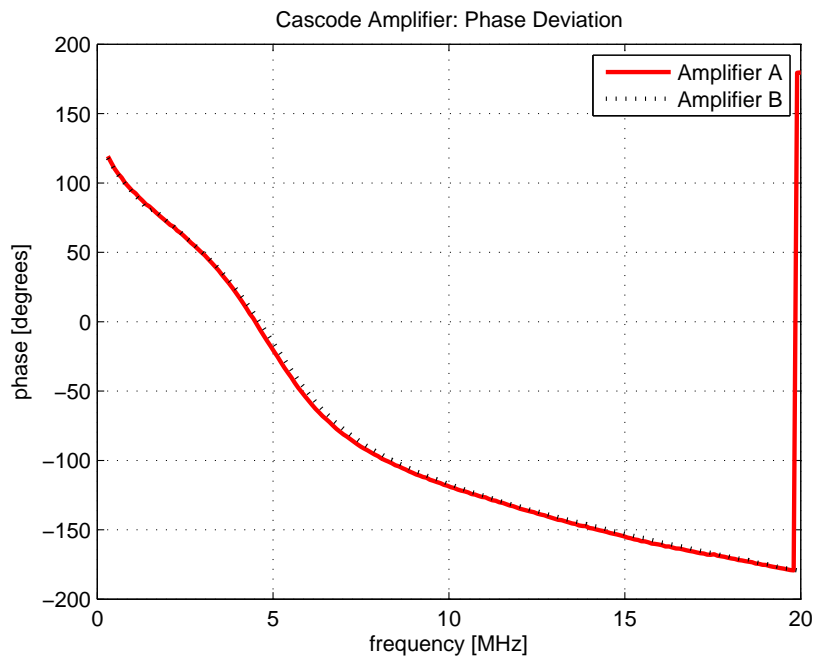


Figure A.10: Cascode amplifier: measured input output phase deviation

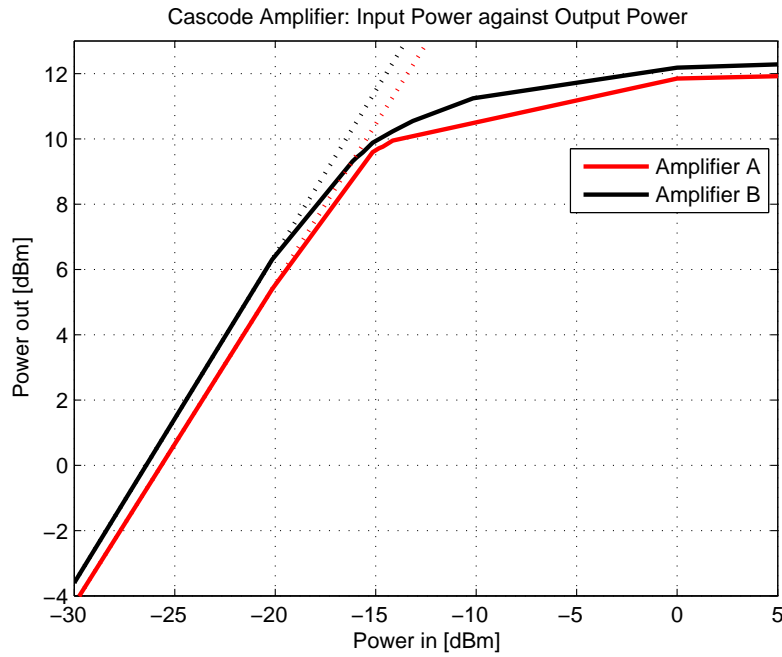


Figure A.11: Cascode amplifier: input power vs. output power



Figure A.12: Wilkinson power dividers used in experiment 1

A.2 Wilkinson Power Divider

The traditional Wilkinson power divider is shown in figure A.13. It consists of two transmission lines of length $L = \frac{\lambda}{4}$, where λ is the wavelength of the operating frequency, with a characteristic impedance of $Z_1 = \sqrt{2}Z_0$, where Z_0 is the characteristic impedance of the ports to be matched. The signal enters at port 1 and is then equally divided between ports 2 and 3. The quarter wave transformer action of these transmission lines, in conjunction with the resistor connecting their outputs, provides good port matching at all 3 ports, as well as isolating the two

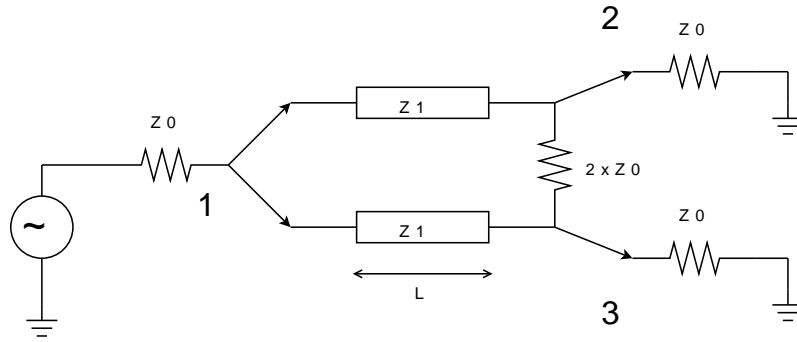


Figure A.13: Wilkinson power divider

output ports from each other. This can be verified by performing even and odd mode analysis on the circuit[1].

The traditional approach to Wilkinson power divider design using transmission lines will, however, not suffice for 5 MHz applications. This is due to the fact that the wavelength of a 5 MHz signal is nearly 60 meters. The problem is, however, easily fixed by designing an LC Wilkinson power divider[20]. LC Wilkinson dividers function on the same principles as their transmission line counterparts. They differ only in the sense that the transmission lines are replaced by LC networks like the ones shown in figureA.14. A quarter wave transmission line equivalent can be designed by setting the element values as follows:

$$C_p = \frac{1}{2\pi f_0 Z} \quad (\text{A.2})$$

$$L_s = \frac{Z}{2\pi f_0} \quad (\text{A.3})$$

where Z is the characteristic impedance of the transmission line to be emulated in ohms and f_0 is the operating frequency in hertz. The values of C_p and L_s are, respectively, calculated in farads and henries.

A.2.1 Design and Simulation

Figure A.15 shows a schematic diagram of an LC Wilkinson power divider. The values of L_s and C_p , for a 5 MHz divider with a characteristic impedance of $Z_0 = 50\Omega$ were calculated using equations A.2 and A.5 and are listed below. Please note that

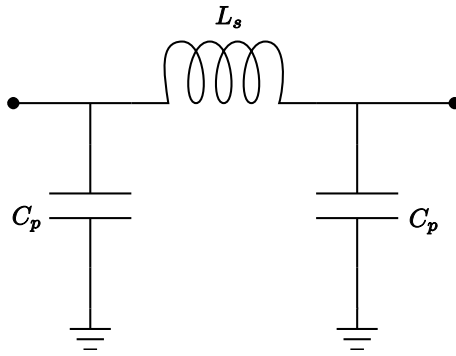


Figure A.14: Quarter wave equivalent LC network

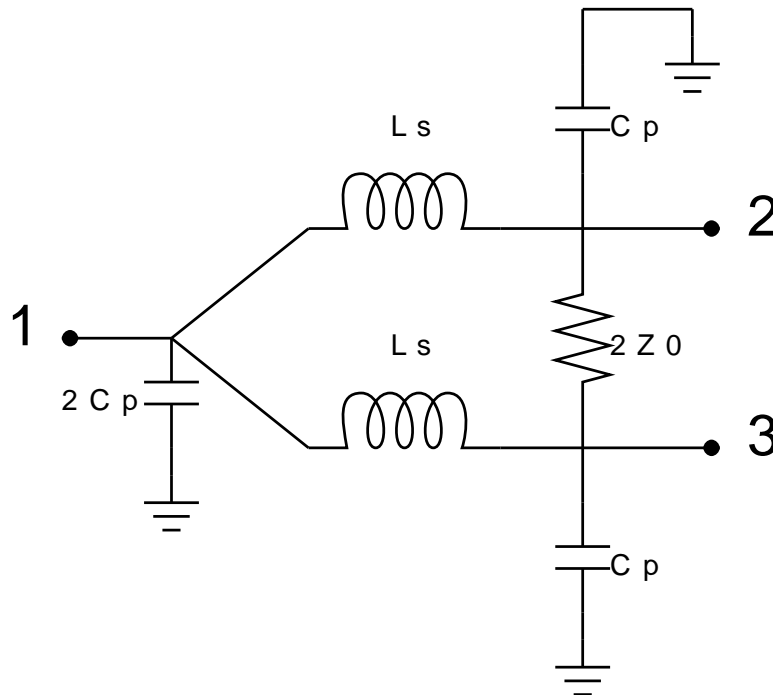


Figure A.15: LC wilkinson power divider

the value of Z in these equations is $\sqrt{2}Z_0$.

$$\begin{aligned} C_p &= 450\text{pF} \\ L_s &= 2.25\mu\text{H} \end{aligned}$$

In order to simplify the manufacturing of the dividers, 470 pF ceramic capacitors were used, since these capacitors are readily available and have high quality factors. The inductors were turned on T50-2 toroids from Micrometals. Their inductances were measured and all found to be approximately $2.2 \mu\text{H}$. Subsequently the entire design was simulated in Microwave Office (MWO) and the results shown in figures A.16, A.17, A.18 and A.19 were obtained.

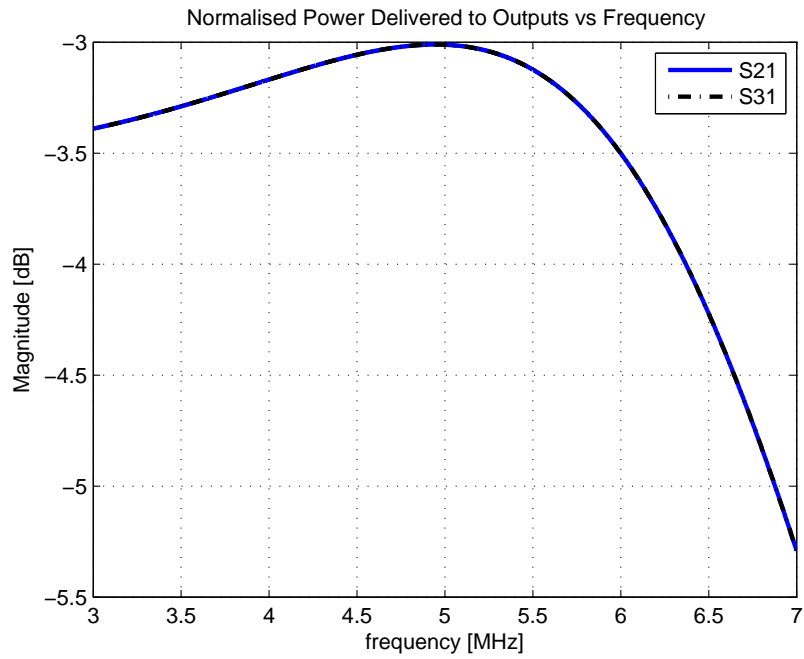


Figure A.16: The simulated normalised power delivered at the output ports of the divider shown against frequency.

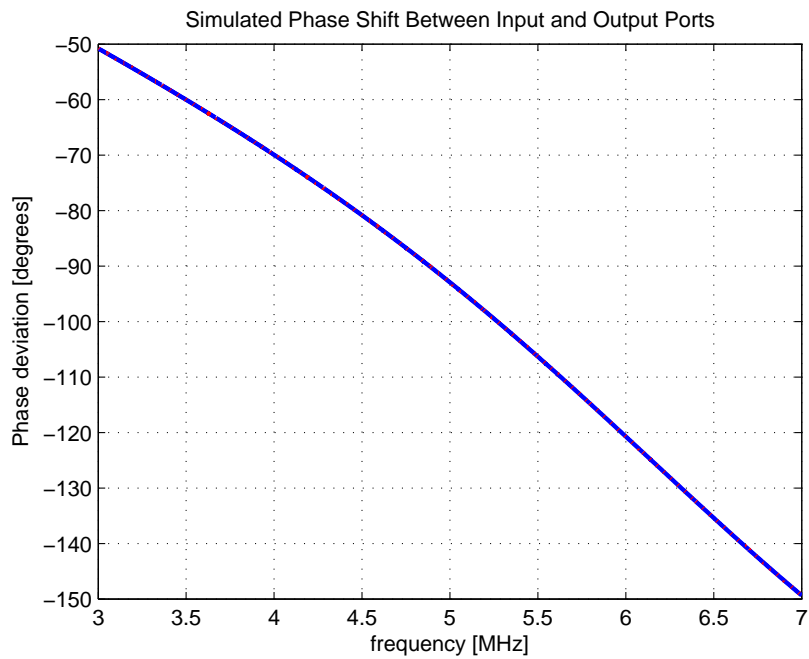


Figure A.17: The simulated phase deviation from input to output against frequency.

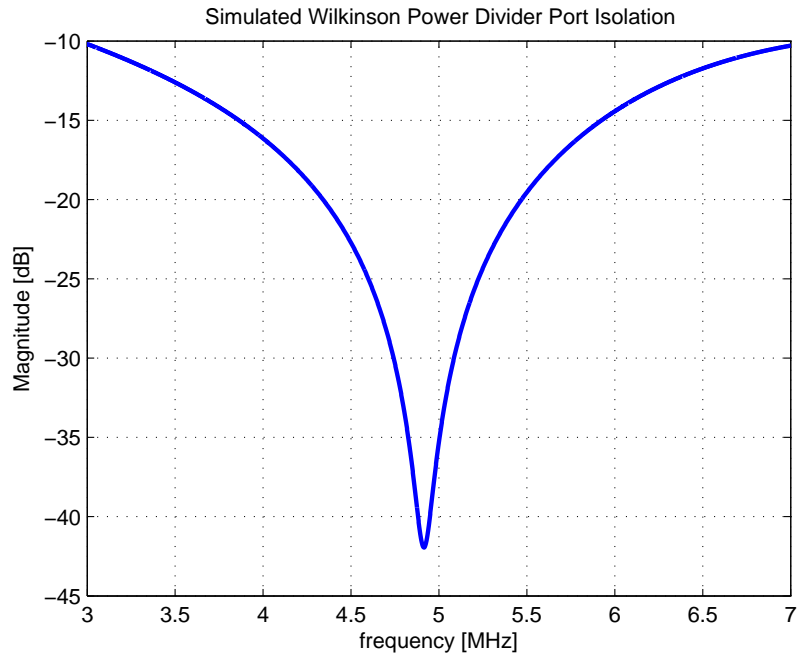


Figure A.18: The simulated isolation factor between the output ports against frequency.

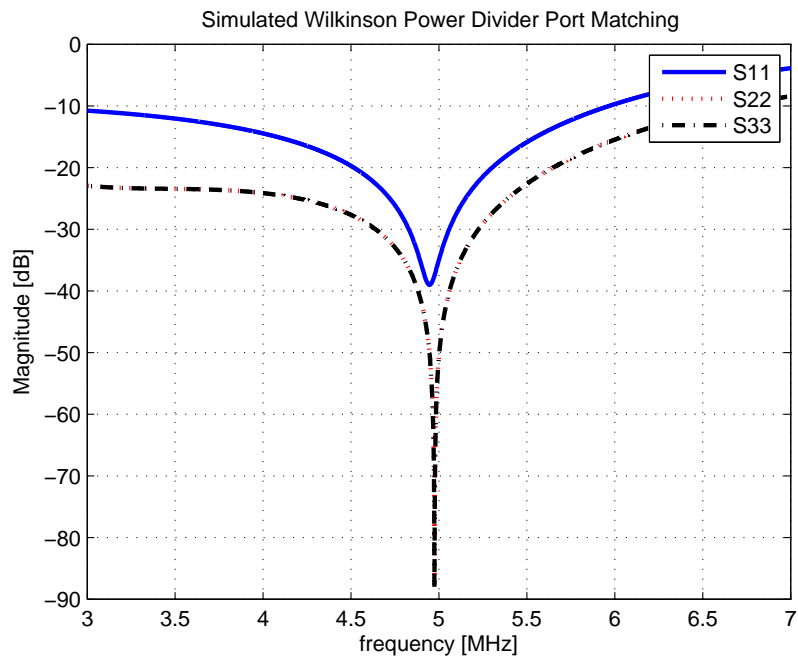


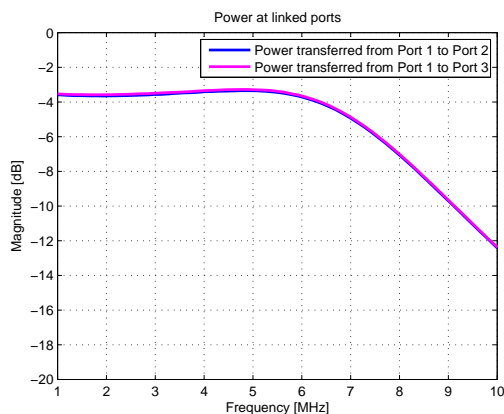
Figure A.19: The simulated reflection coefficient at all three ports

As can be seen from the simulated results, the LC Wilkinson divider acts exactly like its transmission line counterpart at 5 MHz. According to the simulations less than 0.01% of the signal present at the measurement device is expected to leak into the oscillator. It is also shown that all three ports are well matched to 50Ω and that the input power is divided equally between the two output ports.

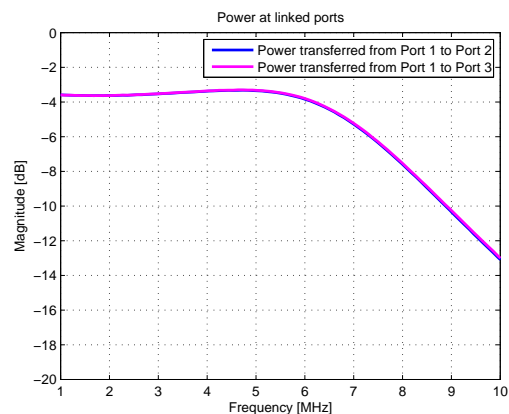
A.2.2 Measurements and Conclusions

Once satisfied with the simulated results, two LC Wilkinson power dividers were built, one for each of the two oscillator circuits mentioned earlier. These were measured using a vector network analyser from Rohde and Schwarz. The measured results for the two dividers are compared in figures A.20, A.21, A.22 and A.23.

In both cases the ports are well matched to 50Ω , the S_{11} -parameter even exceeds the simulated results in MWO. This can be attributed to component losses, since the resistive losses of the capacitors and inductors were not taken into consideration during the simulation of the divider. Furthermore it can be seen that the two dividers are nearly identical in their performance, with only slight variations in their port matching and phase deviation results. One should also note that the output port isolation is not as good as the simulations would suggest. Once again, this can be attributed to component losses. However, with less than a thousandth of the signal power present at the measurement device leaking into the oscillator circuit, the isolation factor is more than adequate for the purposes of the experiment.

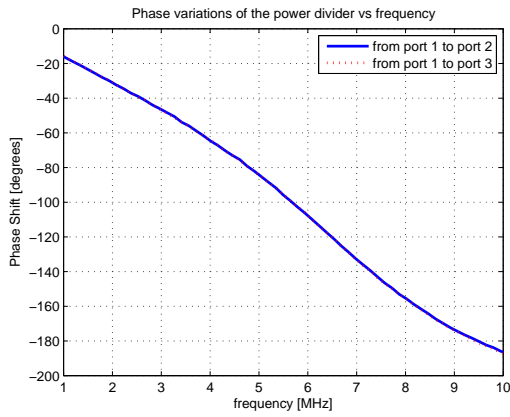


LC Wilkinson divider A

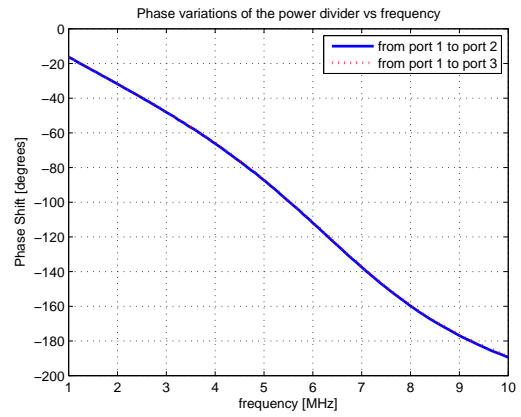


LC Wilkinson divider B

Figure A.20: The measured normalised power delivered at the output ports of the divider shown against frequency.

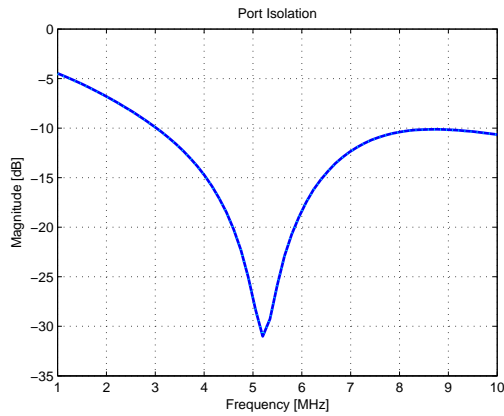


LC Wilkinson divider A

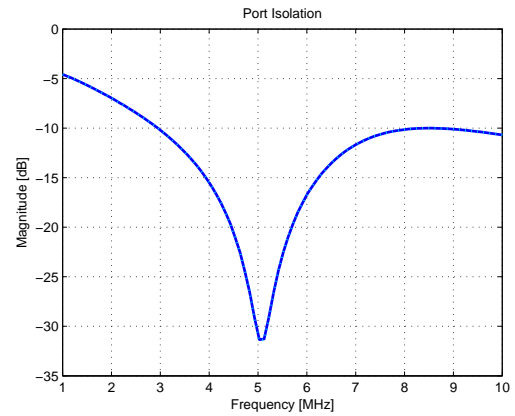


LC Wilkinson divider B

Figure A.21: The measured phase deviation from input to output against frequency.

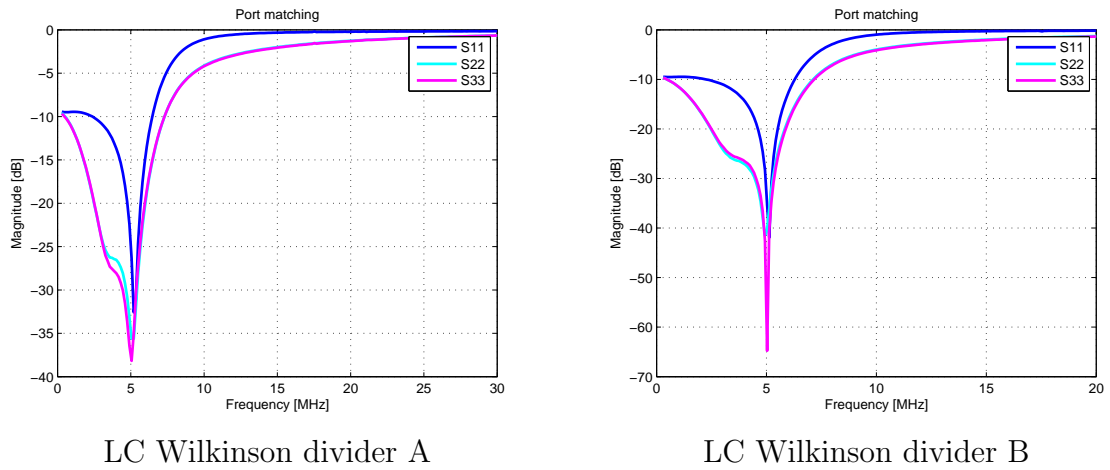


LC Wilkinson divider A



LC Wilkinson divider B

Figure A.22: The measured isolation factor between the output ports against frequency.

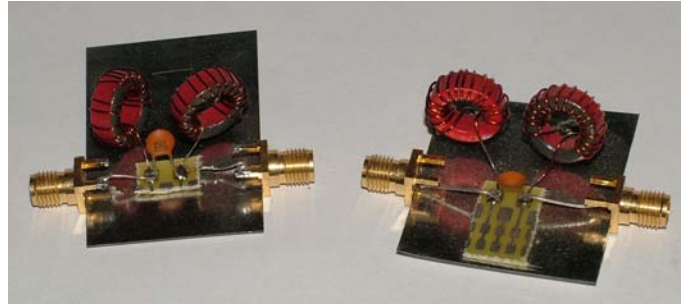


LC Wilkinson divider A

LC Wilkinson divider B

Figure A.23: The measured reflection coefficient at all three ports

A.3 270° Phase Shift Network

**Figure A.24:** 270° Phase shifters

A.3.1 Design and Simulation

The design of a 270° phase shift network is shown in figure A.25. The values of C_s and L_p are defined as follows:

$$C_s = \frac{1}{2\pi f_0 Z} \quad (\text{A.4})$$

$$L_p = \frac{Z}{2\pi f_0} \quad (\text{A.5})$$

where Z is the characteristic impedance of the transmission line to be emulated defined in Ω and where f_0 is the operating frequency. C_s and L_p are calculated in farads and henries respectively. In the case of a 5 MHz phase shifter with a

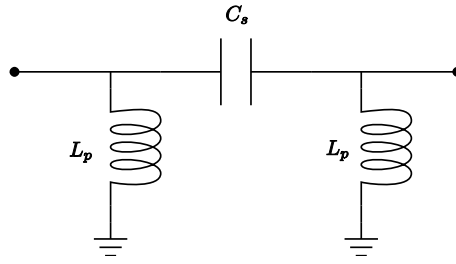


Figure A.25: $\frac{3}{4}$ Wavelength transmission line LC equivalent circuit

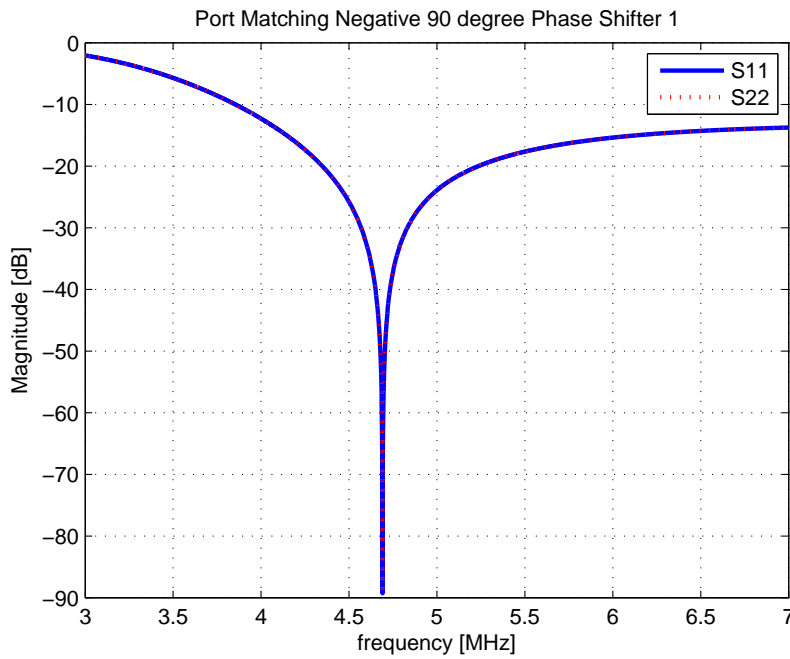


Figure A.26: Simulated reflection coefficient $\frac{3}{4}$ wavelength transmission line equivalent

characteristic impedance of 50Ω , the capacitor and inductor values equates to the following:

$$\begin{aligned} C_s &= 636.3pF \\ L_p &= 1.59\mu H \end{aligned}$$

In order to simplify the manufacturing of the LC network, C_s is set to 680 pF, a readily available ceramic capacitor value. The inductors were turned on T50-2 toroids from Micrometals and their inductances tuned to $1.59\mu H$. The network provides a near 270° phase shift, which should cancel out the phase shift resulting from the power divider. This can be seen in figure A.28. The network also allows for nearly all of the applied signal power to be passed at the operating frequency, while maintaining good port matching (reflection coefficients better than -20dB) at this frequency. This is illustrated at the hand of figures A.27 and A.26.

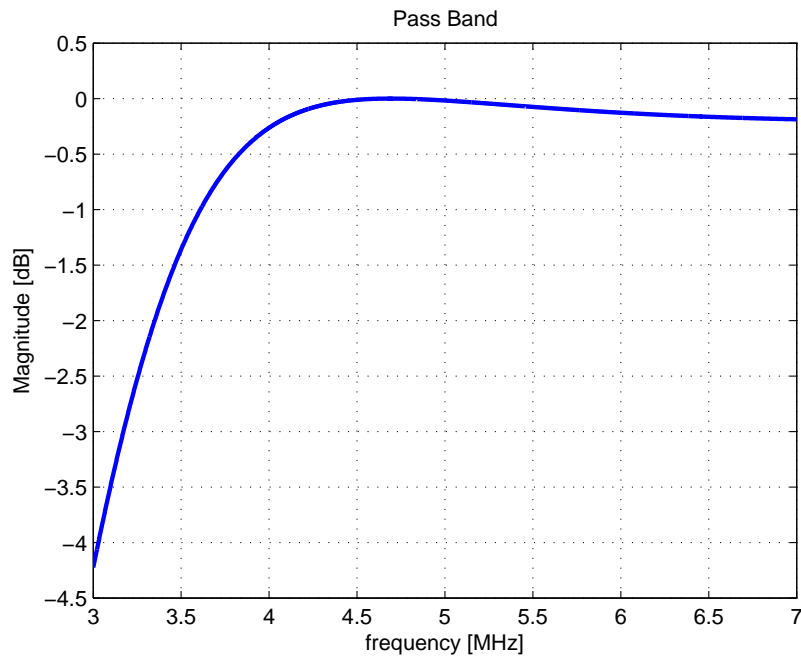


Figure A.27: Simulated pass band of $\frac{3}{4}$ wavelength equivalent.

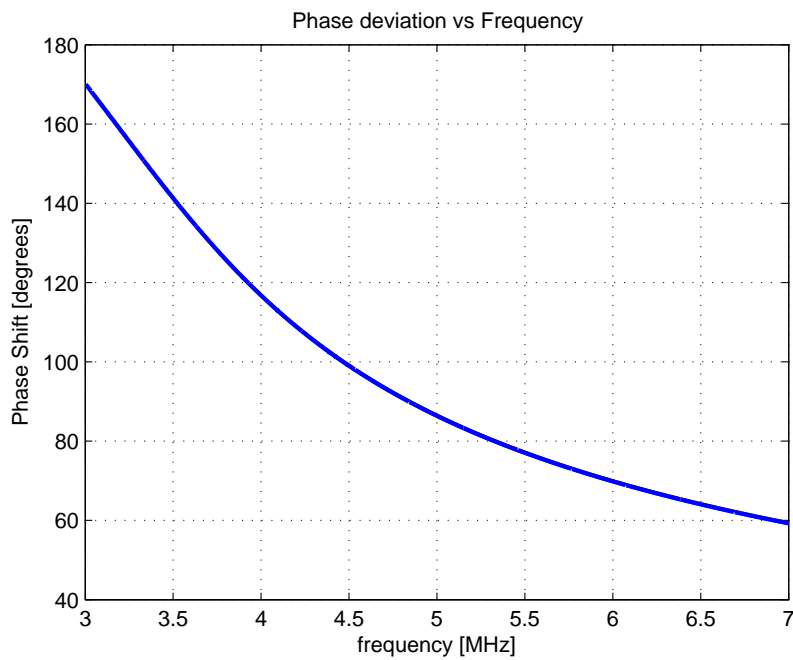


Figure A.28: Simulated phase deviation of $\frac{3}{4}$ wavelength equivalent against frequency.

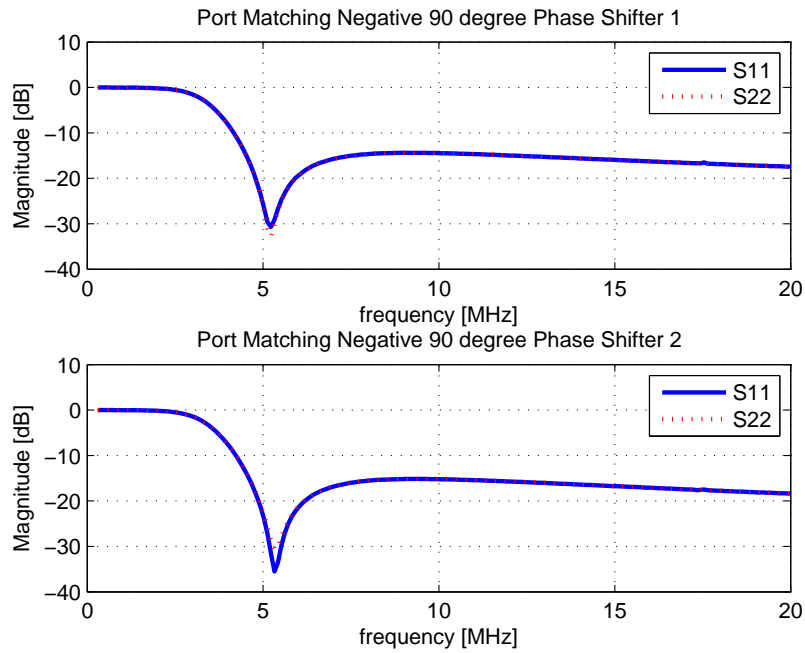


Figure A.29: Measured reflection coefficient $\frac{3}{4}$ wavelength transmission line equivalent

A.3.2 Measurements and Conclusions

Two networks were built in accordance with the previously described design and measured using a Rohde and Schwarz VNA. The measurements are shown in figures A.29, A.30 and A.31, and the two LC networks are compared.

Measurements show that the LC networks are almost identical in their performance. The measured results differ slightly from those simulated. This can be attributed to component tolerances as well as losses that were not considered during simulation. To conclude: the LC networks are functional and will work well for the intended phase shifts in the respective oscillator circuits.

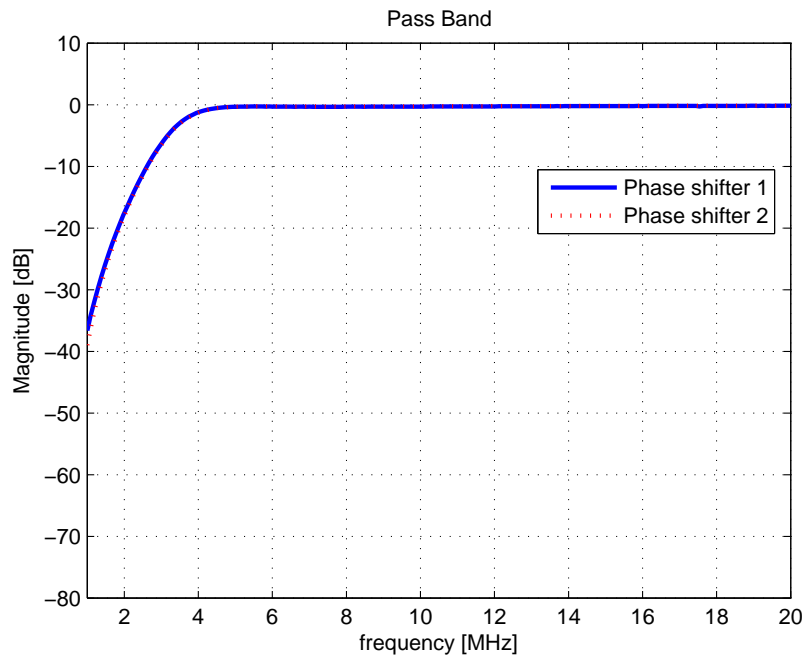


Figure A.30: Measured pass band of $\frac{3}{4}$ wavelength equivalent.

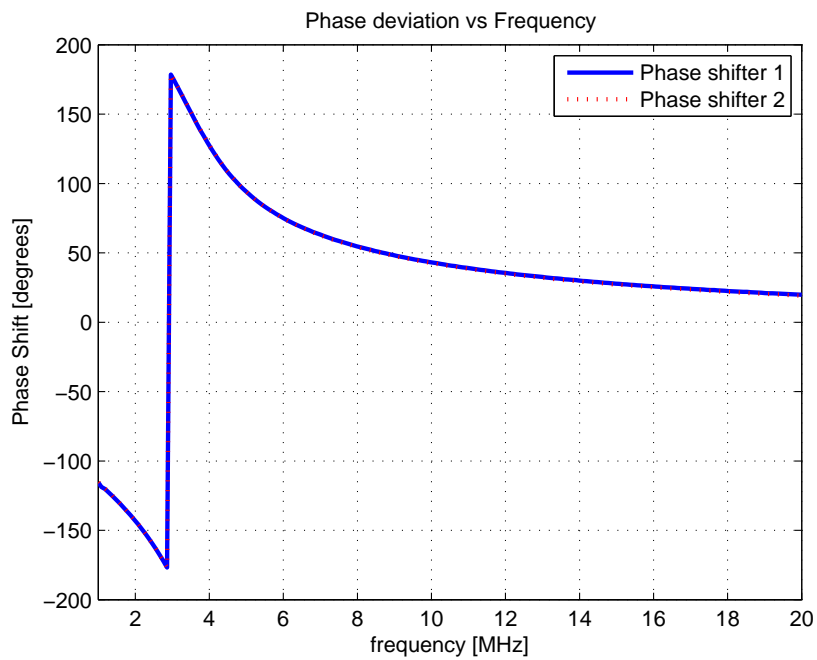


Figure A.31: Measured phase deviation of $\frac{3}{4}$ wavelength equivalent against frequency.

A.4 Π -Attenuators



Figure A.32: Attenuators used

A Π -attenuator like the one in figure A.33 can be designed by using the following equations:

$$R_2 = \frac{1}{2} \left(10^{\frac{L}{10}} - 1 \right) \sqrt{\frac{Z_0^2}{10^{\frac{L}{10}}}} \quad (\text{A.6})$$

$$R_1 = \left\{ \frac{10^{\frac{L}{10}} + 1}{Z_0 \left(10^{\frac{L}{10}} - 1 \right)} - \frac{1}{R_2} \right\}^{-1} \quad (\text{A.7})$$

where R_1 and R_2 are resistor values calculated in ohms, L is the desired attenuation factor in dB and Z_0 is the characteristic impedance of the system to which the attenuator must be matched in ohms. Four such π -attenuator circuits, two 3 dB, an 11 dB and a 15dB attenuator were designed and built. These were measured and the results are shown in figures A.34 to A.42. The measurements show that all the attenuators are well matched to 50Ω and that they would add very little phase shift to the rest of the oscillator circuit. Less than one degree of phase shift was measured at 5 MHz for all four attenuators.

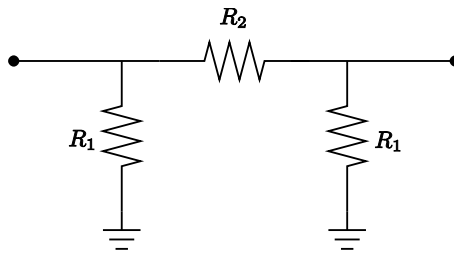


Figure A.33: Schematic diagram of a π -attenuator

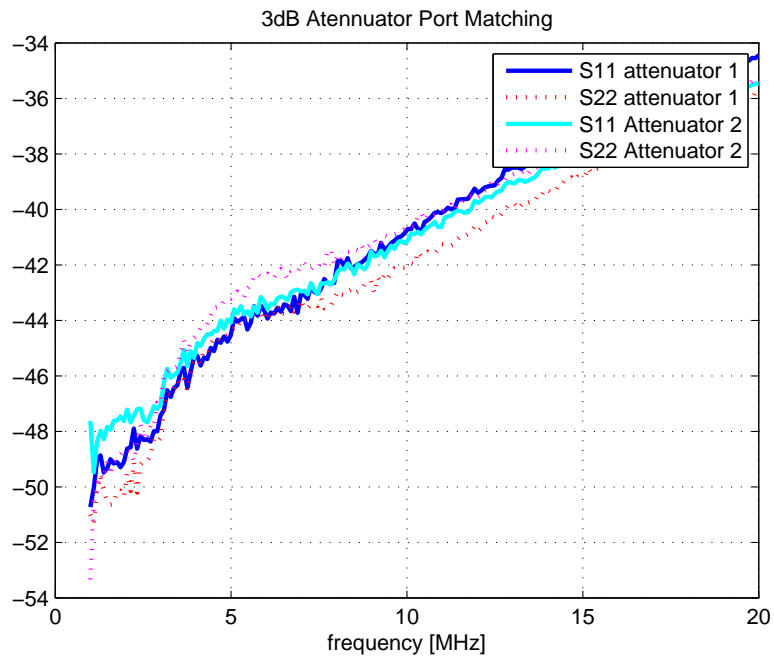


Figure A.34: 3 dB Attenuator port matching

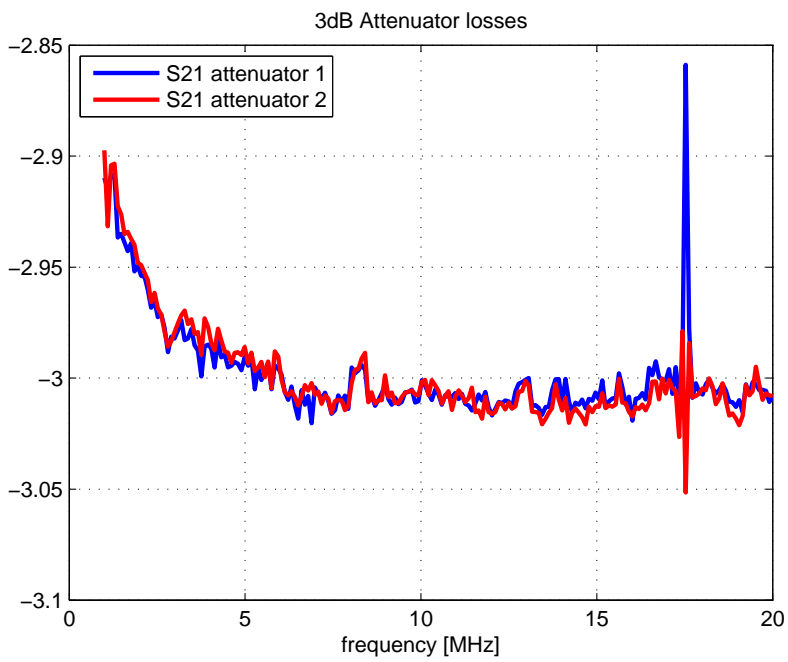


Figure A.35: 3 dB Attenuator losses

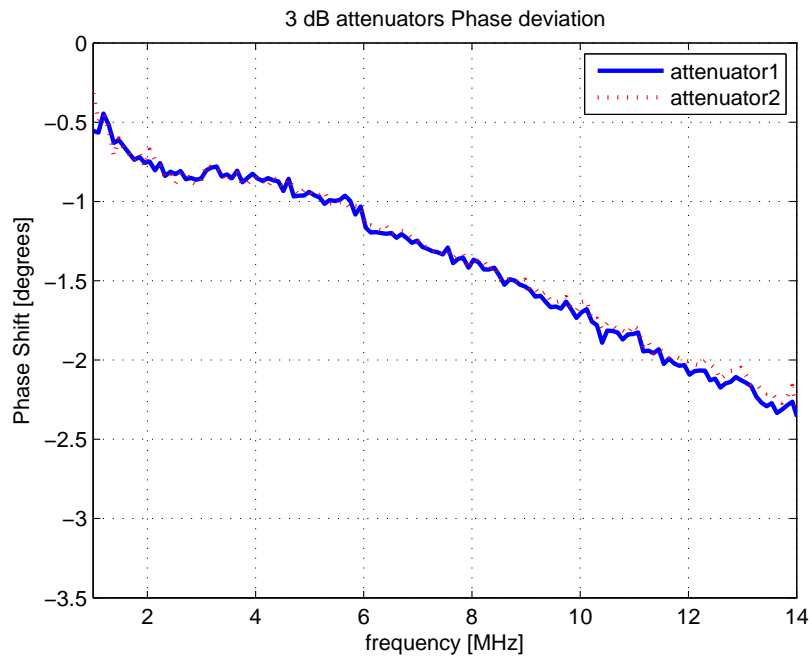


Figure A.36: 3 dB Attenuator phase deviation

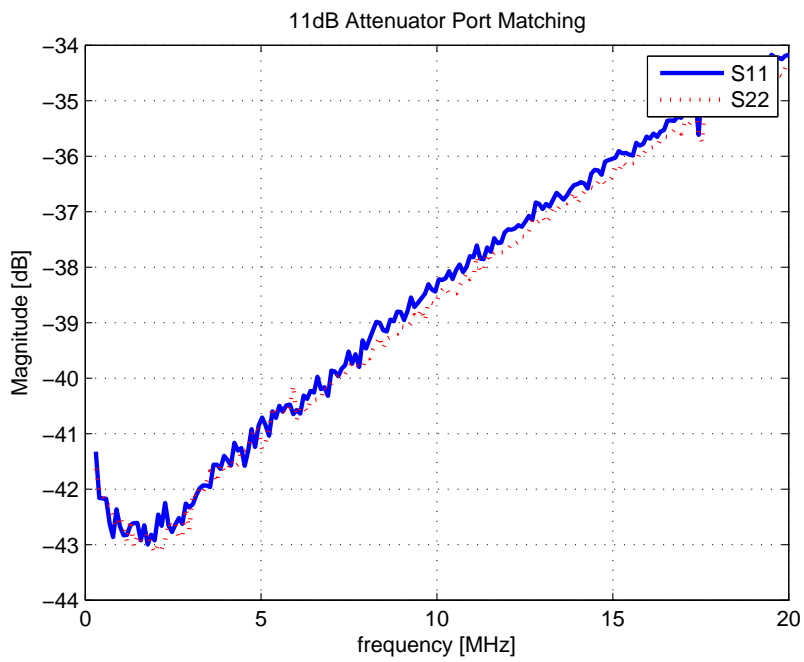


Figure A.37: 11 dB Attenuator port matching

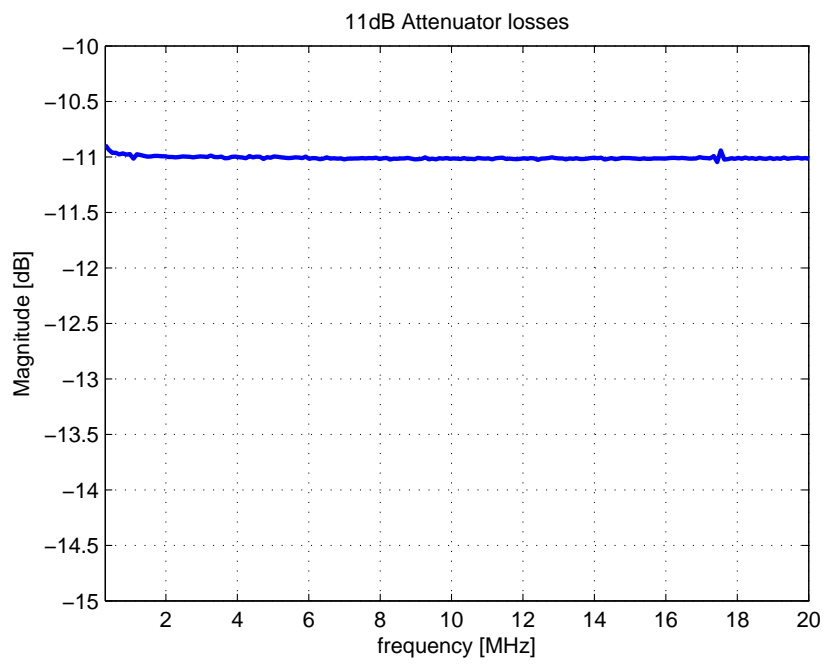


Figure A.38: 11 dB Attenuator loss

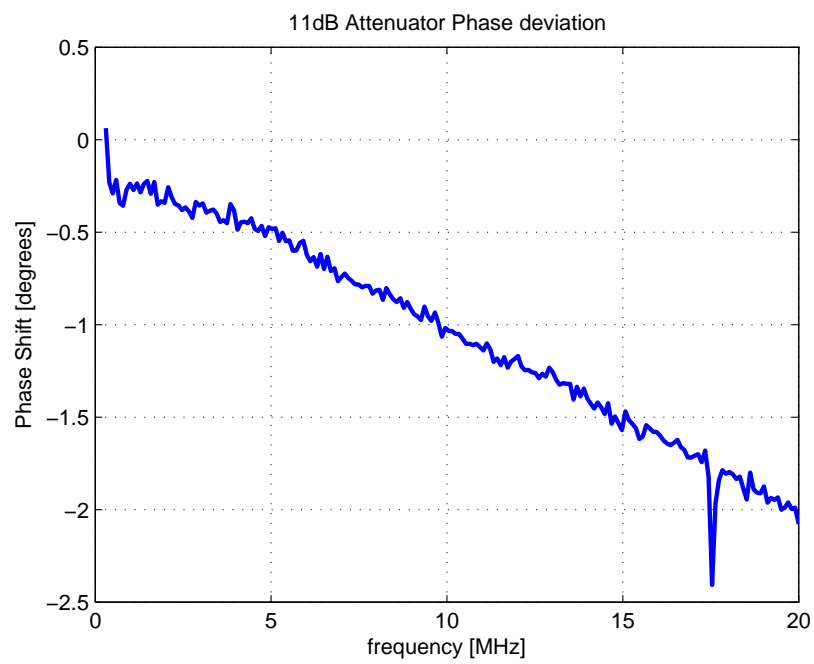


Figure A.39: 11 dB Attenuator phase deviation

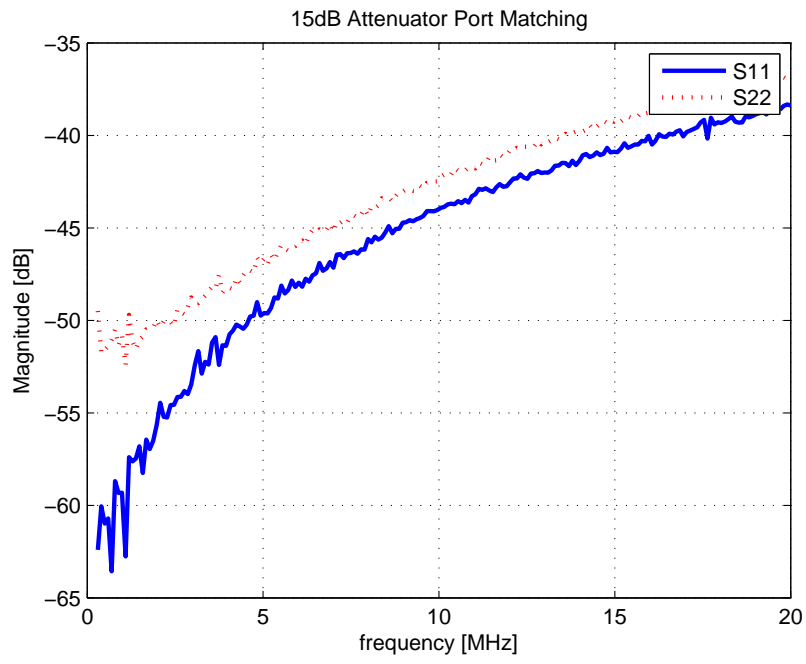


Figure A.40: 15 dB Attenuator port matching

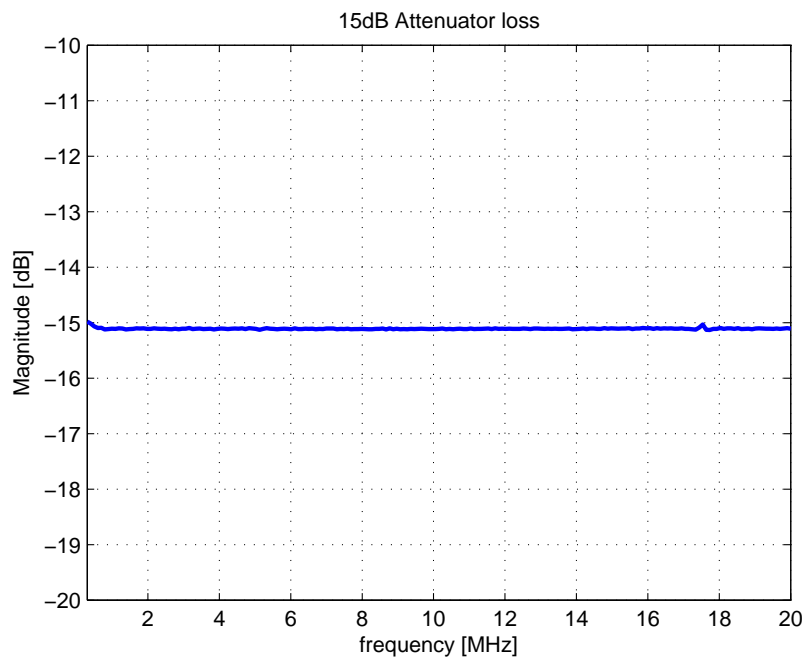


Figure A.41: 15 dB Attenuator loss

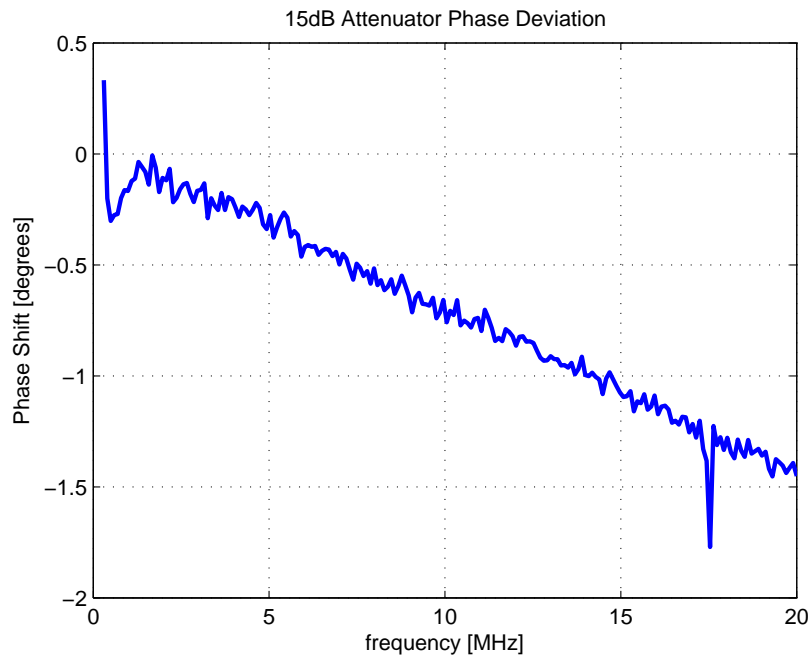


Figure A.42: 15 dB Attenuator phase deviation

The Mini-Circuits Attenuators Datasheets are shown in Appendix B and indicate that these attenuators are suitable for the purposes of the experiment.

A.5 Π -Resonator

Design and Simulation

There are various resonators to choose from. Given the relatively low operating frequency of the oscillator circuits, it was decided upon using an LC resonator in a Π -configuration, like the one shown in figure A.43. Two resonators were designed. One fixed, for the DUT circuit, and the other voltage adjustable, to serve in the reference circuit. First consider the fixed resonator.

The design begins with a simplified model like the one shown in figure A.44. Assume that the unloaded Q of the resonator will effectively be determined by the Q of the inductor. This assumption is valid, since the Q of inductors wound around iron powder cores, like the T50-2 toroids that were used, will typically have a Q of 200 to 250, whereas the Q 's of the capacitors used will typically be of the order 1000 to 5000. The following equations can be used to design a Π -resonator like the one

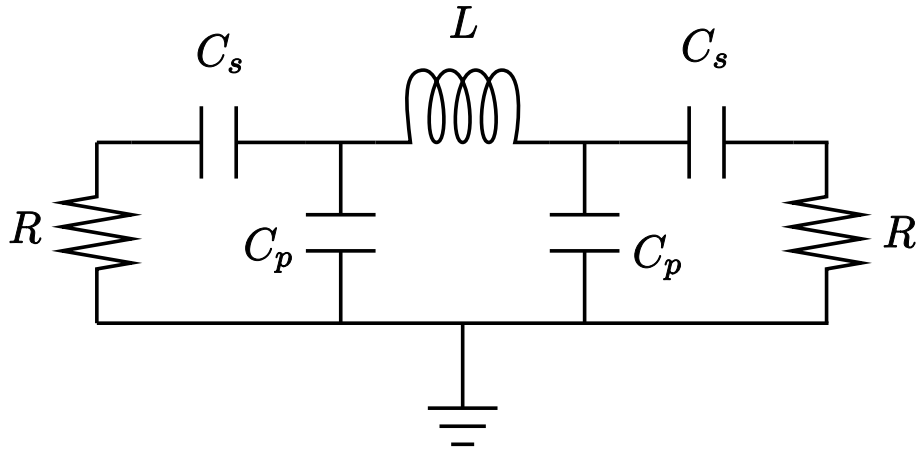


Figure A.43: LC Π-resonator schematic

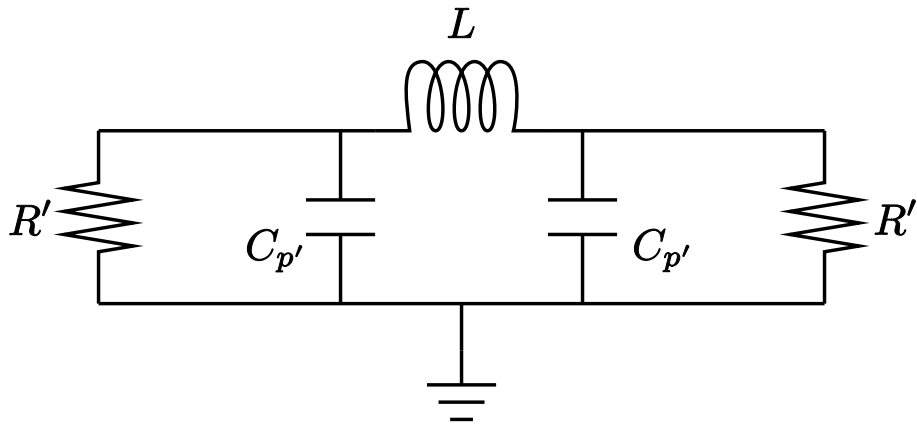


Figure A.44: Simplified Π-resonator schematic

shown in figure A.44[6].

$$X_{C_{p'}} = \frac{R'}{Q_U} \quad (\text{A.8})$$

$$X_L = \frac{2R'Q_U}{Q_U^2 + 1} \quad (\text{A.9})$$

where $X_{C_{p'}}$ is the impedance value of the parallel capacitor and X_L is the impedance value of the series inductor in Ω . In [6] it is assumed that the R' resistors are the only resistors degrading the resonator's Q . In reality there is, however, another resistance value in parallel with the inductor. If we now design the resonator so that R' is equal to half this resistance, the resistor on the left in figure A.44 will see an impedance equal to three times that of its own impedance. By a similar argument the same will be true for the resistor on the right in figure A.44. This implies that the criterion for minimum phase noise, previously derived in Chapter 4.2.5, will be achieved.

Table A.1: Component values of the nonadjustable resonator

Component	value	unit
R	50	Ω
C_s	39	pF
C_p	428	pF
L	4.05	μH

An inductor was turned with an inductance of $L = 4.05\mu H$ and a Q of 250 at 5 MHz. This implies, that for the resonator to perform optimally in terms of phase noise, R' must be approximately 15.9 k Ω . From equation A.8, $C_{p'} \simeq 500pF$ can be calculated.

Since the resonator has to function in a 50 Ω system, $R' \simeq 15.9k\Omega$ must be transformed to $R = 50\Omega$. It should be noted at this point that the schematic diagram in figure A.43 can be transformed into the one in figure A.44 by means of the following equations:

$$Q_e = \frac{1}{\omega_0 \times R \times C_s} \quad (\text{A.10})$$

$$R' = R(1 + Q_e^2) \quad (\text{A.11})$$

$$X = \frac{R'}{Q_e} \quad (\text{A.12})$$

$$C_1 = \frac{1}{\omega_0 X} \quad (\text{A.13})$$

$$C_{p'} = C_1 + C_p \quad (\text{A.14})$$

These equations enable the transformation of R and C_s into their parallel equivalents R' and C_1 . They therefore allow for the calculation of C_s and C_p . In order to simplify the building of the resonator, the values in table A.1 were chosen for the components in figure A.43. Note that R is the characteristic impedance of the system.

The resonator was simulated in MWO and the results are shown figures A.45 through A.47. Since the circuit is symmetrical, the reflection coefficients at both the input and the output ports are the same. This is illustrated in figure A.45. In this figure it can be seen that, at just over 5 MHz, there are reflection coefficients of nearly -6 dB. In other words, almost a quarter of the signal power at the ports is reflected back. This implies that a quarter of the available power is dissipated in the source and another quarter in the load, which means that half of the signal power must be dissipated in the resonator.

The pass band of the resonator denotes a loaded Q of approximately 107, and phase deviation between the input and output ports varies by $\pm 80^\circ$ across the pass band.

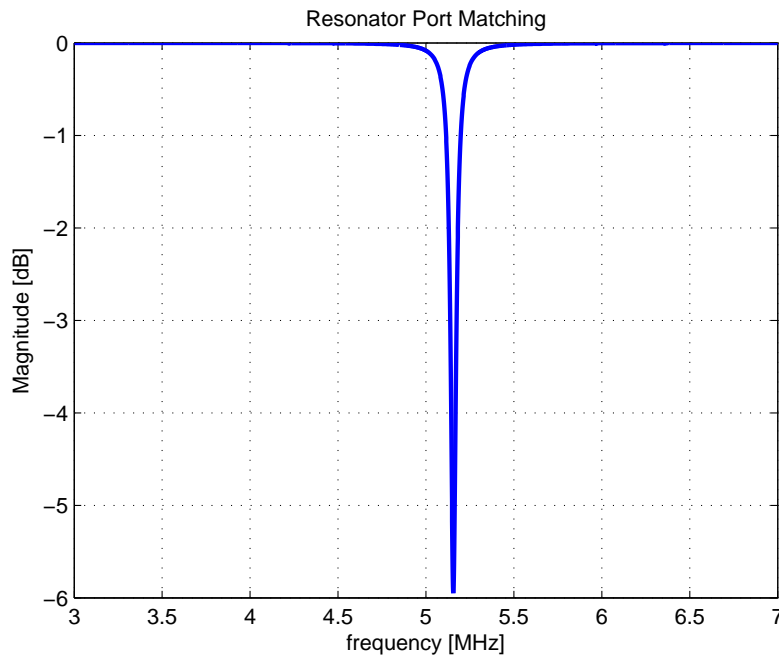


Figure A.45: Simulated fixed resonator: port matching

Next consider the design of the voltage adjustable resonator. The same consideration must be given in terms of the quality factor. For this reason a design similar to that of the fixed resonator was opted for. Two BB804 varactor diodes are used in parallel with capacitor networks, as is shown in figure A.48. This allows the resonance frequency to be adjusted as the voltage, V , over the varactor is varied. The capacitance of the varactor can vary between 26 pF and 42 pF; this implies a relatively small band across which the resonance frequency can be adjusted. It also implies that the variations in the port matching and the pass band of the adjustable resonator will vary only slightly compared with that of the fixed resonator. This can be verified by means of simulation as is shown in figures A.50 and A.51. It can be seen that for a varactor biasing voltage of 10 V the resonance frequency of the adjustable resonator is higher than that of the fixed resonator. Whereas for a varactor biasing voltage of 2 V, its resonance frequency is lower than that of the fixed resonator. This means that the reference oscillator will be capable of tracking the DUT in the experiment detailed in the next section. In both these figures it can also be seen that the magnitude of both the reflection coefficients as well as the peak of the pass band differ by approximately 1 dB between that of the fixed resonator and that of the adjustable resonator. This can be considered a very small difference in magnitude, which means that the adjustable resonator complies to a large degree with the previous criterion for a minimum phase noise level.

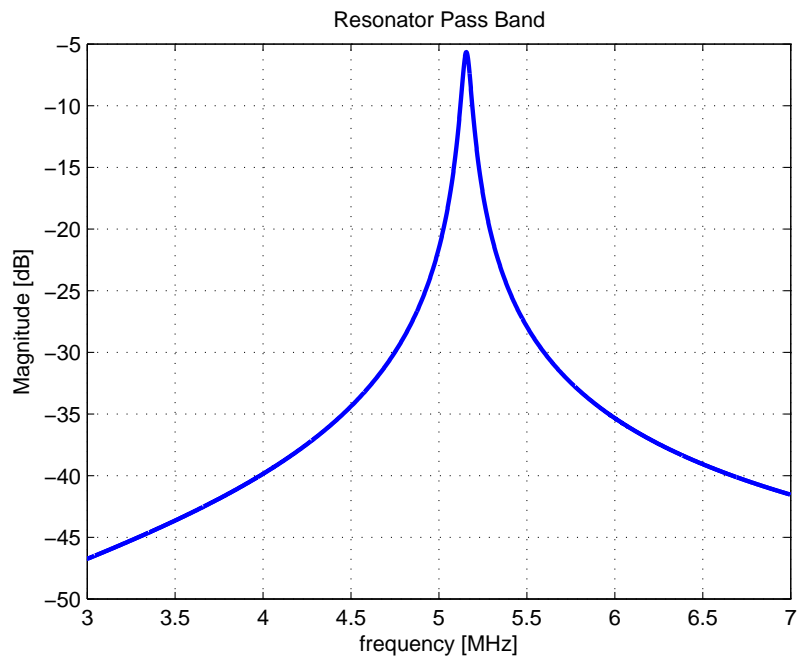


Figure A.46: Simulated fixed resonator: pass band

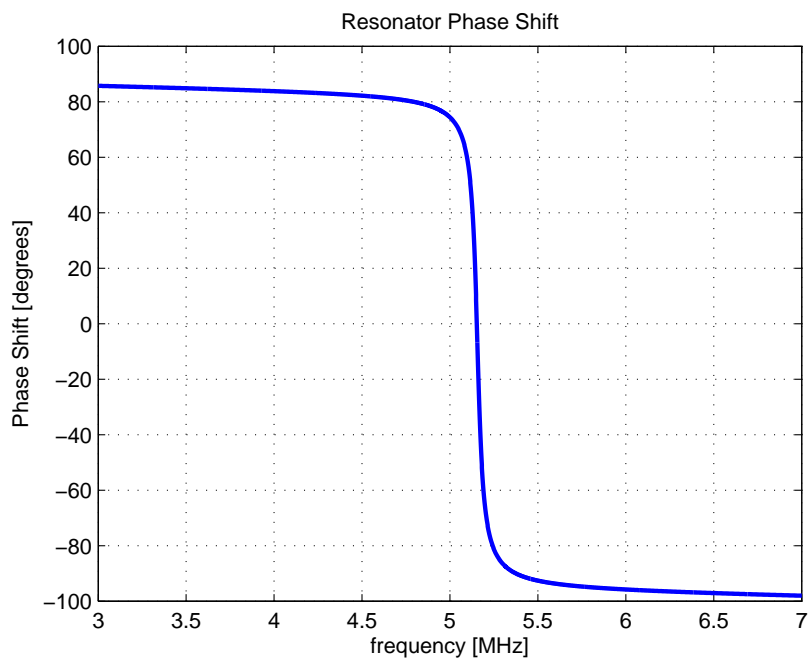


Figure A.47: Simulated fixed resonator: phase shift between input and output ports

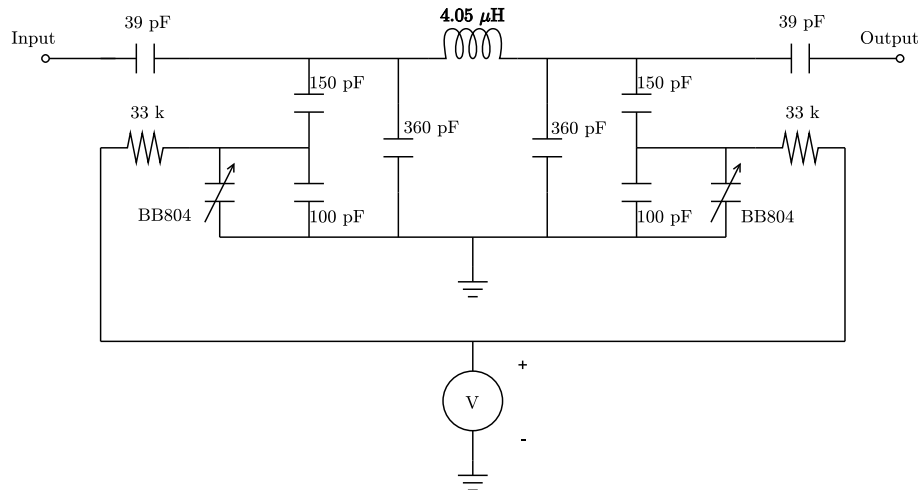


Figure A.48: Schematic diagram of voltage adjustable resonator

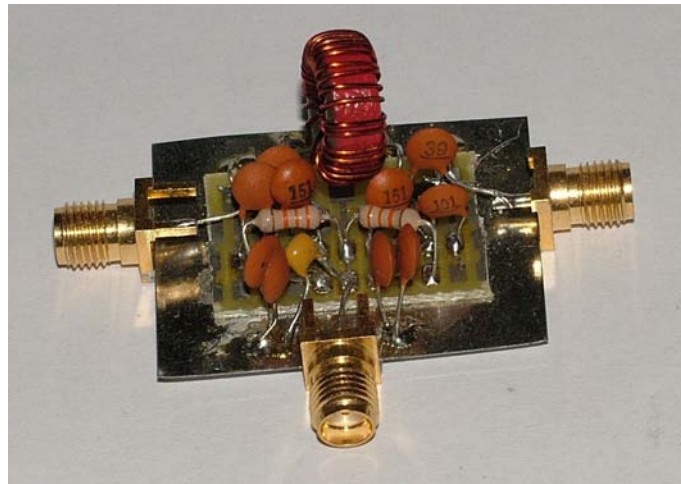


Figure A.49: Adjustable resonator

Care must be taken in choosing the resistor values between the tuning voltage and the varactors shown in figure A.48. They must be large enough to provide isolation between the resonator and the tuning voltage and so as not to degrade the resonator's quality factor, and small enough not to add an extra noise component to the circuit.

It should be noted that both the input and output ports in figure A.48 are terminated in networks with a characteristic impedance of 50Ω .

A.5.1 Measurements and Conclusions

Both of these resonators were built and measured. The results are shown in figures A.52 to A.55. Figure A.52 indicates that the fixed resonator has a reflection coeffi-

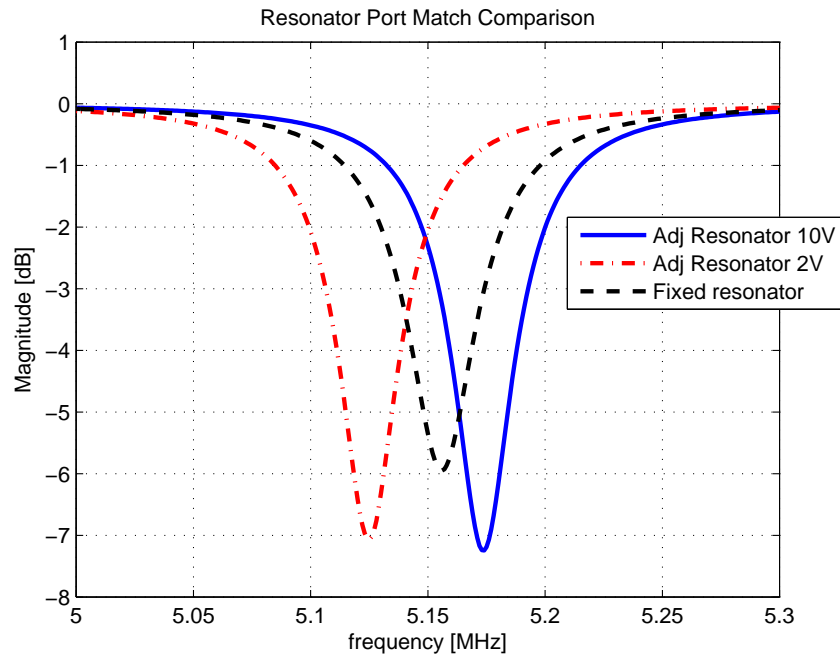


Figure A.50: Comparison of port matching of fixed and adjustable resonators

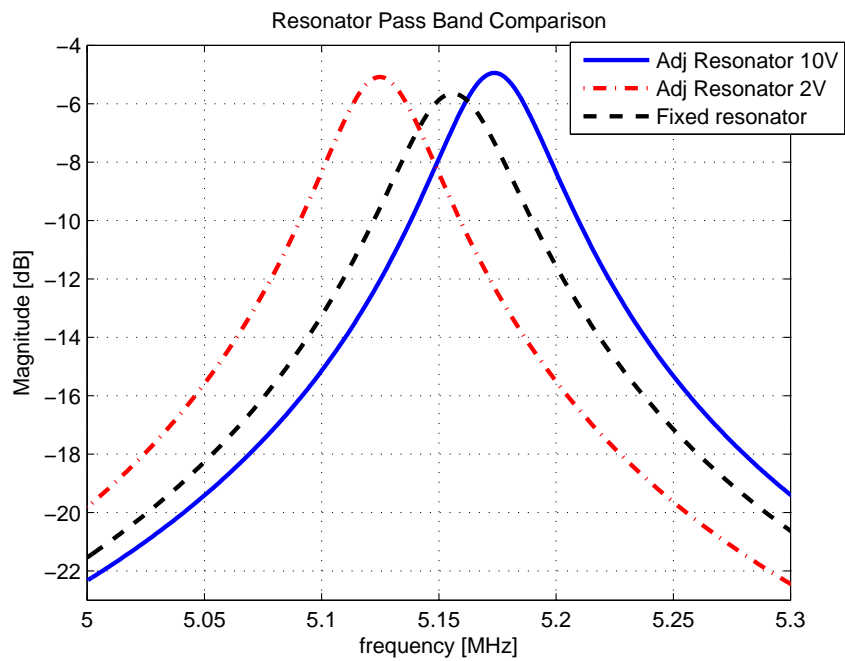


Figure A.51: Simulated comparison of resonance frequencies of fixed and adjustable resonators

cient of approximately 6.5 dB. This is very close to the desired reflection coefficient of 6 dB, implying that almost a quarter of the available signal power is reflected at both the input and output ports. The phase variation between the input and output ports, as well as the resonance frequency shown in figure A.53, are also correlated with their simulated counterparts. In other words: the fixed resonator adheres to the criterion for a minimum phase noise level and its physical performance is close to that which was simulated .

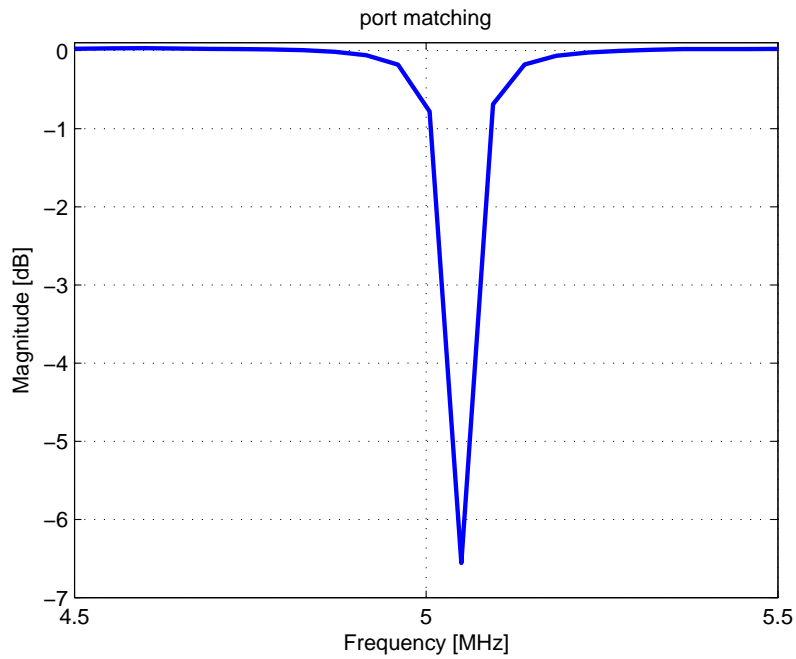


Figure A.52: Measured fixed resonator port matching

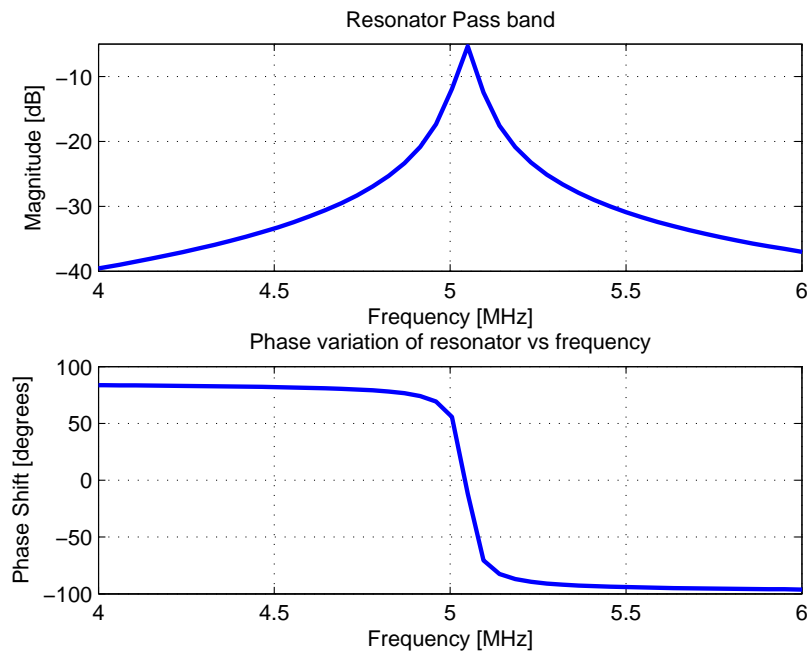


Figure A.53: Measured resonance frequency of fixed resonator

In figure A.54, measurements for different varactor biasing voltages are shown on the same graph, which illustrates how the resonance frequency changes as the biasing voltage varies. The phase shift between output and input, also shown figure A.54, does not vary to the same degree against frequency for the different biasing voltages as does the S_{21} magnitude of the resonator. The amount by which it is off is, however, negligible since this resonator is intended for use in an oscillator which is to be phase locked with our DUT.

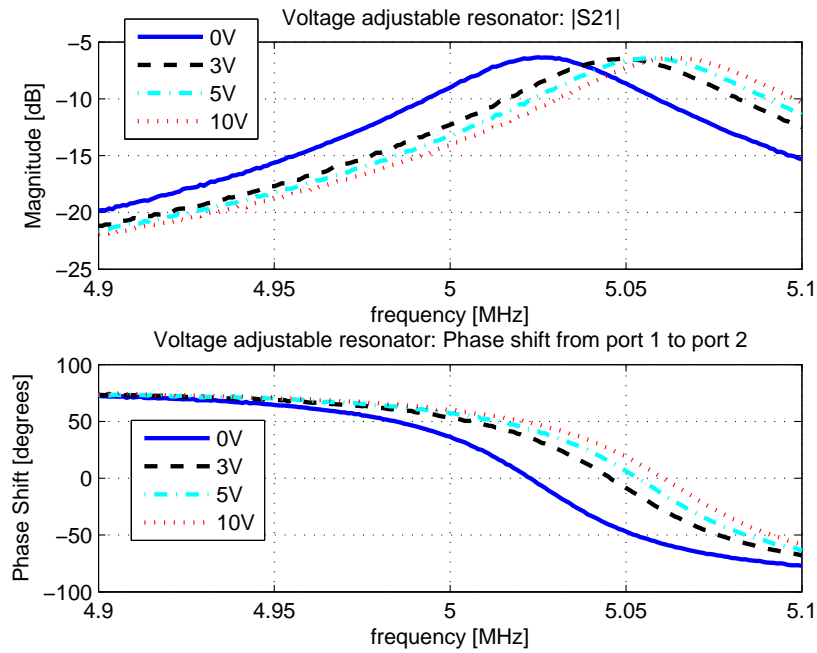


Figure A.54: Resonance frequency of adjustable resonator for various varactor biasing voltages

Figure A.55 illustrates that for a varactor biasing voltage of 10 V, the resonance frequency of the adjustable resonator is higher than that of the fixed resonator and for a biasing voltage of 0V it is far lower than the resonance frequency of the fixed resonator. This means that the voltage controlled oscillator will indeed be capable of tracking the DUT.

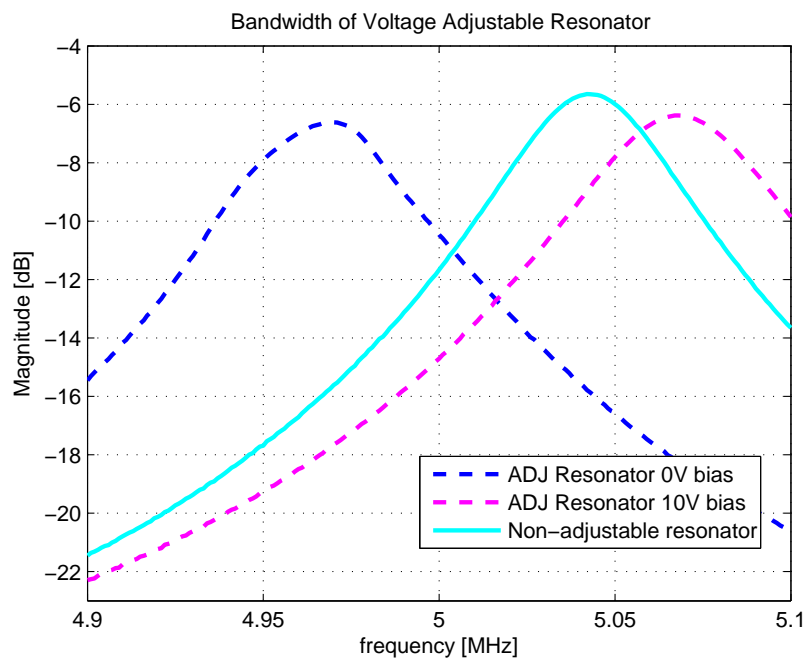


Figure A.55: Measured comparison of resonance frequencies of fixed and adjustable resonators.

Appendix B

Mini-Circuits Attenuators

Coaxial SMA Fixed Attenuator

50Ω 1W 1dB DC to 6000 MHz

VAT-1+



Connectors	Model	Price	Qty.
SMA	VAT-1+	\$11.95 ea.	(1-9)

+ RoHS compliant in accordance with EU Directive (2002/95/EC)

The +Suffix has been added in order to identify RoHS Compliance. See our web site for RoHS Compliance methodologies and qualifications.

Maximum Ratings

Operating Temperature	-45°C to 100°C
Storage Temperature	-55°C to 100°C

Permanent damage may occur if any of these limits are exceeded.

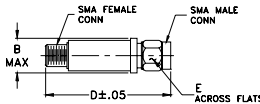
Features

- wideband coverage, DC to 6000 MHz
- 1 watt rating
- rugged unibody construction
- off-the-shelf availability
- very low cost

Applications

- impedance matching
- signal level adjustment

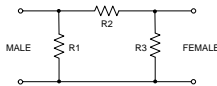
Outline Drawing



Outline Dimensions (inch)

B	D	E	wt
.410	1.43	.312	grams
10.41	36.32	7.92	10.0

Electrical Schematic



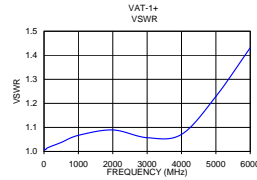
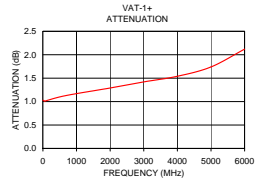
Electrical Specifications

FREQ. RANGE (MHz)	ATTENUATION * (dB)						VSWR (-1)			MAX. INPUT POWER (W)		
	DC-3 GHz		3-5 GHz		5-6 GHz		DC-3 GHz		3-5 GHz		5-6 GHz	
	Nom.	Typ.	Typ.	Typ.	Typ.	Typ.	Typ.	Max.	Typ.		Max.	Typ.
DC-6000	1±0.3	0.20	0.20	0.20	0.20	0.60	1.05	1.20	1.10	1.50	1.40	1.0

* Attenuation varies by 0.3 dB max. over temperature.
** Flatness= variation over band divided by 2.

Typical Performance Data

Frequency (MHz)	Attenuation (dB)	VSWR (-1)
0.03	1.03	1.01
50.00	1.01	1.01
100.00	1.02	1.02
500.00	1.10	1.04
1000.00	1.17	1.07
2000.00	1.29	1.09
3000.00	1.42	1.06
4000.00	1.54	1.07
5000.00	1.74	1.23
6000.00	2.12	1.43



Mini-Circuits®

ISO 9001 ISO 14001 AS 9100 CERTIFIED

P.O. Box 350166, Brooklyn, New York 11235-0003 (718) 934-4500 Fax (718) 332-4661 The Design Engineers Search Engine Provides ACTUAL Data Instantly at minicircuits.com

For detailed performance specs & shipping online see web site

Notes: 1. Performance and quality attributes and conditions not expressly stated in this specification sheet are intended to be excluded and do not form a part of this specification sheet. 2. Electrical specifications and performance data contained herein are based on Mini-Circuits' applicable established test performance criteria and measurement instructions. 3. The parts covered by this specification sheet are subject to Mini-Circuits' standard limited warranty and terms and conditions (collectively, "Standard Terms"). Purchasers of this part are entitled to the rights and benefits contained therein. For a full statement of the Standard Terms and the exclusive rights and remedies thereunder, please visit Mini-Circuits' website at www.minicircuits.com/MC_Store/terms.jsp.

REV. F
M113397
VAT-1+
LC7DC/PIAM
09814

Coaxial SMA Fixed Attenuator

50Ω 1W 3dB DC to 6000 MHz

VAT-3+



CASE STYLE: FF704

Connectors	Model	Price	Qty.
SMA	VAT-3+	\$11.95 ea.	(1-9)

+ RoHS compliant in accordance with EU Directive (2002/95/EC)

The +Suffix has been added in order to identify RoHS Compliance. See our web site for RoHS Compliance methodologies and qualifications.

Maximum Ratings

Operating Temperature	-45°C to 100°C
Storage Temperature	-55°C to 100°C

Permanent damage may occur if any of these limits are exceeded.

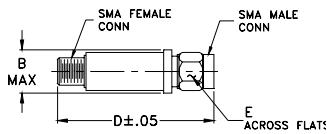
Features

- wideband coverage, DC to 6000 MHz
- 1 watt rating
- rugged unibody construction
- off-the-shelf availability
- very low cost

Applications

- impedance matching
- signal level adjustment

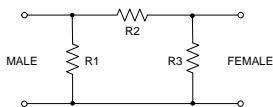
Outline Drawing



Outline Dimensions (inch/mm)

B	D	E	wt
.410	1.43	.312	grams
10.41	36.32	7.92	10.0

Electrical Schematic



Electrical Specifications

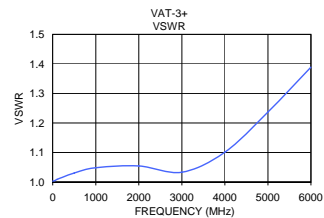
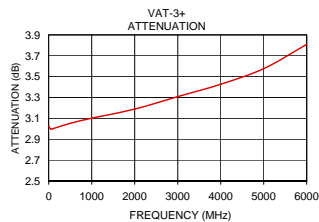
FREQ. RANGE (MHz)	ATTENUATION * (dB)					VSWR (:1)			MAX. INPUT POWER (W)	
	Flatness **					DC-3 GHz	3-5 GHz	5-6 GHz		
f_1 - f_2	Nom.	Typ.	Typ.	Typ.	Typ.	Typ.	Max.	Typ.	Max.	Typ.
DC-6000	3±0.3	0.20	0.15	0.15	0.45	1.05	1.20	1.15	1.40	1.40

* Attenuation varies by 0.3 dB max. over temperature.

** Flatness= variation over band divided by 2.

Typical Performance Data

Frequency (MHz)	Attenuation (dB)	VSWR (:1)
0.03	3.02	1.00
50.00	3.00	1.00
100.00	3.00	1.01
500.00	3.05	1.03
1000.00	3.10	1.05
2000.00	3.19	1.05
3000.00	3.31	1.03
4000.00	3.43	1.10
5000.00	3.58	1.24
6000.00	3.81	1.39



Mini-Circuits
ISO 9001 ISO 14001 AS 9100 CERTIFIED

P.O. Box 350166, Brooklyn, New York 11235-0003 (718) 934-4500 Fax (718) 332-4661 The Design Engineers Search Engine Provides ACTUAL Data Instantly at minicircuits.com

IF/RF MICROWAVE COMPONENTS

For detailed performance specs & shopping online see web site

Notes: 1. Performance and quality attributes and conditions not expressly stated in this specification sheet are intended to be excluded and do not form a part of this specification sheet. 2. Electrical specifications and performance data contained herein are based on Mini-Circuit's applicable established test performance criteria and measurement instructions. 3. The parts covered by this specification sheet are subject to Mini-Circuits standard limited warranty and terms and conditions (collectively, "Standard Terms"); Purchasers of this part are entitled to the rights and benefits contained therein. For a full statement of the Standard Terms and the exclusive rights and remedies thereunder, please visit Mini-Circuits' website at www.minicircuits.com/MCLStore/terms.jsp.

REV. F
M108294
VAT-3+
LC/TD/CP
090814

Coaxial SMA Fixed Attenuator

50Ω 1W 6dB DC to 6000 MHz

VAT-6+



CASE STYLE: FF704

Connectors	Model	Price	Qty.
SMA	VAT-6+	\$11.95 ea.	(1-9)

+ RoHS compliant in accordance with EU Directive (2002/95/EC)

The +Suffix has been added in order to identify RoHS Compliance. See our web site for RoHS Compliance methodologies and qualifications.

Maximum Ratings

Operating Temperature	-45°C to 100°C
Storage Temperature	-55°C to 100°C

Permanent damage may occur if any of these limits are exceeded.

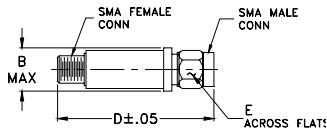
Features

- wideband coverage, DC to 6000 MHz
- 1 watt rating
- rugged unibody construction
- off-the-shelf availability
- very low cost

Applications

- impedance matching
- signal level adjustment

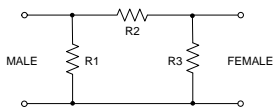
Outline Drawing



Outline Dimensions (inch/mm)

B	D	E	wt
.410	1.43	.312	grams
10.41	36.32	7.92	10.0

Electrical Schematic



Electrical Specifications

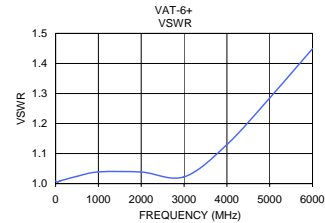
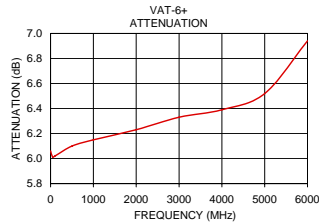
FREQ. RANGE (MHz)	ATTENUATION * (dB)					VSWR (:1)			MAX. INPUT POWER (W)	
	Flatness **					DC-3 GHz		3-5 GHz		5-6 GHz
f_1 - f_2	Nom.	Typ.	Typ.	Typ.	Typ.	Typ.	Max.	Typ.	Max.	Typ.
DC-6000	6±0.3	0.15	0.10	0.20	0.45	1.05	1.20	1.15	1.45	1.50

* Attenuation varies by 0.3 dB max. over temperature.

** Flatness= variation over band divided by 2.

Typical Performance Data

Frequency (MHz)	Attenuation (dB)	VSWR (:1)
0.03	6.06	1.01
50.00	6.01	1.00
100.00	6.02	1.01
500.00	6.10	1.02
1000.00	6.15	1.04
2000.00	6.23	1.04
3000.00	6.33	1.02
4000.00	6.39	1.13
5000.00	6.52	1.29
6000.00	6.94	1.45



Mini-Circuits
ISO 9001 ISO 14001 AS 9100 CERTIFIED

P.O. Box 350166, Brooklyn, New York 11235-0003 (718) 934-4500 Fax (718) 332-4661 The Design Engineers Search Engine Provides ACTUAL Data Instantly at minicircuits.com

IF/RF MICROWAVE COMPONENTS

For detailed performance specs & shipping online see web site

Notes: 1. Performance and quality attributes and conditions not expressly stated in this specification sheet are intended to be excluded and do not form a part of this specification sheet. 2. Electrical specifications and performance data contained herein are based on Mini-Circuit's applicable established test performance criteria and measurement instructions. 3. The parts covered by this specification sheet are subject to Mini-Circuits standard limited warranty and terms and conditions (collectively, "Standard Terms"); Purchasers of this part are entitled to the rights and benefits contained therein. For a full statement of the Standard Terms and the exclusive rights and remedies thereunder, please visit Mini-Circuits' website at www.minicircuits.com/MCLStore/terms.jsp.

REV. F
M108234
VAT-6+
LC/TD/CP
090814

Coaxial SMA Fixed Attenuator

50Ω 1W 10dB DC to 6000 MHz

VAT-10+



CASE STYLE: FF704

Connectors	Model	Price	Qty.
SMA	VAT-10+	\$11.95 ea.	(1-9)

+ RoHS compliant in accordance with EU Directive (2002/95/EC)

The +Suffix has been added in order to identify RoHS Compliance. See our web site for RoHS Compliance methodologies and qualifications.

Maximum Ratings

Operating Temperature	-45°C to 100°C
Storage Temperature	-55°C to 100°C

Permanent damage may occur if any of these limits are exceeded.

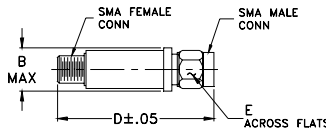
Features

- wideband coverage, DC to 6000 MHz
- 1 watt rating
- rugged unibody construction
- off-the-shelf availability
- very low cost

Applications

- impedance matching
- signal level adjustment

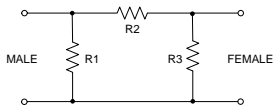
Outline Drawing



Outline Dimensions (inch/mm)

B	D	E	wt
.410	1.43	.312	grams
10.41	36.32	7.92	10.0

Electrical Schematic



Electrical Specifications

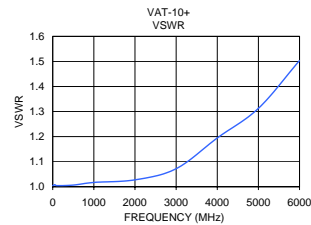
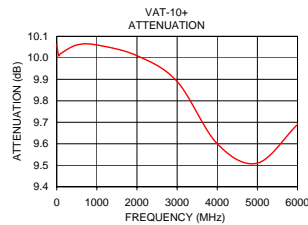
FREQ. RANGE (MHz)	ATTENUATION * (dB)					VSWR (:1)			MAX. INPUT POWER (W)	
	Flatness **					DC-3 GHz	3-5 GHz	5-6 GHz		
f_1 - f_2	Nom.	Typ.	Typ.	Typ.	Typ.	Typ.	Max.	Typ.	Max.	Typ.
DC-6000	10±0.3	0.10	0.20	0.15	0.35	1.05	1.25	1.20	1.60	1.90

* Attenuation varies by 0.3 dB max. over temperature.

** Flatness= variation over band divided by 2.

Typical Performance Data

Frequency (MHz)	Attenuation (dB)	VSWR (:1)
0.03	10.06	1.00
50.00	10.01	1.01
100.00	10.02	1.00
500.00	10.06	1.01
1000.00	10.06	1.02
2000.00	10.01	1.03
3000.00	9.89	1.07
4000.00	9.60	1.19
5000.00	9.51	1.31
6000.00	9.69	1.50



Mini-Circuits
ISO 9001 ISO 14001 AS 9100 CERTIFIED

P.O. Box 350186, Brooklyn, New York 11235-0003 (718) 934-4500 Fax (718) 332-4661 The Design Engineers Search Engine Provides ACTUAL Data Instantly at minicircuits.com

IF/RF MICROWAVE COMPONENTS

For detailed performance specs & shopping online see web site

Notes: 1. Performance and quality attributes and conditions not expressly stated in this specification sheet are intended to be excluded and do not form a part of this specification sheet. 2. Electrical specifications and performance data contained herein are based on Mini-Circuit's applicable established test performance criteria and measurement instructions. 3. The parts covered by this specification sheet are subject to Mini-Circuits standard limited warranty and terms and conditions (collectively, "Standard Terms"); Purchasers of this part are entitled to the rights and benefits contained therein. For a full statement of the Standard Terms and the exclusive rights and remedies thereunder, please visit Mini-Circuits' website at www.minicircuits.com/MCLStore/terms.jsp.

REV. F
M113397
VAT-10+
LC/TD/CP/AM
090814

Appendix C

Hardware Used in Experiment 2 and Experiment 3

C.1 Resistive Feedback Amplifier

A schematic of a resistive feedback amplifier, like the one used in Experiment 2 and Experiment 3, is shown in figure C.2. The component values that were used are shown in table C.1. The collector and base reference voltages, V_C and V_B , are provided by two separate voltage regulators. V_C was set to 6V and V_B was adjusted to 1.9V. The design was adapted from a similar amplifier illustrated in [6]. The measured results are shown in figures C.3 through C.8. These measurements confirm that this amplifier is well matched at both ports, figures C.3 and C.4, and that the isolation between these ports is acceptable at less than -15dB as is illustrated in figure C.6. The measurements also indicate that the amplifier can handle a relatively high input power, 7 dBm, before being driven into saturation, as is illustrated in figure

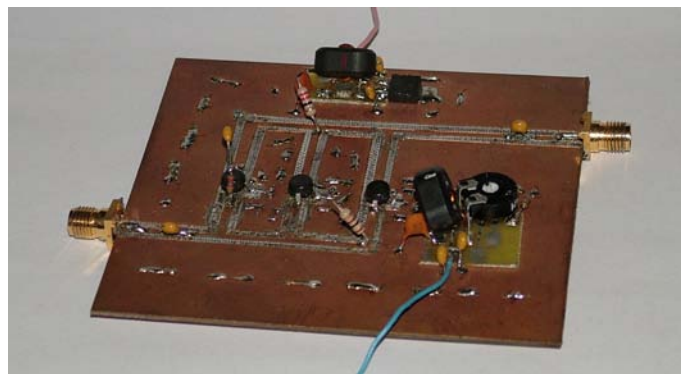


Figure C.1: Resistive feedback amplifier

C.8. Figure C.7 shows that the amplifier's gain stays almost constant up to this input power level.

Table C.1: Component values of the resistive feedback amplifier.

Component	Value
R_C	22Ω
R_B	100Ω
R_E	27Ω
R_{fb}	270Ω
C_{fb}	100nF
C_{in}	100nF
C_{out}	100nF

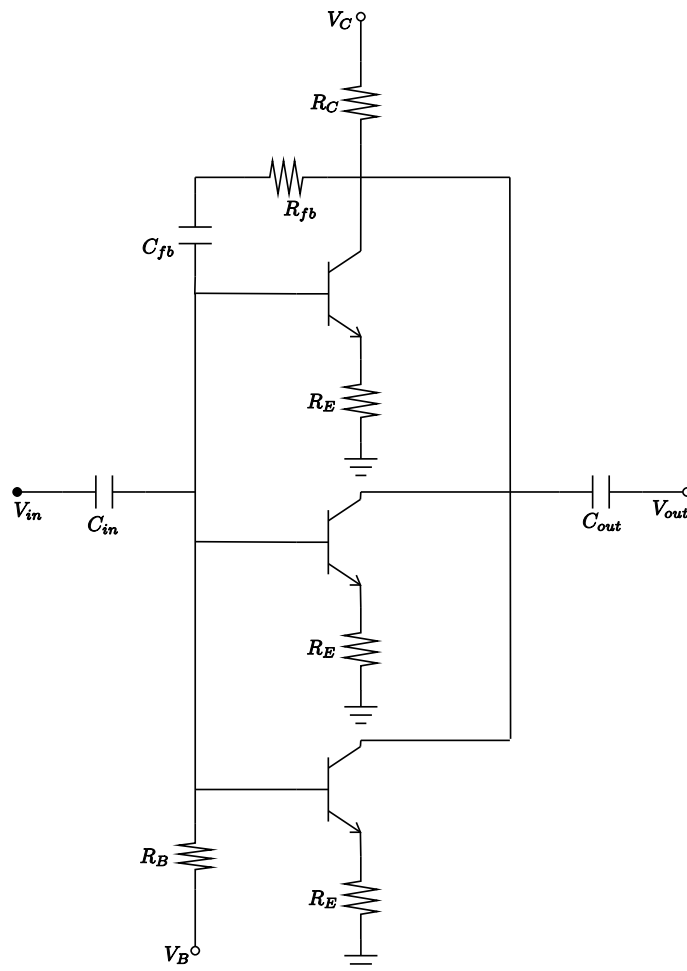


Figure C.2: Schematic of resistive feedback amplifier

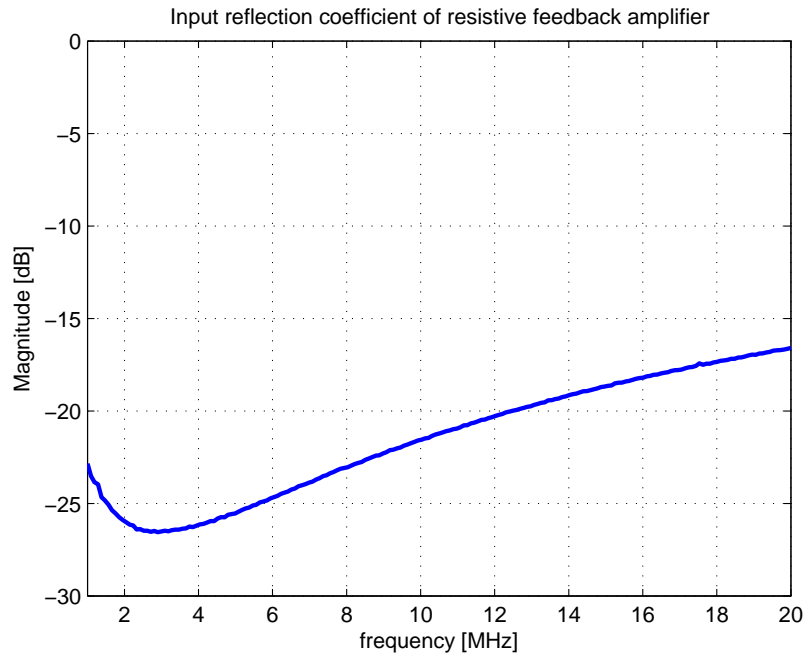


Figure C.3: Resistive feedback amplifier:input port matching

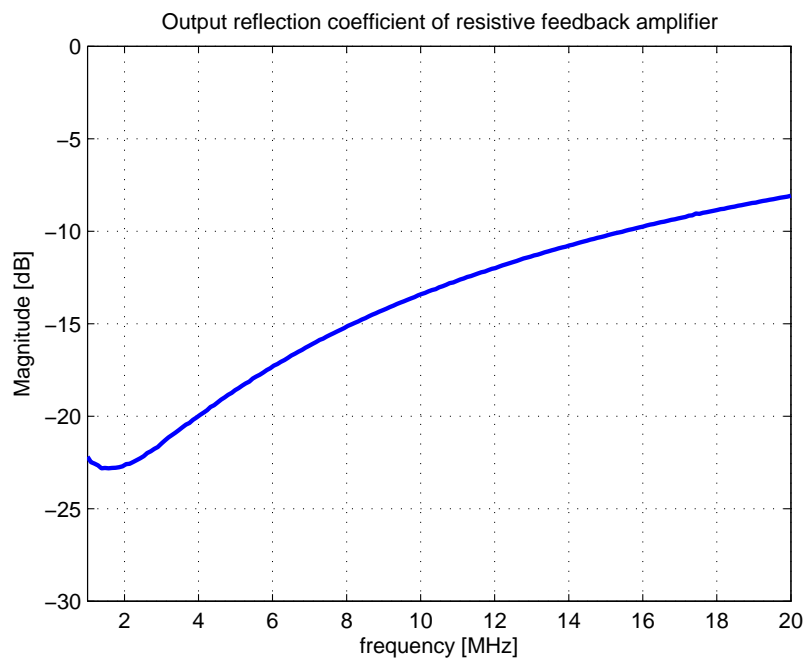


Figure C.4: Resistive feedback amplifier: output port matching

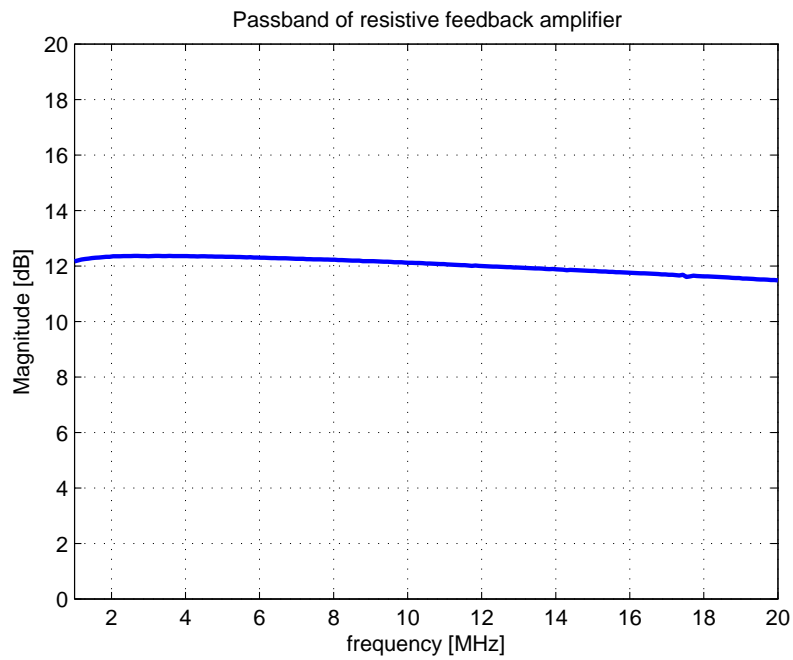


Figure C.5: Resistive feedback amplifier: gain vs frequency

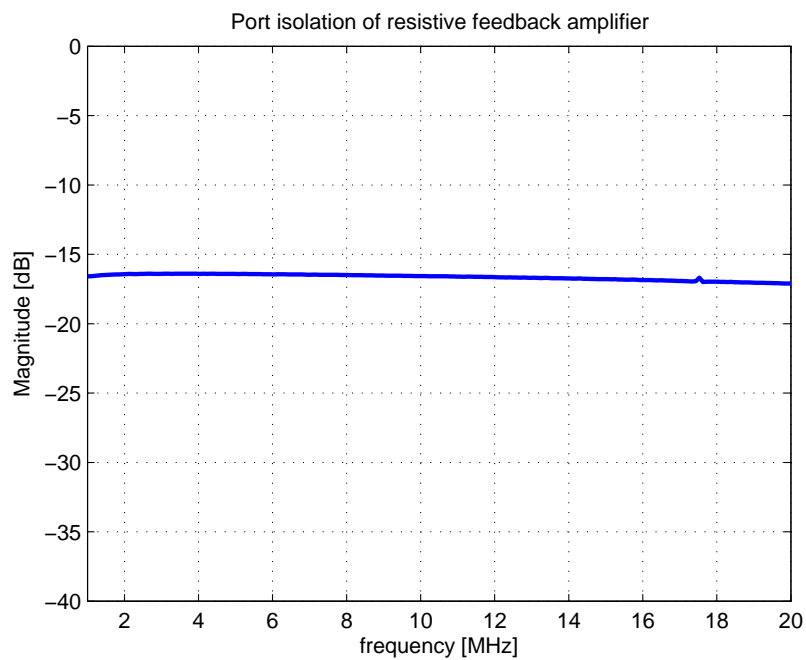


Figure C.6: Resistive feedback amplifier: isolation between the input and output ports

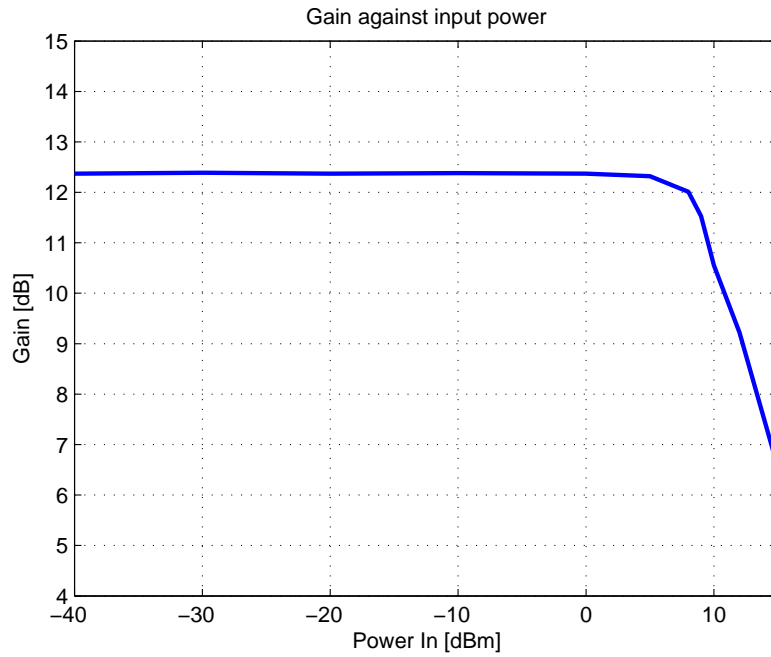


Figure C.7: Resistive feedback amplifier: gain vs input power

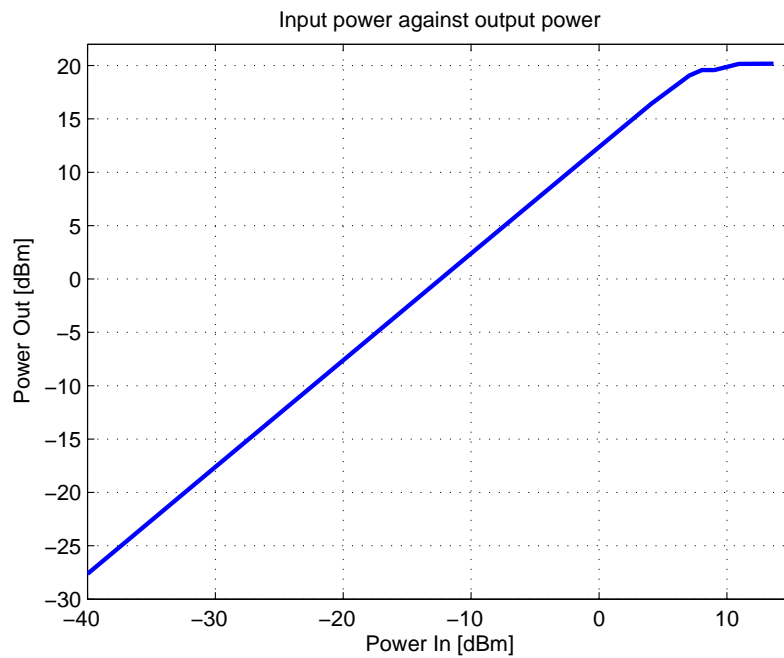


Figure C.8: Resistive feedback amplifier: output power vs input power

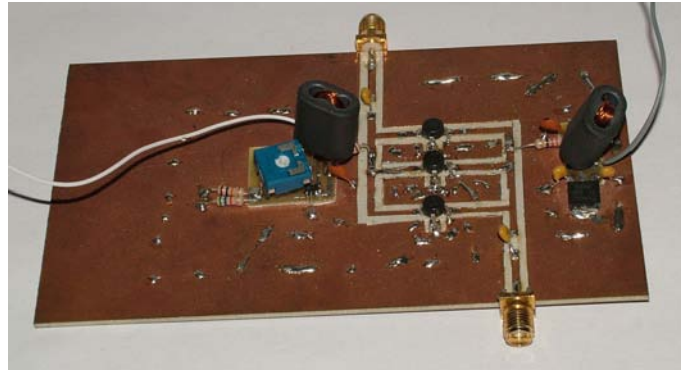


Figure C.9: Amplifier without feedback used in experiment 2

C.2 Amplifier without Feedback

The feedback resistor and capacitor of an amplifier identical to the one described in Appendix C.1, were removed. The base biasing voltage was adjusted and the amplifier was subsequently measured. The results are illustrated in figures C.10 through C.12.

The measurements indicate that the amplifier is poorly matched and that its gain is approximately 5 dB higher than that of the amplifier with feedback.

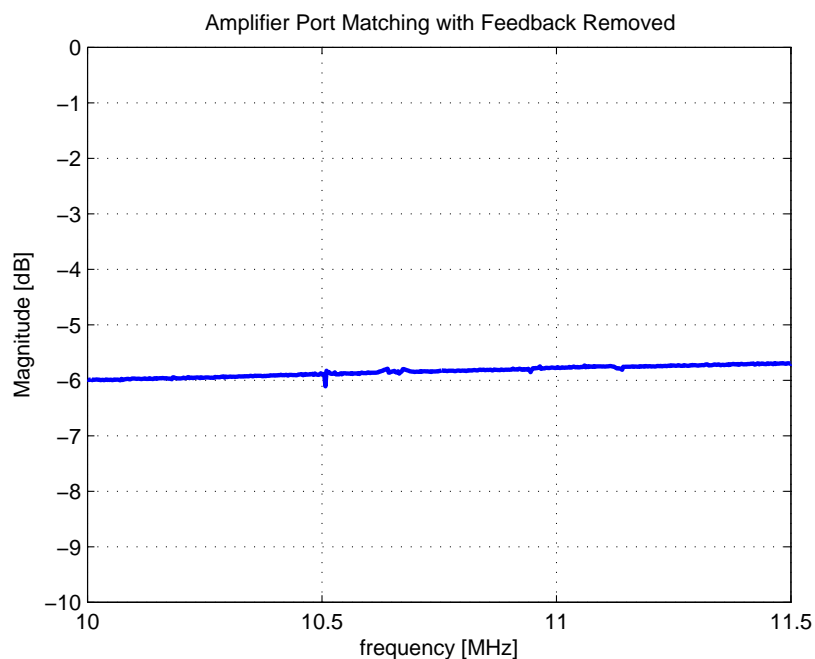


Figure C.10: Amplifier without feedback: input port matching

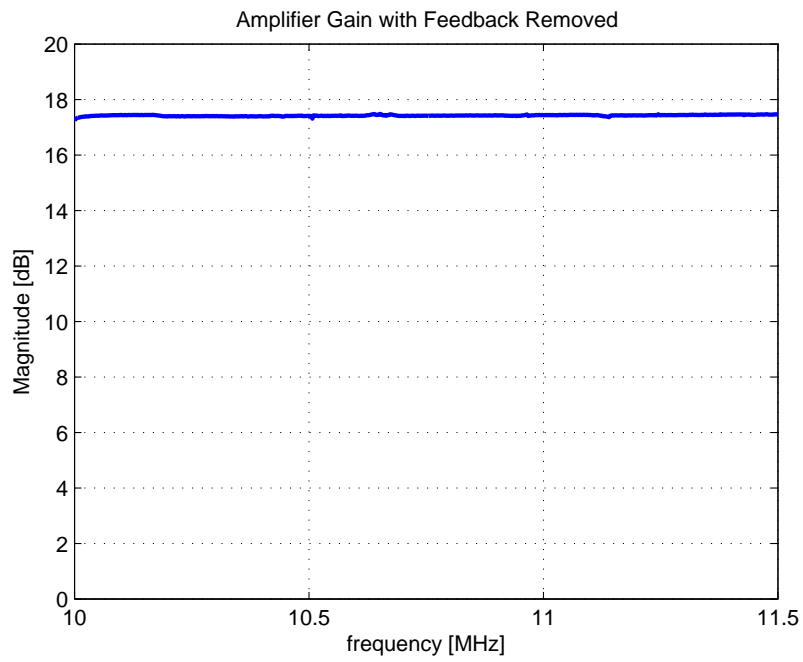


Figure C.11: Amplifier without Feedback: Amplifier Gain

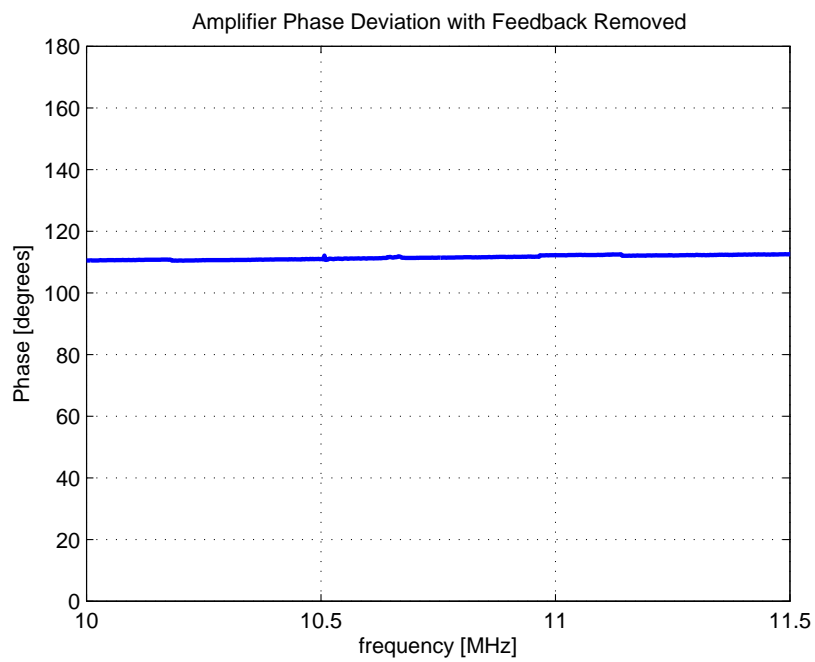


Figure C.12: Amplifier without Feedback: Phase Deviation

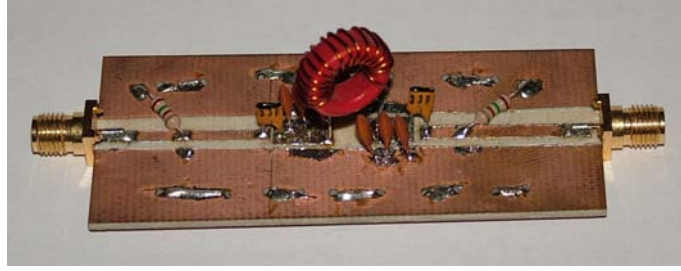


Figure C.13: 10 MHz LC resonator

C.3 10 MHz Resonator

During the design the same procedure discussed in Appendix A.5 was followed, with the exception that the resonator was then resistively matched to 50Ω . The schematic diagram of the resonator is shown in figure C.14 and its component values are listed in table C.2.

Table C.2: Component values of the 10 MHz matched resonator

Component	Value
L	$1.4\mu\text{H}$
C_s	33pF
C_p	300pF
R	120Ω

The resonator was measured and the results are shown in the following figures. These figures clearly indicate that the resonator is well matched at both ports. Figure C.16 also indicates that the resonator performs very close to the criteria for optimal phase noise. Roughly 8 dB of the input power is dissipated within the resonator at the resonant frequency. This may be considered close to the optimal level of 6 dB.

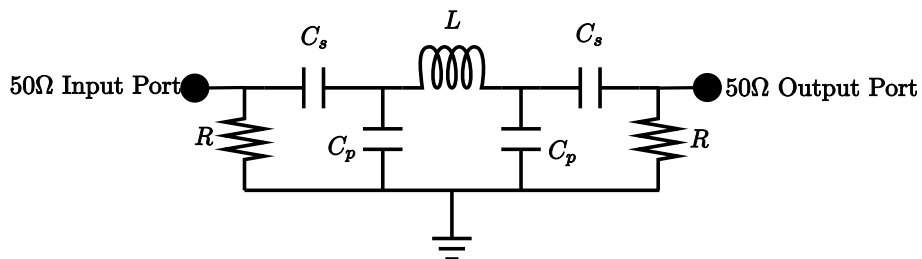


Figure C.14: 10 MHz LC resonator with resistive matching

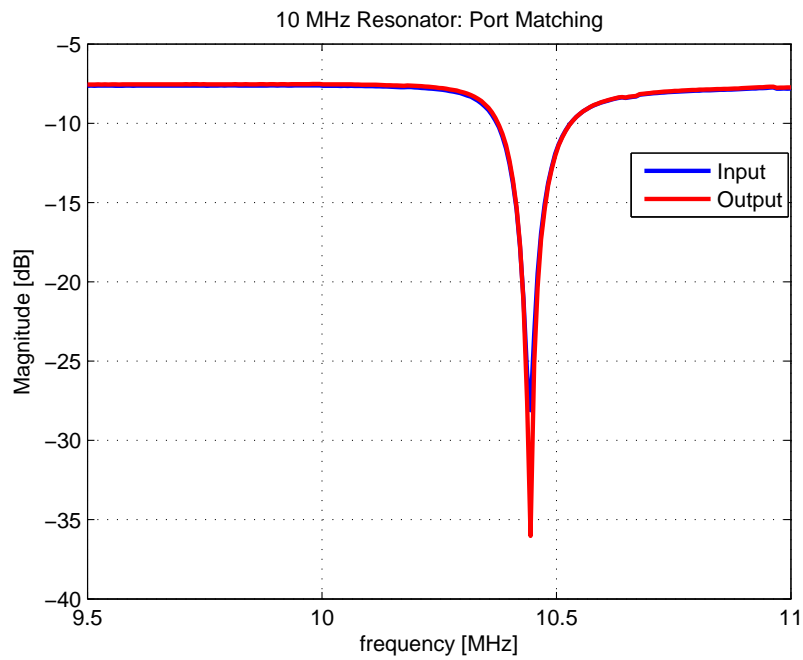


Figure C.15: 10 MHz resonator: port matching

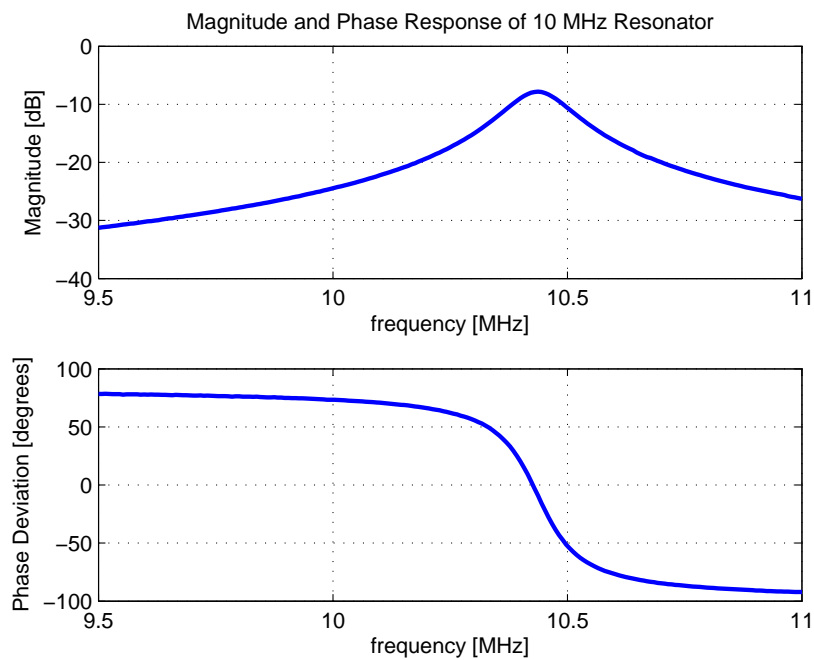


Figure C.16: 10 MHz resonator: magnitude and phase response

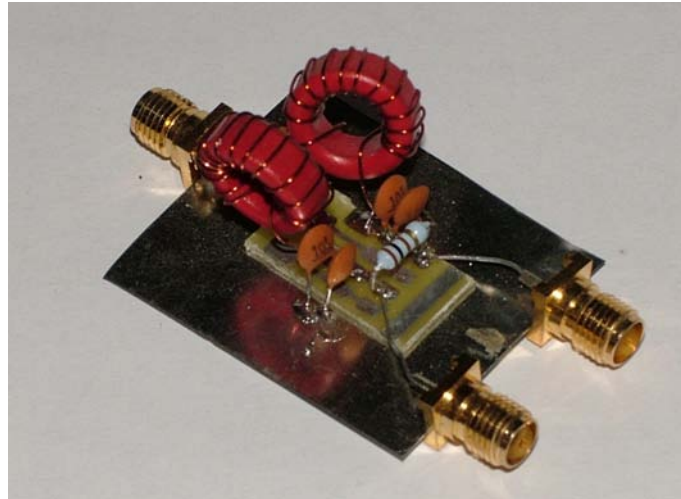


Figure C.17: 10 MHz Wilkinson power divider

C.4 10 MHz Wilkinson Divider

The same principles discussed in Appendix A.2 for LC Wilkinson power dividers apply here and a 10 MHz Wilkinson Power Divider was designed accordingly. The measured results are shown in figures C.18 through C.21 and illustrate that the divider functions admirably.

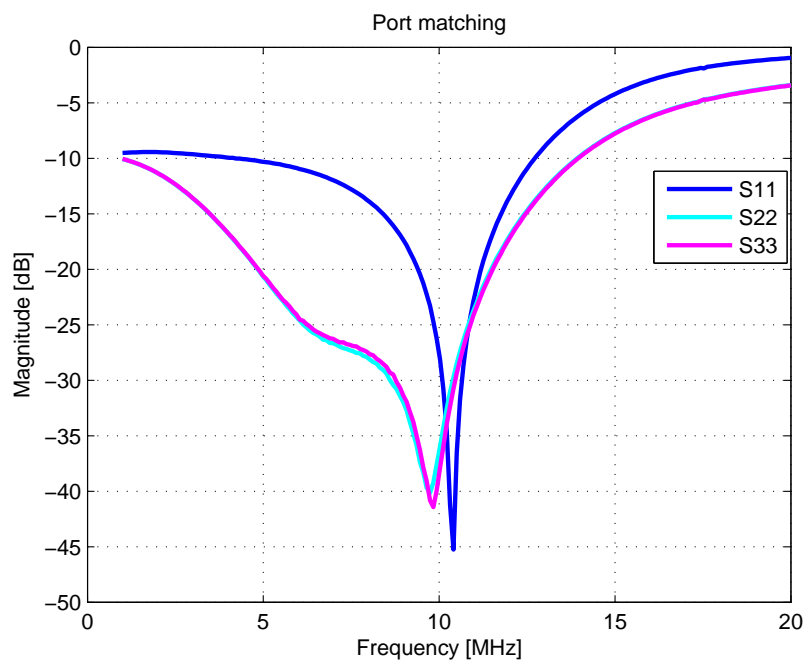


Figure C.18: 10 MHz LC Wilkinson power divider: port matching

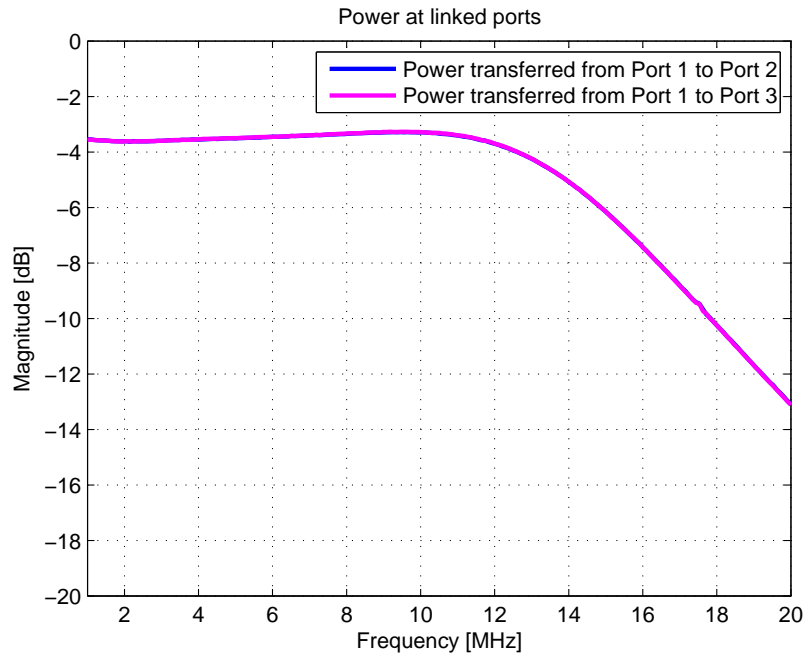


Figure C.19: 10 MHz LC wilkinson power divider:

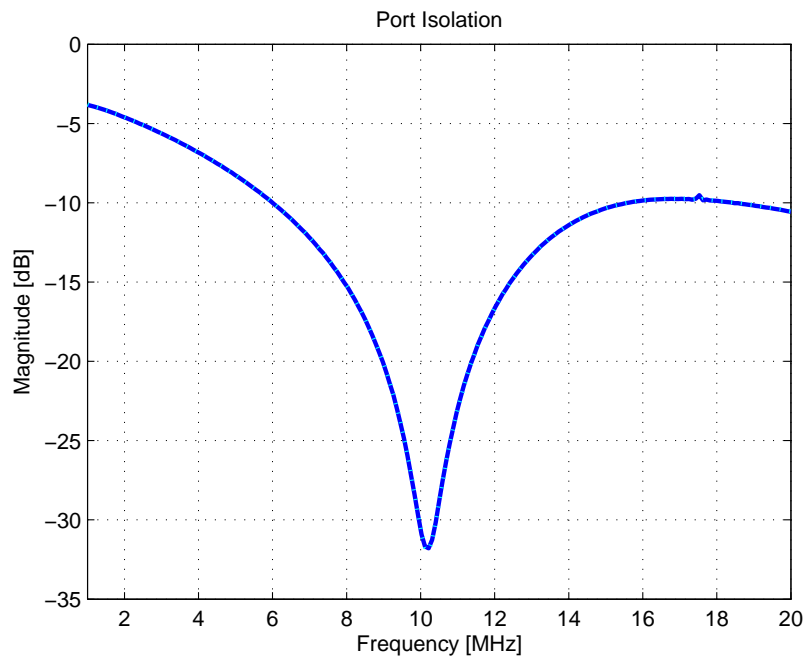


Figure C.20: 10 MHz LC Wilkinson power divider: output port isolation

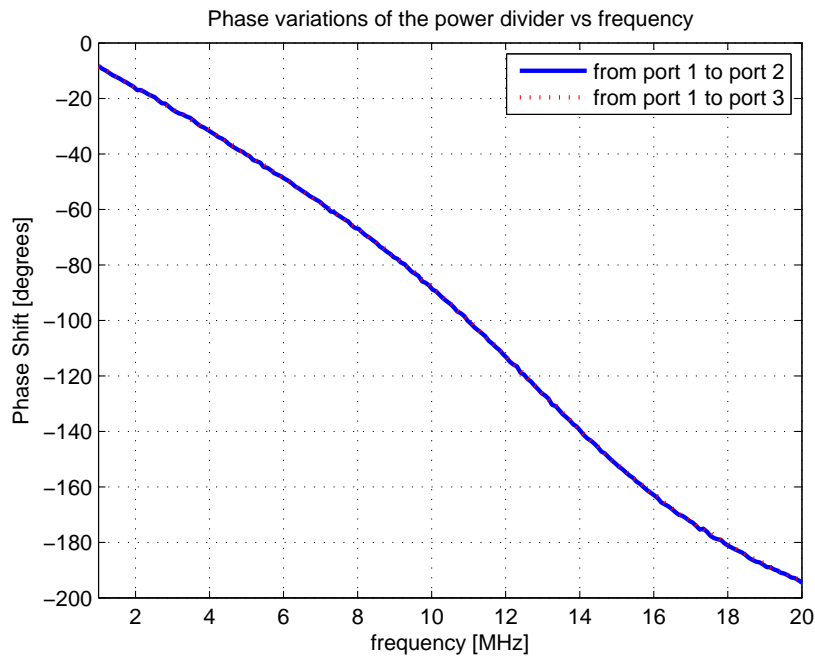


Figure C.21: 10 MHz LC Wilkinson power divider: phase deviation

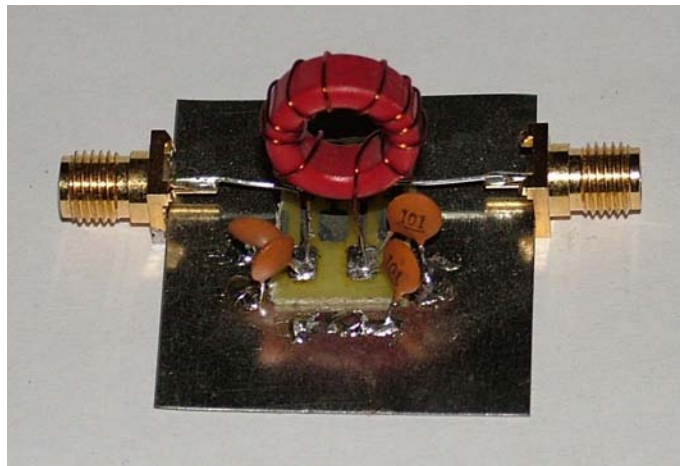


Figure C.22: Phase shifter

C.5 Phase Shift Network

The design of the 68° phase shifter starts off with the quarter wave approximation described in Appendix A.2. In order to change the resulting 90° phase shift to a 68° phase shift an optimisation process was applied in MWO. This resulted in the values C_p and L_s , defined in Appendix A.2, being set to 210 pF and $0.7 \mu\text{H}$ respectively. This design was implemented and the measured results are shown in figures C.23 and C.24. These measurements indicate that the desired phase shift is achieved,

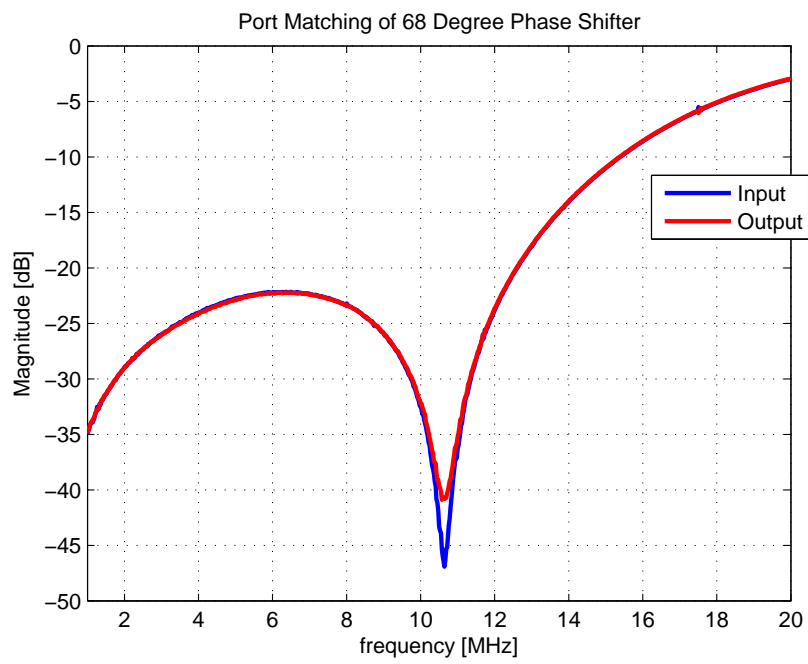


Figure C.23: 68°Phase Shifter: port matching

that the network is well matched and that very few losses occur at the operating frequency of 10 MHz.

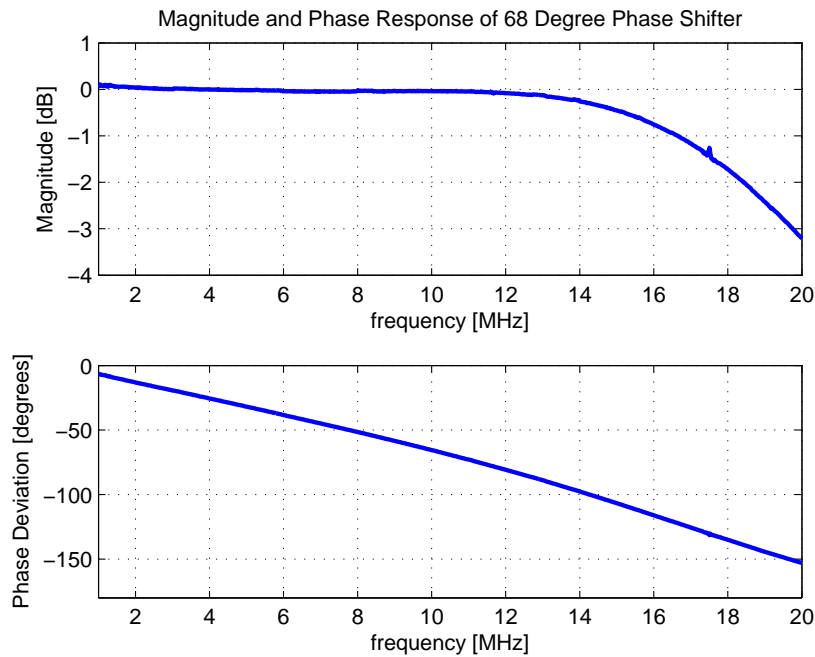


Figure C.24: 68°Phase shifter: magnitude and phase response

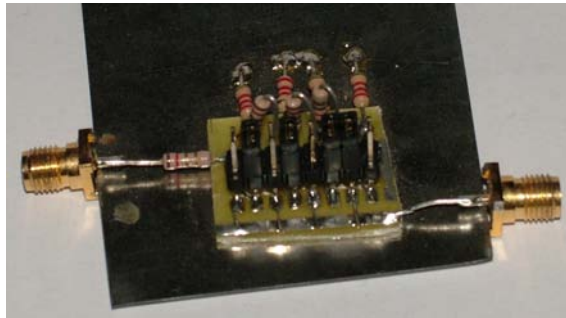


Figure C.25: Variable attenuator

C.6 Variable Attenuator

A resistive, variable attenuator was designed of which the schematic diagram is illustrated in figure C.26. Resistors in the attenuator network can be switched in and out of the network by means of placing or removing jumpers. The various attenuation settings can be realised by placing the previously mentioned jumpers as is indicated in table C.3. The respective jumper positions are indicated on the schematic diagram of figure C.26.

The realised attenuative losses were measured for each of the attenuation settings listed in table C.3 and are shown in figure C.27. The measurements show that these losses closely approximate the attenuation settings which they were designed for.

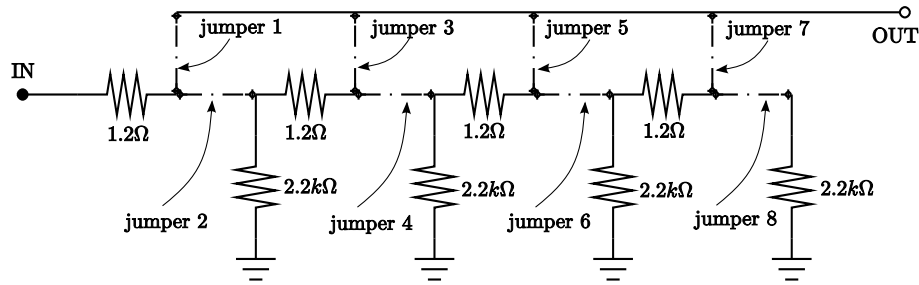


Figure C.26: Variable attenuator: schematic diagram

Table C.3: Variable attenuator: attenuation settings

Attenuation	Jumpers Placed
0.1 dB	1
0.2 dB	1, 2
0.3 dB	2, 3
0.4 dB	2, 3, 4
0.5 dB	2, 4, 5
0.6 dB	2, 4, 5, 6
0.7 dB	2, 4, 6, 7
0.8 dB	2, 4, 6, 7, 8

(Within 0.05 dB.)

In figures C.28 and C.29, it is shown that the attenuator is well matched for all attenuation settings at both its input and output ports.

Figure C.30 illustrates the variations in the phase shift from the input port to the output port of the attenuator for the various attenuation settings. The variations may be associated with the increase in the signal's path length, as more resistors are being switched into the network. At any specific frequency however, these variations differ by no more than three degrees and may be considered negligible.

The attenuator described in this section allows for the adjustment of the amount of its attenuation in steps of approximately 0.1 dB with very little phase deviation between the various attenuation settings. This implies that, when used in an oscillator network, this circuit will have a minimal effect upon the phase conditions for oscillation.

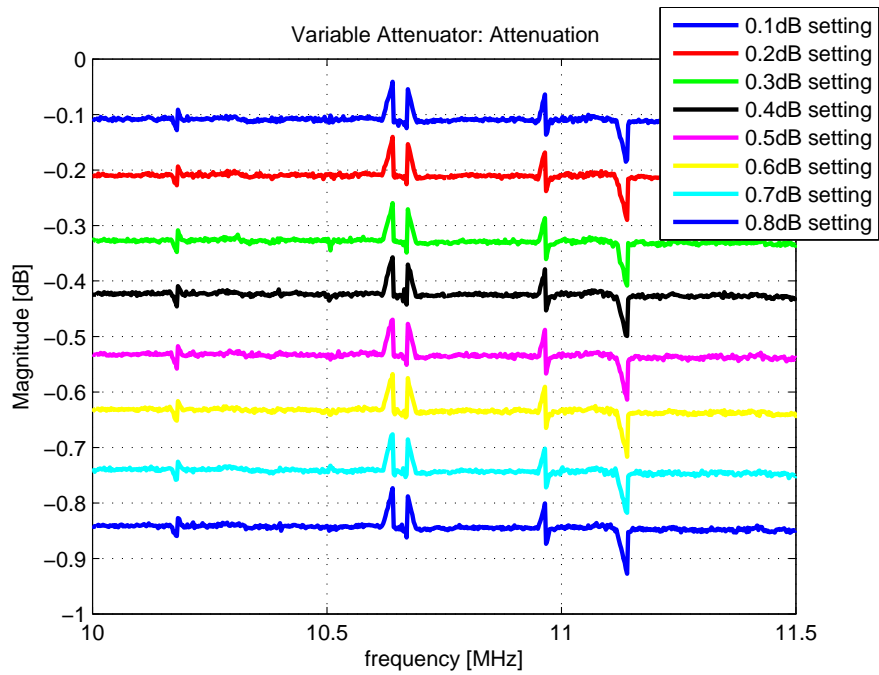


Figure C.27: Variable attenuator: attenuative losses

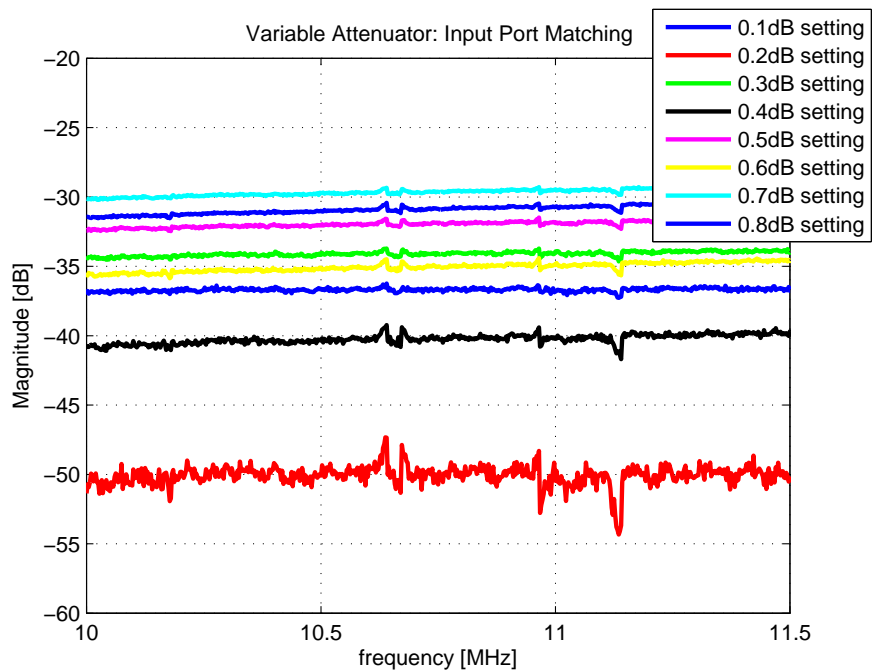


Figure C.28: Variable attenuator: input port matching

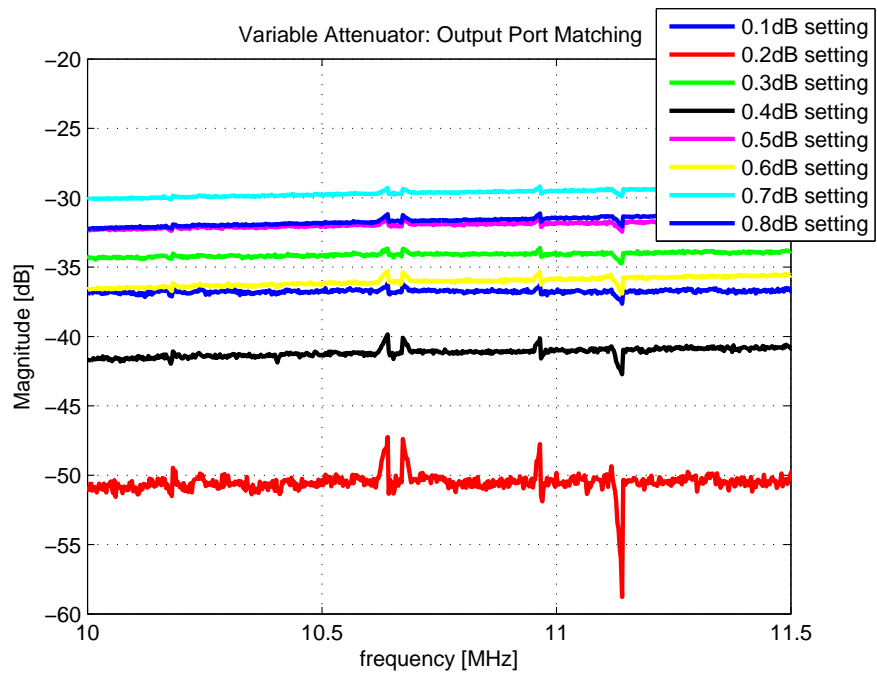


Figure C.29: Variable attenuator: output port matching

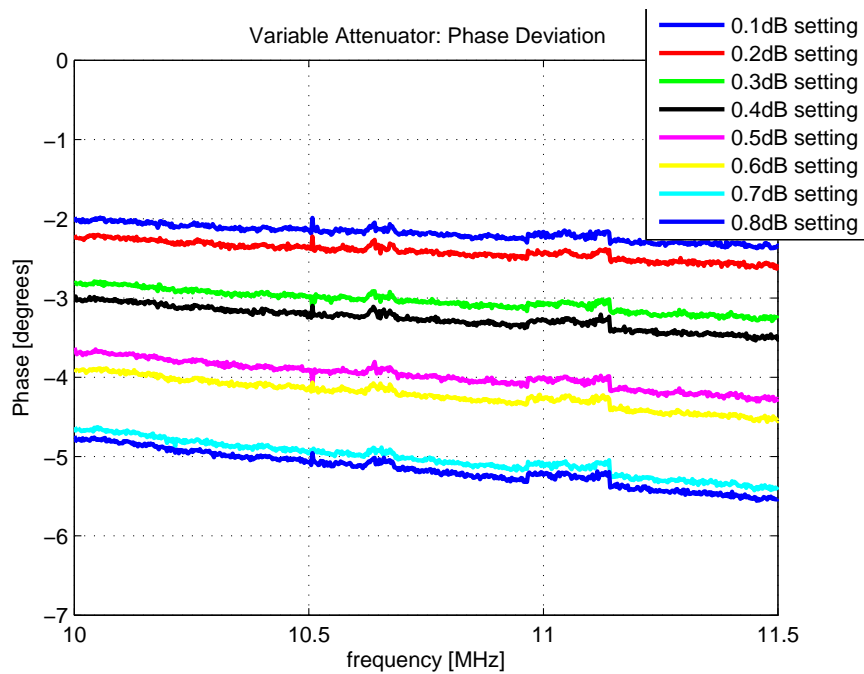


Figure C.30: Variable attenuator: phase deviation

Appendix D

Hardware Used in Experiments 4 to 6

D.1 SC-Cut Crystal Resonator

D.1.1 Design and Measurement

A crystal resonator was designed using an SC-cut crystal. A schematic of the resonator is shown in figure D.2. Since the crystal can handle a maximum of 5 mW, it was decided to couple to and from the crystal using transformers. In order to limit the power absorbed in the crystal, resistive networks were used.

This resonator was built and subsequently measured. The measured results are illustrated in figures D.3 through D.6. The high quality factor of the resonator and the limitation of the measuring equipment's resolution, resulted in the measured data



Figure D.1: Crystal resonator

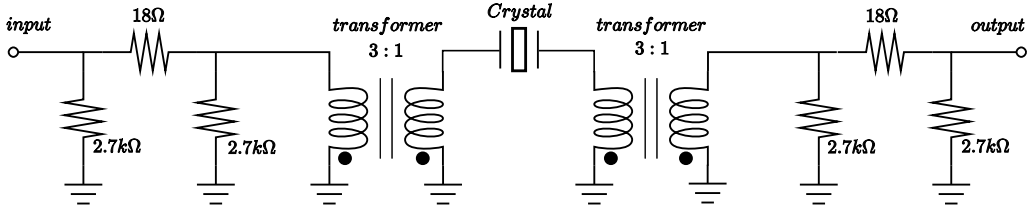


Figure D.2: Crystal resonator schematic

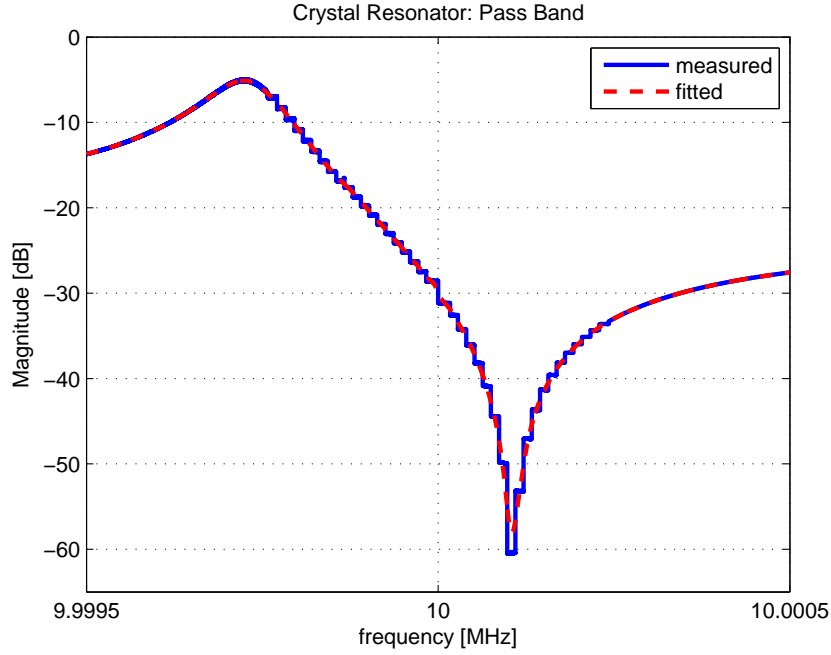


Figure D.3: Crystal resonator: pass band

being discretised. This is depicted in figures D.3 through D.5 by the dashed lines. In order to get a more realistic impression of the crystal resonator's characteristics, the measured data was smoothed using Matlab. These fitted results are illustrated by the solid line in the last mentioned figures. Note that the measurements depicted in figure D.6 are constructed from the fitted curves.

This resonator is matched at the resonant frequency and has a quality factor in excess of 86 000. The quality factor is calculated using the formula

$$Q = \pi f_0 \tau_{g0} = 86799.6 \quad (\text{D.1})$$

where f_0 is the resonant frequency and τ_{g0} is the group delay of the resonator at the resonant frequency.

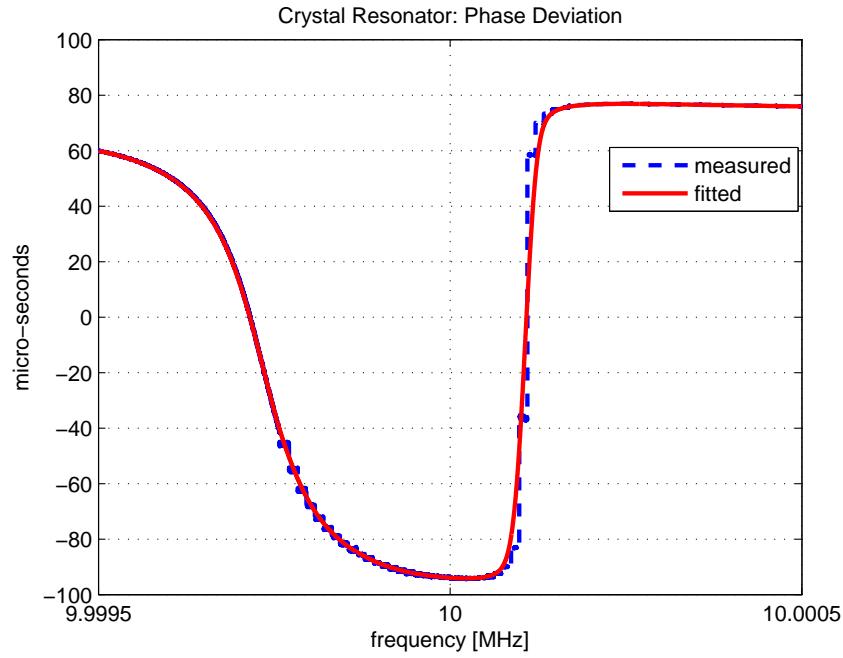
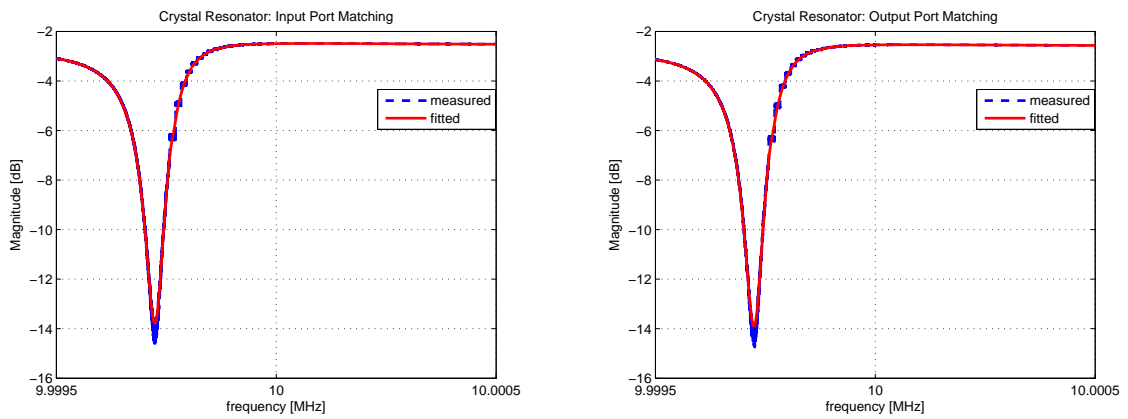


Figure D.4: Crystal resonator: phase deviation



Input port matching

Output port matching

Figure D.5: Crystal resonator: port matching

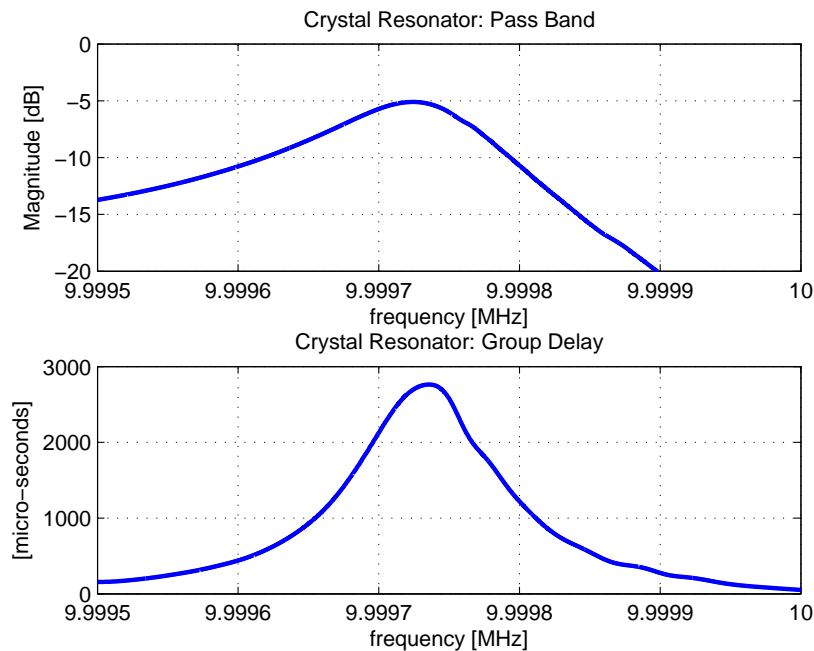


Figure D.6: Crystal resonator: fitted group delay with regard to pass band

D.2 Modified Resistive Feedback Amplifier

In order to suppress the noise entering the oscillator from the voltage source or regulators, the resistive feedback amplifier used in chapters 5, 6 and 7 was modified as follows. The adjustable voltage regulator that had been connected to base side of the amplifier was removed and replaced with a resistive divider network connecting the base to the collector voltage. The amplifier therefore now runs from a single voltage regulator. Before entering the network, the output voltage of this regulator is passed through an operational amplifier circuit in order to suppress any random noise fluctuations. The modifications are shown in figure D.7.

D.2.1 Measurements

The modified resistive feedback amplifier was subsequently measured. It was found that both the input and output ports are sufficiently matched to $50\ \Omega$, as is illustrated in figure D.8. The isolation between the output and input ports, depicted in figure D.9, is also more than adequate as less than one 40th of the output signal leaks back. Figure D.10 shows that the modified amplifier has roughly the same gain as the original and figure D.11 indicates a near linear phase deviation across the band of interest. The modified amplifier's 1 dB compression point is approximately the same as that of the original. This can be obtained from figure D.12.

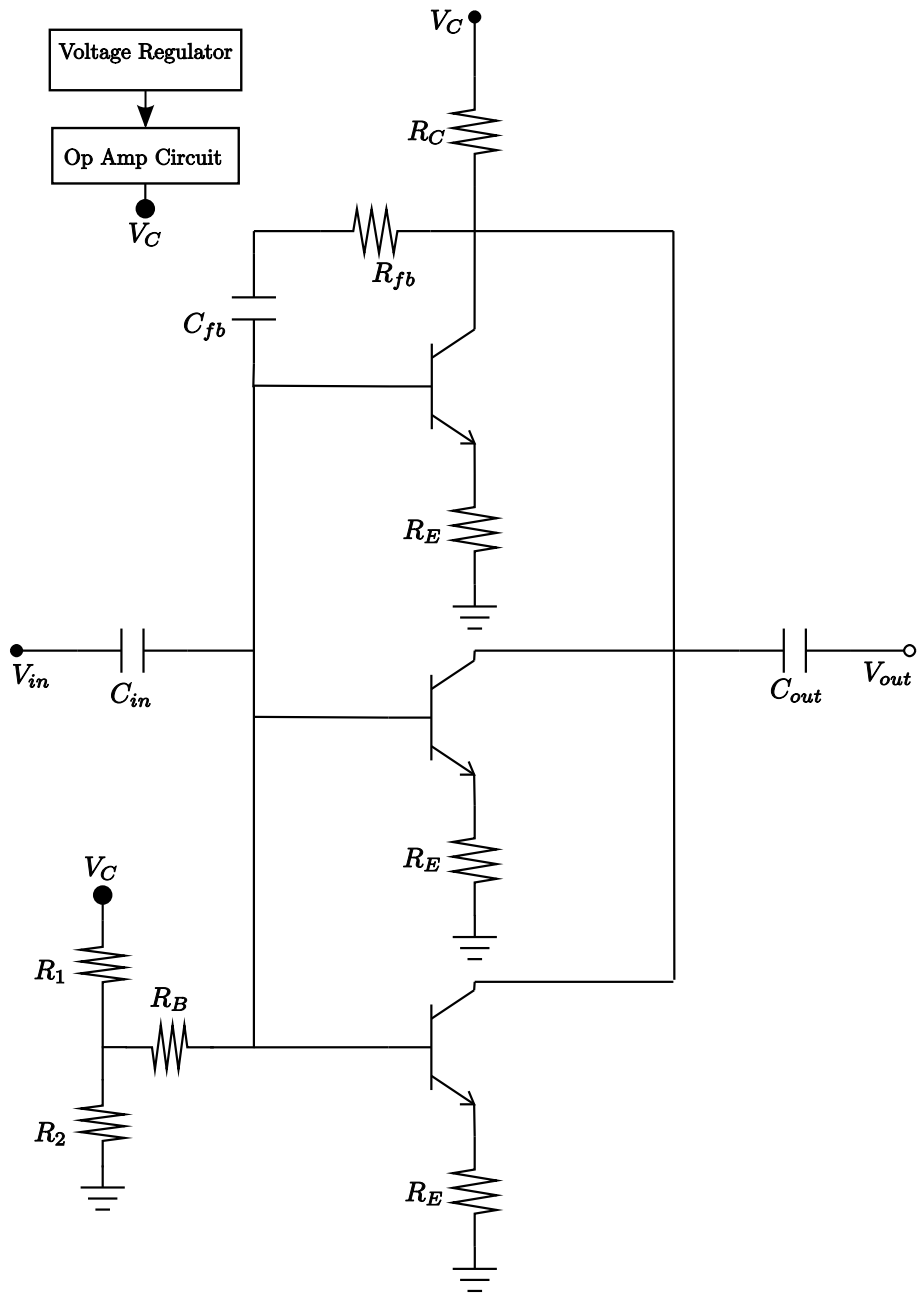


Figure D.7: Modified resistive feedback amplifier schematic

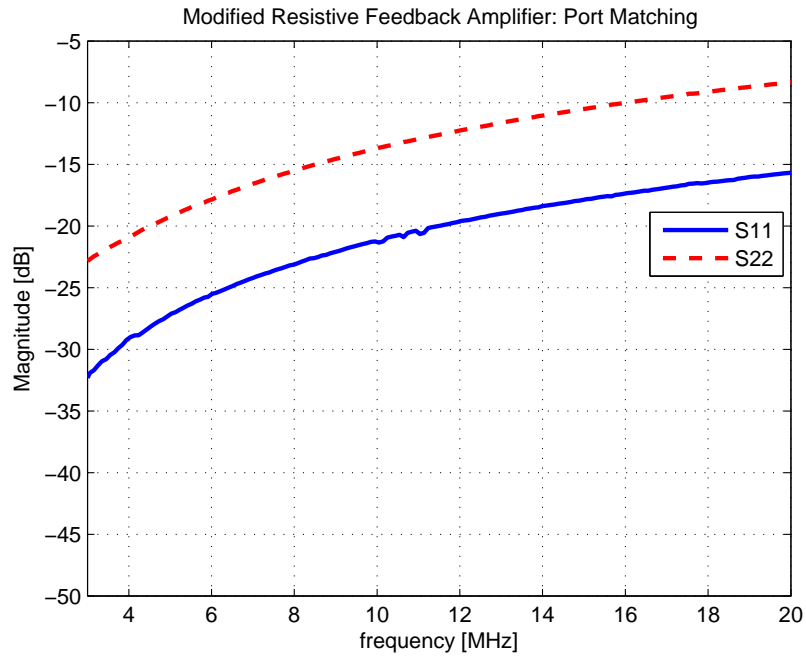


Figure D.8: Modified resistive amplifier: port matching

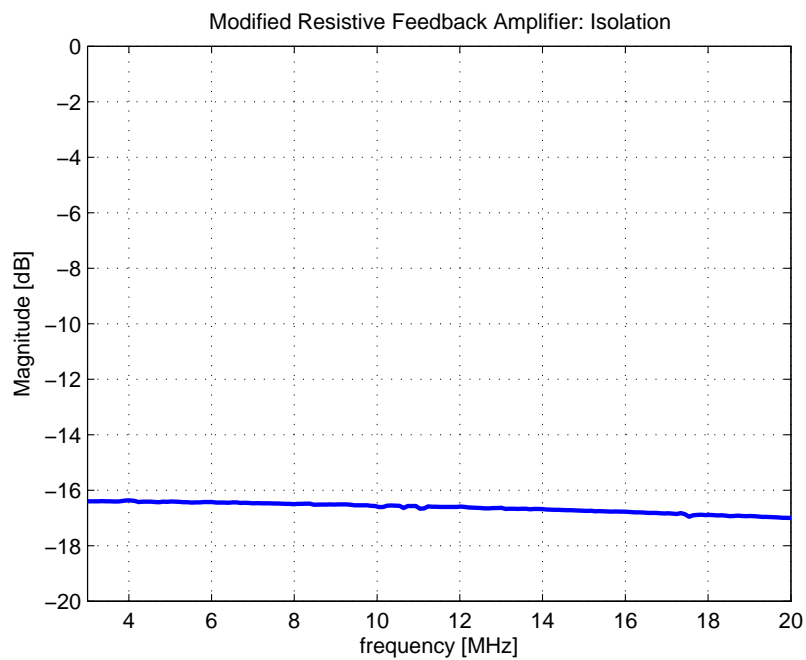


Figure D.9: Modified resistive amplifier: port isolation

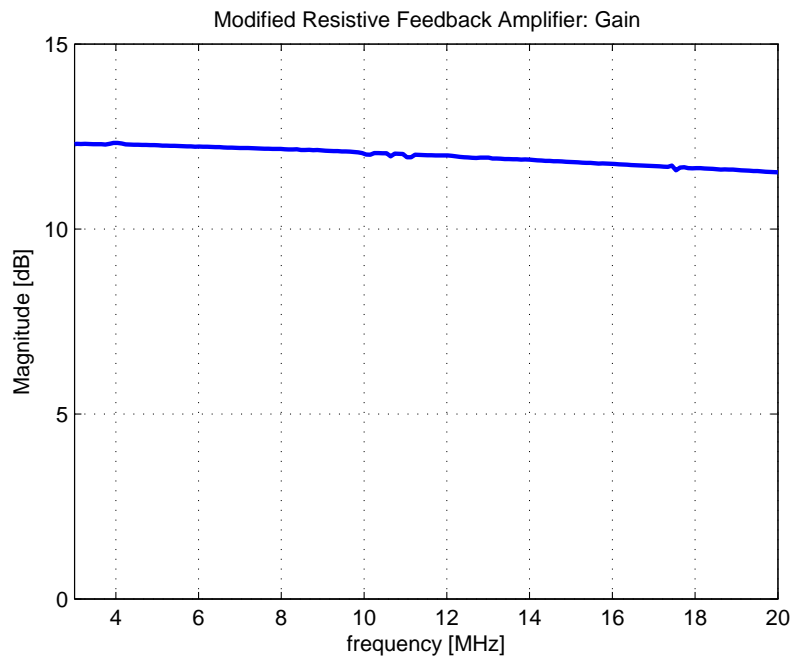


Figure D.10: Modified resistive amplifier: amplifier gain

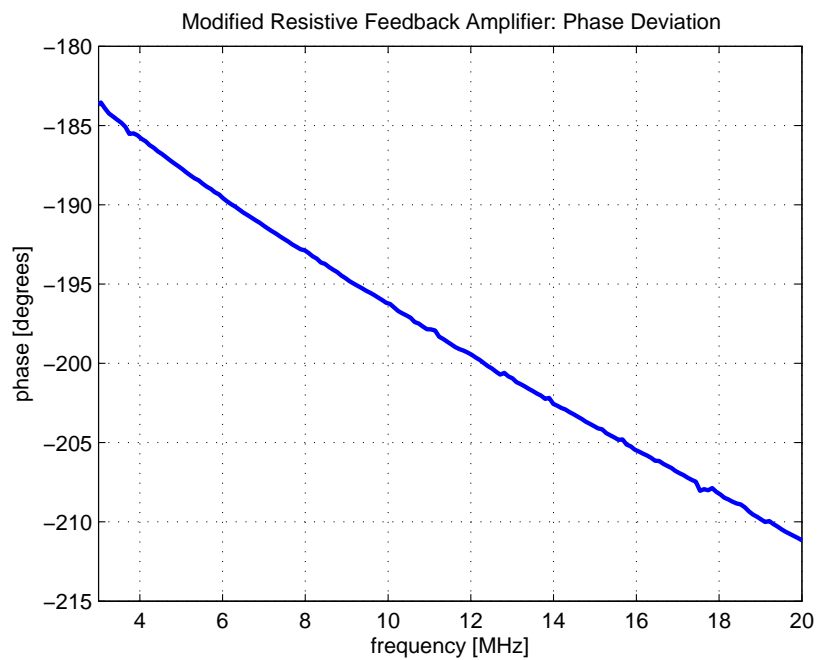


Figure D.11: Modified resistive amplifier: phase deviation

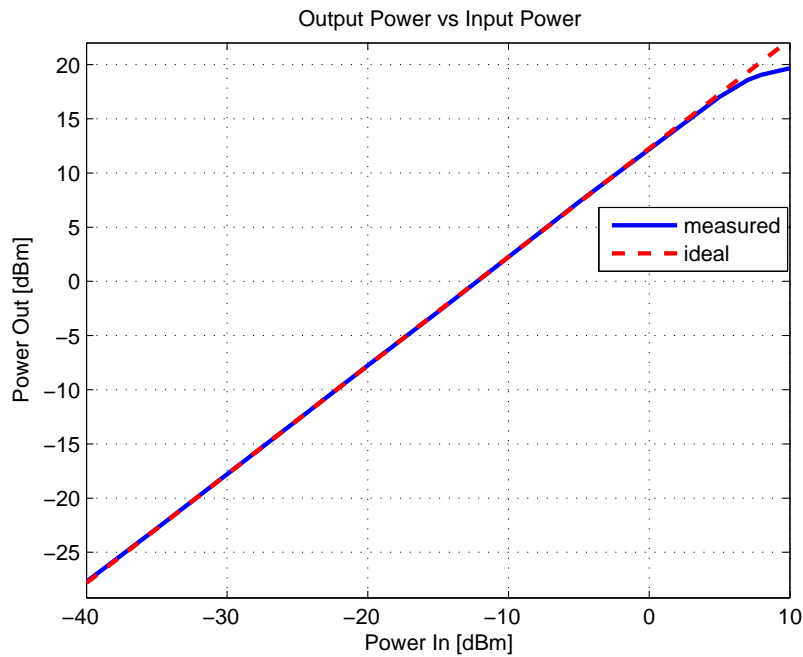


Figure D.12: Modified resistive amplifier: input power vs output power

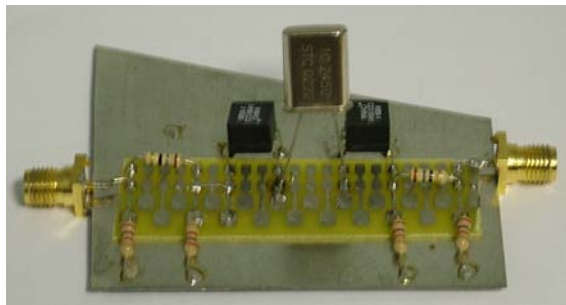


Figure D.13: AT-cut crystal resonator

D.3 AT-Cut Crystal Resonator

D.3.1 Design and Measurements

The same design used in Appendix D.1 was used here again. The only difference between the two resonators is that the SC-cut crystal is replaced here with an 10.245 MHz AT-cut crystal. The reason for this is to reduce the Q of the resonator in order to be able to accurately measure the phase noise of the oscillators in which it is used. This is explained in chapter 9.

The resonator was measured using ZVRE network analyser from Rohde & Schwarz and the results are shown in the following figures. Figure D.14 illustrates the reflection coefficients at the input and output ports of the resonator and indicates that

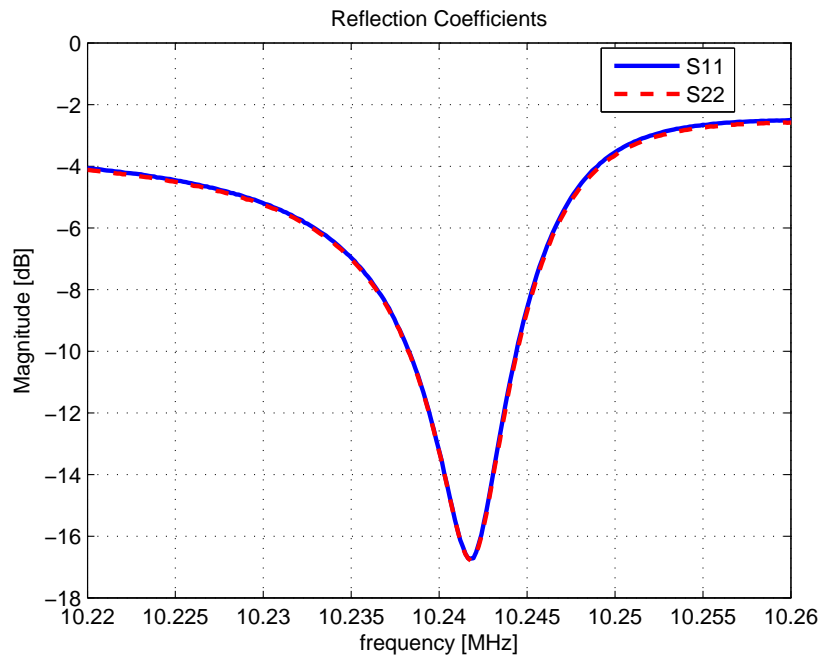


Figure D.14: AT-cut crystal resonator: reflection coefficients

the ports are well matched at the oscillating frequency. (10.245 MHz)

The pass band of the resonator is shown with respect to its phase deviation in figure D.15. In figure D.16, the pass band is depicted with respect to the resonator's group delay. The pass band data is used in chapter 9 in order to determine the ultimate noise floor of the oscillator in question. The measured group delay indicates that the Q of this resonator is considerably lower than that of the SC-cut crystal resonator discussed in Appendix D.1.

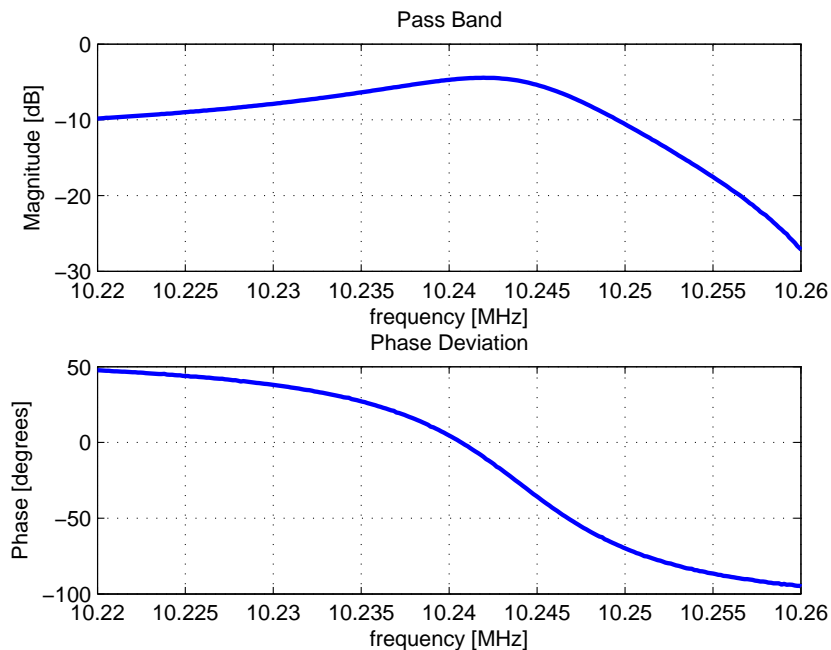


Figure D.15: AT-cut crystal resonator: pass band and phase deviation

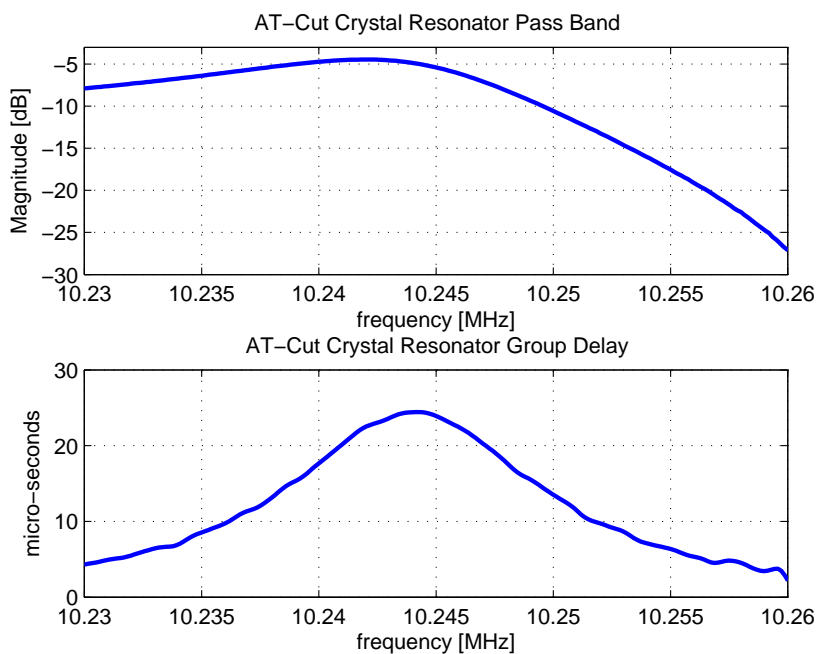


Figure D.16: AT-cut crystal resonator:pass band and group delay